

Elucidating the roles of TRPM4 and Cx40 in cardiovascular function

by

Stephen L. Gust

A thesis submitted in partial fulfillment of the requirements for the degree of

Doctor of Philosophy

Department of Pharmacology
University of Alberta

© Stephen L. Gust, 2024

Abstract

Background

The modulation of resistance artery diameter is crucial for the regulation of tissue perfusion and systemic blood pressure. This is a multi-factorial process which necessitates the integrated activity of vascular endothelial and smooth muscle cells. A wide variety of endothelial and smooth muscle ion channels are involved in the coordination of the electrical and chemical signals governing the contractile state of vascular smooth muscle cells. Smooth muscle contraction is dependent upon an increase in the intracellular concentration of Ca^{2+} via Ca^{2+} release from the sarcoplasmic reticulum and/or Ca^{2+} influx from the extracellular space. This increase in Ca^{2+} can be evoked by any of a large range of stimuli, including intravascular pressure. Pressure-evoked vasoconstriction is the basis of the myogenic response, a phenomenon whereby arteries respond to an increase in pressure by contracting to decrease diameter and maintain constant flow. The transient receptor potential melastatin 4 (TRPM4) channel has emerged as a crucial mediator of pressure-evoked vasoconstriction. Most research into its function has involved the pharmacological TRPM4 inhibitor 9-phenanthrol, though recent studies have questioned its selectivity.

Meanwhile, the endothelium regulates the contractile state of smooth muscle cells through two interrelated Ca^{2+} -dependent mechanisms: by the release of diffusible chemical mediators such as nitric oxide (NO), and by electrical coupling with smooth muscle cells via myoendothelial gap junctions (MEGJs). Gap junctions (GJs) are low resistance channels composed of connexins (Cxs) which allow the passage of ions and small molecules from the cytosol of one cell to another. An increase in intracellular Ca^{2+} causes increased opening of Ca^{2+} -activated K^+ (K_{Ca}) channels, hyperpolarizing the endothelial cell. This hyperpolarization is conducted along the endothelium

by interendothelial GJs and to smooth muscle cells by MEGJs. The hyperpolarization of smooth muscle cells inhibits opening of voltage-operated Ca^{2+} channels, thereby limiting contraction. Endothelial cells express three Cx subtypes: Cx37, Cx40 and Cx43. Of these, Cx40 has been suggested to be necessary for endothelium-dependent vasodilation. A novel Cx40 knockout (KO) rat has only recently been developed, and the cardiovascular function of this rat has yet to be characterized.

Thus, my over-arching goal is to investigate the functional roles of smooth muscle TRPM4 and endothelial Cx40 by addressing three hypotheses:

- 1) TRPM4 plays a role in both myogenic and agonist-induced vasoconstriction in resistance arteries.
- 2) The Cx40 KO rat will demonstrate impaired endothelial modulation of arterial diameter versus wild-type (WT).
- 3) The introduction of a mild hypercaloric diet will impair endothelial modulation of arterial diameter to a greater extent in the Cx40 KO rat than in WT rats.

To test these hypotheses, I have addressed three corresponding aims:

- 1) To investigate the effects of the small-molecule TRPM4 inhibitor 9-phenanthrol on the development of myogenic and agonist-induced vascular tone in isolated resistance arteries.
- 2) To characterize arterial function in the Cx40 KO rat model with exploratory functional assays.
- 3) To investigate the extent to which a hypercaloric diet produces endothelial dysfunction within the Cx40 KO rat model.

Methods

To investigate these aims, I have used a combination of functional and biochemical techniques to investigate the role of TRPM4 in vasoconstriction and characterize the cardiovascular function of the Cx40 KO rat.

Results

Firstly, my data show that pharmacological inhibition of TRPM4 with 9-phenanthrol inhibits agonist-, nerve- and pressure-evoked vasoconstriction in rat mesenteric arteries. The additional presence of the intermediate-conductance K_{Ca} (IK_{Ca}) inhibitors NS6180 and TRAM-34 has no effect on the inhibition of vasoconstriction by 9-phenanthrol, therefore this action of 9-phenanthrol is not mediated by IK_{Ca} . Next, my data show that the Cx40 KO rat exhibits pronounced hypertension and heart enlargement. This is accompanied by a large-magnitude increase in nerve-evoked vasoconstriction in the perfused mesenteric vascular bed. A large component of this effect is endothelium-independent, demonstrating that the ablation of Cx40 affects vascular smooth muscle function. Finally, applying the metabolic stress of a mild high fat diet (HFD) causes further increases in nerve-evoked vasoconstriction in the perfused mesenteric vascular bed, with the largest effect in WT rats.

Conclusion

To conclude, I have shown that 9-phenanthrol does not produce its effect by activating IK_{Ca} and demonstrated that TRPM4 is a necessary mediator of agonist-, nerve- and pressure-evoked vasoconstriction. I have also demonstrated that Cx40 has a crucial physiological role in vascular function and the maintenance of normal systemic BP. The onset of endothelial dysfunction as modelled by a mild HFD appears to share an overlapping mechanism with the Cx40 KO-induced increase in vasoconstriction. These results illustrate crucial physiological roles for TRPM4 and Cx40 in the modulation of resistance artery diameter.

Preface

This thesis is an original work by Stephen Gust. No part of this thesis has been previously published.

All animal care and experimental procedures were approved by the Animal Care and Use Committee (ACUC HS1; AUP 312) of the Faculty of Medicine and Dentistry at the University of Alberta, and performed in accordance with Canadian Council on Animal Care guidelines, and the principles and regulations as described by Grundy, 2015¹.

Acknowledgements

Firstly, I would like to thank my supervisors, Drs. Frances Plane and Paul Kerr, for your invaluable mentorship, support and patience. I would not be the scientist I am today without your guidance. It's not possible to capture all my years in the lab in a few sentences here, so suffice to say, my sincere thanks for everything.

I would like to thank the donors of the grants and awards which funded this research: the Heart & Stroke Foundation of Canada, the University of Alberta Cardiovascular Research Centre and the Faculty of Medicine & Dentistry. These awards include the Motyl Graduate Studentship in Cardiac Sciences, the Faculty of Medicine & Dentistry 75th Anniversary Award (awarded but declined) and the Faculty of Medicine & Dentistry Dean's Doctoral Award.

I would like to thank Dr. Paul Jurasz for sitting on my supervisory committee. Thank you for your advice, expertise and guidance. I also thank Dr. Fred Tse for sitting on my supervisory committee until your health prohibited. I truly appreciate your involvement and I am sorry it could not continue.

I would like to thank Drs. Harley Kurata and Darren DeLorey for serving as examiners for my candidacy.

I would like to thank several labs for facilitating my research. I thank Dr. Stephane Bourque and his lab for your generous contributions to my research. In particular, to Jad Julian-Rachid for the donation of your time and expertise performing tail-cuff plethysmography and to Claudia Holody for procuring the QIAGEN RNeasy Micro Kit I needed. I would also like to thank Dr. Nadia Jahroudi and her graduate student Parnian Alavi for your instruction, advice and equipment. I truly appreciate the time you took from your own research in order to help me. Thanks as well to Nicholas Ruel and Dr. James Hammond's lab for your resources and advice that were instrumental in my success with PCR.

I would like to thank Nichole Vestby, Colin Sanders and Margaret Mackenzie in HSLAS for your management of the rat colony and your constant help.

I would like to thank Dr. Ahmed El-Yazbi for your professional encouragement and your insightful collaboration.

I would like to thank Drs. Stephanie Lunn and Ran Wei for your friendship and supervision through my undergraduate studies. The lab was always fun with you two around!

I would like to thank my fellow graduate students, Erika Poitras, Alexia Maheux and Caleb McInroy for your friendship, your great company throughout the years and your contributions to my data.

Finally, I would like to thank my parents, Tom and Kathy, and my brother, Michael, for your unending support, your undeserved generosity and your extreme patience with me. I could not have done it without you.

Table of Contents

Abstract	ii
Preface	v
Acknowledgements	vi
Table of Contents	vii
List of Tables	x
List of Figures	xi
Abbreviations	xiv

Chapter 1: Introduction and background

1.1 Introduction.....	1
1.1.1 Impact of cardiovascular disease	1
1.1.2 Blood vessel structure	1
1.1.3 Blood vessel function.....	2
1.2 Relationship between arterial resistance and blood flow.....	3
1.3 Mechanisms of contraction in vascular smooth muscle cells	4
1.3.1 Ca ²⁺ -dependent contraction	4
1.3.2 Ca ²⁺ homeostasis in vascular smooth muscle cells.....	10
1.3.2.1 Release of Ca ²⁺ from intracellular stores	11
1.3.2.2 Ca ²⁺ signals mediated by release from intracellular stores	15
1.3.2.3 Ca ²⁺ influx pathways.....	19
1.3.2.4 Ca ²⁺ signals mediated by influx from the extracellular space	31
1.3.3 Ca ²⁺ sensitization of the contractile apparatus in vascular smooth muscle cells	34
1.3.4 Myogenic reactivity	36
1.4 Endothelium-dependent modulation of resistance artery diameter	38
1.4.1 Ca ²⁺ signalling in endothelial cells	39
1.4.1.1 Release of Ca ²⁺ from intracellular stores	40
1.4.1.2 Ca ²⁺ influx pathways.....	41
1.4.2 Endothelium-derived NO.....	43
1.4.3 Endothelium-dependent hyperpolarization.....	48
1.4.4 Crosstalk between NO synthesis and EDH.....	53
1.5 Endothelial cell junctions.....	55
1.5.1 Endothelial gap junctions.....	57
1.5.2 Role of Cx40.....	59
1.6 Myocardial ischemia/reperfusion injury	61
1.7 Hypothesis and aims	63

Chapter 2: Materials and methods

2.1 Ethics approval.....	65
2.2 Animal care and use.....	65
2.3 Perfused mesenteric vascular bed	66
2.3.1 Electric field stimulation of perivascular nerves	67

2.4	Wire myography	68
2.4.1	Concentration-response curves	68
2.5	Pressure myography	69
2.5.1	Myogenic responses to increases in intraluminal pressure	70
2.6	Genotyping.....	70
2.6.1	DNA extraction.....	71
2.6.2	Polymerase chain reaction	71
2.6.3	Gel electrophoresis.....	71
2.6.4	PCR product extraction.....	71
2.6.5	DNA sequencing and analysis	72
2.6.6	Primers for PCR and sequencing.....	72
2.7	Quantitative reverse transcription PCR (RT-qPCR).....	72
2.7.1	RNA extraction and cDNA synthesis	72
2.7.2	Sample preparation and RT-qPCR.....	73
2.8	Blood glucose measurement	74
2.9	Tail-cuff plethysmography.....	74
2.10	Langendorff heart perfusion	75
2.10.1	Ischemia/reperfusion protocol	76
2.11	Mild hypercaloric challenge via high-fat diet.....	76
2.12	Drugs and chemicals	77
2.13	Statistical analysis.....	79

Chapter 3: TRPM4 blockade impairs myogenic, agonist-induced, and nerve-evoked vasoconstriction independent of IK_{Ca}

3.1	Introduction.....	80
3.2	Methods.....	82
3.3	Results.....	82
3.3.1	TRPM4 mRNA is highly expressed in rat mesenteric arteries	82
3.3.2	Characterization of nerve-evoked vasoconstriction in the rat perfused mesenteric vascular bed.....	82
3.3.3	9-Phenanthrol limits nerve-evoked vasoconstriction in a dose-dependent manner without acting at IK_{Ca} channels.....	84
3.3.4	Characterization of pressure-evoked vasoconstriction in isolated mesenteric arteries using pressure myography	86
3.3.5	9-Phenanthrol abolishes myogenic tone without acting at IK_{Ca} channels	87
3.3.6	9-Phenanthrol induces vasodilation without acting at IK_{Ca} channels	91
3.3.7	9-Phenanthrol limits phenylephrine-induced vasoconstriction.....	93
3.4	Discussion.....	95

Chapter 4: Characterization of cardiovascular function in a novel Cx40 knockout rat

4.1	Introduction.....	106
4.2	Methods.....	109
4.3	Results.....	109

4.3.1	Cx40 KO does not upregulate relative mRNA expression of Cx37 and Cx43.....	109
4.3.2	Genetic ablation of Cx40 produces hypertension and heart enlargement.....	110
4.3.3	Genetic ablation of Cx40 enhances nerve-evoked vasoconstriction in the rat perfused mesenteric vascular bed.....	113
4.3.4	Genetic ablation of Cx40 does not affect myogenic reactivity in isolated mesenteric arteries.....	121
4.3.5	Genetic ablation of Cx40 enhances PE-induced vasoconstriction without affecting ACh-induced vasodilation in isolated rat mesenteric arteries	125
4.3.6	Genetic ablation of Cx40 impairs post-ischemic functional recovery in the Langendorff-perfused rat heart.....	130
4.4	Discussion.....	132
Chapter 5: Genetic ablation of Cx40 decreases the magnitude of vascular dysfunction incurred in mild hypercaloric challenge		
5.1	Introduction.....	145
5.2	Methods.....	148
5.3	Results.....	149
5.3.1	Hypercaloric challenge does not affect Cx40 KO-induced hypertension or heart enlargement	149
5.3.2	Hypercaloric challenge enhances nerve-evoked vasoconstriction but does not impair EDH or NO production	154
5.3.3	Mild hypercaloric challenge does not affect myogenic reactivity in isolated mesenteric arteries.....	161
5.3.4	HFD enhances post-ischemic functional recovery in the Langendorff-perfused rat heart	164
5.4	Discussion.....	166
Chapter 6: General discussion and future directions		
6.1	General discussion	175
6.2	Future directions	179
References		182
Appendix A: Diet compositions		250
Appendix B: Absolute values of organ weights		256

List of Tables

Chapter 2: Materials and methods

Table 2.1: Forward and reverse primers used for the amplification of <i>Trpc6</i> , <i>Trpm4</i> , <i>Kcnn4</i> and <i>Actb</i> in RT-qPCR	73
Table 2.2: Forward and reverse primers used for the amplification of <i>Gja4</i> , <i>Gja5</i> , <i>Gja1</i> and <i>Actb</i> in RT-qPCR	74
Table 2.3: Drugs used in the experiments described in this thesis	78

Chapter 4: Characterization of cardiovascular function in a novel Cx40 knockout rat

Table 4.1: logEC ₅₀ values of ACh-induced vasodilation in isolated second- and third-order mesenteric arteries from male and female WT, HET, and KO rats using wire myography	125
---	-----

Appendix A: Diet compositions

Table A.1: Chemical composition of the first control diet, PicoLab [®] Laboratory Rodent Diet 5L0D	250
Table A.2: Chemical composition of the second control diet, PicoLab [®] Rodent Diet 20 5053	252
Table A.3: Chemical composition of the mild HFD, Teklad custom diet TD.210490	254

List of Figures

Chapter 1: Introduction and background

Figure 1.1: Structure of the arterial wall	2
Figure 1.2: Organization of contractile filaments in smooth muscle cells	7
Figure 1.3: Mechanism of smooth muscle contraction	8
Figure 1.4: Activation of BK _{Ca} channels by Ca ²⁺ sparks	17
Figure 1.5: Membrane topology of VOCCs	21
Figure 1.6: Membrane topology of TRP channels	25
Figure 1.7: Compartmentalization of Ca ²⁺ signalling in vascular smooth muscle	33
Figure 1.8: Ca ²⁺ sensitization pathways	35
Figure 1.9: Pressure-diameter relationship in the myogenic response in arterioles	37
Figure 1.10: Schematic diagram of eNOS electron transfer states	44
Figure 1.11: Membrane topology of SK _{Ca} /IK _{Ca} channels	50
Figure 1.12: Twofold symmetry of SK _{Ca} /IK _{Ca} channels	50
Figure 1.13: Schematic diagram of EDH and NO synthesis pathways of endothelium-dependent vasodilation	55
Figure 1.14: Membrane topology of connexins	58
Figure 1.15: Schematic diagram of conduction of membrane potential along the vessel wall via gap junctions	60

Chapter 3: TRPM4 blockade impairs myogenic, agonist-induced, and nerve-evoked vasoconstriction independent of IK_{Ca}

Figure 3.1: mRNA encoding TRPM4 is expressed at higher levels than TRPC6 or IK _{Ca} in rat mesenteric arteries	83
Figure 3.2: Electric stimulus-evoked vasoconstriction in the rat perfused mesenteric vascular bed is frequency-dependent, time-independent, and is mediated by α_1 -adrenoceptors	83
Figure 3.3: 9-Phenanthrol produces concentration-dependent inhibition of nerve-evoked vasoconstriction	85
Figure 3.4: Inhibition of nerve-evoked vasoconstriction by 9-phenanthrol is not mediated by IK _{Ca}	85
Figure 3.5: Myogenic reactivity of isolated rat mesenteric arteries is time-independent and is not affected by DMSO	88
Figure 3.6: Myogenic reactivity of isolated rat mesenteric arteries is endothelium-independent	89
Figure 3.7: 9-Phenanthrol abolishes pressure-evoked vasoconstriction in isolated mesenteric arteries without acting at IK _{Ca}	90
Figure 3.8: 9-Phenanthrol produces concentration-dependent relaxation of isolated mesenteric arteries	92
Figure 3.9: 9-Phenanthrol inhibits PE-induced vasoconstriction of isolated mesenteric arteries without affecting EDH or NO synthesis	92
Figure 3.10: 9-Phenanthrol inhibits depolarization-dependent contraction to PE in an IK _{Ca} -independent manner	95

Figure 3.11: Schematic diagram of voltage-dependent vasoconstriction in a vascular smooth muscle cell 98

Chapter 4: Characterization of cardiovascular function in a novel Cx40 knockout rat

Figure 4.1: Relative mRNA expression of endothelial Cx subtypes is not altered across genotypes 110

Figure 4.2: Genetic ablation of Cx40 causes increased systolic blood pressure and heart mass in male and female rats 111

Figure 4.3: Representative traces of nerve-evoked vasoconstriction in the rat perfused mesenteric vascular bed 114

Figure 4.4: EDH and NO synthesis are significant contributors to inhibition of nerve-evoked vasoconstriction in perfused mesenteric vascular beds from Cx40 WT, HET and KO rats 115

Figure 4.5: Genetic ablation of Cx40 enhances nerve-evoked vasoconstriction in the rat perfused mesenteric vascular bed 116

Figure 4.6: Removal of endothelium abolishes the effects of apamin, TRAM-34 and L-NAME but not the effect of Cx40 ablation in the rat perfused mesenteric vascular bed 118

Figure 4.7: Perfused mesenteric vascular beds from Cx40 KO rats maintain a significant increase in nerve-evoked pressure responses versus WT and HET rats upon removal of endothelium 119

Figure 4.8: Removal of endothelium in the perfused mesenteric vascular bed enhances pressure responses in beds from males but not from females 120

Figure 4.9: Representative trace of pressure-diameter relationships in an isolated mesenteric artery from a male WT rat 122

Figure 4.10: Pressure-evoked vasoconstriction occurs in isolated mesenteric arteries from Cx40 WT, HET and KO rats 123

Figure 4.11: Myogenic response of isolated rat mesenteric arteries is not affected by genetic ablation of Cx40 124

Figure 4.12: Representative traces of concentration-response curves to ACh in isolated mesenteric arteries from male and female WT, HET and KO rats 126

Figure 4.13: EDH and NO pathways both contribute to ACh-induced vasodilation in isolated mesenteric arteries from male WT, HET and KO rats 128

Figure 4.14: EDH and NO pathways both contribute to ACh-induced vasodilation in isolated mesenteric arteries from female WT, HET and KO rats 129

Figure 4.15: U46619-induced, but not PE-induced tone is impaired in isolated mesenteric arteries from male KO and female HET and KO rats 130

Figure 4.16: Post-ischemic functional recovery is impaired in Langendorff-perfused hearts from male and female KO rats 131

Chapter 5: Genetic ablation of Cx40 decreases the magnitude of vascular dysfunction incurred in mild hypercaloric challenge

Figure 5.1: HFD does not alter Cx40 KO-induced increase in systolic blood pressure and heart mass 149

Figure 5.2: Comparisons of phenotypic changes between control and HFD-fed rats 152

Figure 5.3: HFD does not impair contribution of EDH and NO synthesis to inhibition of nerve-evoked vasoconstriction in perfused mesenteric vascular beds from Cx40 WT, HET and KO rats	156
Figure 5.4: Genetic ablation of Cx40 enhances nerve-evoked vasoconstriction in the perfused mesenteric vascular bed from HFD-fed rats	157
Figure 5.5: HFD significantly enhances nerve-evoked vasoconstriction in perfused mesenteric vascular beds from Cx40 WT rats	158
Figure 5.6: HFD significantly enhances nerve-evoked vasoconstriction in perfused mesenteric vascular beds from female, but not male Cx40 HET rats	159
Figure 5.7: HFD significantly enhances nerve-evoked vasoconstriction in perfused mesenteric vascular beds from Cx40 KO rats	160
Figure 5.8: Pressure-evoked vasoconstriction occurs in isolated mesenteric arteries from HFD-fed Cx40 WT, HET and KO rats	162
Figure 5.9: Myogenic response of isolated rat mesenteric arteries is not affected by HFD	163
Figure 5.10: Post-ischemic functional recovery in Langendorff-perfused hearts from HFD-fed male and female rats	164
Figure 5.11: HFD enhances post-ischemic functional recovery in Langendorff perfused rat hearts	165
Figure 5.12: Schematic diagram illustrating the formation of ONOO ⁻ and its role in vascular dysfunction	170

Appendix B: Absolute values of organ weights

Figure B.1: Weight of kidneys and hearts from control and HFD-fed WT, HET and KO rats before correcting for body weight	256
--	-----

Abbreviations

5-HT	5-hydroxytryptamine (serotonin)
ACh	acetylcholine
ADP	adenosine 5'-diphosphate
AKAP	A-kinase anchoring protein
apoCaM	apocalmodulin (Ca ²⁺ -free calmodulin)
AT₁R	angiotensin II type 1 receptor
ATP	adenosine 5'-triphosphate
BK_{Ca}	big-conductance Ca ²⁺ -activated K ⁺ channel
BP	blood pressure
Ca²⁺	calcium ion
[Ca²⁺]_i	intracellular concentration of Ca ²⁺
Ca²⁺/CaM	Ca ²⁺ -calmodulin complex
CaD	caldesmon
CaM	calmodulin
CaMKII	Ca ²⁺ /CaM-dependent protein kinase II
cAMP	cyclic adenosine-3',5'-monophosphate
CD	control diet
cGMP	cyclic guanosine-3',5'-monophosphate
CICR	Ca ²⁺ -induced Ca ²⁺ release
Cl_{Ca}	Ca ²⁺ -activated chloride channel
COX	cyclooxygenase
CPI-17	PKC-potentiated PP1 inhibitory protein of 17 kDa
CVD	cardiovascular disease
Cx	connexin
DAG	diacylglycerol
DMSO	dimethyl sulfoxide
EC	endothelial cell
EDH	endothelium-dependent hyperpolarization
ELC or LC₁₇	essential light chain
eNOS	endothelial nitric oxide synthase
ER	endoplasmic reticulum
GJ	gap junction
GPCR	G protein-coupled receptor
GTP	guanosine-5'-triphosphate
HET	heterozygous
HFD	high-fat diet
HUVEC	human umbilical vein endothelial cell
IK_{Ca}	intermediate-conductance Ca ²⁺ -activated K ⁺ channel
IP₃	inositol 1,4,5-trisphosphate
IP₃R	inositol 1,4,5-trisphosphate receptor
JCaT	junctional Ca ²⁺ transient
K⁺	potassium ion
KO	knockout
L-NAME	N ^G -nitro-L-arginine methyl ester hydrochloride

LTCC	L-type Ca ²⁺ channel
LVDP	left ventricular developed pressure
MEGJ	myoendothelial gap junction
MEP	myoendothelial projection
MLCK	myosin light chain kinase
MLCP	myosin light chain phosphatase
NA	noradrenaline
Na⁺	sodium ion
NADPH	reduced nicotinamide-adenine-dinucleotide phosphate
NO	nitric oxide
NOX	NADPH oxidase
NS6180	4-[[3-(trifluoromethyl)phenyl]methyl]-2 <i>H</i> -1,4-benzothiazin-3(4 <i>H</i>)-one
O₂⁻	superoxide anion
ONOO⁻	peroxynitrite
P2X	purinergic ionotropic receptor
P2Y	G-protein coupled purinergic receptor
PE	phenylephrine
P_i	inorganic phosphate
PIP₂	phosphatidylinositol 4,5-bisphosphate
PK	protein kinase
PLC	phospholipase C
PMCA	plasma membrane Ca ²⁺ -ATPase
PP	protein phosphatase
RLC or LC₂₀	regulatory light chain
ROS	reactive oxygen species
RyR	ryanodine receptor
SERCA	sarcoplasmic/endoplasmic reticulum Ca ²⁺ -ATPase
sGC	soluble guanylyl cyclase
SK_{Ca}	small-conductance Ca ²⁺ -activated K ⁺ channel
SR	sarcoplasmic reticulum
T2DM	type 2 diabetes mellitus
TM	transmembrane domain
TMEM16A	transmembrane protein 16A
TRAM-34	1-[(2-chlorophenyl)diphenylmethyl]-1 <i>H</i> -pyrazole
TRP	transient receptor potential
TRPA	ankyrin transient receptor potential channel
TRPC	canonical transient receptor potential channel
TRPM	melastatin transient receptor potential channel
TRPV	vanilloid transient receptor potential channel
TTCC	T-type Ca ²⁺ channel
U46619	(5 <i>Z</i>)-7-[(1 <i>R</i> ,4 <i>S</i> ,5 <i>S</i> ,6 <i>R</i>)-6-[(1 <i>E</i> ,3 <i>S</i>)-3-hydroxy-1-octen-1-yl]-2-oxabicyclo[2.2.1]hept-5-yl]-5-heptenoic acid
VOCC or Cav	voltage-operated Ca ²⁺ channel
VSMC	vascular smooth muscle cell
WKY	Wistar-Kyoto
WT	wild-type

Chapter 1: Introduction and background

1.1 Introduction

1.1.1 Impact of cardiovascular disease

The World Health Organization reports that cardiovascular disease (CVD) is the leading cause of death worldwide, responsible for an estimated 17.9 million deaths (32% of all global deaths) in 2019, of which 15.2 million are due to heart attack and stroke². Metabolic disease and diabetes are major risk factors of CVD^{3,4}. In the United States, an estimated 8.5-12% of the adult population have type 2 diabetes mellitus (T2DM)^{3,5}, and over 50% of T2DM-related deaths are attributable to CVD³. Despite the efficacy of lifestyle interventions⁶, the prevalence of T2DM in both adults and youth continues to increase^{2,3,5}, underscoring the need for the identification of new drug targets and the development of novel pharmacological therapies for CVD, especially within the context of metabolic disease and diabetes.

1.1.2 Blood vessel structure

In the body, blood vessels (i.e. arteries, veins and capillaries) are responsible for tissue perfusion, thereby facilitating gas exchange, nutrient distribution and waste removal by the blood. Arteries and veins are composed of three tissue layers: the tunica externa, tunica media, and tunica intima (**Figure 1.1**). The tunica externa, or adventitia, is the outermost layer which consists primarily of elastin and collagen aligned longitudinally along the vessel, but also includes fibroblasts, mast cells, macrophages, and perivascular nerves with surrounding Schwann cells⁷⁻⁹. The middle layer is the tunica media, comprising vascular smooth muscle cells (VSMCs) and an internal elastic lamina, which is a fenestrated sheet of elastin bordering the luminal side of the media⁷⁻⁹. Finally, the tunica intima consists of the endothelium, which is a single layer of squamous endothelial cells (ECs), and an 80-nm thick basal lamina separating the endothelium from the

media. Additionally, in large, elastic vessels such as the aorta, a subendothelial space containing fibrous collagen and elastin is present between the basal lamina and the media^{7,8}.

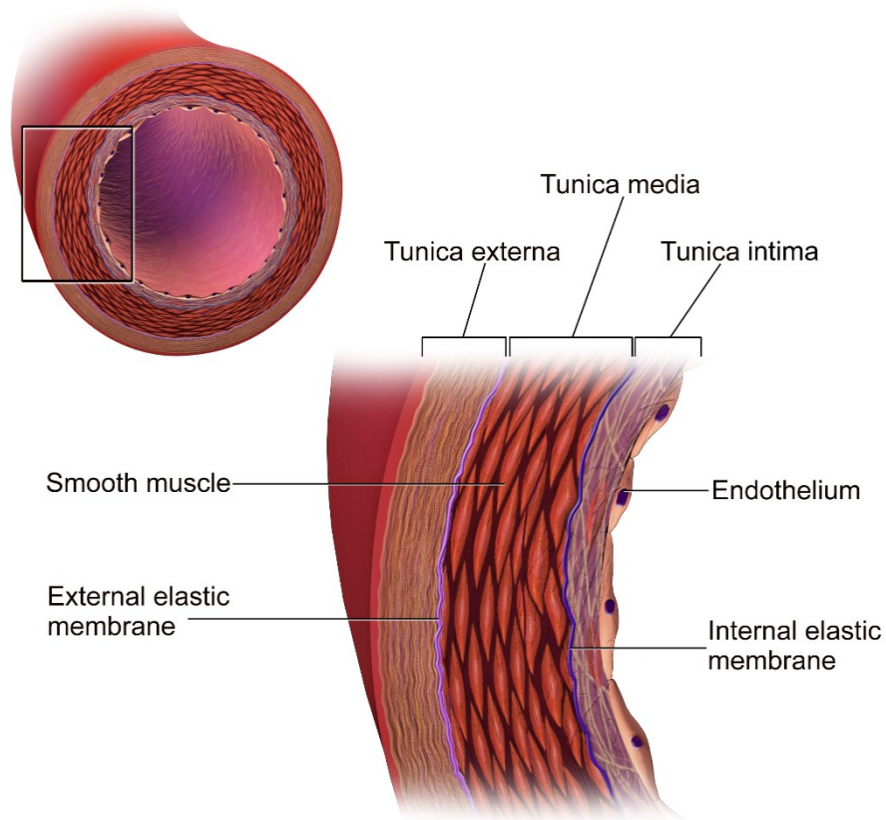


Figure 1.1: Structure of the arterial wall. Diagram illustrating the three tissue layers of the arterial wall: the tunica externa or adventitia, the tunica media, and the tunica externa (from Blausen Medical, 2014)¹⁰.

1.1.3 Blood vessel function

Resistance arteries, which comprise precapillary arteries and arterioles with diameters of 20 to 500 μm ^{7,11,12}, account for over 80% of haemodynamic resistance in the body⁹. They are a primary regulator of systemic blood pressure and tissue perfusion due to their ability to rapidly change diameter in response to chemical and mechanical stimuli^{9,13,14}. Depending upon the arteriolar diameter, the media of resistance arteries ranges from 1 cell layer in 20-50 μm arterioles to approximately 6 cell layers of VSMCs in 500 μm arteries, with little intercellular space between

VSMCs^{7,8}. The endothelium plays a crucial role in the regulation of smooth muscle contraction by two predominant mechanisms: firstly by the release of diffusible vasoconstrictors (e.g. endothelin-1, thromboxane A₂) and vasodilators (e.g. nitric oxide (NO), prostacyclin (PGI₂), epoxyeicosatrienoic acids (EETs)), and secondly by electrical coupling between ECs and VSMCs via myoendothelial gap junctions (MEGJs)¹³⁻¹⁷. By regulating the contractile state of VSMCs, the endothelium controls arterial diameter, which determines vascular resistance and subsequently blood flow and blood pressure. In addition to modulating blood flow, the endothelium produces factors which influence inflammation¹⁸, platelet function¹⁹, and angiogenesis²⁰⁻²³. Although the endothelium was once considered to be no more than a physical barrier between the blood and the vessel wall, it is now considered an endocrine organ due to its integral role in these regulatory pathways²⁴.

Most forms of CVD, including atherosclerosis, hypertension and T2DM, begin with the development of endothelial dysfunction²⁵⁻³², whereby the endothelium's ability to regulate blood vessel diameter is impaired. Thus, there is growing interest in the development of therapies to prevent or reverse endothelial dysfunction in order to treat the etiology of CVD more directly. This approach requires a greater understanding of endothelial function and the identification of putative drug targets.

1.2 Relationship between arterial resistance and blood flow

Flow, in any fluid system, is driven by a pressure gradient³³. Within a cylindrical tube, such as a blood vessel, this difference in pressure is calculated by the Hagen-Poiseuille equation:

$$\Delta P = \frac{8\mu L Q}{\pi r^4}$$

where μ is the dynamic viscosity of the fluid (in Pa·s), L is the length of the tube (in m), Q is the volumetric flow rate (in m³·s⁻¹), r is the tube radius (in m), and the pressures at $x = 0$ and $x = L$

are $P = P$ and $P = P + \Delta P$, respectively³³⁻³⁵. The relationship between pressure, flow rate, and fluidic resistance is analogous to the relationship between voltage (V), current (I), and electrical resistance (R), respectively, described by Ohm's law ($V = IR$)³⁴. Thus, substituting Ohm's law into the Hagen-Poiseuille equation yields a formula to determine fluid resistance in a tube:

$$R = \frac{8\mu L}{\pi r^4}$$

This equation demonstrates that fluid resistance is inversely proportional to the tube radius raised to the fourth power (i.e. $R \propto r^{-4}$). In the context of resistance arteries, this means that relatively small changes in the luminal diameter result in much larger changes in vascular resistance. This is the guiding principle by which the contractile state of VSMCs is a major determinant of systemic blood pressure.

1.3 Mechanisms of contraction in vascular smooth muscle cells

The membrane potential of VSMCs determines their contractile state by regulating the activity of a wide variety of ion channels. This in turn controls the entry and release of calcium ions (Ca^{2+}) into the cytoplasm, thereby regulating smooth muscle contraction. This section will provide detail into this multi-factorial process.

1.3.1 Ca^{2+} -dependent contraction

Muscle tissues in vertebrates comprise three categories: skeletal, cardiac, and smooth muscle^{36,37}. Each type of muscle is composed of myocytes which are phenotypically distinct from the other categories; however, all muscle contraction requires both ATP and an increase in the intracellular concentration of calcium ($[\text{Ca}^{2+}]_i$)^{38,39}. ATP hydrolysis fuels the sliding of myosin filaments, or thick filaments, along corresponding actin filaments, or thin filaments, in order to contract the myocyte.

Skeletal and cardiac muscle are together known as striated muscle due to the organization of actin and myosin filaments into a repeating functional unit called a sarcomere^{36,37}. The sarcomere is a bipolar^{40,41} arrangement of actin and myosin filaments, bounded between two structural Z-disks composed mostly of α -actinin⁴². The thin filament primarily consists of polymerized actin monomers, regulated by associated proteins tropomyosin and troponins T, I and C³⁷. Tropomyosin is a long molecule composed of two α -helical chains twisted together to form a “coiled coil,” helically wrapped around the actin filament⁴¹. Tropomyosin covers the myosin binding site on actin when the cell is in a relaxed state; the binding of Ca^{2+} to troponin C elicits a conformational change in tropomyosin, exposing the myosin binding sites^{36,37,41}. Myosin filaments are composed of muscle-myosin II, a hexameric protein comprising two heavy chains; two essential light chains, 17 kDa each (ELC or LC₁₇); and two regulatory light chains, 20 kDa each (RLC or LC₂₀)^{36,43}. The S1 fragment of the heavy chain is called the myosin head, and contains a nucleotide-binding site and an actin-binding site^{36,44}. Once the myosin binding sites on actin are exposed, ATP binds to the nucleotide-binding site on the myosin head to be hydrolysed, causing a conformational change which cocks the myosin head to allow cross-bridge formation with the actin molecule³⁹. The release of P_i produces the power stroke of the filaments sliding past one another, and the cycle is complete with the release of ADP, which causes the myosin head to return to an uncocked position. This process is called cross-bridge cycling, and is the underlying mechanism of contraction or shortening in all myocytes (reviewed by Sweeney and Holzbaur, 2018)⁴⁵.

Like striated muscle cells, smooth muscle cells contain actin and myosin filaments which require both ATP and an increase in $[\text{Ca}^{2+}]_i$ for contraction; however, the cellular machinery of contraction is organized very differently. Most prominently, smooth muscle cells do not contain

sarcomeres^{36,37,40,41,46-49}. Smooth muscle actin and myosin have been demonstrated to be morphologically and functionally similar to striated muscle actin and myosin, thus it is accepted that cross-bridge cycling is the process responsible for smooth muscle shortening^{40,50,51}. However, the ultrastructure of actin and myosin filaments in smooth muscle cells is not clearly defined^{40,48}, in large part due to the fact that striated muscle sarcomeres are clearly visible via electron micrograph, whereas myosin is undetectable in native smooth muscle cells by electron micrograph^{41,52}. The current model of the functional unit of contraction in smooth muscle is a side-polar filament model (**Figure 1.2a**)⁴⁰, wherein cross-bridges have the same polarity along one side of the myosin thick filament, and the opposite polarity along the other side. Actin thin filaments are bound at one end by cytoplasmic or membrane-associated dense bodies composed mostly of α -actinin, analogous to Z-disks in striated muscle (**Figure 1.2b**)^{40,49,53-56}. Dense bodies have also been demonstrated to bind the cytoskeletal intermediate filaments desmin and vimentin^{36,49,55,57-59}, creating a structural network which allows the cell to support passive tension, or basal tone⁴⁷. Additionally, it has been demonstrated that unlike in striated muscle, smooth muscle myosin filaments undergo polymerization and depolymerization to regulate contractility and to adapt to large changes in cell length (reviewed by Wang *et al.*, 2021)⁴⁴.

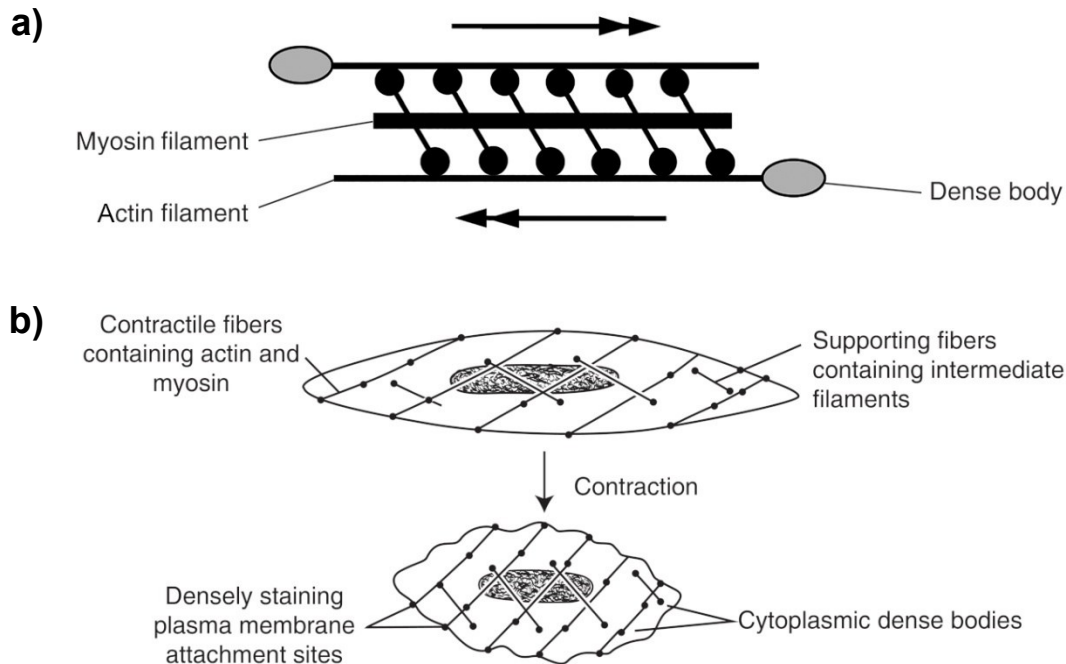


Figure 1.2: Organization of contractile filaments in smooth muscle cells. a) Schematic diagram of the side-polar filament model of the smooth muscle contractile unit. The double arrows indicate the direction of actin sliding relative to myosin. **b)** Diagram illustrating the arrangement of contractile units within the smooth muscle cell at rest and during contraction (adapted from Seow, 2019 and Sweeney and Hammers, 2018)^{36,40}.

Smooth muscle also differs from striated muscle in the mechanisms by which actomyosin interactions are regulated. In striated muscle, a Ca^{2+} -dependent conformational change in the thin filament initiates cross-bridge formation, whereas in smooth muscle, cross-bridge formation is initiated by a Ca^{2+} -dependent conformational change in the thick filament⁶⁰. Upon the influx of Ca^{2+} from either the extracellular space or intracellular stores (See §1.3.2)⁶¹, four Ca^{2+} ions bind to one calmodulin (CaM) molecule to form a Ca^{2+} /CaM complex⁶², which subsequently binds to myosin light chain kinase (MLCK)⁶³. MLCK contains an auto-inhibitory domain which is ordinarily bound to its catalytic site⁵⁴; the binding of Ca^{2+} /CaM to MLCK elicits a dissociation of the auto-inhibitory domain from the catalytic site, thereby activating MLCK⁶⁴⁻⁶⁷. Subsequently, MLCK phosphorylates residues Ser19 and, at relatively high concentrations of MLCK, Thr18 on

both RLCs of myosin II⁶⁸⁻⁷⁰. The phosphorylation of Ser19 induces a conformational change in the myosin head, facilitating actomyosin cross-bridge formation and increasing the actin-activated Mg^{2+} -ATPase activity of myosin II^{43,45,54,71}. The hydrolysis of ATP then drives cross-bridge cycling in the same manner as occurs in striated muscle (**Figure 1.3**). Due to the action of Ca^{2+} ATPase pumps at the sarcoplasmic/endoplasmic reticulum (SERCA) and plasma membrane (PMCA) to remove Ca^{2+} from the cytosol, $[Ca^{2+}]_i$ decreases following contraction^{37,56,72}. This initiates relaxation by causing the dissociation of Ca^{2+} from CaM, which inactivates MLCK^{54,62,65}. The myosin RLCs may then be dephosphorylated by protein phosphatases 1 (PP1) and 2A (PP2A), together known as myosin light chain phosphatases (MLCP)⁷³. Dephosphorylation of Ser19 returns myosin II to its inactive conformation, disrupting the actomyosin cross-bridge and precipitating relaxation^{54,56,67,74}.

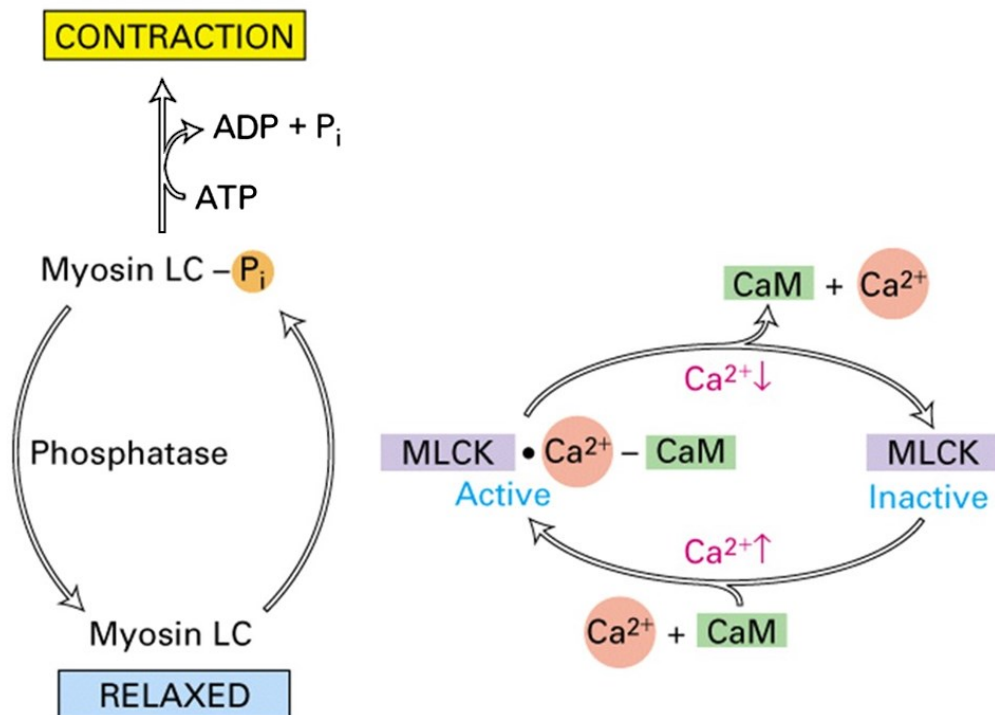


Figure 1.3: Mechanism of smooth muscle contraction. Schematic diagram illustrating the pathway of Ca^{2+} -dependent contraction in smooth muscle cells. An increase in $[Ca^{2+}]_i$ leads to the activation of MLCK by Ca^{2+} /CaM. MLCK then phosphorylates myosin RLC, enhancing its Mg^{2+} -ATPase activity and initiating crossbridge cycling (adapted from Lodish *et al.*, 2000)⁷⁵.

Smooth muscle contraction and relaxation are modulated by secondary Ca^{2+} -dependent pathways as well. The two most influential of these modulators are the actin-binding proteins and Ca^{2+} -dependent kinases. Firstly, instead of troponin found in skeletal muscle thin filaments, smooth muscle cells express the functionally analogous actin-binding proteins caldesmon (CaD) and calponin (CaP) which bind both actin and tropomyosin^{46,76-80}. CaD has been demonstrated to directly inhibit actomyosin Mg^{2+} -ATPase activity in a tropomyosin-dependent manner, and competitively inhibits myosin S1-ATP binding to actin^{71,81-85}. Upon $[\text{Ca}^{2+}]_i$ increase, Ca^{2+} /CaM binds to CaD, dissociating it from actin and allowing cross-bridge formation^{86,87}. CaD is also reversibly phosphorylated by kinases including protein kinase C (PKC), mitogen-activated protein kinase (MAPK) and Ca^{2+} /CaM-dependent protein kinase II (CaMKII), causing its dissociation from actin and decreasing its inhibition of actomyosin Mg^{2+} -ATPase activity^{46,88-91}. CaP has also been shown to inhibit actomyosin Mg^{2+} -ATPase activity; however, unlike CaD, its effect is not dependent upon tropomyosin⁹². It has been demonstrated that the regulation of actin by CaD and CaP in smooth muscle is structurally distinct from the regulation of actin by troponin in striated muscle^{85,93}. Furthermore, it is generally accepted that smooth muscle cells do not express troponin^{36,54,94,95}. However, recent evidence in the primary literature suggests that certain troponin isoforms may be expressed in some VSMCs^{96,97}, perhaps due to the demand for a quicker onset of contraction in vessels such as the renal afferent arteriole relative to the rest of the vasculature⁹⁷.

Secondly, there are two main Ca^{2+} -dependent kinases which regulate smooth muscle contraction: PKC and CaMKII^{54,71,98,99}. Smooth muscle cells express the Ca^{2+} -dependent classical PKC isoforms α and β , which also require diacylglycerol (DAG) for activation^{54,100-102}. In response to an increase in both $[\text{Ca}^{2+}]_i$ and DAG, such as through agonism at the α_1 -adrenergic receptor (See §1.3.2), PKC α and β are activated and move to phosphorylate a small protein called PKC-

potentiated PP1 inhibitory protein of 17 kDa (CPI-17) at Thr38^{98,103,104}. This activates CPI-17, which is a competitive false substrate at MLCP. Thus, by occupying MLCP, CPI-17 prolongs contraction since MLCP can no longer dephosphorylate the myosin RLC. While PKC is activated by Ca²⁺ ions, CaMKII is activated by the binding of Ca²⁺/CaM. Smooth muscle cells express two of four existing CaMKII isoforms: δ and γ (cf. α and β isoforms are restricted to neurons)^{98,99}. CaMKII contains an auto-inhibitory domain which occupies its active site; Ca²⁺/CaM binding causes CaMKII to autophosphorylate at Thr287, dissociating the auto-inhibitory domain from the active site. This active form is retained even after the removal of Ca²⁺/CaM, and is therefore implicated in Ca²⁺ sensitization (See §1.3.3)^{98,105}. When activated, CaMKII phosphorylates a wide range of downstream targets, including key contractile proteins such as MLCK, myosin RLC, CaD, SERCA, L-type Ca²⁺ channels, IP₃ and ryanodine receptors, and canonical transient receptor potential (TRPC) channels^{98,99,106}. Despite the fact that CaMKII inhibits MLCK by phosphorylation¹⁰⁷, the sum of its actions produce a net pro-contractile effect^{108,109}.

1.3.2 Ca²⁺ homeostasis in vascular smooth muscle cells

In order to initiate smooth muscle cell contraction, there are two sources from which Ca²⁺ ions may enter the cytoplasm: intracellular stores and the extracellular space (reviewed by Ghosh *et al.*, 2017)⁶¹. The resting [Ca²⁺]_i of vascular smooth muscle is maintained at approximately 100 nM, three and four orders of magnitude lower than the Ca²⁺ concentrations within the sarcoplasmic reticulum and the extracellular space, at 200 μ M and 2 mM, respectively^{110,111}. This relatively extreme concentration gradient is maintained by the constitutive action of SERCA, PMCA, and the Na⁺/Ca²⁺ exchanger (NCX) to remove Ca²⁺ ions from the cytosol^{37,110,112}. Due to the relatively low diffusion coefficient of Ca²⁺ ions^{113,114}, Ca²⁺ signalling in VSMCs, as in other cell types, is compartmentalized^{71,110,115}. This refers to the spatial and temporal organization of cellular

functions into signalling microdomains, whereby associated proteins of a particular pathway are localized to the same region or structure of a cell in order to optimize the efficiency and efficacy of second messenger signalling¹¹⁰. Ca^{2+} is a ubiquitous second messenger in all cell types; thus, compartmentalization in VSMCs allows for the activation of specific pathways via localized, subcellular increases in $[\text{Ca}^{2+}]$ without necessarily increasing the global $[\text{Ca}^{2+}]_i$ ^{110,114}. VSMCs exhibit several types of local Ca^{2+} signals which can be categorized according to their distinct spatiotemporal patterns and mechanisms by which they are generated (reviewed by Amberg and Navedo, 2013)¹¹⁵. These local Ca^{2+} signals contribute both directly and indirectly to changes in $[\text{Ca}^{2+}]_i$ of the VSMC, thereby influencing vascular tone and subsequently controlling systemic blood flow and pressure^{71,115}.

1.3.2.1 Release of Ca^{2+} from intracellular stores: Within VSMCs, there are two main organelles which serve as Ca^{2+} stores: the sarcoplasmic reticulum (SR) and mitochondria^{61,110,116-118}. The SR is a specialized endoplasmic reticulum found in myocytes, and it is the primary intracellular Ca^{2+} store associated with the initiation of contraction in VSMCs^{112,119-122}. The resting $[\text{Ca}^{2+}]$ inside the SR is approximately three orders of magnitude greater than the resting cytosolic $[\text{Ca}^{2+}]_i$ ^{110,111}. While up to 90% of the volume of smooth muscle cells is occupied by myofilaments, intermediate filaments and dense bodies, the SR occupies approximately 2-7% of the cell volume depending on the tissue^{112,118,122,123}. It was hypothesized and demonstrated that smooth muscle subtypes with larger SR volumes (e.g. VSMCs from large elastic arteries such as the aorta) continue to contract after prolonged exposure to Ca^{2+} -free media, whereas subtypes with smaller SR volumes (e.g. visceral smooth muscle; VSMCs from resistance arteries) experience significantly less contraction after exposure to Ca^{2+} -free media¹²⁴⁻¹²⁶. Thus, it was believed that SR volume correlates with the relative contribution of Ca^{2+} release, as opposed to Ca^{2+} influx, to

smooth muscle contraction^{118,124}. However, the correlation between SR volume and contraction time in Ca²⁺-free media fell out of favour due to reports of low SR volumes in phasic smooth muscles, such as the vas deferens and taenia coli, which maintain phasic contractions in Ca²⁺-free media^{112,126-128}. Subsequently, confocal imaging using fluorescent probes of free Ca²⁺ and of SR proteins such as SERCA and ryanodine receptors have elucidated the ultrastructure of the SR as a network of interconnected tubules, sacs and cisternae continuous with the nucleus^{112,119,129-133}. SR is both concentrated around the nucleus and distributed peripherally. Currently the functional and compositional differences between central and peripheral SR are not clear; however, it has been demonstrated that phasic SMCs have predominantly peripheral SR relative to non-phasic SMCs^{112,131,132}.

Mitochondria are the second notable intracellular Ca²⁺ store; however, there is no evidence to suggest that Ca²⁺ release from the mitochondria is linked to smooth muscle contraction^{110,115,116,122}. The role of mitochondria in smooth muscle Ca²⁺ homeostasis is not fully understood; the current model suggests that due to their higher capacity for Ca²⁺ uptake than release, with release being saturable¹³⁴, mitochondria act as a buffer for cytosolic [Ca²⁺]_i¹³⁵. Mitochondria are likely minimally loaded with Ca²⁺ under physiological conditions, but remove Ca²⁺ from the cytosol during “Ca²⁺ overload” events of pathologically high [Ca²⁺]_i (≥ 5 μM; 50 times the resting concentration)¹³⁵⁻¹³⁷. For the purposes of this thesis, I will focus on the role of the SR in VSMC Ca²⁺ handling rather than the mitochondria, due to the latter’s lack of direct involvement in VSMC contraction.

IP₃Rs: Free Ca²⁺ may be released from the SR into the cytoplasm via activation of two ligand-gated Ca²⁺-channels: the inositol 1,4,5-trisphosphate (IP₃) receptor (IP₃R), and the ryanodine receptor (RyR)^{138,139}. The first of these, the IP₃R, is a homo- or heterotetramer in which

each subunit contains a cytosolic N-terminal domain, six hydrophobic transmembrane (TM) domains with a central pore domain between TM5 and TM6, and finally a cytosolic C-terminal domain¹⁴⁰. The N-terminus contains the IP₃ binding site as well as a suppressor domain that inhibits IP₃ binding, a regulatory domain comprising Ca²⁺ and ATP binding sites, and a coupling domain which facilitates direct interaction between the IP₃R and TRPC channels^{61,140,141}. Three isoforms of the IP₃R have been identified: IP₃R1, IP₃R2 and IP₃R3; these isoforms are derived from three separate genes sharing approximately 60-70% sequence identity, and differ in their affinity for IP₃ binding as well as their relative expression in different tissues^{61,140-148}. IP₃Rs are ubiquitously expressed, and have been found localized to the SR of myocytes and ER of many other cell types¹⁴¹. All three isoforms have been shown to be expressed by VSMCs, with IP₃R1 being the primary form expressed in both large conduit arteries and small resistance arteries¹⁴⁹⁻¹⁵¹.

IP₃ is a second messenger which is produced through the hydrolysis of the membrane phospholipid phosphatidylinositol 4,5-bisphosphate (PIP₂) into IP₃ and DAG by phospholipase C (PLC; reviewed by Kadamur and Ross, 2013)¹⁵². G_{q/11} protein-coupled receptors activate PLC, thereby increasing the production of IP₃. Endogenous agonists such as noradrenaline (NA), acetylcholine (ACh), angiotensin II, endothelin-1 (ET-1), and serotonin (5-hydroxytryptamine, or 5-HT) increase IP₃ production, and subsequently increase IP₃R activity by binding to G_{q/11}-coupled receptors on smooth muscle such as the α₁ adrenergic receptor, the M₃ muscarinic receptor, the angiotensin II receptor (AT), the ET-1 receptor A (ET_A), and the 5-HT_{2A} receptor, respectively^{61,117,139,153,154}.

The binding of IP₃ to its N-terminal binding site causes a conformational change in the subunit, allowing the binding of obligate factors ATP and Ca²⁺ to their respective binding sites to stabilize the open conformation of the channel^{155,156}. The channel stoichiometry is such that four

IP₃ molecules, one to each subunit, are necessary for channel activation¹⁵⁷. The stoichiometry of ATP and Ca²⁺ are currently unclear; however, there is evidence to suggest that only two ATP molecules may be required for pore opening¹⁵⁸. The Ca²⁺-gating of the IP₃R1 channel is biphasic, wherein a high nanomolar Ca²⁺ concentration is optimal for channel activation, but a micromolar concentration is inhibitory¹⁵⁹⁻¹⁶³. It has been suggested that this mechanism may contribute to autoregulation of Ca²⁺ signalling; however, many other extrinsic factors including channel density and spatial arrangement of channels may contribute to this regulation as well¹⁴¹.

RyRs: The second channel responsible for Ca²⁺ release from the SR is the RyR, which is the largest known ion channel, at over 2 MDa¹⁶⁴. RyRs are a family of Ca²⁺ channels localized to the SR membrane which are structurally homologous with IP₃Rs¹⁶⁵, and the two channels share many similarities. Like the IP₃R, the RyR is a homotetramer in which each subunit contains 6 TM domains, a pore domain between TM5 and TM6, and cytosolic N- and C-termini^{166,167}. Another similarity is that the RyR, like the IP₃R, occurs in three known mammalian isoforms (RyR1, RyR2 and RyR3) encoded by three separate genes¹⁶⁸⁻¹⁷². Transcription and translation of all three subtypes have been demonstrated in VSMCs; however, RyR2 is the predominant form expressed by VSMCs in resistance arteries including mesenteric and cerebral arteries¹⁷³⁻¹⁷⁵. RyRs are activated by the binding of Ca²⁺ and ATP, and cryo-EM studies have revealed that the Ca²⁺-coordinating residues of its binding site are conserved between the IP₃Rs and RyRs¹⁷⁶. Additionally, multiple Ca²⁺ binding sites in each subunit allow the RyR to be activated by either cytosolic Ca²⁺ at the canonical *A*-site, or by a sufficiently high [Ca²⁺] within the SR to occupy the lower affinity, lumenal-facing *L*-site^{177,178}. Ca²⁺ binding at an inhibitory site, the *I*-site, stabilizes a closed conformation of the RyR at millimolar [Ca²⁺]_i^{177,179}. Together with the *A*-site's *K_a* of

approximately 1-5 μM , the RyR exhibits a bell-shaped activation curve to increasing $[\text{Ca}^{2+}]_i$, similar to the IP_3R ¹⁷⁷.

In addition to Ca^{2+} and ATP, RyRs are modulated by interactions with a large number of other factors and agents, including inhibition by Mg^{2+} , activation by caffeine and diamide insecticides, and concentration-dependent activation/inhibition by both $\text{Ca}^{2+}/\text{CaM}$ and unbound CaM (apoCaM)^{164,177,180,181}. The RyR is named for its interaction with the plant alkaloid ryanodine, which binds with high affinity and selectivity to the open conformation of the channel. Single-channel recordings have demonstrated that, when applied at nanomolar concentrations, ryanodine stabilizes the open conformation of the channel, in what is suspected to be a positive allosteric mechanism^{182,183}. When applied at micromolar concentrations, ryanodine binds to a low-affinity site in order to stabilize a subconductance state of the channel with an open probability (P_o) of ~ 1 , but approximately half of its maximal conductance; and finally at millimolar concentrations ryanodine binds to the central pore and blocks the channel¹⁸⁴⁻¹⁸⁶.

1.3.2.2 Ca^{2+} signals mediated by release from intracellular stores: As described earlier, the compartmentalization of Ca^{2+} signalling within VSMCs allows Ca^{2+} release and influx events to fulfill different functions based upon their localization and spatiotemporal pattern. Ca^{2+} signals may be mediated by Ca^{2+} release from the SR as in Ca^{2+} sparks, Ca^{2+} puffs, and Ca^{2+} waves; or they may be mediated by Ca^{2+} influx as in junctional Ca^{2+} transients and Ca^{2+} sparklets^{61,115,187}. This variety of mechanistically distinct Ca^{2+} signals allows for nuanced modulation of the contractile state of VSMCs. This section will discuss Ca^{2+} sparks, Ca^{2+} puffs, and Ca^{2+} waves.

Ca^{2+} sparks: Ca^{2+} sparks (reviewed by Cheng and Lederer, 2008)¹⁸⁸ are discrete, local, and transient Ca^{2+} release events from the SR through clusters of RyRs^{61,71,187}. In contrast to the tight lattice-patterned organization of RyRs in striated muscle cells^{188,189}, immunofluorescence and

electron microscopy studies have demonstrated that in SMCs, RyRs are clustered into calcium release units (CRUs) with variable density and no apparent geometry, and that the distribution of RyRs matches the helical distribution of SR cisternae^{112,190,191}. Therefore, phasic smooth muscle cells with primarily peripheral SR exhibit peripheral distribution of RyRs, whereas tonic smooth muscle cells, such as VSMCs in resistance arteries, exhibit both perinuclear and peripheral distribution of RyRs^{190,191}. RyR2, the primary isoform in VSMCs, is predominantly located in peripheral SR, which has been shown to be as close as 18 nm to the inner side of the plasma membrane^{190,192,193}. Due to the low spatial reach of Ca²⁺ sparks (approximately 10-15 μm²)^{194,195}, they have little direct impact on global [Ca²⁺]_i; however, this localization of RyRs near the plasma membrane allows them to functionally couple with plasmalemmal ion channels such as big-conductance Ca²⁺-activated potassium (BK_{Ca}) channels and Ca²⁺-activated chloride (Cl_{Ca}) channels in order to regulate global [Ca²⁺]_i indirectly (**Figure 1.4**)^{71,112,115}. Activation of BK_{Ca} channels by Ca²⁺ sparks precipitates an efflux of K⁺ ions known as a spontaneous transient outward current (STOC), which contributes to hyperpolarization of the SMC, and thus vasorelaxation in resistance arteries^{195,196}. The coupling of Ca²⁺ sparks to STOCs in VSMCs was first described by Nelson *et al.* in 1995¹⁹⁶, wherein they demonstrated that Ca²⁺ release from the SR through RyRs counterintuitively elicited vasorelaxation of rat cerebral resistance arteries. In contrast, however, VSMCs in other vascular beds (e.g. portal vein^{197,198}, pulmonary artery¹⁹⁹) exhibit spatial coupling between RyRs and Cl_{Ca} channels, whereby Ca²⁺ sparks activate Cl_{Ca} channels and allow efflux of Cl⁻ ions^{115,188,200,201}. Unlike the hyperpolarizing K⁺ efflux that occurs in STOCs, Cl⁻ efflux creates a depolarizing current, called a spontaneous transient inward current (STIC), which indirectly amplifies vasoconstrictor stimuli^{71,201-204}. In VSMCs expressing both BK_{Ca} and Cl_{Ca} channels, spontaneous transient outward then inward currents (STOICs) elicited by Ca²⁺ sparks have been

recorded, the physiological purpose of which is suspected to be a finer modulation of membrane potential and cell excitability²⁰⁵.

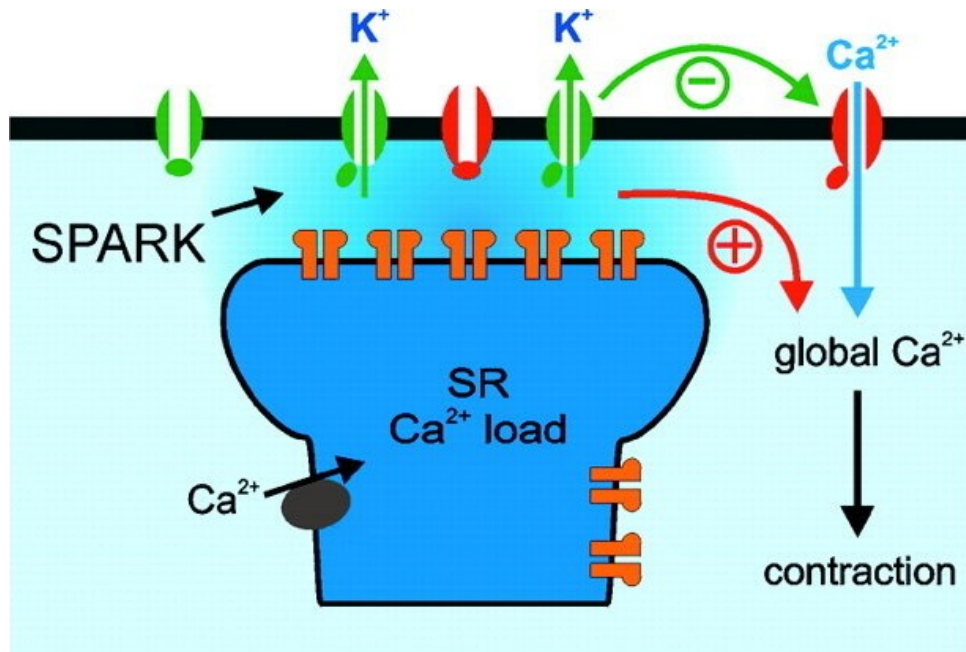


Figure 1.4: Activation of BK_{Ca} channels by Ca²⁺ sparks. Activation of RyRs (orange) in the SR membrane allows local release of Ca²⁺ from the SR in a Ca²⁺ spark. The resultant increase in local [Ca²⁺]_i activates colocalized BK_{Ca} channels (green) to induce a hyperpolarizing outward current of K⁺. Hyperpolarization of the membrane potential decreases the activity of L-type Ca²⁺ channels (red) and inhibits contraction. The activity of SERCA (grey) maintains SR Ca²⁺ levels (adapted from Jaggar *et al.*, 2000)²⁰⁶.

Ca²⁺ puffs: Analogous to Ca²⁺ sparks, Ca²⁺ puffs are discrete, local Ca²⁺ transients from the SR mediated by CRUs of IP₃Rs rather than RyRs^{61,112,207-209}. Ca²⁺ puffs are not as well-characterized as Ca²⁺ sparks, and have not been directly recorded or visualized in VSMCs to date, despite the confirmed expression and localization of all three IP₃R isoforms at the SR in VSMCs^{61,112,115}. G_{q/11}PCR agonist-evoked, ryanodine-insensitive Ca²⁺ puffs have only been directly recorded in two smooth muscle types: ureteric^{210,211} and colonic^{212,213} smooth muscle. Nevertheless, indirect evidence suggests that Ca²⁺ puffs may modulate the contractile state of VSMCs via spatial coupling with plasmalemmal ion channels in a similar manner to Ca²⁺ sparks. In rat cerebral artery smooth muscle, pressure-induced Na⁺ influx through the melastatin transient

receptor potential (TRPM) channel TRPM4, a Ca^{2+} -dependent Na^+ channel, was shown to be insensitive to ryanodine, but reduced by both the SERCA inhibitor cyclopiazonic acid, and the IP_3R blocker xestospongine $\text{C}^{214,215}$. The lack of direct evidence for Ca^{2+} puffs in VSMCs may be due to complicating factors such as IP_3R localization or distribution versus other types of SMCs⁶¹. Moreover, Ca^{2+} released from the SR in a puff may activate neighbouring IP_3Rs in a process termed Ca^{2+} -induced Ca^{2+} release (CICR)^{150,216-218}. Once Ca^{2+} puff activity reaches the threshold at which CICR occurs, a global, propagating increase in $[\text{Ca}^{2+}]_i$ called a Ca^{2+} wave is initiated^{208,219,220}. It is possible that this threshold is lower in VSMCs than phasic SMCs, making isolated Ca^{2+} puffs difficult to record without initiating global Ca^{2+} waves.

Ca²⁺ waves: Ca^{2+} waves are regenerative, cyclical elevations in global $[\text{Ca}^{2+}]_i$ which are initiated by local Ca^{2+} release from the SR via IP_3Rs and/or RyRs , and are subsequently propagated by CICR^{61,221,222}. A Ca^{2+} wave is propagated when Ca^{2+} released from the SR activates successive adjacent CRUs of IP_3Rs and RyRs , creating a wave front which travels the entire length of the cell^{188,223}. In electrophysiological recordings, these waves appear as asynchronous oscillations in global $[\text{Ca}^{2+}]_i$ ^{221,224-226}. Within the current model, the oscillations of Ca^{2+} waves reflect the biphasic activation of IP_3Rs and RyRs at lower $[\text{Ca}^{2+}]$ and inactivation at higher $[\text{Ca}^{2+}]$ ²²². However, counter-evidence indicates that Ca^{2+} occupation of the IP_3R Ca^{2+} -inhibitory site is not necessary for channel inactivation, and that obligatory intrinsic inactivation of the channel may be sufficient for terminating Ca^{2+} release²¹⁷. Ca^{2+} waves are abolished in the presence of SERCA inhibitors, but insensitive to VOCC inhibitors, suggesting that Ca^{2+} waves are maintained by a cycle of Ca^{2+} release from and reuptake into the SR, and are not dependent upon extracellular Ca^{2+} entry^{224,225,227,228}. Moreover, it has been demonstrated that simultaneous Ca^{2+} waves propagating

in opposite directions will “collide”, terminating both waves due to the depletion of Ca^{2+} from the SR on either side of the collision²²³.

In VSMCs, Ca^{2+} waves may arise spontaneously^{150,229}, be evoked by $G_{q/11}$ PCR agonists such as UTP and NA^{221,225,230-232}, or be evoked by electrical field stimulation of perivascular nerves²²⁶. Although they were originally thought to be mediated only by IP_3Rs , Ca^{2+} waves have since been shown to arise from activation of either or both IP_3Rs and RyRs ^{221,222,231}. The relative contribution of IP_3Rs and RyRs varies depending on the tissue and the nature of the stimulus^{61,222}. For example, Heppner *et al.* (2002) demonstrated in VSMCs from rat cerebral arteries that Ca^{2+} waves may be evoked by the application of caffeine (which activates RyRs but not IP_3Rs) and are abolished by ryanodine, but are insensitive to the IP_3R blockers xestospongin C and 2-aminoethoxydiphenyl borate (2-APB)²³³. Meanwhile, both IP_3Rs and RyRs were found to contribute significantly to Ca^{2+} waves in portal vein VSMCs^{216,231}.

Ca^{2+} waves have been shown to elicit contraction in VSMCs and subsequently vasoconstriction in whole arteries^{150,229,231,234}, which is proposed to occur by two mechanisms: 1) the Ca^{2+} wave directly elevates global $[\text{Ca}^{2+}]_i$, thereby increasing MLCK activity and initiating cross-bridge cycling, and 2) the Ca^{2+} wave interacts with plasmalemmal Ca^{2+} -activated ion channels, such as Cl_{Ca} and TRPM4 channels, in order to depolarize the cell and leading to further Ca^{2+} entry through VOCCs in a positive feedback mechanism²³⁵. It has been demonstrated that Ca^{2+} waves may underlie specific vasoconstrictive behaviours including the initiation of pressure-induced myogenic tone^{229,236}, and the initiation of vasomotion in response to tissue hypoperfusion^{227,237-239}.

1.3.2.3 Ca^{2+} influx pathways: In addition to Ca^{2+} release from the SR, extracellular Ca^{2+} entry through plasmalemmal Ca^{2+} -permeable channels is a major source of cytoplasmic Ca^{2+} for

the initiation of smooth muscle contraction^{61,115}. This involves a wide variety of ion channels, such as voltage-operated Ca^{2+} channels (VOCCs or Ca_v channels); transient receptor potential (TRP) channels; and ligand-gated Ca^{2+} -permeable channels including the P2X family of purinergic receptors, and Orai channels^{61,115,117,187}.

VOCCs: The VOCC family of Ca^{2+} channels are arguably the most crucial driver of cellular Ca^{2+} dynamics in most cell types, and they are required for normal excitation-contraction coupling in all myocytes, including VSMCs^{187,240}. Two main subtypes of VOCCs are expressed by VSMCs: L-type (LTCC or Ca_v1) and T-type (TTCC or Ca_v3) Ca^{2+} channels, wherein the “L” and “T” stand for “long-lasting” and “transient”, respectively. Ca^{2+} currents through LTCCs and TTCCs are distinguishable from one another by several physiological and pharmacological features. The Ca^{2+} current through LTCCs is typified by a high voltage of activation, high unitary conductance, slow voltage-dependent inactivation, and a well-characterized blockade by selective antagonists including dihydropyridines (e.g. nifedipine), phenylalkylamines, and benzothiazepines^{240,241}. In contrast, the Ca^{2+} current through TTCCs has a more hyperpolarized voltage of activation, low unitary conductance, rapid inactivation, and was initially found to be insensitive to classical LTCC inhibitors^{240,242,243}.

LTCCs are heteromultimeric channels containing a pore-forming α_1 subunit regulated by accessory subunits β , $\alpha_2\delta$, and γ (**Figure 1.5**). The α_1 subunit contains four repeated domains (I-IV), each with six transmembrane segments (S1-S6), surrounded by cytosolic N- and C-termini^{187,240,244}. This single subunit functions similarly to a homotetrameric ion channel, whereby a membrane-associated P loop linking S5 and S6 in each domain forms the central pore and selectivity filter of the channel^{245,246}. The S4 segment of each domain contains four or five positively-charged arginine and lysine residues which act as a voltage sensor; membrane

depolarization reverses the surrounding electrical field, forcing the S4 segments outward to open the central pore²⁴⁷⁻²⁵⁰. Four subtypes of LTCCs have been identified, each containing distinct α_1 subunits encoded by separate genes sharing approximately 70% sequence homology: these are Cav1.1, 1.2, 1.3, and 1.4, containing α_{1S} , α_{1C} , α_{1D} , and α_{1F} , respectively^{244,251}. Of these subtypes, cardiomyocytes and VSMCs primarily express Cav1.2 channels^{244,252}.

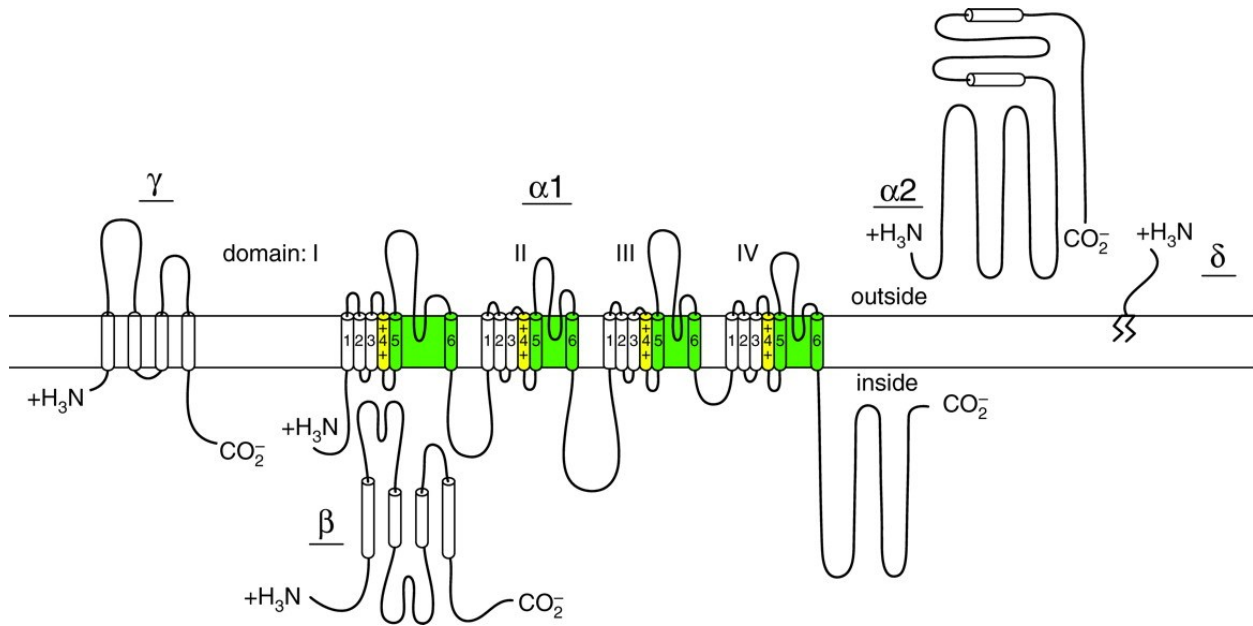


Figure 1.5: Membrane topology of VOCCs. Schematic diagram illustrating the pore-forming α_1 subunit and the accessory subunits β , $\alpha_2\delta$, and γ . The α_1 subunit assembles similarly to a homotetrameric ion channel, except that the ‘monomers’ are four domains of the same subunit. Each domain contains a P loop between TM segments S5 and S6 (green) which form the central pore of the channel. The S4 segment of each domain (yellow) forms the channel’s voltage sensor (from Catterall, 2011)²⁴⁰.

The three auxiliary subunits regulate the channel’s voltage-dependence and gating, as well as facilitate interactions between VOCCs and other proteins^{240,253}. The β subunit has no transmembrane segments and binds α_1 at the cytoplasmic loop between domains I and II²⁵⁴. This subunit is responsible for increasing channel expression by activating nuclear transcription factors, as well as hyperpolarizing the voltage of activation and increasing the P_o of the channel^{253,255}. The $\alpha_2\delta$ subunit is composed of one gene product which is post-translationally proteolysed into two

subunits, α_2 and δ , then joined by a single disulfide bond²⁵⁶. The δ portion is bound to the extracellular side of the plasma membrane via a glycosylphosphatidylinositol membrane anchor^{240,256,257}, while the α_2 portion has emerged as a putative pharmacological target for allosteric blockade of the channel^{258,259}. Finally, the γ subunit is an integral protein with four transmembrane segments which mediates interactions with AMPA channels²⁶⁰. To date, four subtypes of the β subunit, four subtypes of the $\alpha_2\delta$ subunit, and eight subtypes of the γ subunit have been identified, which in combination confer a wide range of gating and regulatory properties to VOCCs²⁵⁶. Furthermore, both the α_1 and auxiliary subunits of VOCCs experience a wide range of alternative splicing that is often tissue-specific^{240,255,256}. Splicing of exons 1, 9, and 33 yields a VSMC-specific isoform of α_{1C} which experiences decreased plasmalemmal insertion, and a voltage-dependence of activation that is shifted by approximately -15 mV versus cardiac α_{1C} ²⁶¹⁻²⁶⁴. Vascular Cav1.2 is activated by membrane depolarization above approximately -40 mV^{265,266}.

The activation of Cav1.2 channels in response to membrane depolarization in VSMCs is necessary for maintaining the tonic constriction of resistance arteries, thereby regulating systemic blood pressure. For example, mice with a tamoxifen-inducible smooth muscle knockout of Cav1.2 exhibited a reduced mean arterial pressure (MAP), and pressure-induced myogenic tone was abolished in isolated resistance arteries²⁶⁷. Meanwhile, hypertension is associated with the upregulation of Cav1.2 channels^{268,269}. Evidence in cell culture and animal models illustrates a positive feedback loop whereby membrane depolarization both acutely activates LTCCs and chronically upregulates their expression, leading to increased capacity for Ca^{2+} influx and contributing to prolonged depolarization²⁷⁰⁻²⁷². Interestingly, the relative expression of LTCCs to TTCCs decreases along the vascular tree, to the point where Cav1.2 mRNA was undetectable in

arterioles less than 40 μm in diameter²⁷³⁻²⁷⁵. This suggests an increased role of TTCCs over LTCCs in regulating Ca^{2+} handling in the microvasculature versus in large, elastic vessels^{275,276}.

Three subtypes of TTCCs have been identified: $\text{Cav}3.1$, 3.2 , and 3.3 , composed of the pore-forming subunits α_{1G} , α_{1H} , and α_{1I} , respectively^{244,256}. TTCCs are characterized by a more hyperpolarized voltage of activation and faster rate of voltage-dependent inactivation relative to other Ca^{2+} channels, and are thus well-suited to the generation of rhythmic action potentials^{240,244}. Unlike LTCCs, TTCCs function as monomers and do not require the association of auxiliary β , $\alpha_2\delta$, or γ subunits^{277,278}; however, these auxiliary subunits likely modulate TTCCs by other mechanisms. β and $\alpha_2\delta$ subunits have been shown to upregulate functional $\text{Cav}3$ expression at the plasma membrane, but it is unclear whether any direct mechanisms of modulation take place²⁷⁹⁻²⁸¹. To date there is contradictory evidence for and against the modulation of the electrophysiological and gating properties of $\text{Cav}3$ by β , $\alpha_2\delta$, and γ subunits^{278,281-285}.

VSMCs in rodents have been shown to express $\text{Cav}3.1$ and 3.2 , whereas human VSMCs favor expression of $\text{Cav}3.2$ and 3.3 and only minimally express $\text{Cav}3.1$ ^{286,287}. The physiological roles of these channels appear to vary, with $\text{Cav}3.1$ contributing to myogenic constriction^{287,288}, and $\text{Cav}3.2$ apparently opposing myogenic constriction due to localization near RyRs and interaction with BK_{Ca} channels^{289,290}. It is likely that TTCCs are a major contributor to Ca^{2+} influx in VSMCs, but distinguishing between LTCC and TTCC currents has been notoriously difficult due to the low selectivity of pharmacological VOCC blockers such as mibefradil²⁸⁶. Dihydropyridines, which inhibit LTCCs at nanomolar concentrations, were subsequently found to additionally inhibit TTCCs at micromolar concentrations²⁹¹⁻²⁹³. Novel compounds derived from 3,3'-diindolylmethane are currently under investigation as putative selective TTCC blockers²⁹⁴.

TRP channels: TRP channels are a superfamily of cation channels with 28 mammalian isoforms from separate genes divided into six subfamilies: canonical (TRPC1-7), vanilloid (TRPV1-6), melastatin (TRPM1-8), ankyrin (TRPA1), mucolipin (TRPML1-3), and polycystic (TRPP1-3)^{295,296}. Each of these genes encodes a TRP subunit containing six TM helices (S1-S6) bounded by cytoplasmic N- and C-termini (**Figure 1.6**)²⁹⁵. Of the 28 isoforms, 27 are expressed in humans: TRPC2 is expressed in rodents but is only present as a pseudogene in humans²⁹⁷. Similarly to voltage-operated ion channels, TRP subunits form functional channels as homo- or heterotetramers, with a pore loop between S5 and S6 which creates the central pore and selectivity filter^{298,299}. All TRP channels are Ca²⁺-permeable except for TRPM4 and TRPM5, which are activated by Ca²⁺, but are only permeable to monovalent cations²⁹⁵. Despite their structural similarity to voltage-operated channels, TRP channels do not contain a classical voltage-sensing domain in S4. Instead, they are sensitive to a wide range of other stimuli including temperature, pressure, mechanical stretch, shear stress, oxidative stress, and changes to the surrounding phospholipid environment, as well as modulation by endogenous and exogenous ligands and phosphorylation by protein kinases (reviewed by Yue *et al.*, 2015)³⁰⁰. Due to a lack of conserved basic residues in S4, it was initially believed that TRP channels were voltage-insensitive; however, it has since been demonstrated that several isoforms (including TRPV1, TRPV3, TRPM4, TRPM5, and TRPM8) are weakly voltage-dependent³⁰¹⁻³⁰⁶. Although TRP channels were first discovered decades ago³⁰⁷, crystal structures of assembled tetrameric TRP channels remained unsolved until only recently^{299,308-310}, and the voltage-sensing residues have not yet been elucidated. However, in TRPV and TRPM channels, a conserved sequence of six basic amino acids in the C-terminal region called the “TRP box” may be necessary for voltage-dependent gating, as well as subunit assembly^{295,311-313}.

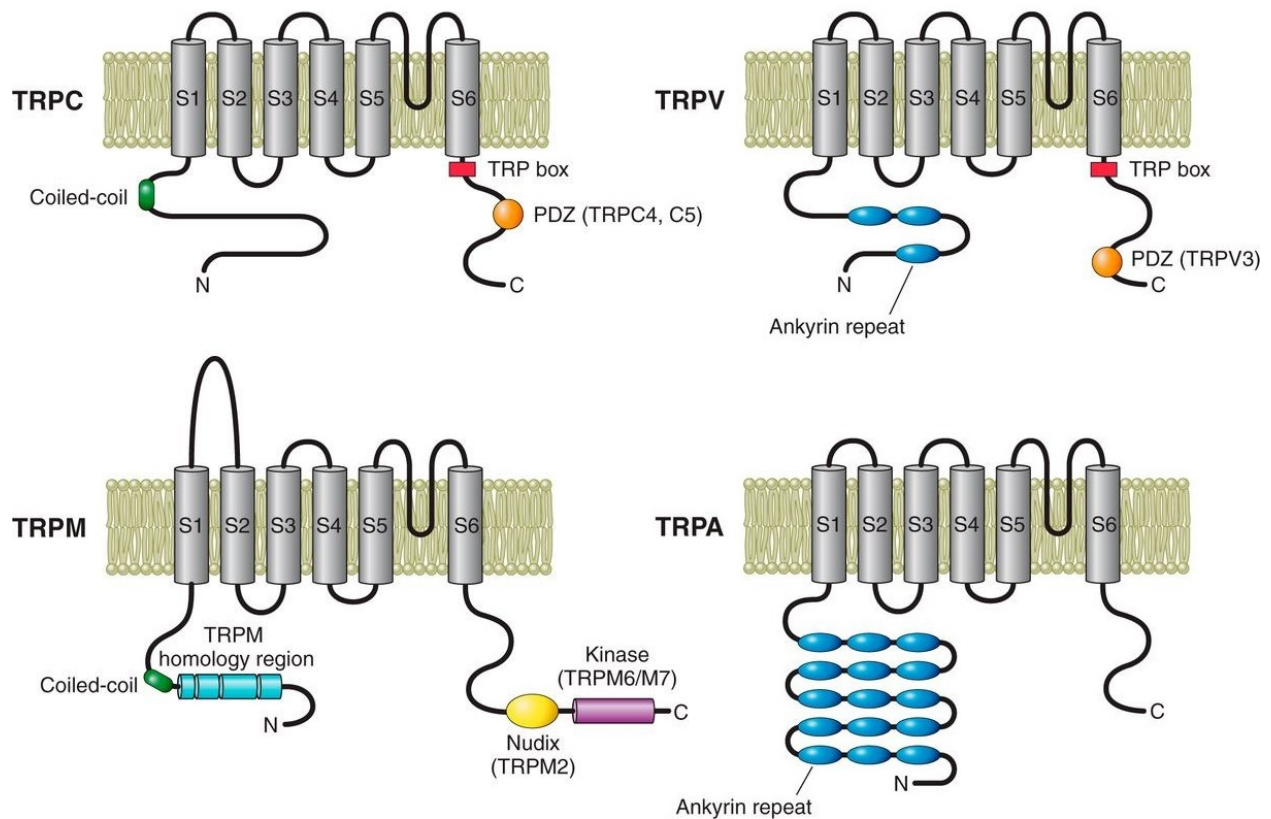


Figure 1.6: Membrane topology of TRP channels. Schematic diagrams of the generalized structures of four TRP subfamilies: TRPC, TRPV, TRPM, and TRPA channels. All TRP channels contain six TM domains with a P loop between S5 and S6. Subfamilies are distinguishable by features of their N- and C-terminal domains which determine the functional properties of the channel (from Earley and Brayden, 2015)²⁹⁵.

VSMCs express a wide range of TRP channels, including members of the TRPC, TRPV, TRPM, TRPA and TRPP subfamilies^{300,314}. This section will highlight the TRP isoforms which, to date, have been found to be the most influential in modulating the contractile state of VSMCs. Firstly, from the TRPC subfamily, VSMCs have been shown to express all isoforms except TRPC2^{300,315,316}. TRPC channels are non-selective cation channels with a slight preference for Ca^{2+} permeability, with selectivity ratio $P_{\text{Ca}^{2+}}/P_{\text{Na}^{+}}$ ranging from approximately 1 to 5 depending on the isoform³¹⁶. TRPC isoforms share complex relationships of heteromultimerization; for example, TRPC1 forms heterotetramers with TRPC4 and TRPC5^{317,318}, but also with isoforms outside of its

subfamily, such as TRPV4³¹⁹. This feature has made it difficult to isolate the functions of individual TRPC isoforms. The main role of TRPC channels is facilitating receptor-operated Ca²⁺ entry (ROCE), whereby the activation of G_{q/11}PCRs results in the cleavage of PIP₂ by PLC into IP₃ and DAG; the latter of which directly binds TRPC3/C6/C7 at S6 to cause channel opening and cation influx³²⁰⁻³²³. TRPC1/C4/C5 channel activation also depends upon G_{q/11}PCR activation, but this is not due to direct activation by DAG and instead appears to be mediated by IP₃R activation^{300,324,325}. Furthermore, the C-terminus of TRPC channels contains a CaM and IP₃R-binding (CIRB) domain³²⁶; the current model suggests that IP₃ induces direct physical coupling of IP₃R1 and TRPC3, leading to cation influx in VSMCs and vasoconstriction that is independent of IP₃R-mediated Ca²⁺ release from the SR³²⁷⁻³²⁹. Additionally, TRPC channels were once thought to mediate store-operated Ca²⁺ entry (SOCE), whereby depletion of Ca²⁺ from the SR elicits extracellular Ca²⁺ influx in order to replenish SR Ca²⁺. This role of TRPC channels remains controversial^{295,314}; there is a body of evidence which contraindicates the involvement of TRPC in SOCE, such as the finding that a TRPC3 KO and a TRPC1/C4/C6 triple-KO had no effect on SOCE in mouse Purkinje neurons³³⁰. Also noteworthy is the activation of TRPC6 by mechanical stimuli, putatively suggesting the involvement of TRPC6 in pressure-induced myogenic vasoconstriction^{331,332}.

TRPV channels are also crucial modulators of the contractile state of VSMCs. Of the six mammalian TRPV isoforms, VSMCs express TRPV1-4^{295,333,334}, but the most well-characterized of these is TRPV4¹⁸⁷. TRPV4 channels have a higher preference for Ca²⁺ conduction ($P_{Ca^{2+}}/P_{Na^{+}}$ of 6-10) and a higher unitary conductance than TRPC channels, and are activated by a variety of stimuli including G_{q/11}PCR signalling, arachidonic acid, and epoxyeicosatrienoic acids (EETs)^{187,295,335}. In VSMCs, activation of TRPV4 facilitates vasodilation and negative feedback

inhibition of vasoconstrictor stimuli^{336,337}. This occurs when activation of the angiotensin II type 1 receptor (AT₁R), a G_qPCR, increases production of DAG, which in turn activates PKC. PKC then phosphorylates TRPV4, increasing its P_o ; Ca²⁺ influx through TRPV4 activates colocalized RyRs, causing a Ca²⁺ spark (see §1.3.2.2) that results in the activation of hyperpolarizing BK_{Ca} channels^{295,336,337}. However, TRPV4 activity likely precipitates different effects in the contexts of different microdomains within VSMCs, as evidenced by a recent study wherein an inducible, SMC-specific TRPV4 KO counterintuitively lowered systemic blood pressure in mice³³⁸.

The expression of most TRPM isoforms has been detected in VSMCs^{333,339}, but TRPM4 and TRPM8 appear to have the greatest influence on vascular function^{314,339,340}. As mentioned earlier, TRPM4 is Ca²⁺-activated and weakly voltage-dependent, but not Ca²⁺-permeable. Instead, TRPM4 activation allows an influx of Na⁺ which depolarizes the cell membrane potential and activates LTCCs, which then elicit whole-cell depolarization and smooth muscle contraction^{314,341}. The [Ca²⁺]_i necessary for TRPM4 activation is extremely high, at approximately 10-100 μM (cf. VSMC resting [Ca²⁺]_i of 100 nM); however, this is solved by Ca²⁺ compartmentalization whereby TRPM4 channels are colocalized with IP₃Rs and activated by discrete Ca²⁺ puffs^{214,215}. This mechanism appears to underlie the development of pressure-induced myogenic tone in a process that is co-dependent upon TRPC6 and PLCγ1 activation³⁴². TRPM8 exhibits higher levels of expression in VSMCs than TRPM4, but its contribution to whole-vessel function *in vivo* is less clearly understood^{333,339}. TRPM8 is mildly selective for Ca²⁺ conductance, activated by cold temperatures and agonists such as menthol and icilin, and notably expressed at both the plasmalemmal and SR membranes^{339,343}. Using wire myography, Johnson *et al.* (2009)³⁴⁴ found that TRPM8 activation elicited vasodilation in precontracted arteries, but elicited vasoconstriction in resting arteries. However, Melanaphy *et al.* (2016)³⁴⁵ later demonstrated that experimental

concentrations of menthol and icilin used to induce TRPM8 currents also act off-target to inhibit LTCCs. They propose that LTCC inhibition may be responsible for the vasodilatory effects that had previously been attributed to TRPM8 activation which were observed in many studies^{343,345-347}. Despite this, studies of TRPM8 function which avoid the use of non-selective agonists are still inconclusive whether TRPM8 activation precipitates vasoconstriction³⁴⁸ or vasodilation³⁴⁹, suggesting that its role is likely context-dependent.

Purinergic receptors: Purinergic (P) receptors constitute another important family of receptors contributing to Ca²⁺ influx in VSMCs. The P2 superfamily of purinergic receptors comprises the ionotropic P2X receptors, which are non-selective cation channels activated by ATP; and the metabotropic P2Y receptors, which are GPCRs activated by several purine and pyrimidine nucleotides (reviewed by Ralevic and Dunn, 2015)³⁵⁰. VSMCs express many P2Y subtypes, including several vasoconstrictive subtypes such as P2Y₁, P2Y₂, P2Y₄ and P2Y₆ that are G_{q/11}-coupled^{351,352}. These receptors can indirectly promote Ca²⁺ influx and subsequent vasoconstriction by increasing production of DAG and IP₃ by PLC, thereby contributing to both TRP channel activation and Ca²⁺ release from the SR³⁵³.

In contrast, the P2X family mediate ATP-induced Ca²⁺ influx directly³⁵⁴. There are seven isoforms of P2X subunits (P2X₁-P2X₇) produced by separate genes; each contains two TM domains linked by an extracellular loop^{350,355}. P2X channels assemble as either homo- or heterotrimers, containing a central pore formed by TM2 of each subunit, and three ATP binding sites in the extracellular domain of the channel^{355,356}. Resistance artery VSMCs predominantly express P2X₁ homomers and P2X₁/P2X₄ heteromers, with additional evidence for lesser expression of P2X₅ and P2X₇ subunits depending on the vascular bed³⁵⁷⁻³⁶². Heteromerization yields P2X receptors with different kinetic and functional properties, allowing them to fulfill a

wider range of tissue-specific roles³⁵⁴. For example, P2X₁ homomers are fast activating and desensitizing, whereas P2X₄ homomers are slow activating and desensitizing; accordingly, P2X₁/P2X₄ heteromers exhibit the slow kinetics of the P2X₄ channel with the pharmacological profile of the P2X₁ channel^{363,364}. In VSMCs, activation of P2X channels by ATP raises [Ca²⁺]_i by two routes of Ca²⁺ influx: direct influx via P2X, and activation of LTCCs in response to the P2X-induced membrane depolarization³⁶⁵. Ca²⁺ entry through these channels elicits CICR from the SR through IP₃Rs to elicit vasoconstriction³⁶⁶. Sukhanova *et al.* (2013) found that in guinea pig mesenteric artery VSMCs, the ATP-induced increase in [Ca²⁺]_i was approximately 11% due to direct Ca²⁺ entry through P2X, 8% due to direct Ca²⁺ entry through LTCCs, 25% due to P2X-induced CICR, and 56% due to LTCC-induced CICR³⁶⁵. Perivascular sympathetic nerves which innervate resistance arteries co-store and co-release NA and ATP^{367,368}, and P2X channels have been found to be localized in clusters at sympathetic varicosities³⁶⁹, underscoring a prominent role for P2X in VSMCs as a mediator of nerve-evoked vasoconstriction and autoregulation of blood flow^{370,371}. In resistance arteries, the effects of ATP at P2X channels and NA at α -adrenoceptors have been found to be synergistic rather than simply additive^{372,373}.

Orai channels: The most recently discovered family of ion channels responsible for mediating Ca²⁺ influx in VSMCs are the Orai channels (which is not an acronym, but rather a name derived from the *Horae* of Greek mythology). Their discovery was preceded by the characterization of an inward Ca²⁺ current elicited by depletion of intracellular Ca²⁺ stores, termed the Ca²⁺-release-activated Ca²⁺ (CRAC) current (I_{CRAC})³⁷⁴. The pore-forming protein responsible for mediating I_{CRAC} was discovered over a decade later in 2006 as the plasmalemmal channel subunit Orai1³⁷⁵⁻³⁷⁷. The Orai subunit is a 4-TM protein with cytoplasmic N- and C-termini³⁷⁸⁻³⁸⁰. Three isoforms of the Orai subunit (Orai1-3) are encoded by three separate genes and form

hexameric, highly selective CRAC channels with heteromerization that does not appear to be preferential for any particular combination or order of subunits³⁸⁰⁻³⁸³. Expression of both mRNA and protein of all three Orai subtypes has been detected in VSMCs^{384,385}, although Orai1 is much more well-studied than Orai2 or Orai3. CRAC channels, along with stromal interaction molecules (STIM) 1 and 2, are the most prominent mediators of SOCE³⁸⁶⁻³⁸⁸. STIM is a single TM protein ubiquitously expressed in many cell types that is inserted in the ER or SR membrane³⁸⁹⁻³⁹¹. The ER-luminal N-terminus contains two EF-hand domains and a sterile α -motif (SAM) domain which together compose the Ca^{2+} sensor of STIM^{392,393}. Upon depletion of Ca^{2+} from the ER, apoSTIM undergoes oligomerization, forming a cluster of STIM proteins which translocates to nearby plasmalemma-ER junctions to facilitate its direct interaction with Orai³⁹⁴⁻³⁹⁶. STIM allosterically stabilizes the open conformation of CRAC channels by a mechanism that is yet to be fully elucidated; interaction at a STIM binding site on the C-terminus of Orai is known to be necessary, but an additional binding site on the N-terminus may be involved as well (reviewed by Yeung *et al.*, 2020)³⁷⁸.

Under physiological conditions, STIM1 appears to be a more prominent mediator of SOCE events than STIM2, whereas STIM2 is suspected to have a larger role in maintenance of basal Ca^{2+} levels due to its higher sensitivity to changes in $[\text{Ca}^{2+}]_{\text{ER}}$ ^{388,397,398}. Interestingly, STIM2 has been shown to be upregulated in VSMCs under pathophysiological conditions such as pulmonary arterial hypertension^{385,399}. This is consistent with evidence demonstrating that SOCE is absent in quiescent VSMCs but active in VSMCs undergoing proliferation and migration such as occurs in vascular remodeling^{386,400}. Thus, the physiological relevance of SOCE to VSMC contractility is controversial, and the prevailing view suggests that SOCE has a greater role in VSMC proliferation and vascular remodeling than in regulating VSMC contractility^{327,386,399-404}. Nevertheless, recent

evidence in SMC-specific STIM1 KO mice demonstrates that the absence of STIM1 significantly impairs both myogenic tone and PE-induced vasoconstriction in isolated segments of aorta as well as cerebral and mesenteric arteries without altering VOCC function^{388,405}.

In addition to CRAC channels, Orai subunits can form arachidonic acid-regulated Ca^{2+} (ARC) channels which are store-independent⁴⁰⁶. Unlike hexameric CRAC channels, ARC channels are a pentameric formation containing three Orai1 subunits and two Orai3 subunits^{407,408}. Little is known about the extent to which these channels contribute to VSMC contractility; however, evidence indicates that they are present in rat aortic VSMCs and mediate a leukotriene Ca_4 -induced Ca^{2+} current that is Orai1/3- and STIM1-dependent^{409,410}.

1.3.2.4 Ca^{2+} signals mediated by influx from the extracellular space: As described previously, two main varieties of Ca^{2+} signals are mediated by Ca^{2+} influx pathways rather than Ca^{2+} release from the SR: these are junctional Ca^{2+} transients and Ca^{2+} sparklets.

Junctional Ca^{2+} transients: Sympathetic perivascular nerves are responsible for the simultaneous release of three vasoconstrictive co-transmitters at sympathetic varicosities: NA, ATP, and neuropeptide Y (NPY)⁴¹¹⁻⁴¹³. Postjunctionally, NA acts at metabotropic α_1 -adrenoceptors to increase production of IP_3 and produce Ca^{2+} waves (See §1.3.2.2)^{234,414}, and NPY acts at metabotropic Y_1 and Y_5 receptors to modulate the frequency of NA-evoked Ca^{2+} waves^{415,416}. In contrast, ATP acts at ionotropic P2X receptors to elicit short-lived, non-propagating Ca^{2+} influx events called junctional Ca^{2+} transients (JCaTs)^{417,418}. JCaTs are distinguishable from the adrenergic response by pharmacological tools, as they are abolished by the P2X antagonist suramin and insensitive to the α_1 antagonist prazosin⁴¹⁷. Additionally, a P2X₁ KO mouse model has demonstrated that P2X₁ receptors are necessary for the observation of JCaTs in isolated mesenteric arteries evoked by either electrical field stimulation or the P2X agonist α,β -

methylene-ATP⁴¹⁹. JCaTs have a larger spread and longer $t_{1/2}$ than RyR-mediated Ca^{2+} sparks⁴¹⁷, and are capable of initiating vasoconstriction^{418,419}.

Ca²⁺ sparklets: The term “ Ca^{2+} sparklet” refers to local increases in $[\text{Ca}^{2+}]_i$ caused by Ca^{2+} influx through individual or small clusters of plasmalemmal Ca^{2+} -permeable ion channels, the two most prominent being LTCCs and TRPV4 channels^{71,115}. Despite their similar names, Ca^{2+} sparklets are unrelated to RyR-mediated Ca^{2+} sparks.

Whereas whole-cell depolarization of VSMCs leads to extensive opening of LTCCs to cause a global increase in $[\text{Ca}^{2+}]_i$ and precipitate vasoconstriction^{267,420,421}, LTCC sparklets are constitutive, and their frequency and amplitude are modulated by local changes in membrane potential (**Figure 1.7**)^{422,423}. Additionally, LTCC sparklet activity is bimodal, depending upon recruitment of PKC α to LTCCs by a signalling complex formed by a plasmalemmal scaffolding protein named A-kinase anchoring protein 5 (AKAP5)^{422,424,425}. As one of over 50 known AKAP members, AKAP5 is a family comprising three orthologs: bovine AKAP75, rodent AKAP150 and human AKAP79 (reviewed by Guo *et al.*, 2015)⁴²⁶. Without the binding of the AKAP5 complex, LTCC sparklets display a low-activity state characterized by stochastic, single-channel openings with low amplitude and short duration⁴²³⁻⁴²⁵. Conversely, both AKAP5 and PKC α are necessary for a high-activity state of persistent LTCC sparklets, as demonstrated by Navedo *et al.* (2008) in VSMCs from AKAP150 KO mice⁴²⁴. The AKAP5 complex also binds PKA and protein phosphatase-2B, also called calcineurin (CaN)^{71,427}. PKA canonically phosphorylates two residues, Ser1700 and Ser1928, in the C-terminus of the $\text{Ca}_v1.2$ α_{1C} subunit in order to modulate channel activity⁴²⁷⁻⁴³⁰. The mechanism by which PKC α increases LTCC sparklets has not been directly shown; however, biochemical evidence shows that PKC is capable of phosphorylating Ser1928⁴³¹, and *ex vivo* evidence shows a correlation between enhanced PKC activity and high

levels of α_{1C} phosphorylation in aortic VSMCs from a mouse model of coronary spastic angina⁴³². In the latter study, administration of the LTCC-blocker diltiazem decreased both PKC activity and α_{1C} phosphorylation without affecting PKA activity. Furthermore, AKAP5-bound CaN opposes the effects of PKC and PKA on Cav1.2 by dephosphorylating α_{1C} at Ser1928, but not Ser1700^{430,433}. Taken together, these data suggest that PKC α may increase LTCC sparklets by phosphorylation at Ser1928, although it is unclear whether or not the mechanism is direct.

TRPV4 sparklets are also regulated by the AKAP5 signalling complex (**Figure 1.7**)^{336,434}. The phosphorylation of TRPV4 by both PKC and PKA at several specific residues elicits an increase in channel activity and flux⁴³⁵. In contrast to vasoconstrictive LTCC sparklets, TRPV4 sparklets mediate vasodilation due to the colocalization of TRPV4 channels near RyRs and BK_{Ca} channels as discussed earlier (§1.3.2.3).

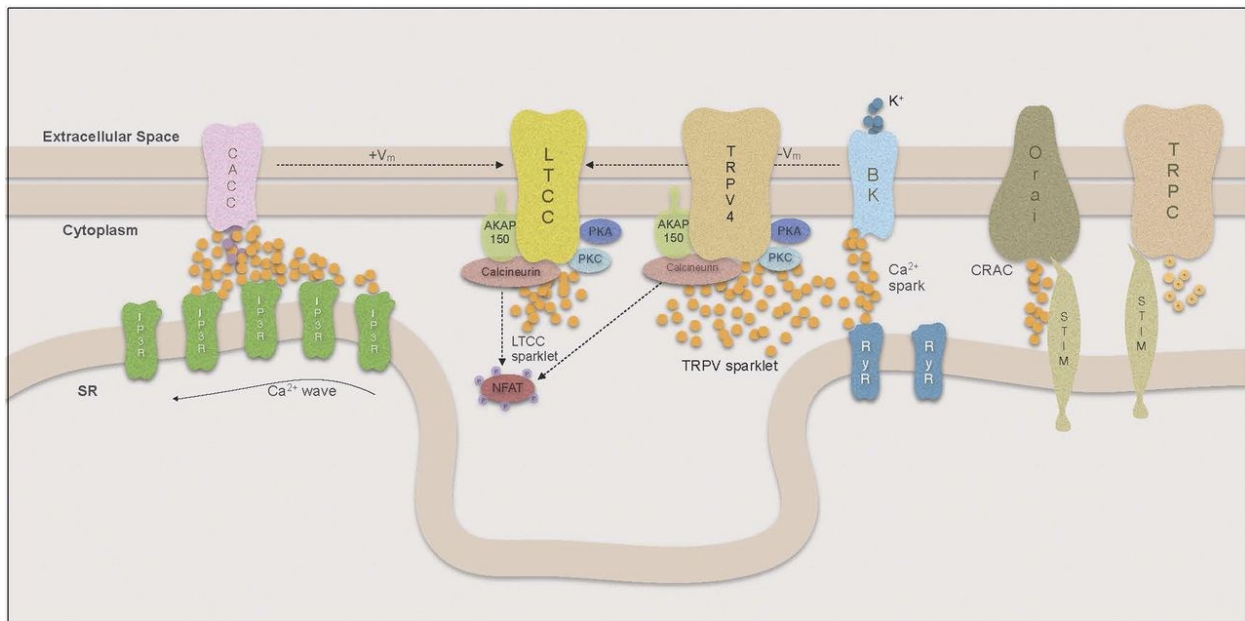


Figure 1.7: Compartmentalization of Ca²⁺ signalling in vascular smooth muscle. Schematic diagram illustrating the relationships of Ca²⁺ release and influx events in VSMCs. LTCC and TRPV4 sparklets are regulated by the AKAP5 signalling complex. Due to colocalization, TRPV4 sparklets can result in RyR-mediated Ca²⁺ sparks, subsequently activating BK_{Ca} and hyperpolarizing the cell membrane potential (from Brozovich *et al.*, 2016)⁷¹.

1.3.3 Ca²⁺ sensitization of the contractile apparatus in vascular smooth muscle cells

Over three decades ago, the observation was made in SMCs that GPCR agonists produce a greater ratio of contractile force to Ca²⁺ influx than that produced by depolarization induced by high extracellular [K⁺]⁴³⁶⁻⁴³⁸. This discrepancy is due to Ca²⁺ sensitization, a process wherein contractile agonists at metabotropic receptors precipitate downstream effects which increase contractile force without further increasing [Ca²⁺]_i^{37,98}.

The main mechanism underlying Ca²⁺ sensitization is the inhibition of MLCP⁴³⁹⁻⁴⁴¹, which leads to increased phosphorylation of myosin RLC and prolongation of cross-bridge cycling (see §1.3.1). Two main pathways contribute to MLCP inhibition: the DAG-PLC-PKC pathway and the RhoA pathway (**Figure 1.8**)³⁷. Firstly, agonism at G_{q/11}PCRs such as α₁-adrenoceptors activates PLCβ, causing an increase in production of DAG, which subsequently activates classical PKC isoforms α and β, as well as Ca²⁺-independent novel PKC isoforms δ and ε^{102,442}. As described earlier (§1.3.1), PKC activates CPI-17 by phosphorylating it at Thr38; CPI-17 then binds MLCP as a false substrate, inhibiting its ability to dephosphorylate myosin RLC^{103,104}.

The RhoA pathway is activated by agonism at G_{12/13}PCRs; the Gα_{12/13} subunit couples to a range of receptors including the α₁-adrenoceptor, AT₁, P2Y, 5-HT_{2C}, ET_A, and sphingosine-1-phosphate receptors, among others⁴⁴³⁻⁴⁴⁶. Rho (from *Ras homolog*) proteins are a subfamily within the Ras (from *rat sarcoma virus*) superfamily of ubiquitously expressed small GTPases⁴⁴⁷. The α-subunits of G_{12/13}PCRs directly activate Rho guanine nucleotide-exchange factors (RhoGEFs)⁴⁴⁸⁻⁴⁵¹, which in turn catalyze the conversion of inactive, GDP-bound RhoA into active, GTP-bound RhoA⁴⁵². RhoA-GTP then binds to Rho kinase (ROCK1 and 2), which activates ROCK by dissociating its autoinhibitory C-terminal domain from its catalytic N-terminal domain⁴⁵³. Finally, ROCK phosphorylates the myosin phosphatase target subunit (MYPT1) of MLCP at Thr696 and

Thr853^{103,454}. In particular, the phosphorylated Thr696 site on MYPT1 autoinhibits the catalytic subunit of MLCP to impair its phosphatase activity⁴⁵⁵, thereby prolonging phosphorylation of myosin RLC. In addition to phosphorylating MYPT1, ROCK feeds into the DAG-PLC-PKC pathway by phosphorylating CPI-17 in the same manner as PKC, albeit to a lesser extent than PKC^{440,456-458}. The relative contributions of the DAG-PLC-PKC pathway and the RhoA pathway to VSMC Ca²⁺ sensitization vary along the vasculature: α_{1A} -adrenoceptors and the DAG-PLC-PKC pathway predominate in resistance arteries, whereas α_{1D} -adrenoceptors and the RhoA pathway predominate in large, elastic arteries^{459,460}.

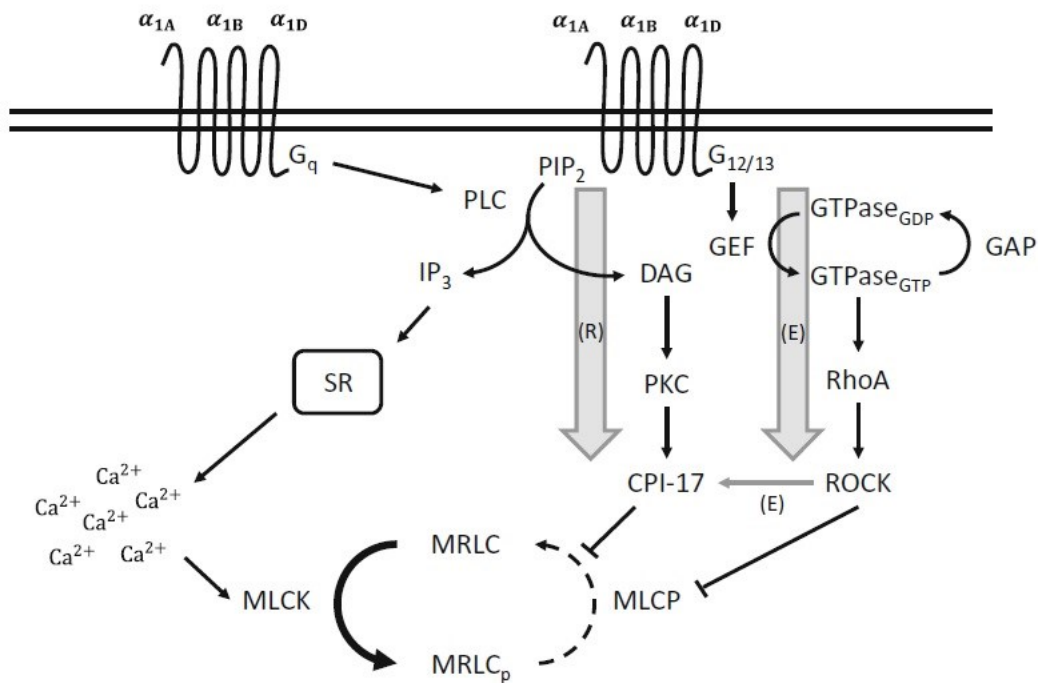


Figure 1.8: Ca²⁺ sensitization pathways. Schematic diagram illustrating the DAG-PLC-PKC and RhoA pathways of Ca²⁺ sensitization in VSMCs. The DAG-PLC-PKC pathway is more active in resistance arteries (R), and the RhoA pathway is more active in elastic arteries (E). Both of these GPCR-mediated pathways lead to inhibition of MLCP activity, prolonging phosphorylation of the myosin RLC without further increase in [Ca²⁺]_i (from Murtada and Humphrey, 2018)⁴⁶⁰.

Although more controversial than the well-established model of GPCR-mediated Ca^{2+} sensitization, there are also believed to be mechanisms of depolarization-mediated Ca^{2+} sensitization which were initially overlooked⁴⁶¹. CaMKII is activated by KCl-induced Ca^{2+} influx, and retains its activity after the removal of Ca^{2+} /CaM¹⁰⁵. Additionally, CaMKII interacts with the canonical Ca^{2+} -sensitization pathways; Sakurada *et al.* (2003) found in rabbit VSMCs that pharmacological inhibition of CaMKII reduced Rho activation and impaired KCl-induced contraction, but not ionomycin-induced contraction⁴⁶². CaMKII is also proposed to activate extracellular-regulated kinases (ERKs)¹⁰⁸ which in turn activate MLCK and increase myosin RLC phosphorylation⁴⁶³.

Ca^{2+} sensitization is necessary for the development of myogenic tone in isolated arteries *ex vivo*⁴⁶⁴⁻⁴⁶⁶, and correspondingly is a crucial component in the maintenance of vascular tone under physiological conditions^{467,468}. In excess, however, Ca^{2+} sensitization contributes to the pathophysiology of hypertension^{103,465}. Many animal models of hypertension have demonstrated an associated increase in VSMC Ca^{2+} sensitization due to increased activity and/or expression of PKC, CPI-17, RhoA and ROCK. These models include spontaneously hypertensive rats (SHRs)^{467,469,470}, salt hypertension⁴⁷⁰, chronic artery occlusion^{471,472}, hypercaloric challenge-induced prediabetes⁴⁷³, and many others (reviewed by Yang and Hori, 2021)⁴³⁹.

1.3.4 Myogenic reactivity

First described in 1902 by Bayliss⁴⁷⁴, myogenic reactivity, or the myogenic response, is a property of small resistance arteries whereby they constrict in response to increases in transmural pressure and dilate in response to decreases in transmural pressure⁴⁷⁵. The most prominent purposes of this mechanism are firstly to establish basal vascular tone, and secondly to maintain a constant blood flow despite changes in blood pressure⁴⁷⁶. In response to increases in blood

pressure, resistance arteries are able to increase resistance to prevent a spike in blood flow which could damage downstream arterioles and capillaries⁴⁷⁶. The myogenic response follows a well-characterized biphasic pattern (**Figure 1.9**) and has been recorded in a wide variety of vascular beds^{475,477-482}. Moreover, the role of myogenic reactivity in pathophysiological states is controversial: some studies suggest that vascular dysfunction in disease states such as hypertension and diabetes mellitus may be associated with an increase in myogenic tone⁴⁸³⁻⁴⁸⁷, though this is contradicted by other results wherein myogenic reactivity was unaffected or decreased⁴⁸⁸⁻⁴⁹⁰.

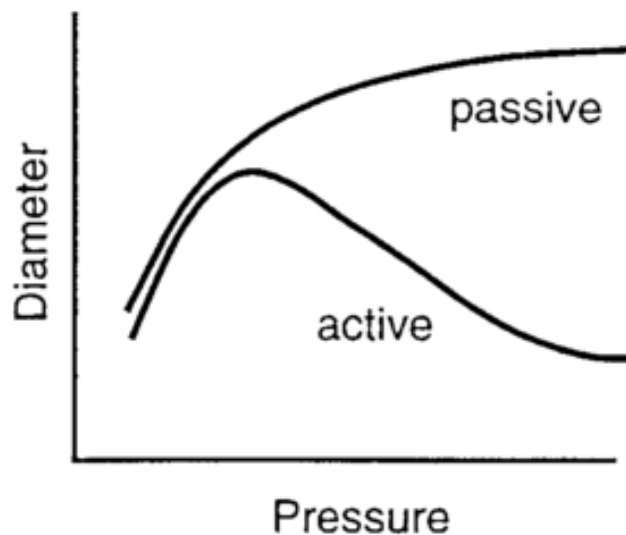


Figure 1.9: Pressure-diameter relationship in the myogenic response in arterioles. Generalized graph illustrating the pressure-diameter relationship observed in arterioles in the presence (active) and absence (passive) of Ca^{2+} in the organ bath media. Myogenically active arteries will passively dilate under low intraluminal pressure, and will gradually constrict as intraluminal pressure increases. In the absence of Ca^{2+} or presence of VOCC inhibitors, arterial diameter increases as pressure increases (from Davis and Hill, 1999)⁴⁷⁵.

The underlying mechanisms responsible for myogenic reactivity are still unclear. Currently, the “wall tension hypothesis” first put forward in 1981 by Burrows and Johnson suggests that pressure-induced increases in smooth muscle tension cause depolarization in VSMCs, leading to Ca^{2+} influx through VOCCs and precipitating vasoconstriction^{475,491}. This is corroborated by findings that the development of myogenic tone is accompanied by VSMC

depolarization, and is impaired by small-molecule VOCC blockers^{479,492-494}. The mechanism by which smooth muscle tension results in a depolarization of membrane potential has not been elucidated, but is hypothesized to be mediated by an unidentified mechanosensor in the VSMC plasmalemma⁴⁷⁶. Several candidates have been proposed, including integrins, GPCRs, and stretch-activated ion channels such as certain TRP channels (reviewed by El-Yazbi and Abd-Elrahman, 2017; and Davis *et al.*, 2023)^{465,495}. Although most recent evidence suggests that TRP channels themselves are not mechanosensitive^{338,496-498}, it is clear that many TRP channels are crucial mediators of mechanically-induced cation entry in VSMCs^{314,499}. In particular, TRPM4 has emerged as a crucial component in the development of myogenic tone. For example, in rat cerebral, mesenteric, and skeletal muscle arteries, application of the TRPM4 inhibitor 9-phenanthrol was shown to eliminate pressure-induced depolarization of VSMCs and abolish the myogenic response^{500,501}. Suppression of TRPM4 expression using an antisense oligodeoxynucleotide has also been demonstrated to inhibit myogenic tone by 70-85% in rat cerebral arteries⁵⁰². Furthermore, single-channel recordings indicate that TRPM4 is activated by stretch in cerebral artery myocytes, albeit likely through an indirect mechanism, as it was found to be dependent upon SR Ca²⁺ release⁵⁰³. TRPM4 activity has also been suggested to couple with mechanosensitive P2Y₄ and P2Y₆ receptors⁵⁰⁴. Lastly, a recent study supports both the role of TRPM4 and the view that myogenic reactivity is increased in vascular dysfunction: Gong *et al.* (2019) found that TRPM4 was upregulated in rat cerebral arteries after induced subarachnoid hemorrhage, increasing myogenic tone and reducing cerebral blood flow⁵⁰⁵.

1.4 Endothelium-dependent modulation of resistance artery diameter

Prior to the 1970s, the vascular endothelium was thought to only function as a physical barrier separating VSMCs from the blood²⁴. However, in 1980, Furchgott and Zawadzki published

a seminal paper demonstrating that removing the endothelium, either mechanically or using collagenase, eliminated ACh-induced vasodilation in isolated segments of rabbit aorta⁵⁰⁶. This finding provided the first example of endothelium-dependent vasodilation and led to the discovery of NO as a crucial vasodilator produced by ECs^{507,508}. Thus opened a new field of research into the functional role of the vascular endothelium in health and disease. Decades later, the endothelium is now understood as an endocrine organ which regulates VSMC contractility both by electrical coupling through MEGJs and by secreting diffusible vasodilators and vasoconstrictors²⁴. Both of these mechanisms are obligately initiated by an increase in the $[Ca^{2+}]_i$ of ECs⁵⁰⁹.

1.4.1 Ca^{2+} signalling in endothelial cells

Just as in VSMCs, ECs depend upon compartmentalized Ca^{2+} signalling for mediating cellular functions; these include the modulation of not only vascular diameter^{509,510}, but also endothelial permeability^{511,512}, inflammation⁵¹³, platelet function⁵¹⁴ and angiogenesis⁵¹⁵. Again similarly to VSMCs, there are two sources from which free Ca^{2+} can enter the cytoplasm of ECs to cause an increase in $[Ca^{2+}]_i$: intracellular stores (i.e. the ER and mitochondria), and the extracellular space. However, unlike VSMCs, endothelial cells do not express voltage-operated Ca^{2+} , Na^+ or K^+ channels, making them nonexcitable cells⁵¹⁶. Thus, endothelial Ca^{2+} signalling is typically initiated by GPCR agonism and TRP channel activation rather than changes in membrane potential^{509,517}. While increases in $[Ca^{2+}]_i$ in VSMCs precipitate depolarization of membrane potential and activation of the contractile apparatus, increases in $[Ca^{2+}]_i$ in ECs are associated with hyperpolarization of membrane potential due to the activation of small- and intermediate-conductance Ca^{2+} activated K^+ channels ($K_{Ca2.1-3}$ or SK_{Ca} , and $K_{Ca3.1}$ or IK_{Ca} , respectively; see §1.4.3), producing a net vasodilatory effect^{516,517}.

1.4.1.1 Release of Ca²⁺ from intracellular stores: The visualization of intracellular Ca²⁺ dynamics proved to be more difficult in vascular ECs than in VSMCs due to the relative inaccessibility of the intimal layer. Thus, the first characterization of Ca²⁺ release events from the ER of ECs was published relatively recently by Ledoux *et al.* in 2008⁵¹⁸. These Ca²⁺ release events were termed Ca²⁺ pulsars, which are similar to, but spatiotemporally distinct from, both Ca²⁺ sparks and Ca²⁺ puffs in VSMCs^{518,519}. Ca²⁺ pulsars are constitutively active, spatially fixed Ca²⁺ release events from the ER through IP₃Rs, which were found to be localized to myoendothelial projections (MEPs)⁵¹⁸. They are unresponsive to RyR modulators ryanodine^{518,519} and caffeine⁵²⁰, but decreased by IP₃R and PLC inhibitors⁵¹⁸. Moreover, pulsar frequency is increased in response to G_{q/11}PCR agonist-evoked increases in IP₃, such as by ACh at M₃ receptors⁵¹⁸ and ATP at P2Y₁ receptors⁵²¹. Pulsars may be propagated by CICR to elicit a global increase in [Ca²⁺]_i as either synchronous or asynchronous Ca²⁺ waves, which are increased in both number and frequency by G_{q/11}PCR agonists^{518,522}. Even without propagation, the localization of Ca²⁺ pulsars to MEPs allows for coupling with IK_{Ca} channels to facilitate the development of endothelium-dependent hyperpolarization and subsequent vasodilation (see §1.4.3)^{518,523}. Due to the lack of evidence for expression of functional RyRs in resistance artery ECs, Ca²⁺ pulsars are thought to be the predominant mechanism of Ca²⁺ release from the ER⁵²³.

While the ER accounts for approximately 75% of the Ca²⁺ storage capacity of ECs, mitochondria are responsible for the remaining 25%⁵²⁴. It is generally accepted that mitochondria in ECs cooperate with the ER and act as a buffer to prevent an overload of cytosolic Ca²⁺, just as they do in VSMCs⁵²⁵. Interestingly, mitochondria have been shown localized to the base of MEPs⁵²⁶, where their uptake of free Ca²⁺ may limit high [Ca²⁺]-induced inhibition of IP₃Rs (based upon evidence in colonic SMCs)^{213,527}. Some studies suggest that mitochondria exhibit a

mechanism of CICR via the permeability transition pore^{524,528}, but there is no evidence that this mitochondrial Ca^{2+} release contributes to EC membrane potential hyperpolarization or vasodilation. Conversely, recent evidence suggests that the main role mitochondria serve in endothelial Ca^{2+} signalling is as producers of ATP rather than as a source of Ca^{2+} release. ATP is an obligate factor in the activation of IP_3Rs , and thus decreases in ATP production result in decreased Ca^{2+} release from the ER⁵²⁹. Furthermore, mitochondria have recently been implicated in shear stress-induced Ca^{2+} influx in ECs. It has been demonstrated that shear stress evokes an increase in ATP production by mitochondria, subsequently activating P2X_4 and P2Y_2 purinergic receptors to allow Ca^{2+} influx^{530,531}. The mechanism by which mitochondria respond to mechanical stress remains unclear, but may involve the shear stress-evoked internalization of plasmalemmal cholesterol⁵³².

1.4.1.2 Ca^{2+} influx pathways: TRP channel-mediated Ca^{2+} sparklets (as described in §1.3.2.4) are the predominant Ca^{2+} influx signal in ECs. The most well-characterized of these is the TRPV4 sparklet (reviewed by Chen and Sonkusare, 2020)⁴⁹⁹. TRPV4 is a cation channel which is activated by IP_3 ⁵³³⁻⁵³⁶, shear stress^{537,538}, and changes in intracellular osmotic pressure⁵³⁹; however, it is thought not to be a direct mechanosensor, but an important mediator in mechanosensitive pathways^{338,496}. TRPV4 sparklets in ECs have been implicated in both NO production and K_{Ca} activation leading to endothelium-dependent vasodilation^{434,536-538,540,541}. Unlike Ca^{2+} pulsars, which occur mainly at MEPs, TRPV4 sparklets are approximately evenly distributed between MEPs (39%), ends of cells (31%), and non-domain-associated locations (30%)⁵⁴⁰. ECs also express AKAP5, which is highly localized to MEPs^{434,536,540}. Thus, MEP-associated TRPV4 channels are associated with the AKAP5 complex, which facilitates the activation of TRPV4 by AKAP5-bound PKC⁴³⁴. Muscarinic receptor stimulation selectively

activates MEP-associated TRPV4 channels in a PKC- and AKAP5-dependent manner. Like Ca^{2+} pulsars, the localization of TRPV4 channels in MEPs allows TRPV4 sparklets to couple with IK_{Ca} channels in order to hyperpolarize the EC and contribute to vasodilation^{434,523,540,542}. Non-MEP-associated TRPV4 channels contribute to endothelium-dependent vasodilation as well, but through the activation of eNOS rather than K_{Ca} channels⁵⁴³. In order to be visualized, endothelial TRPV4 sparklets had to be isolated from Ca^{2+} pulsars by inhibiting SERCA and/or PLC⁵⁴⁰. However, when the ER is not depleted of Ca^{2+} , activation of TRPV4 may produce an increase in global $[\text{Ca}^{2+}]_i$, suggesting cooperation between TRPV4 sparklets and IP_3R pulsars^{540,542}.

Some counter-evidence contradicts TRPV4 sparklets as a significant contributor to endothelium-dependent vasodilation: Pankey *et al.* (2014) found that *in vivo* administration of the TRPV4 antagonist GSK-219387 did not affect ACh-induced vasodilation in rats⁵⁴⁴. Hong *et al.* (2018) showed in mice that a global TRPV4 KO did not alter resting systemic blood pressure vs control⁵³⁶. However, the TRPV4 KO mice did exhibit a significantly greater increase in blood pressure than control mice in response to intraperitoneal phenylephrine, suggesting that TRPV4 sparklets may facilitate negative feedback inhibition of vasoconstriction rather than directly evoking vasodilation.

Several other TRP channels also contribute to Ca^{2+} influx and dynamics in ECs. Pharmacological inhibition and knockout of TRPC3 channels both attenuate endothelium-dependent hyperpolarization and vasodilation⁵⁴⁵⁻⁵⁴⁸. Moreover, evidence indicates that TRPC3 is involved in mediating shear stress-induced vasodilation. For example, *in vivo* administration of a TRPC3 antisense oligonucleotide in rats produced a modest but statistically significant decrease in flow-induced vasodilation⁵⁴⁵. However, there is limited evidence in support of or against TRPC3 itself being a mechanosensor. Overexpression of TRPC3 in the ND-C hybrid neuronal cell line

produced a mechanically-evoked current, but this was not reproducible in other cell lines⁵⁴⁹. Two other TRP channels, TRPV3⁵⁵⁰ and TRPA1⁵⁵¹, may facilitate Ca²⁺ entry events similar to TRPV4 sparklets and have been shown contribute to endothelium-dependent vasodilation in cerebral arteries.

1.4.2 Endothelium-derived NO

As stated earlier, increases in [Ca²⁺]_i in ECs are associated with vasodilation. This is due to the action of Ca²⁺ at several key effectors, which in most cases is mediated by Ca²⁺/CaM rather than free Ca²⁺ ions⁵⁰⁹. One of two main effectors responsible for endothelium-dependent vasodilation is endothelial nitric oxide synthase (eNOS or NOS3), an oxidoreductase which catalyzes the conversion of L-arginine and O₂ into citrulline and NO⁵⁵²⁻⁵⁵⁶. eNOS is one of three mammalian isoforms of nitric oxide synthase (NOS) encoded by three separate genes, along with neuronal NOS (nNOS or NOS1) and inducible NOS (iNOS or NOS2)^{552,553,557}. eNOS and nNOS are constitutively expressed in vascular ECs and neurons respectively, while iNOS expression is an immune function evoked by bacterial lipopolysaccharides and cytokines^{552,557}. The induction of iNOS primarily occurs in macrophages, but has been shown to occur in many other cell types as well⁵⁵⁸.

All three NOS isoforms catalyze the same reaction, requiring L-arginine as the substrate; molecular oxygen and reduced nicotinamide-adenine-dinucleotide phosphate (NADPH) as co-substrates; and flavin adenine dinucleotide (FAD), flavin mononucleotide (FMN), and (6*R*)-5,6,7,8-tetrahydro-L-biopterin (BH₄) as cofactors^{552,553,556,559}. The active form of NOS is a homodimer in which each NOS monomer requires activation by a Ca²⁺/CaM group⁵⁵³. The NOS monomer comprises an N-terminal oxygenase domain which binds Fe³⁺-protoporphyrin IX (heme), BH₄, and L-arginine; and a C-terminal reductase domain which binds FAD, FMN, and

NADPH⁵⁶⁰⁻⁵⁶². The Ca²⁺/CaM binding site is located in the linker region between the two domains. Additionally, the dimer interface in the NOS complex contains a zinc ion, tetrahedrally coordinated by a CXXXXC motif in the oxygenase domain of each NOS monomer⁵⁶³. The role of this zinc center is structural rather than catalytic, stabilizing both the dimerization of NOS and the structural integrity of the BH₄ binding site^{563,564}.

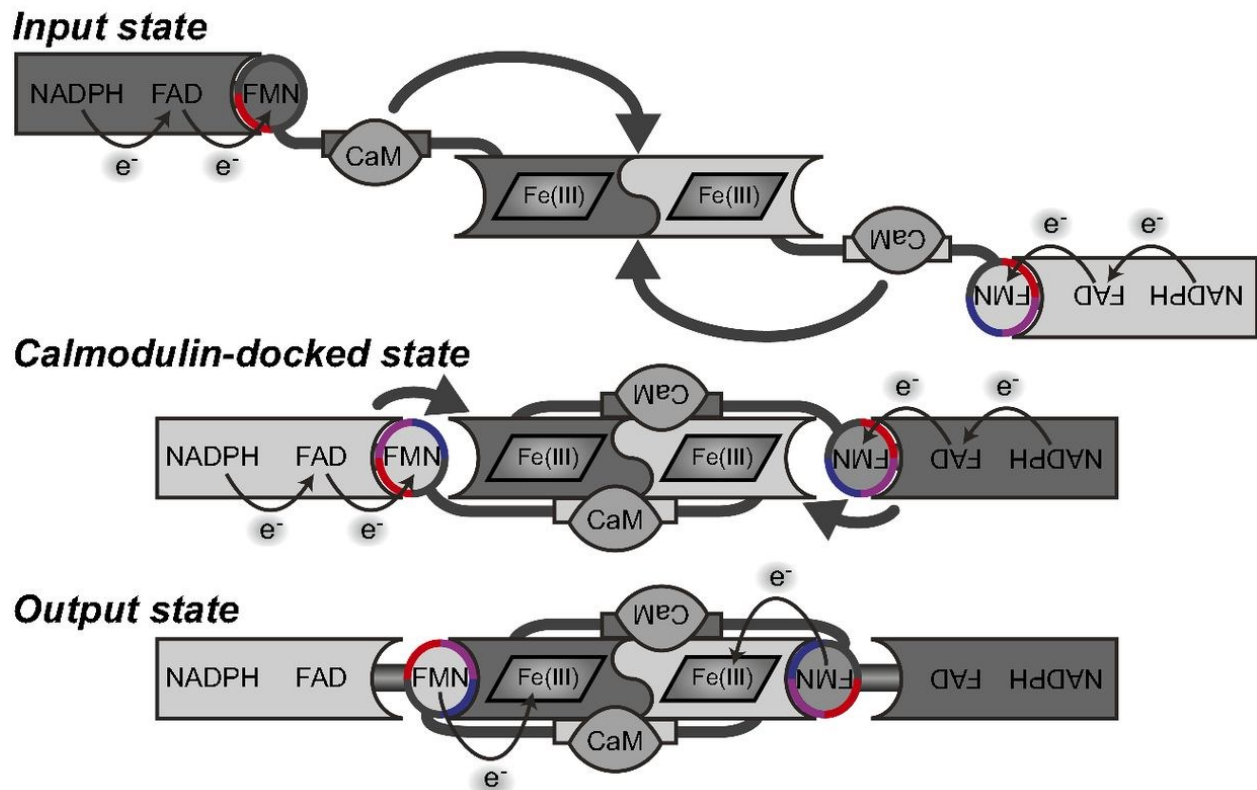


Figure 1.10: Schematic diagram of eNOS electron transfer states. Diagrams of the eNOS electron transfer pathway. Ca²⁺/CaM binds to the linker region in each eNOS monomer (input state). NADPH donates an electron to FAD and FAD then donates the electron to FMN (calmodulin-docked state). FMN reduces the ferric heme of the opposite eNOS monomer (output state). This allows O₂ to bind to heme to initiated NO synthesis (from Smith *et al.*, 2013)⁵⁶⁵.

The biosynthesis of NO by NOS is preceded by a series of electron transfers. An electron is first donated by NADPH to FAD and subsequently transferred to FMN^{552,556}. Next, the electron is transferred from the FMN in the reductase domain to the heme in the oxygenase domain of the opposite monomer (**Figure 1.10**)^{552,565,566}. The binding of Ca²⁺/CaM to NOS inhibits suppression

of the electron transfer between the flavins, and is necessary for the cross-subunit transfer from FMN to heme^{556,565-570}. The reduction of heme facilitates O₂ binding at the heme, allowing NO biosynthesis to begin⁵⁷¹. The oxidation of L-arginine occurs in two steps, with N-hydroxy-L-arginine (NOHA) as an intermediate before citrulline and NO are produced^{556,572}. The role of BH₄ was originally thought to be only structural, but it was later discovered that BH₄ donates a second electron to the heme-dioxy species to prevent it from splitting into superoxide anion (O₂⁻) and ferric heme in a process called uncoupling⁵⁷³.

Several proteins aside from CaM are also involved in modulating NOS function, including caveolin-1 (Cav-1)⁵⁷⁴. Caveolin is an integral membrane protein localized to caveolae, which are very small (50-100 nm diameter) invaginations in the plasmalemma of most cell types^{575,576}. Of three mammalian subtypes (Cav-1, -2, and -3), ECs express Cav-1⁵⁷⁷. In ECs, most eNOS is targeted to caveolae due to co- and post-translational fatty acid acylation of residues in the oxygenase domain^{574,578,579}. This proximity allows Cav-1 to bind to eNOS at a site in its heme-containing hydrophobic pocket, thereby inhibiting eNOS activity and NO release⁵⁸⁰⁻⁵⁸³. By this mechanism, most eNOS in resting ECs is inactive; however, in response to an increase in [Ca²⁺]_i, Ca²⁺/CaM binding to eNOS displaces Cav-1 and activates eNOS⁵⁸⁴. This process is aided by the binding of a chaperone protein, heat shock protein 90 (HSP90), at a site proximal to the Cav-1 binding site to allosterically enhance Ca²⁺/CaM association^{584,585}.

In addition to these regulatory mechanisms, eNOS may also be phosphorylated by a number of kinases in response to shear stress^{552,586}. Phosphorylation of Ser1177 by PKA, Akt (PKB), CaMKII, and AMP-activated protein kinase (AMPK) enhances eNOS activity, whereas phosphorylation of Thr495 by PKC reduces eNOS activity^{552,587}. Several other phosphorylation

sites contribute to eNOS regulation, including Tyr81, Ser114, Ser615, Ser633, and Tyr657 (reviewed by Fleming, 2010)⁵⁸⁸.

NO is a messenger molecule that is crucial to numerous biological processes throughout the body, including the regulation of vascular tone, neurotransmission, gene transcription and translation, gastrointestinal physiology, genitourinary function, and immune function (reviewed by Moncada and Higgs, 1993; and Kapil *et al.*, 2020)^{589,590}. NO exists in three redox states: nitrosonium cation (NO^+), uncharged free radical (NO^\bullet), and nitroxyl anion (NO^- or HNO)⁵⁹¹. It is assumed that the biological effects of NO are primarily mediated by the radical NO^\bullet ^{13,591}; however, NO^- has emerged as a significant contributor to smooth muscle relaxation as well^{592,593}. The neutral charge of NO^\bullet means that it has a low dipole moment, allowing it to cross plasma membranes by simple diffusion⁵⁹⁴⁻⁵⁹⁷. In the vascular context, this means that once NO is synthesized by eNOS, it can diffuse in a paracrine manner from ECs into VSMCs where it acts as a potent vasodilator¹³. The primary mechanism by which NO precipitates smooth muscle relaxation is its activation of the hemoprotein soluble guanylyl cyclase (sGC)^{598,599}. sGC is responsible for converting guanosine-5'-triphosphate (GTP) into cyclic guanosine-3',5'-monophosphate (cGMP)⁵⁹⁸. NO binds to the heme moiety of sGC to induce an allosteric conformational change in its catalytic domain that increases the activity of sGC over 100-fold vs its basal activity⁵⁹⁹⁻⁶⁰². The increase in cGMP production leads to the activation of cGMP-dependent protein kinase (protein kinase G, or PKG), which phosphorylates a number of downstream targets to precipitate vasodilation^{13,599}. For example, PKG phosphorylation increases the P_o of BK_{Ca} channels, leading to VSMC hyperpolarization and reduced Ca^{2+} entry through VOCCs⁶⁰³⁻⁶⁰⁵. PKG also phosphorylates PLC in order to reduce production of IP_3 ⁶⁰⁶; it phosphorylates RhoA to decrease phosphorylation of MLC⁶⁰⁷; it phosphorylates the IP_3R -associated cGMP-kinase substrate (IRAG) to inhibit Ca^{2+}

release from the SR through IP₃Rs⁶⁰⁸; and it phosphorylates MYPT1 of MLCP at Ser962, Ser695 and Ser852 to promote Ca²⁺ desensitization⁶⁰⁹. The phosphorylation of all of these targets, and still many others, by PKG produces a multi-faceted vasodilatory effect (reviewed by Schlossmann and Desch, 2011)⁶⁰⁸.

NO[•], though unstable, is less reactive than many other free radicals such as HO[•]^{594,610}; this property means that it is able to diffuse to remote targets with less chance of being inactivated. However, the greatest limiting factor on the bioavailability of NO is its reaction with other free radicals, particularly reactive oxygen species (ROS) such as O₂⁻^{552,590}. NO and O₂⁻ undergo an irreversible diffusion-limited reaction to form peroxynitrite (ONOO⁻) at a rate approximately six times faster than O₂⁻ is rescued by superoxide dismutase (SOD)⁶¹¹⁻⁶¹⁵. Pathophysiological states such as elevated glucose in diabetes increase O₂⁻ production by mitochondria, leading in turn to increased ONOO⁻ formation¹³. ONOO⁻ is a highly reactive oxidizer which can oxidize BH₄, disrupting eNOS dimer formation and uncoupling eNOS^{13,616-618}. Uncoupled eNOS produces O₂⁻ instead of NO, leading to a positive feedback mechanism that exacerbates conditions of oxidative stress⁵⁸⁷. Another factor that was thought to limit the bioavailability of NO is the abundance of hemoproteins in the blood; conversely, studies from Kleschyov *et al.* (2023) and DeMartino *et al.* (2023) show that NO bound to hemoproteins such as hemoglobin and myoglobin is still able to activate sGC⁶¹⁹⁻⁶²¹.

The identification of NO as the “endothelium-derived relaxing factor” was initially controversial^{508,594}. However, the use of false substrate NOS inhibitors such as L-N^G-nitro arginine (L-NOARG) and N^G-nitro-L-arginine methyl ester hydrochloride (L-NAME) elucidated the role of NO in regulating arterial diameter^{622,623}. Furthermore, deletion of eNOS from ECs in mice eliminates flow-induced vasodilation and precipitates hypertension^{624,625}. Interestingly, deletion of

eNOS from erythrocytes does not affect flow-induced vasodilation but still produces hypertension, though the contribution of erythrocyte eNOS to NO signalling is as yet poorly understood⁶²⁴.

1.4.3 Endothelium-dependent hyperpolarization

In addition to the chemical pathway of NO synthesis, endothelium-dependent hyperpolarization (EDH) is a concomitant electrical pathway responsible for endothelium-dependent vasodilation in the vasculature⁶²⁶. EDH was originally isolated and identified as a vasodilatory hyperpolarization of VSMCs that was insensitive to NOS inhibitors and cyclooxygenase (COX) inhibitors, and was shown to occur without an increase in cGMP or cAMP in VSMCs⁶²⁷⁻⁶³¹. This vasodilatory response was initially thought to be facilitated by an unidentified chemical mediator, named endothelium-dependent hyperpolarizing factor (EDHF) in a wide body of literature. However, the current model entails that this response is due to the direct electrical coupling of ECs to VSMCs via MEGJs^{626,632,633}.

EDH depends upon the activity of SK_{Ca} and IK_{Ca} channels in ECs^{517,634}. Ca²⁺-activated K⁺ (K_{Ca}) channels are a family of K⁺ channels that includes three subfamilies which have been discussed separately in previous sections of this chapter (reviewed by Orfali and Albanyan, 2023)⁶³⁵. The subfamilies are named for their single-channel conductance levels: small-conductance K_{Ca} (SK_{Ca} or K_{Ca}2.1-3) channels (~4-14 pS), intermediate-conductance K_{Ca} (IK_{Ca} or K_{Ca}3.1) channels (~32-39 pS), and large-conductance K_{Ca} (BK_{Ca} or K_{Ca}1.1) channels (~200-300 pS)⁶³⁵⁻⁶³⁸. BK_{Ca} channels are tetramers composed of four 7TM α subunits that are activated by depolarization or by binding Ca²⁺ ions directly, and are expressed in VSMCs but not in ECs^{635,639-642}. In contrast, SK_{Ca} and IK_{Ca} channels are tetramers of four 6TM α subunits that are activated by Ca²⁺/CaM instead of free Ca²⁺ ions^{635,643}. Under physiological conditions, SK_{Ca} and IK_{Ca} channels are only expressed in ECs, and not in VSMCs^{635,640,641,644}.

The SK_{Ca} subfamily comprises three isoforms (K_{Ca}2.1-3 or SK1-3) encoded by three separate genes (*KCNN1-3*, respectively)⁶⁴⁵. In ECs, K_{Ca}2.3 is the predominantly expressed isoform, while expression of K_{Ca}2.1 and K_{Ca}2.2 is negligible^{644,646,647}. Thus, throughout this thesis, the use of the term “SK_{Ca}” will refer specifically to K_{Ca}2.3 channels. ECs also highly express IK_{Ca} (K_{Ca}3.1 or SK4) which is the only member of its subfamily, encoded by the gene *KCNN4*^{641,645,647}. The α subunit of SK_{Ca} and IK_{Ca} channels possesses cytoplasmic N- and C-termini and contains a pore domain between TM helices S5 and S6 (**Figure 1.11**)^{635,641}. CaM is believed to be constitutively bound to a domain in the C-terminus^{648,649}, conferring the channel with Ca²⁺ sensitivity at EC₅₀s ranging from 95 to 300 nM^{636,648,650}. It has been shown that SK_{Ca} channels do not assemble with fourfold symmetry like most other homotetramers; instead, two α subunits and two CaMs form an antiparallel dimer arrangement, and the whole channel assembles as a “dimer of dimers” with twofold symmetry (**Figure 1.12**)^{651,652}. This arrangement blocks the C-lobe of CaM, so that even at high [Ca²⁺]_i, only the N-lobe of CaM is exposed and available to bind two Ca²⁺ ions⁶⁵¹. Some evidence suggests that the Ca²⁺ sensitivity of these channels may be modulated by phosphorylation and dephosphorylation of SK_{Ca}-bound CaM at Thr80 by colocalized casein kinase 2 (CK2); however, this has only been demonstrated in non-vascular tissues^{653,654}. Unlike BK_{Ca} channels, SK_{Ca} and IK_{Ca} channels are voltage-insensitive since their S4 domain contains only two positively charged residues compared to six in voltage-operated potassium (K_V) channels or five in LTCCs^{247,638,650,655}.

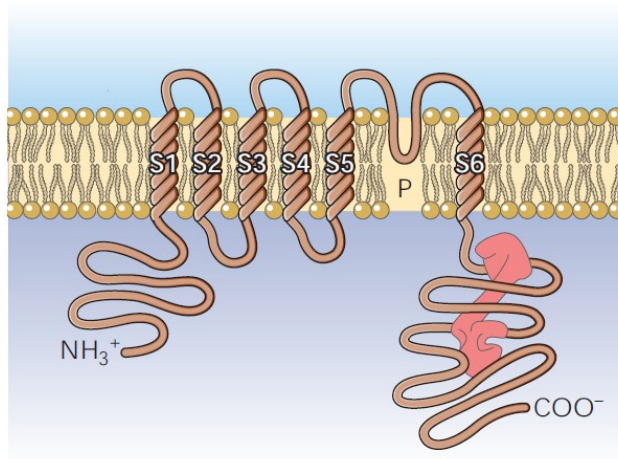


Figure 1.11: Membrane topology of SK_{Ca}/IK_{Ca} channels. Each α subunit of the SK_{Ca} or IK_{Ca} channel contains six TM domains, with a P loop between S5 and S6. ApoCaM is constitutively bound to the C-terminus (from Ledoux *et al.*, 2006)⁶⁴¹.

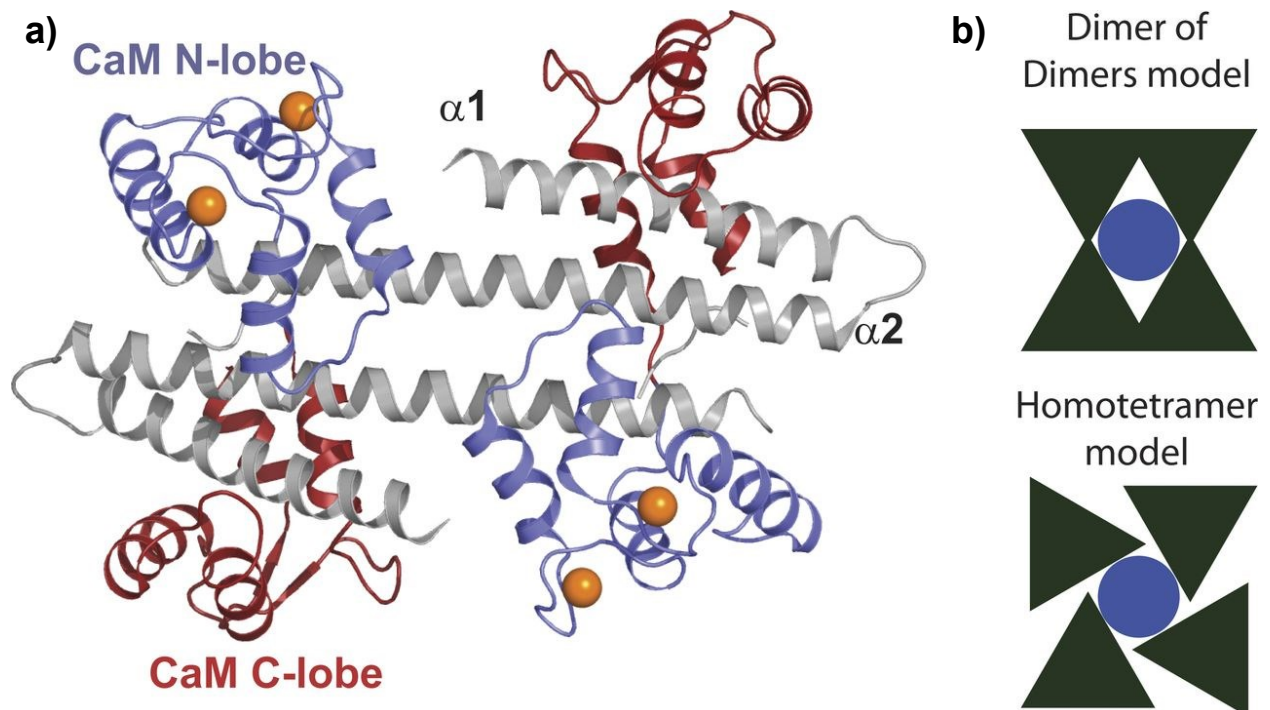


Figure 1.12: Twofold symmetry of SK_{Ca}/IK_{Ca} channels. **a)** Antiparallel arrangement of two CaM molecules (blue, N-lobe; and red, C-lobe) and two SK proteins (grey; sequence from R396 to Q487 of SK2). The N-lobe of each CaM is occupied by Ca²⁺ ions (orange spheres) as in the open conformation of the channel. **b)** Schematic illustration of the “dimer of dimers” model versus a canonical homotetramer. Dark green triangles represent SK_{Ca} α subunits; blue circles represent the central pore (from Halling *et al.*, 2014)⁶⁵¹.

EDH begins in ECs, where an agonist- or shear stress-induced increase in $[Ca^{2+}]_i$ activates SK_{Ca} and IK_{Ca} channels^{517,523,634}. The binding of Ca^{2+} to channel-bound CaM increases the P_o of SK_{Ca} and IK_{Ca} channels^{636,648,651}, allowing an efflux of K^+ ions that hyperpolarizes the EC^{644,647,656-659}. The change in membrane potential is then able to spread via the movement of ions from the EC to adjacent VSMCs through MEGJs, causing the VSMC to become hyperpolarized as well^{656,660-663}. In the VSMC, hyperpolarization decreases the P_o of VOCCs, reducing Ca^{2+} entry and thereby inducing relaxation of the smooth muscle^{633,657,664,665}. Additionally, it has been shown that K^+ efflux from ECs through SK_{Ca} and IK_{Ca} leads to a localized increase in $[K^+]$ near MEPs, which in turn may activate inwardly rectifying K^+ (K_{IR}) channels and/or Na^+/K^+ -ATPases on VSMCs and/or ECs, depending on the tissue^{661,666-669}. This pathway serves to amplify the initial K_{Ca} -induced hyperpolarization⁵¹⁷.

EDH provides a higher relative contribution to vasodilation than NOS in smaller arteries such as resistance arteries and arterioles, whereas the NOS pathway is more prominent in large elastic arteries^{631,670,671}. This makes EDH a particularly crucial regulator of local tissue perfusion. Despite the varying degrees of its contribution, SK_{Ca} - and IK_{Ca} -mediated EDH and its subsequent spread to VSMCs have been recorded in a wide range of vascular tissue, including rat aorta⁶⁵⁹, mesenteric artery^{663,672,673}, and hepatic artery⁶⁵⁷; guinea pig carotid artery⁶⁵⁶; porcine coronary artery⁶⁴⁴; canine mesenteric artery⁶⁴⁷; human umbilical vein endothelial cells (HUVECs)⁶⁷⁴; and still many others. The investigation and isolation of SK_{Ca} - and IK_{Ca} -mediated EDH in these studies was aided by the well-developed pharmacology of SK_{Ca} and IK_{Ca} channels. The classical inhibitors of SK_{Ca} and IK_{Ca} channels are the venom-derived peptides apamin (from bee venom) and charybdotoxin (from scorpion venom), respectively⁶⁷⁵. Apamin blocks SK_{Ca} with high selectivity; it has the highest affinity for SK2 ($IC_{50} \approx 0.03-0.2$ nM), followed by SK3 ($IC_{50} \approx 0.6-4$ nM) and

finally SK1 ($IC_{50} \approx 0.7-12$ nM)^{655,675}. It was initially thought that apamin blocks SK_{Ca} by binding to two residues in opposite sides of the pore⁶⁷⁶, and that the differences in selectivity between SK1, 2 and 3 are due to apamin's interaction with a third residue in the outer vestibule of the pore⁶⁷⁷. Evidence that apamin interacts with the extracellular S3-S4 loop of SK_{Ca} has led some to believe that apamin's action is allosteric instead^{678,679}. However, the mechanism is still unclear, as the crystal structure of SK_{Ca} has not yet been solved⁶⁸⁰. While apamin is still widely used experimentally⁶⁸⁰, charybdotoxin was found to block BK_{Ca} and K_V1.3 in addition to IK_{Ca}, so it has been replaced by more selective small molecule blockers of IK_{Ca}⁶⁷⁵. These include 1-[(2-chlorophenyl)diphenylmethyl]-1*H*-pyrazole (TRAM-34; $IC_{50} \approx 20$ nM)^{681,682} and 4-[[3-(trifluoromethyl)phenyl]methyl]-2*H*-1,4-benzothiazin-3(4*H*)-one (NS6180; $IC_{50} \approx 9-14$ nM)^{683,684}, which block the central pore from the cytoplasmic side of the selectivity filter⁶⁸⁵. Selective small-molecule activators of SK_{Ca} and IK_{Ca} have also been developed, such as *N*-cyclohexyl-*N*-[2-(3,5-dimethyl-pyrazol-1-yl)-6-methyl-4-pyrimidinamine (CyPPA) and naphtho[1,2-*d*]thiazol-2-ylamine (SKA-31), respectively. These molecules are positive allosteric modulators which bind at the interface between the α subunit and CaM and increase the apparent Ca²⁺-sensitivity of the channel⁶⁸⁶⁻⁶⁸⁹.

SK_{Ca} and IK_{Ca} share many structural and functional similarities, but have distinct roles in regulating vascular tone based on their disparate localization within the EC^{14,672,690}. SK_{Ca} channels are localized in caveolae on the luminal surface of ECs, especially near interendothelial gap junctions (see §1.5.1)^{672,690-692}. In caveolae, SK_{Ca} channels are colocalized with TRP channels such as TRPV4 and TRPC1^{693,694}. Shear stress activates TRP channels, and the resultant local increase in [Ca²⁺]_i activates SK_{Ca}, leading to endothelium-dependent vasodilation^{691,695}. In particular, Brähler *et al.* (2009) demonstrated using pressure myography in isolated carotid arteries from mice

deficient in either or both SK_{Ca} and IK_{Ca} channels that the loss of SK_{Ca}, but not IK_{Ca}, impaired shear-stress induced vasodilation⁶⁹¹. In contrast to SK_{Ca}, endothelial IK_{Ca} channels are localized to MEPs^{690,696-698}. In addition to contributing to endothelium-dependent vasodilation, this unique position allows IK_{Ca} channels to mediate a negative feedback response termed myoendothelial feedback⁵⁴⁶. The activation of α_1 -adrenoceptors on VSMCs increases the production of IP₃ by PLC; IP₃ is then able to diffuse through MEGJs into adjacent ECs⁶⁹⁹. Here, IP₃ activates both TRPC3 channels on the plasma membrane⁵⁴⁶ and IP₃Rs on sections of the ER localized to MEPs⁵¹⁸, leading to Ca²⁺ influx and release in an event called a “Ca²⁺ wavelet”^{14,698} that is characteristically distinct from a Ca²⁺ pulsar. The wavelet creates a local [Ca²⁺]_i increase in the MEP that activates IK_{Ca}, subsequently producing EDH which spreads back to the VSMCs to limit the initial vasoconstrictor stimulus^{14,546,698,700}. Regardless of their discrete, specialized roles, SK_{Ca} and IK_{Ca} are both capable of hyperpolarizing ECs. Activation of either channel precipitates vasodilation, and both channels must be blocked in order to fully inhibit EDH^{687,701-703}. The physiological importance of endothelial K_{Ca} channels is underscored by evidence that suppression or knockout of SK_{Ca} and/or IK_{Ca} impairs ACh-induced vasodilation and produces systemic hypertension in mice^{691,704,705}.

1.4.4 Crosstalk between NO synthesis and EDH

For many years, the two Ca²⁺-induced mechanisms of endothelium-dependent vasodilation, NO synthesis and EDH, were considered to be parallel, but ultimately separate. Conversely, over the past decade, evidence has emerged that NO and EDH are heavily interconnected, and might be more correctly framed as two facets of a single pathway (**Figure 1.13**). For example, our lab has previously demonstrated in isolated basilar arteries from rats that EDH-mediated myoendothelial feedback depends upon NO synthesis, which was impaired in the

presence of IK_{Ca} and TRPC3 inhibitors⁵⁴⁶. This is congruent with a study from Biwer *et al.* (2016) showing that a population of eNOS is localized to MEPs and is activated by PKC in response to IP_3 entry from smooth muscle⁷⁰⁶. Moreover, Brähler *et al.* (2009) found that genetic ablation of endothelial SK_{Ca} impaired NO-mediated dilation to ACh in mouse cremaster arterioles⁶⁹¹. It has also been shown that SK_{Ca} and IK_{Ca} blockers eliminate ATP- and histamine-induced NO production in HUVECs⁶⁷⁴. One mechanism which likely contributes to this effect involves the production of ROS. NADPH oxidase (NOX) is a constitutively active enzyme complex found in the plasmalemma of ECs, and is the primary producer of O_2^- in the vasculature⁷⁰⁷⁻⁷⁰⁹. It has been reported that NOX is activated by membrane depolarization in endothelial cells⁷¹⁰; increased production of O_2^- decreases NO bioavailability by scavenging NO and forming $ONOO^-$ which uncouples eNOS^{599,615}. Thus, SK_{Ca} - and IK_{Ca} -mediated hyperpolarization leads to a decrease in O_2^- production, thereby increasing the bioavailability of NO⁶¹⁵. Our lab has previously shown using pressure myography coupled with dihydroethidium (DHE) visualization of O_2^- that SK_{Ca} and IK_{Ca} activators decrease O_2^- production in isolated mesenteric arteries from rats⁷¹¹.

In the opposite direction, another body of literature demonstrates that NOS inhibitors impair EDH, suggesting that endothelial-derived NO may provide a necessary contribution to EDH⁷¹²⁻⁷¹⁵. Taken together, these findings suggest that EDH and NO are interrelated pathways wherein EDH enhances the bioavailability of NO, and NO may in turn enhance K_{Ca} activity (reviewed by Alaaeddine *et al.*, 2019)⁷¹⁶.

Shear stress \longrightarrow

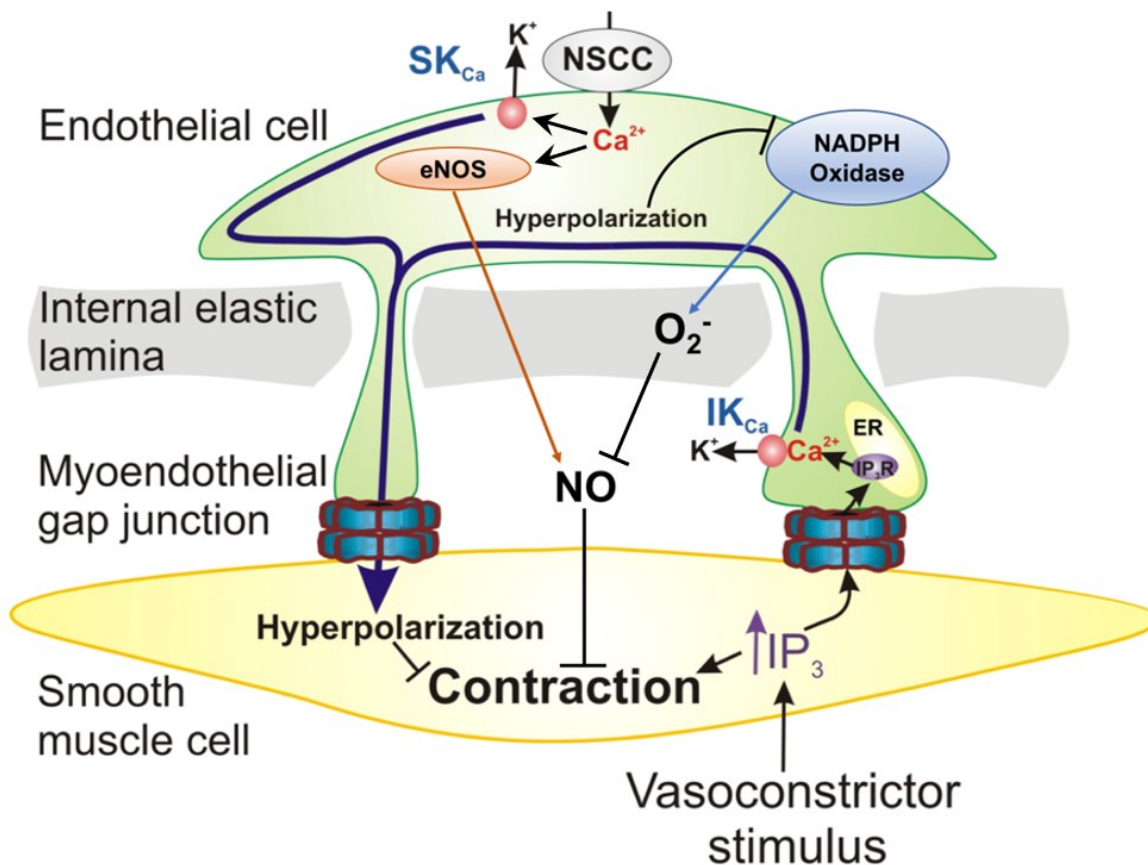


Figure 1.13: Schematic diagram of EDH and NO synthesis pathways of endothelium-dependent vasodilation. Ca^{2+} influx through non-selective cation channels (NSCCs) such as TRP channels leads to activation of SK_{Ca} , IK_{Ca} , and eNOS. Opening of K_{Ca} channels hyperpolarizes the endothelial cell membrane potential, and this hyperpolarization spreads to adjacent VSMCs via MEGJs to inhibit contraction. Activation of eNOS leads to the synthesis of diffusible NO which also inhibits contraction.

1.5 Endothelial cell junctions

The endothelium exhibits structural and functional heterogeneity throughout the vasculature (reviewed by Aird, 2007)^{717,718}. The ultrastructure of the endothelium may be either continuous or discontinuous; continuous endothelium may be further categorised as fenestrated or nonfenestrated^{718,719}. Nonfenestrated continuous endothelium is the most common ultrastructure

throughout the body, found in arteries, veins and capillaries of the brain, skin, lungs, heart, and skeletal muscle, as well as resistance arteries such as the mesenteric vascular bed^{24,719,720}. It is characterized by the presence of tight junctions between endothelial cells, and a continuous basal lamina. Fenestrated continuous endothelium is marked by transcellular pores (approximately 50-70 nm diameter) occupied by a glycoprotein diaphragm, and is observed in locations requiring increased transport or filtration, such as glomeruli, endocrine glands, and gastrointestinal mucosa^{24,717,721-723}. Finally, discontinuous endothelium contains larger pores (approximately 100-200 nm diameter) with no diaphragm, as well as gaps in the basal lamina^{24,717,721}. It is found in sinusoidal vascular beds in the liver, bone marrow and spleen⁷²⁴.

The ultrastructure of the endothelium is determined by the quantity and nature of intercellular junctions between ECs^{718,721,725}. Interendothelial junctions belong to several categories, namely adherens junctions (AJs), tight junctions (TJs) and gap junctions (GJs)⁷²⁵. All of these junctions depend upon the extracellular interaction of transmembrane proteins with those of adjacent cells^{717,725}. Endothelial AJs have the widest intermembrane distance of the three junctions, providing mechanical adhesion between cells⁷²⁶. AJs are composed primarily of vascular endothelial cadherin (VE-cadherin) that is anchored on the intracellular side to the actin cytoskeleton and/or vimentin filaments^{725,727}. Endothelial TJs bridge a smaller intermembrane distance than AJs, and serve two main functions: a “fence” function preventing the mixing of apical and basolateral membrane proteins, and a “gate” function controlling the paracellular passage of water, ions and solutes^{726,728}. They contain members of several protein families, including claudins, occludins, junctional adhesion molecules (JAMs) and endothelial cell-selective adhesion molecules (ESAMs)^{725,729}. Both AJs and TJs play important roles in the modulation of

endothelial permeability, leukocyte extravasation and angiogenesis which has been reviewed elsewhere^{725,727,730}; however, this thesis will instead focus on the role of endothelial GJs.

1.5.1 Endothelial gap junctions

The coordination of vasodilatory function in the endothelium, particularly in EDH and myoendothelial feedback, is dependent upon intercellular communication through GJs (reviewed by Pogoda *et al.*, 2019)⁷³¹. GJs are intercellular channels linking the cytosol of two adjacent cells, either in homocellular couplings (e.g. EC-EC) or heterocellular couplings (e.g. EC-VSMC at MEGJs)⁷³². These channels comprise two hemichannels called connexons, each belonging to the plasmalemma one of the coupled cells (**Figure 1.14**). Connexons are hexamers composed of connexins (Cxs), a family of 4TM proteins with 21 members expressed in humans⁷³³. Four Cx subtypes are expressed in the vasculature: ECs express Cx37, Cx40, and to a lesser extent Cx43, whereas VSMCs express Cx43 and Cx45⁷³⁴⁻⁷⁴⁰. Connexons may be either homomers comprising units of a single Cx subtype, or heteromers comprising more than one Cx subtype⁷⁴¹⁻⁷⁴³. Notably, the two main EC connexins, Cx40 and Cx37, have not been demonstrated to form heteromers together, but have each been shown to readily heteromerize with Cx43^{731,743-745}. Two connexons forming a functional channel may either contain the same Cx composition (homotypic) or distinct Cx compositions (heterotypic)⁷⁴¹. This leads to a wealth of possible combinations for intercellular channels with varying unitary conductances^{742,743}, which can be homomeric-homotypic, homomeric-heterotypic, heteromeric-homotypic, or heteromeric-heterotypic⁷³². The formation of intramolecular disulfide bonds in the extracellular loops of each Cx creates a β -sheet formation necessary for intercellular docking of connexons⁷⁴⁶⁻⁷⁴⁹. The pore-to-pore docking of connexons is a tight interaction involving the staggering and interdigitation of Cx extracellular loops so as to prevent leakage between the cytosol and the extracellular space^{747,750,751}. In order to facilitate

docking and formation of GJ channels, connexons localize in clusters called plaques, each containing up to 2000 individuals and occupying an area of diameter 0.5-2 μm ^{752,753}. The half-lives of GJ channels are much shorter than most integral membrane proteins, ranging from 1.5-5 hours depending on the Cx subtypes and the tissue^{752,754-757}. The central pore of the channel creates an electrical continuity between cells which facilitates the spread of membrane potential, while also being large enough to facilitate the passage of polar small molecules (<1 kDa)^{758,759}. This includes the diffusion of vasoactive molecules such as Ca^{2+} ions, IP_3 , cAMP, cGMP, ATP, NAD^+ , and prostaglandins, as well as linear oligopeptides and microRNAs^{760,761}.

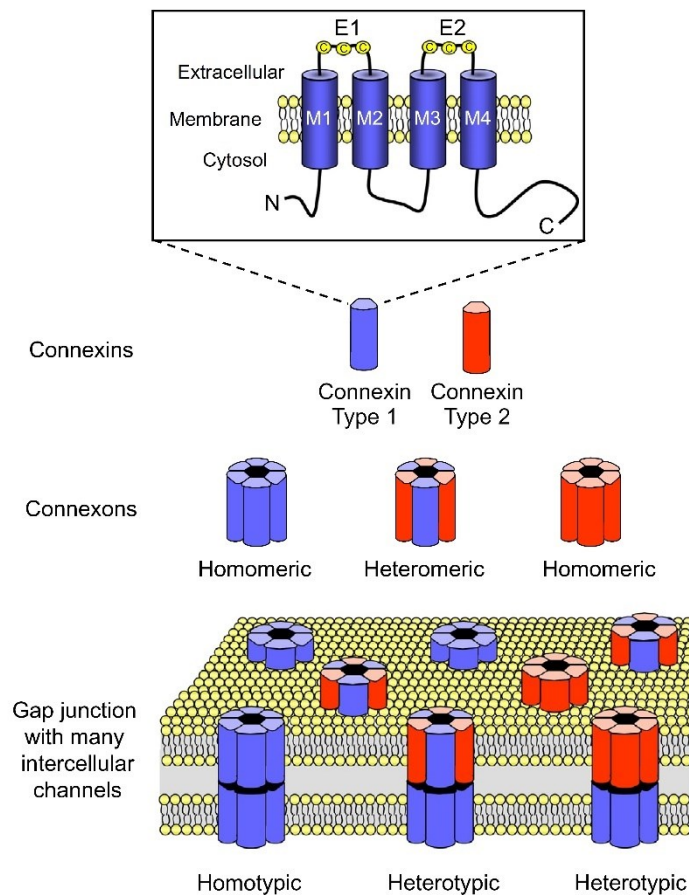


Figure 1.14: Membrane topology of connexins. Connexins contain four TM domains with cytosolic N- and C-termini. Connexins assemble into hexameric connexons (or hemichannels) which may be homomeric or heteromeric. Connexons of one cell dock with connexons of an adjacent cell to form gap junction channels which may be homotypic or heterotypic (adapted from Schmidt *et al.*, 2016)⁷³².

1.5.2 Role of Cx40

In ECs, gap junctions are responsible for the longitudinal conduction of hyperpolarization up- or downstream from the focal site of a vasodilatory stimulus (reviewed by Welsh *et al.*, 2018)⁷⁶². The conducted vasomotor response is a crucial mechanism whereby a vasodilatory stimulus in a small artery can spread up the vascular tree (i.e. opposite to blood flow) in order to increase tissue perfusion to match energetic demand^{762,763}. Cx40 has been shown to be a crucial mediator of this response. For example, Figueroa *et al.* (2008) demonstrated using mouse germline knockout models that Cx40, but not Cx37, is necessary for the upstream conduction of ACh-induced endothelium-dependent vasodilation in cremaster arteries⁷⁶⁴. The authors also found that neither deletion of Cx40 nor Cx37 affected conduction of dilation to pinacidil, which opens ATP-sensitive K⁺ (K_{ATP}) channels on VSMCs. These findings were expounded upon by Jobs *et al.* (2012), who used mice with a point mutation yielding non-functional Cx40; they demonstrated that functional Cx40 is necessary for the conduction of ACh- or bradykinin-induced vasodilation in cremaster arterioles⁷⁶⁵. Cx40 is also implicated in other forms of haemodynamic control: studies in Cx40 knockout mice have observed elevated systemic blood pressure, impaired magnitude of endothelium-dependent vasodilation, and decreased eNOS expression in vessels such as the aorta and renal artery^{661,766,767}. However, the myogenic response was preserved in the renal afferent arteriole of Cx40 knockout mice⁷⁶⁸. Interestingly, some evidence also suggests that the conducted vasomotor response allows for hyperpolarized membrane potentials to be amplified as they are conducted (**Figure 1.15**)⁶⁶². In mouse cremaster arterioles, Rodenwaldt *et al.* (2007) observed that conducted vasoconstrictor responses decay exponentially with distance along the vessel, whereas conducted dilations decay with distance much less than modelling predicts^{769,770}. A prominent candidate for this mechanism is smooth muscle K_{IR} channels⁶⁶⁷, but endothelial IK_{Ca} channels may

be involved as well, despite being voltage-insensitive⁷⁷¹. Evidence has also emerged associating disease states of endothelial dysfunction, such as T2DM, with decreased expression of Cx40 in the cardiovascular system⁷⁷². Taken together, these observations indicate that Cx40 is a major contributor to endothelium-dependent vasodilation, and subsequently the regulation of arterial diameter and systemic blood pressure.

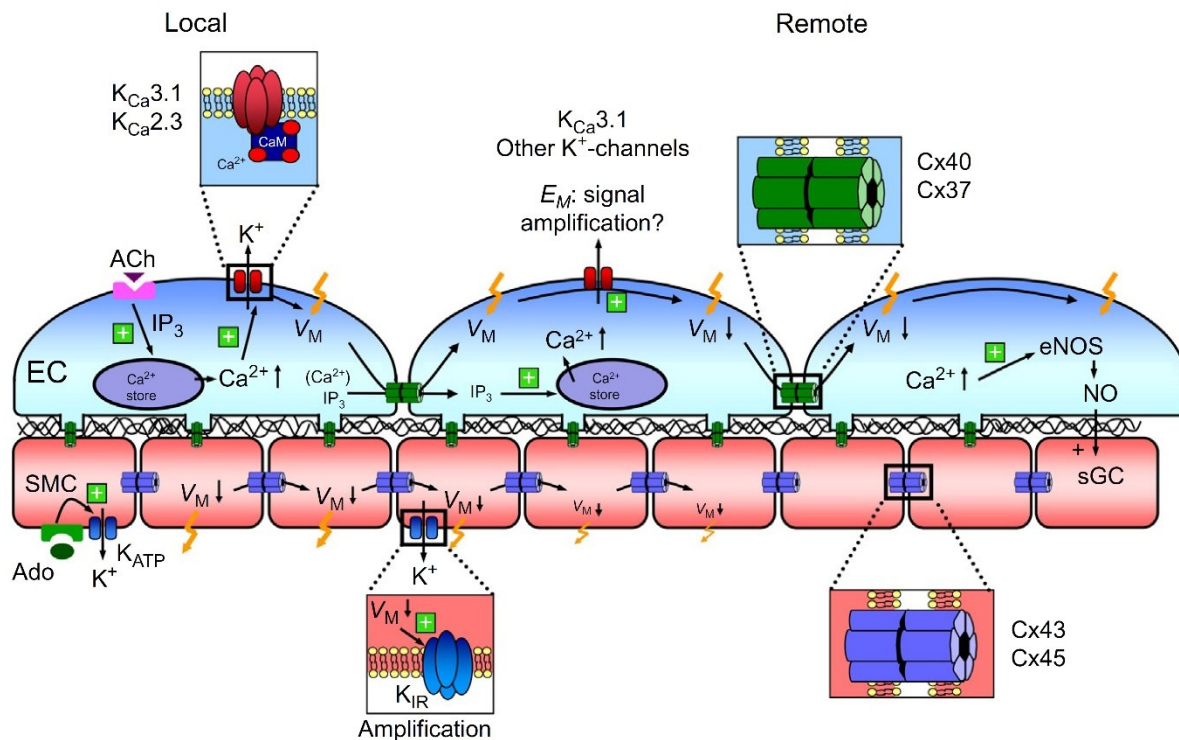


Figure 1.15: Schematic diagram of conduction of membrane potential along the vessel wall via gap junctions. Local stimulation of M₃ receptors by ACh leads to the activation of SK_{Ca} and IK_{Ca} channels, hyperpolarizing the endothelial cell. The hyperpolarization is amplified as it spreads to adjacent ECs through interendothelial GJs, though the underlying mechanism is unclear (from Schmidt *et al.*, 2016)⁷³².

Conversely, knockout of Cx37 in mice produces phenotypic changes outside of the cardiovascular system, including female infertility and disrupted lymphatic valve development, but does not produce obvious vascular dysfunction⁷⁷³⁻⁷⁷⁷. The main vascular effects reported to date in Cx37 knockout mice are enhanced angiogenesis, and partial resistance to angiotensin II-

induced hypertension^{764,778,779}. Meens *et al.* (2015) also showed that L-NAME significantly enhanced phenylephrine-induced contraction of isolated aorta segments from wild-type mice, but this was reversed in Cx37 knockout mice, suggesting a putative role for Cx37 in basal NO release⁷⁸⁰. Where Cx37 or Cx40 knockout animals are viable, the deletion of both Cx37 and Cx40 in mice results in perinatal death⁷⁷³. However, despite the crucial role of Cx37 in other systems, Cx40 appears to be a larger contributor to intercellular coordination in the vascular endothelium and modulation of arterial diameter.

Until recently, only mouse models of Cx knockouts have been available. This has restricted most physiological assays to the use of large elastic arteries such as the aorta, rather than resistance arteries, due to the physical limitations of fine dissection in techniques such as wire and pressure myography. Our research group received a novel strain of Cx40 knockout rats as a gift from collaborator Dr. William Cupples; this has allowed me to perform experiments assessing the functional physiological role of Cx40 in the modulation of resistance artery diameter, which was not possible in mouse models.

1.6 Myocardial ischemia/reperfusion injury

Ischemic heart disease is the most prevalent form of CVD worldwide, causing approximately 8.9 million deaths (16% of total global mortality) in 2019 according to the World Health Organization⁷⁸¹. Ischemic heart disease occurs as a result of full or partial occlusion of one or more coronary arteries in conditions such as atherosclerosis or thrombosis. This creates a period of acute myocardial ischemia, during which the myocardium receives insufficient oxygen resulting in necrotic death of cardiomyocytes⁷⁸². Current preventative therapies for ischemic heart disease focus on reducing the occurrence of acute myocardial ischemic attacks by treating the associated risk factors: T2DM, obesity, atherosclerosis and hypertension⁷⁸³⁻⁷⁸⁵. Once an ischemic attack

occurs, primary myocardial reperfusion via pharmacological or mechanical means remains the gold standard treatment⁷⁸⁶. Paradoxically, reperfusion following the ischemic attack also induces myocardial damage and contributes to subsequent heart failure in a phenomenon called ischemia/reperfusion injury⁷⁸⁷⁻⁷⁸⁹. Reperfusion of the ischemic myocardium produces a state of oxidative stress⁷⁹⁰ which results in greater tissue injury than ischemia alone by mechanisms including the reduced bioavailability of NO, intracellular and mitochondrial Ca²⁺ overload, the recruitment of neutrophils and the induction of inflammation (reviewed by Yellon and Hausenloy, 2007)⁷⁸⁷. Animal models have shown that the damage caused by reperfusion accounts for up to 50% of the final size of a myocardial infarct caused by an ischemic attack⁷⁸⁷.

Atrial cardiomyocytes are one of the few locations outside of the vascular endothelium where Cx40 expression is well-established⁷⁹¹. During early embryonic development, Cx40 is broadly expressed in the heart, but by the time of birth through to adulthood, expression is restricted to atrial cardiomyocytes and cells of the conduction system including the bundle of His, bundle branches and Purkinje fibers^{792,793}. In fact, Cx40 has been demonstrated to participate in embryonic cardiac morphogenesis, as Cx40 knockout mice were found to have greater incidence of septal defects and other cardiac malformations⁷⁹⁴. Due to this localization pattern, Cx40 is an important mediator of intercellular conduction of electrical signals in the heart. It follows that somatic mutations in the Cx40-encoding gene *GJA5* which reduce conduction of the assembled GJ channel have been linked to idiopathic atrial fibrillation and arrhythmias in human patients^{795,796}. Gemel *et al.* (2014) found in cultured cells that several Cx40 mutants associated with atrial fibrillation undergo more rapid proteasomal degradation than wild-type Cx40, thereby reducing their cell-surface expression⁷⁹⁷. Furthermore, Zhang *et al.* (2017) found that mRNA

expression of Cx40 in atrial cardiomyocytes is significantly decreased in atrial fibrillation patients versus controls with rheumatic heart disease⁷⁹⁸.

Thus, Cx40 is understood to serve a crucial role in the myocardial conduction system, but it is unclear whether or not Cx40-mediated conduction has a role in cardiac ischemia/reperfusion injury. Evidence suggests that the absence of Cx40 is associated with increased oxidative stress⁷⁹⁹, making it reasonable to hypothesize that the physiological role of Cx40 may be protective in ischemia/reperfusion. Unfortunately, current data is limited as this question has not been widely investigated. Nevertheless, Morel *et al.* (2014) demonstrated that EC-specific Cx40 knockout mice incur a greater area of cardiac infarction than wild-type mice in response to *in vivo* ischemia/reperfusion⁸⁰⁰. However, this difference was not observed in response to *ex vivo* ischemia/reperfusion in the Langendorff isolated heart perfusion. The authors further demonstrate that this discrepancy is due to greater neutrophil infiltration in the myocardium of the EC-specific Cx40 knockout mouse. Together, these data suggest that Cx40 may serve a protective role in ischemia/reperfusion injury; however, further research is necessary.

1.7 Hypothesis and aims

The coordinated action of ECs and VSMCs is crucial for the modulation of resistance artery diameter, and subsequently the control of systemic BP. This coordination depends upon electrical signalling through a wide range of ion channels. In particular, TRPM4 in VSMCs is reputed to be necessary for myogenic vasoconstriction, and Cx40-containing GJ channels in ECs have been put forward as a major contributor to endothelium-dependent vasodilation. Thus, through this thesis I investigate these roles by addressing three hypotheses:

- 1) TRPM4 plays a role in both myogenic and agonist-induced vasoconstriction in resistance arteries.

- 2) The Cx40 knockout rat will demonstrate impaired endothelial modulation of arterial diameter versus wild-type.
- 3) The introduction of a mild hypercaloric diet will impair endothelial modulation of arterial diameter to a greater extent in the Cx40 knockout rat than in wild-type rats.

To test these hypotheses, I have addressed three corresponding aims:

- 1) To investigate the effects of the small-molecule TRPM4 inhibitor 9-phenanthrol on the development of myogenic and agonist-induced vascular tone in isolated resistance arteries.
- 2) To characterize arterial function in the Cx40 knockout rat model with exploratory functional assays.
- 3) To investigate the extent to which a hypercaloric diet produces endothelial dysfunction within the Cx40 knockout rat model.

Chapter 2: Materials and methods

2.1 Ethics approval

All animal care and experimental procedures were approved by the Animal Care and Use Committee (ACUC HS1; AUP 312) of the Faculty of Medicine and Dentistry at the University of Alberta, and performed in accordance with Canadian Council on Animal Care guidelines, and the principles and regulations as described by Grundy, 2015¹.

2.2 Animal care and use

Two separate rat strains are used in this research; the experiments described in **Chapter 3** use Sprague-Dawley rats, whereas the experiments described in **Chapters 4** and **5** use Cx40^{+/+} (wild-type or WT), Cx40^{+/-} (heterozygous or HET), and Cx40^{-/-} (knock-out or KO) rats bred from the WKY-Gja5^{em1M_{ewi}} mutant strain.

Male (250-300 g) and female (175-225 g) Sprague-Dawley rats were obtained from Charles River Laboratories (Montréal, Canada).

The WKY-Gja5^{em1M_{ewi}} strain was developed by Drs. Melinda Dwinell and Aron Geurts at the Medical College of Wisconsin⁸⁰¹ under a R24 Resource grant (R24 HL114474) awarded by the National Heart, Lung, and Blood Institute (NHLBI) on behalf of the National Institutes of Health (NIH). This strain is based on a Wistar-Kyoto (WKY) background and was produced by injecting a CRISPR plasmid targeting the sequence CGATGACCGTAGAGTGCTTG on the *Gja5* gene coding for Cx40 (NCBI GenBank Accession #NM_019280)⁸⁰² into WKY embryos. The plasmid introduces a 1-bp substitution into exon 1 (c.25G>T)⁸⁰³ resulting in a premature stop codon in place of Glu9^{804,805}. Our research group received WKY-Gja5^{em1M_{ewi}} rats as a gift from collaborator Dr. William Cupples at Simon Fraser University.

The colony was bred and maintained in conjunction with University of Alberta Health Sciences Laboratory Animal Services (HSLAS). Initial breeding pairs comprised WKY-Gja5^{em1Mcwi} rats and WKY stock rats; in subsequent generations breeding pairs comprised HET × HET crossings yielding offspring with a genotype distribution of approximately 25% WT, 50% HET, and 25% KO. Ear notch samples were collected by HSLAS staff. Genotyping was completed using polymerase chain reaction (PCR) and direct sequencing as described in §2.6. Rats were age-matched at 6 months of age (\pm 1 month) when euthanized for tissue collection.

All rats were housed by HSLAS in an enriched environment maintained on a 12:12 h light–dark cycle at \sim 23°C with fresh tap water and standard or hypercaloric chow (§2.11) available ad libitum. Blood glucose (§2.8) and body weight were measured immediately prior to euthanasia. Rats used for Langendorff heart perfusion (§2.10) were euthanized by i.p. injection of pentobarbital followed by decapitation; otherwise rats were euthanized by inhalation of isoflurane followed by decapitation. The gut, heart, brain and kidneys were excised post-mortem and placed in ice-cold Krebs buffer containing (mM): NaCl (119.0), NaHCO₃ (25.0), KCl (4.7), MgSO₄·7H₂O (1.2), KH₂PO₄ (1.18), glucose (11), and CaCl₂ (2.5). Organs and isolated arteries were flash-frozen in liquid nitrogen for use in RT-qPCR (§2.7). For experiments requiring a nominally Ca²⁺-free solution, CaCl₂ was omitted from the above composition.

2.3 Perfused mesenteric vascular bed

The mesenteric vascular bed was perfused by the superior mesenteric artery and electrically stimulated as described previously⁸⁰⁶. For this procedure, the mesenteric vascular bed was separated from the intestine, and the superior mesenteric artery was isolated from surrounding adipose and connective tissue before being cannulated with a blunted hypodermic needle (20 G). The needle was secured with 3-0 surgical silk (Ethicon; Livingston, UK) and flushed with Krebs

buffer to remove blood. In experiments using endothelium-denuded vascular beds, the endothelium was removed by flushing the bed with 0.5% Triton X-100 (Fisher Scientific; Fair Lawn, USA) in water for 15-30 seconds followed by rapid washout with Krebs buffer. The mesentery was placed on a wire mesh and secured in a water jacket maintained at an internal temperature of 37°C. Next, the mesentery was perfused with heated (37°C) and gassed (95% O₂ / 5% CO₂) Krebs buffer by a Minipuls 2 peristaltic pump (Gilson; Villiers-le-Bel, France) at a constant flow rate of 5 mL·min⁻¹. Changes in perfusion pressure were recorded via an in-line pressure transducer through a PowerLab 2/20 data acquisition system using Chart 5.0 software (ADInstruments; Colorado, USA).

Endothelium-denuded tissues were assessed for endothelial function using the α_1 -adrenoceptor agonist methoxamine (MOX; 1 μ M) to induce vasoconstriction, followed by the endothelium-dependent vasodilator acetylcholine (ACh; 1 μ M). Tissues in which ACh caused \leq 30% reversal of constriction by MOX were considered to be denuded. If ACh failed to evoke a vasodilatory response, endothelium-independent vasodilation was induced by administration of non-selective β -adrenoceptor agonist isoproterenol (10 μ M) in order to confirm smooth muscle function.

2.3.1 Electric field stimulation of perivascular nerves

Electrodes were attached to the hypodermic needle and the wire mesh to facilitate electrical field stimulation of the mesentery using a Grass SD9 Stimulator (Grass Medical Instruments; Quincy, USA). Tissues were equilibrated for 20 minutes before applying a single stimulation (30 Hz; 90 V; 1 ms pulse width; 30 s duration) to determine the viability of the preparation. After another 10 minutes, viable tissues were subjected to stimulations of increasing frequency ranging from 1 to 40 Hz (90 V; 1 ms pulse width; 30 s duration) every 10 minutes in order to construct a

frequency-response curve⁸⁰⁷⁻⁸⁰⁹. In order to assess their effects on nerve-evoked vasoconstriction, pharmacological agents were added to the Krebs buffer and allowed to perfuse through the preparation for 20 minutes before constructing a second or third frequency-response curve.

2.4 Wire myography

Isolated second and third order mesenteric arteries were cleaned of surrounding adipose and connective tissue, cut into approximately 2 mm-long segments, and mounted between two gold-plated tungsten wires (25 μm diameter; Goodfellow Cambridge Ltd.; Huntingdon, UK) in a Malvany-Halpern myograph (Model 610M; Danish Myo Technology; Aarhus, Denmark) as described previously^{700,806}. Changes in isometric tension were recorded via a PowerLab 4/25 using Chart 5.0 or 8.0 software (ADInstruments). Artery segments were maintained in a 7 mL bath of heated (37°C) and gassed (95% O₂ / 5% CO₂) Krebs buffer (pH 7.4) and were held at a pre-determined optimal resting tension of 5 mN for 20 minutes. 5 mN was determined from active length-tension curves to be the resting tension at which the α_1 -adrenoceptor agonist phenylephrine (PE; 10 μM) elicited 75% of its maximal response. After this equilibration period, endothelial function was assessed as % relaxation to ACh (3 μM) after pre-stimulation with PE (3 μM). Arteries in which ACh elicited $\geq 90\%$ reversal of PE-induced tone were considered to have a functional, intact endothelium and were used to construct concentration-response curves; otherwise, arteries were discarded.

2.4.1 Concentration-response curves

Cumulative concentration-response curves (CRCs) to vasodilatory and vasoconstrictive agents were constructed in the presence and absence of SK_{Ca} inhibitor apamin (50 nM), IK_{Ca} inhibitor TRAM-34 (1 μM), eNOS inhibitor L-NAME (100 μM), and/or TRPM4 inhibitor 9-phenanthrol (10 μM). These pharmacological pre-treatments were allowed to equilibrate in the

myograph chamber for 20 minutes before CRCs were constructed. Cumulative CRCs to vasodilatory agents were constructed following pre-stimulation of artery segments with either PE (3 μ M), 5-HT (3 μ M) or the TXA₂ mimetic U46619 (3 μ M) and results were expressed as % reversal of agonist-induced tone. Cumulative CRCs to vasoconstrictive agents were constructed without pre-stimulation and results were expressed as a % of maximal response.

2.5 Pressure myography

Leak-free 2-4 mm-long segments of fourth to sixth order mesenteric artery were cleaned of surrounding adipose and connective tissue, mounted between two glass cannulae in an arteriograph chamber (Model CH-1-LIN; Living Systems Instrumentation; Burlington, USA). The glass cannulae were pulled from borosilicate glass capillary tubes (1.2 mm outer diameter and 0.69 mm inner diameter; Sutter Instrument Company; Novato, USA) using a P-87 Flaming/Brown micropipette puller (Sutter Instrument Company). Artery segments were secured on the cannulae by nylon monofilament sutures (30 μ m diameter; Living Systems Instrumentation) and maintained in a 7 mL bath of heated (37°C) and gassed (20.96% O₂ / 4.94% CO₂ / balance N₂) Krebs buffer (pH 7.4). The arteriograph chamber was placed on the stage of a Nikon Eclipse TE300 inverted microscope (Nikon Instruments Inc.; Melville, USA) and vessels were visualized using a CCD video camera module (Model XC-73CE; Sony; Atsugi, Japan) and an automated video dimension analyzer (Model VDA-10; Living Systems Instrumentation) in order to measure the internal diameter of the vessel in real time. Transmural pressure (i.e. intraluminal pressure relative to atmospheric pressure) was recorded via an in-line pressure transducer and maintained by a pressure servo controller with a peristaltic pump (Model PS-200; Living Systems Instrumentation) connected to the inflow cannula. In all experiments, the outflow cannula was closed and vessels were pressurized with no luminal flow. The pressure servo was set in automatic mode, wherein a

stable pressure value indicated that no leaks were present in the system. Pressure and internal diameter measurements were recorded via a PowerLab 4/20 using Chart 5.0 software (ADInstruments).

2.5.1 Myogenic responses to increases in intraluminal pressure

Arteries were held at an intraluminal pressure of 80 mmHg for a period of 45 minutes to allow for the spontaneous development of myogenic tone. Arteries which failed to exhibit a sustained decrease in diameter $\geq 50 \mu\text{m}$ within this period were considered not myogenically reactive and were discarded. 80 mmHg was chosen as the intraluminal pressure for equilibration because it approximates the mean arterial blood pressure of a rat *in vivo*⁸¹⁰⁻⁸¹².

Following equilibration, intraluminal pressure was decreased to 20 mmHg and a pressure ramp was constructed under control conditions by increasing the pressure from 20 mmHg to 120 mmHg in stepwise increments of 20 mmHg. Each step was held for a minimum of 3 minutes, holding longer if required for the vessel diameter to plateau. The pressure was returned to 20 mmHg at the end of the pressure ramp. Pharmacological agents were added to the bath and allowed to equilibrate for 20 minutes before second and third pressure ramps were constructed. At the end of each experiment, the Krebs in the bath was replaced with Ca^{2+} -free Krebs (§2.2) and a final pressure ramp was constructed to reveal the passive diameter of the vessel at each pressure step. Myogenic reactivity is reported as the difference between passive and active diameters as a percentage of maximum passive diameter:

$$\% \text{ myogenic tone} = \frac{\text{passive diameter} - \text{active diameter}}{\text{passive diameter}} \cdot 100\%$$

2.6 Genotyping

The genotype of individual rats bred from the WKY-Gja5^{em1M_{cwi}} strain was determined prior to their experimental use, through the following procedure.

2.6.1 DNA extraction

Ear notch samples collected by HSLAS staff were placed in an alkaline lysis reagent (pH ~12) containing (mM): NaOH (25), and Na₂-EDTA·2H₂O (0.2). Samples were heated at 95°C for one hour, after which an equal volume of neutralization buffer (pH ~5) was added, containing (mM): Tris-HCl (40). Samples were then cooled to 4°C and DNA concentrations were measured using a NanoDrop ND-1000 spectrophotometer (Thermo Fisher Scientific; Waltham, USA).

2.6.2 Polymerase chain reaction

PCR was performed for each sample at a 25 µL reaction volume in an ICycler thermocycler (Bio-Rad; Hercules, USA). Each reaction contained: 12.5 µL 2×Taq FroggaMix (FroggaBio; Concord, Canada), 6.5 µL PCR grade water (FroggaBio), 0.5 µM *Gja5* forward primer (Integrated DNA Technologies; Coralville, USA), 0.5 µM *Gja5* reverse primer (Integrated DNA Technologies) and 1 µL extracted DNA from sample. PCR cycling conditions were: 94°C for 15 minutes; 30 cycles of 94°C for 1 minute, 68°C for 30 seconds, and 72°C for 1 minute; 72°C for 10 minutes; and 4°C hold.

2.6.3 Gel electrophoresis

In order to confirm that PCR yielded the desired product, PCR reactions were run by electrophoresis on a 1.5% agarose gel containing ethidium bromide and visualized under ultraviolet light.

2.6.4 PCR product extraction

The PCR product was purified using a PCR cleanup kit (TruIn Science; Edmonton, Canada) according to the manufacturer's protocol. The final DNA concentration of the purified product was measured using a NanoDrop ND-1000 spectrophotometer (Thermo Fisher Scientific) as described in §2.6.1.

2.6.5 DNA sequencing and analysis

Samples were prepared for sequencing as 10 μL aliquots containing approximately 10-15 $\text{ng}\cdot\mu\text{L}^{-1}$ DNA from the purified PCR product and 0.25 μM *Gja5* forward primer (Integrated DNA Technologies). Sequencing reactions were performed in a 3730 Genetic Analyzer (Applied Biosystems; Foster City, USA) at the University of Alberta's Molecular Biology Services Unit (MBSU) by MBSU staff. Data files were analysed in SnapGene Viewer Version 6.2.2 (Dotmatrix; Boston, USA). At coding position 25, samples found to have a guanine base were considered WT; samples found to have a thymine base were considered KO; and samples in which both guanine and thymine bases were detected were considered HET.

2.6.6 Primers for PCR and sequencing

Gja5 forward and reverse primers were manufactured by Integrated DNA Technologies (Coralville, USA) and contained the sequences 5'-TGGATCAGTGGTCCAGAGCATGATG-3', and 5'-GCGTGGCCCATGTACACCAGAGAT-3', respectively.

2.7 Quantitative reverse-transcription PCR (RT-qPCR)

Expression levels of mRNA coding for TRPC6, TRPM4 and IK_{Ca} in mesenteric arteries from male Sprague-Dawley rats and Cx37, Cx40 and Cx43 in mesenteric arteries from male and female Cx40 WT, HET and KO rats were measured using real-time RT-qPCR. Results represent arteries from n different rats, with each measurement performed in triplicate.

2.7.1 RNA extraction and cDNA synthesis

Isolated second- and third-order mesenteric arteries were stored at -80°C until extraction. Arteries were placed in QIAzol Lysis Reagent (QIAGEN Cat. No. 79306) and homogenized using a TissueLyser II (QIAGEN). 100 μL chloroform (Sigma-Aldrich; St. Louis, USA) was added to each sample. Total RNA was extracted from homogenates using the RNeasy[®] Micro Kit (QIAGEN

Cat. No. 74004) according to the manufacturer's protocol. RNA concentration was measured using a NanoDrop ND-1000 spectrophotometer (Thermo Fisher Scientific). For each sample, 250 ng of extracted RNA was used to synthesize cDNA using the QuantiTect Reverse Transcription Kit (QIAGEN Cat. No. 205313) according to the manufacturer's protocol. cDNA samples were diluted 1:5 in nuclease-free water and stored at -20°C.

2.7.2 Sample preparation and RT-qPCR

RT-qPCR experiments were performed using SYBR green reagents. Reactions were performed in a total volume of 10 µL containing: 5 µL SYBR Green PCR Master Mix (Applied Biosystems; Thermo Fisher Scientific), 2 µL nuclease-free water, 0.5 µL forward primer, 0.5 µL reverse primer and 2 µL cDNA sample. Primers used are listed in **Tables 2.1** and **2.2**. Reactions were carried out in a 7500 Fast & 7500 Real-Time PCR System (Applied Biosystems).

Primers for RT-qPCR (TRP and IK_{Ca} Expression)		
Species-Gene (Product)	Sequence	Manufacturer
Rat-Trpc6 (TRPC6)	F 5'-GCGGCAGACAGTTCTTCGTGAG-3'	Integrated DNA Technologies
	R 5'-CTTCTAGCATCTTCCGCACCACTG-3'	
Rat-Trpm4 (TRPM4)	F 5'-TGC GCGCCGAGATGTAT-3'	Integrated DNA Technologies
	R 5'-AAAGAAGCAGGTCGCTCCAG-3'	
Rat-Kcnn4 (IK _{Ca})	F 5'-ATGCTGCTACGTCTCTAC-3'	Integrated DNA Technologies
	R 5'-GAATCGGACTTGGTTGAG-3'	
Rat-Actb (β-actin)	F 5'-CACCATTGGCAATGAGCGGTTC-3'	Integrated DNA Technologies
	R 5'-AGGTCTTTGCGGATGTCCACGT-3'	

Table 2.1: Forward and reverse primers used for the amplification of *Trpc6*, *Trpm4*, *Kcnn4* and *Actb* in RT-qPCR.

Primers for RT-qPCR (Connexin Expression)		
Species-Gene (Product)	Sequence	Manufacturer
Rat-Gja4 (Cx37)	F 5'-GGTGGCAGAGGACGGTTCGTCT-3'	Integrated DNA Technologies
	R 5'-CCATGGTCCAGCCGTAGAGA-3'	
Rat-Gja5 (Cx40)	F 5'-GGAAAGAGGTGAACGGGAAG-3'	Integrated DNA Technologies
	R 5'-GGGCCTCGAGACATAACAGTT-3'	
Rat-Gja1 (Cx43)	F 5'-TCTGCCTTTCGCTGTAACACT-3'	Integrated DNA Technologies
	R 5'-GGGCACAGACACGAATATGAT-3'	
Rat-Actb (β -actin)	F 5'-AGATTACTGCCCTGGCTCCT-3'	Integrated DNA Technologies
	R 5'-ACTCCTGCTTGCTGATCCAC-3'	

Table 2.2: Forward and reverse primers used for the amplification of *Gja4*, *Gja5*, *Gja1* and *Actb* in RT-qPCR.

mRNA expression of each gene was compared to the expression of reference gene *Actb*. Threshold cycle (C_t) values were obtained for each gene; ΔC_t is the difference between C_t values obtained for the gene of interest and *Actb*, i.e. $\Delta C_t = C_t(\text{gene}) - C_t(\text{Actb})$. Fold-difference is expressed as $2^{-\Delta C_t}$.

2.8 Blood glucose measurement

Random (i.e. non-fasting) blood glucose concentration was measured immediately prior to euthanasia. Blood sample was collected by lateral tail vein prick and glucose concentration was measured using a OneTouch Ultra 2 glucometer (LifeScan Europe; Zug, Switzerland).

2.9 Tail-cuff plethysmography

Systolic blood pressure (BP) of male and female Cx40 rats was measured non-invasively by tail-cuff plethysmography using a CODA high-throughput system (Kent Scientific; Torington, USA)⁸¹³⁻⁸¹⁶. CODA relies upon volume-pressure recording (VPR) to determine BP indirectly by

measuring changes in tail blood volume⁸¹⁴. Rats were placed on a warming platform maintained at 37°C and lightly sedated (1.25% isoflurane in oxygen; 1 L·min⁻¹ via nose-cone). An appropriately sized occlusion tail-cuff and VPR sensor were fitted onto the tail. After an equilibration period of 5 minutes to isoflurane, the CODA system automatically took 20 BP measurements with a 15 second cuff deflation time and 5 seconds between cycles. The first 10 cycles were conducted for the purpose of acclimatization and equilibration, but were not used for data. Systolic BP measurements were taken exclusively from the final 10 cycles. The integrity of systolic BP measurements was determined based upon the successful measurement of diastolic BP and heart rate (HR) during the same cycle. Cycles during which no meaningful diastolic BP or heart rate data could be recorded were discarded. Systolic BP values reported for each rat represent the mean systolic BP value of successful cycles.

2.10 Langendorff heart perfusion

Male and female Cx40 rats were anaesthetized (>100 mg·kg⁻¹ pentobarbital sodium by intraperitoneal injection) and decapitated (§2.2). Hearts were rapidly excised and placed briefly into ice-cold Krebs buffer. Hearts were then cannulated via the ascending aorta, secured with 3-0 surgical silk (Ethicon), and perfused in Langendorff mode⁸¹⁷ with heated (37°C) and gassed (95% O₂ / 5% CO₂) Krebs buffer by a MHRE200 peristaltic pump (Watson-Marlow; Falmouth, UK) at a constant flow rate of 13 mL·min⁻¹. A water-filled latex balloon connected to a pressure transducer was inserted into the left ventricle through an incision in the left atrium. The volume of the balloon was adjusted to achieve a baseline left ventricular end-diastolic pressure (LVEDP) of 18-20 mmHg. Left ventricular pressure and HR were recorded via a PowerLab 2/26 data acquisition system using LabChart 8 software (ADInstruments). Left ventricular developed pressure (LVDP) was calculated as the difference between left ventricular systolic pressure (LVSP) and LVEDP.

HR was automatically calculated in LabChart 8 (ADInstruments) from the wavelength of the cardiac cycle. LVDP, LVEDP and HR were retrieved from the continuous trace at 5 minute intervals for data analysis.

2.10.1 Ischemia/reperfusion protocol

Hearts were perfused under normoxic conditions for 30 minutes to establish baseline pressure and HR. After equilibration, global no-flow ischemia was induced by clamping the aortic inflow line and switching off the pump. The heart was immersed in Krebs buffer in a water-jacketed organ bath maintained at 37°C without gassing. Ischemia was maintained for 15 minutes, followed by a 45 minute period of aerobic reperfusion wherein the pump was restarted and the clamp reopened.

2.11 Mild hypercaloric challenge via high-fat diet

The mildly hypercaloric high-fat diet (HFD) used in this research is based upon a formulation by our collaborator Dr. Ahmed El-Yazbi at Alalamein International University^{473,818,819}. Their HC rat chow was prepared in-house using 8604 Teklad Rodent Diet (Envigo; Madison, USA) as a base, to which they added food grade fructose and hydrogenated vegetable oil, and replaced sodium and potassium by adding NaCl and KCl. The composition of the final product was determined via bomb calorimetry and was found to comprise by weight 18.1% fat, 15.8% protein, and 46.1% carbohydrates. In calorie content this was 38.7% kcal from fat, 15.6% kcal from protein and 45.7% kcal from carbohydrates, with a total caloric density of 4.035 kcal·g⁻¹.

Based upon this diet formulation from the El-Yazbi research group, an analogous custom diet, TD.210490, was formulated in consultation with Dr. Derek Martin, RD, a laboratory animal nutritionist at Envigo. Teklad custom diet TD.210490 contains (g·kg⁻¹): 8604 Teklad Rodent Diet

(643.85), fructose (200.0), Crisco[®] hydrogenated vegetable shortening (150.0), NaCl (1.05), KCl (3.5), US Rodent Mineral Mix 99115 (0.89), and US Rodent Vitamin Mix 99114 (0.71). The diet contains by weight 17.9% fat, 15.8% protein, and 46.4% carbohydrates. The diet offers 4.1 kcal·g⁻¹ in metabolizable energy^{820,821}, distributed as follows: 39.3% kcal from fat, 15.4% kcal from protein, and 45.3% kcal from digestible carbohydrates. The chow was mixed, pelleted and irradiated to order by Envigo. Throughout this thesis, the term HFD will refer to Teklad custom diet TD.210490.

The term “control diet” will refer to one of two standard rodent diets: 5L0D PicoLab[®] Laboratory Rodent Diet (LabDiet; Richmond, USA) was used until March 2023, after which a similar diet, 5053 PicoLab[®] Rodent Diet 20 (LabDiet), was used instead due to low availability of 5L0D. 5L0D offers 2.91 kcal·g⁻¹ in metabolizable energy and contains by weight (calorie content): 5.0% fat (13.4% kcal), 25.0% protein (29.8% kcal) and 47.5% digestible carbohydrates (56.7% kcal). 5053 offers 3.03 kcal·g⁻¹ in metabolizable energy and contains by weight (calorie content): 5.0% fat (13.1% kcal), 21.0% protein (24.5% kcal) and 53.4% digestible carbohydrates (62.3% kcal). Detailed nutritional information for the 5L0D, 5053, and TD.210490 diets may be found in **Appendix A (Table A.1)**.

Male and female Cx40 rats were divided into two groups: 1) rats fed with control chow for 6 months and 2) rats fed with control chow for 3 months followed by HFD chow for 3 months before euthanasia and experimental use (§2.2).

2.12 Drugs and chemicals

Salts such as those used in the preparation Krebs buffer were purchased from Fisher Scientific or from Sigma-Aldrich. All other chemicals and their mechanisms of action, solvents,

and manufacturers may be found in **Table 2.3** below. Experimental concentrations were derived from accepted literature values.

Name	Mechanism of Action	Solvent	Experimental Concentration	Manufacturer
Acetylcholine (ACh)	Muscarinic agonist ⁸²²⁻⁸²⁴	Water	1 nM to 10 μ M	Sigma-Aldrich
Apamin	SK _{Ca} channel inhibitor ⁸²⁵	Water	50 nM	Tocris
Isoproterenol (ISO)	β -adrenoceptor agonist ⁸²⁶⁻⁸²⁹	Water	10 μ M	Sigma-Aldrich
N^G-nitro-L-arginine methyl ester hydrochloride (L-NAME)	NOS inhibitor ^{622,830,831}	Water	100 μ M	Sigma-Aldrich
Methoxamine (MOX)	α_1 -adrenoceptor agonist ^{832,833}	Water	1 μ M	Sigma-Aldrich
Nifedipine	LTCC ^{266,834-836} and TTCC ²⁹¹⁻²⁹³ inhibitor	DMSO	1 μ M to 10 μ M	Sigma-Aldrich
4-[[3-(Trifluoromethyl)phenyl]methyl]-2H-1,4-benzothiazin-3(4H)-one (NS6180)	IK _{Ca} channel inhibitor ⁶⁸⁴	DMSO	1 μ M	Tocris
9-Phenanthrol	TRPM4 channel inhibitor ^{837,838}	DMSO	1 μ M to 20 μ M	Sigma-Aldrich
Phenylephrine (PE)	α_1 -adrenoceptor agonist ^{833,839-842}	Water	1 nM to 100 μ M	Sigma-Aldrich
Prazosin	α_1 -adrenoceptor antagonist ⁸⁴²⁻⁸⁴⁴	Water	0.1 μ M to 1 μ M	Tocris
1-[(2-Chlorophenyl)diphenylmethyl]-1H-pyrazole (TRAM-34)	IK _{Ca} channel inhibitor ^{681,682}	DMSO	1 μ M	Cayman Chemical
(5Z)-7-[(1R,4S,5S,6R)-6-[(1E,3S)-3-Hydroxy-1-octen-1-yl]-2-oxabicyclo[2.2.1]hept-5-yl]-5-heptenoic acid (U46619)	TXA ₂ receptor agonist ⁸⁴⁵	DMSO	1 nM to 100 μ M	Cayman Chemical

Table 2.3: Drugs used in the experiments described in this thesis. For each of these drugs, control experiments were carried out using appropriate concentrations of DMSO.

2.13 Statistical analysis

All statistical analyses were performed using GraphPad Prism 9.5.1 (GraphPad Software; La Jolla, USA). Data are reported as mean \pm SEM (n) where n is the number of animals used. Unless otherwise indicated, responses in the absence and presence of drugs were obtained from the same tissues. Normalized agonist CRCs were fitted to a sigmoidal curve with a variable slope using a four parameter logistic equation. Data from repeated measures (i.e. having two independent variables) were analysed using two-way ANOVA followed by either a Tukey's multiple comparison post-hoc test for three or more experimental groups (e.g. comparing between genotypes), or Šídák method post-hoc test for two experimental groups (e.g. comparing between CD and HFD). Data with one independent variable (e.g. body weight, blood glucose, BP, etc.) were analysed using one-way ANOVA followed by either a Tukey's multiple comparison post-hoc test for three or more experimental groups, or a Šídák's multiple comparison post-hoc test for two experimental groups. $P < 0.05$ was considered to be statically significant.

Chapter 3: TRPM4 blockade impairs myogenic, agonist-induced, and nerve-evoked vasoconstriction independent of IK_{Ca}

3.1 Introduction

As discussed in §1.3.4, myogenic reactivity is a crucial vascular mechanism underlying the autoregulation of blood flow in response to changes in blood pressure⁴⁷⁴⁻⁴⁷⁶. The myogenic response is initiated when an increase in transmural pressure in resistance arteries causes membrane depolarization in VSMCs, leading to increased $[Ca^{2+}]_i$ through VOCC activation, and subsequently causing activation of MLCK, crossbridge cycling, and vasoconstriction. The mechanism responsible for linking increased transmural pressure to a depolarization of smooth muscle membrane potential is believed to be an as-yet unidentified mechanosensor on smooth muscle cells⁴⁶⁵. Several candidates for this linking mechanism have emerged, including integrins⁸⁴⁶, GPCRs⁸⁴⁷, and TRP channels such as TRPM4 and TRPC6^{341,342}. Recent studies suggest that TRP channels themselves are not direct mechanosensors^{338,342,496-498}; however, several TRP channels have been shown to be necessary for mechanically-induced cation entry in VSMCs^{314,499}. It has recently been shown in rat cerebral arteries that TRPM4 activity depends upon the activation of PLC³⁴² downstream from $G_{q/11}$ PCRs such as the AT_1R , which may be directly mechanosensitive⁸⁴⁸⁻⁸⁵⁰.

A large portion of the literature investigating the role of TRPM4 in the myogenic response has relied upon use of the small-molecule TRPM4 inhibitor, 9-phenanthrol^{214,215,500,501,504,505,851}. For example, in rat cerebral, mesenteric, and skeletal muscle arteries, application of 9-phenanthrol was shown to eliminate pressure-induced depolarization of VSMCs and abolish the myogenic response^{500,501}. In cerebral parenchymal arterioles from rats, 9-phenanthrol was found to partially inhibit vasoconstriction evoked by the selective $P2Y_4$ and $P2Y_6$ receptor agonists, UTP γ S and UDP, respectively⁵⁰⁴. $P2Y$ receptors are $G_{q/11}$ PCRs, thus the suggestion that $P2Y$ activity is

coupled to TRPM4 activity is consistent with the finding that PLC is necessary for TRPM4-mediated myogenic constriction³⁴². 9-phenanthrol has also been used to examine the role of TRPM4 in cardiovascular functions other than myogenic tone; for instance, Hurley *et al.* (2023) demonstrate that TRPM4 is abundantly expressed in rat Purkinje fibres, and that the application of 9-phenanthrol to Langendorff perfused rat hearts reduces the frequency of ectopic arrhythmias⁸⁵². Most recently, 9-phenanthrol has also been investigated for therapeutic use *in vivo*. Administration of 9-phenanthrol (70 $\mu\text{g}\cdot\text{kg}^{-1}$) was shown to attenuate cerebral edema in a rat model of induced traumatic brain injury⁸⁵³. The authors attribute this effect to the inhibition of Na^+ influx in neurovascular ECs and SMCs, and reduced expression and activity of matrix metalloproteinase-9 (MMP-9) which is able to degrade the blood brain barrier.

Since its action as a TRPM4 inhibitor was discovered in 2008⁸³⁷, the pharmacological properties of 9-phenanthrol have been thoroughly investigated (reviewed by Guinamard *et al.*, 2014)⁸³⁸. 9-phenanthrol inhibits TRPM4 with an IC_{50} of approximately 17 μM , but does not affect its closest relative, TRPM5⁸³⁷. It has also shown no inhibitory effect on several other TRP channels including TRPC3, TRPC6 and TRPM7^{500,854}. Thus, 9-phenanthrol was believed to be quite selective for TRPM4. However, recent studies propose that 9-phenanthrol may have off-target actions as an inhibitor of K_{IR} channels⁸⁵⁵, an inhibitor of transmembrane protein 16A (TMEM16A; a Cl_{Ca} channel)⁸⁵⁶, and an activator of IK_{Ca} channels⁸⁵⁷. These findings have raised doubts about the usefulness of 9-phenanthrol as a pharmacological tool for investigating the role of TRPM4. The action of 9-phenanthrol at K_{IR} is controversial: Veress *et al.* (2018) reported that transient outward, rapid delayed rectifier, and inward rectifier K^+ currents were suppressed by 9-phenanthrol at 10 and 30 μM in canine ventricular myocytes⁸⁵⁵. However, this is contradicted by previous studies describing no effect of 9-phenanthrol on global K^+ currents in rat cerebral artery VSMCs

or mouse ventricular cardiomyocytes at concentrations under 100 $\mu\text{M}^{500,858}$. Currently, no evidence contradicts the findings that 9-phenanthrol activates IK_{Ca} and inhibits TMEM16A, so it is unclear whether these mechanisms contribute to 9-phenanthrol's inhibition of myogenic reactivity. Thus, I have tested the hypothesis that *9-phenanthrol's primary mechanism of action is TRPM4 inhibition rather than IK_{Ca} activation.*

3.2 Methods

A full description of methods is provided in **Chapter 2**. As stated in §2.2, experiments in this chapter use male (250-300 g) and female (175-225 g) Sprague-Dawley rats.

3.3 Results

3.3.1 TRPM4 mRNA is highly expressed in rat mesenteric arteries

mRNA encoding two TRP channels, TRPC6 and TRPM4, as well as IK_{Ca} channels, was measured in isolated mesenteric arteries from male Sprague-Dawley rats using quantitative reverse-transcription PCR (RT-qPCR; **Figure 3.1**). mRNA expression of *Trpc6*, *Trpm4* and *Kcnn4* was compared to the expression of *Actb* (reference gene encoding β -actin). Fold-difference is expressed as $2^{-\Delta\text{C}_t}$, where $\Delta\text{C}_t = \text{C}_t(\text{gene}) - \text{C}_t(\text{Actb})$. TRPM4 and IK_{Ca} mRNA were both detected. Relative expression of TRPM4 is significantly greater than relative expression of TRPC6 ($P < 0.05$).

3.3.2 Characterization of nerve-evoked vasoconstriction in the rat perfused mesenteric vascular bed

Nerve-evoked vasoconstriction in the rat perfused mesenteric vascular bed was characterized using tissue from male Sprague-Dawley rats. Pressure responses were shown to be frequency-dependent and time-independent ($P > 0.05$, **Figure 3.2a**). Pressure responses were abolished in the presence of the α_1 -adrenoceptor antagonist prazosin (0.1 μM), indicating that electric stimulus-evoked vasoconstriction in the perfused mesenteric bed is attributable to the

action of NA at α_1 -adrenoceptors on VSMCs ($P < 0.05$, **Figure 3.2b**). This experiment was performed in order to demonstrate that pressure responses to electrical stimulation were mediated by neurotransmitter release from perivascular nerves rather than direct electrical stimulation of vascular smooth muscle.

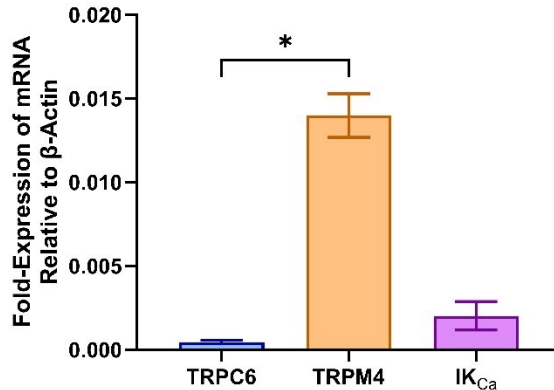


Figure 3.1: mRNA encoding TRPM4 is expressed at higher levels than TRPC6 or IK_{Ca} in rat mesenteric arteries. RT-qPCR results showing expression of mRNA coding for TRPC6, TRPM4 and IK_{Ca} relative to β -actin in mesenteric arteries from male Sprague-Dawley rats. Data are presented as mean \pm SEM ($n = 4$). * denotes $P < 0.05$ between mRNA products; one-way ANOVA. *Data contributed by Ran Wei.*

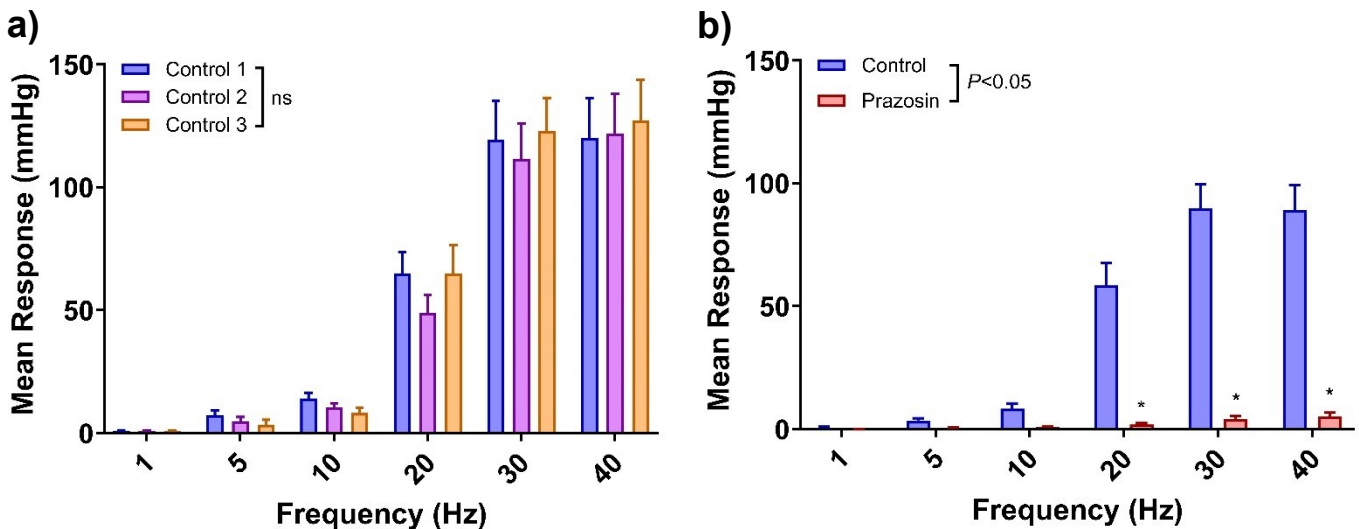


Figure 3.2: Electric stimulus-evoked vasoconstriction in the rat perfused mesenteric vascular bed is frequency-dependent, time-independent, and is mediated by α_1 -adrenoceptors. Frequency-response relationships constructed using endothelium-intact mesenteric beds from male Sprague-Dawley rats perfused at a constant flow rate **a**) in time controls ($n = 5$) and **b**) in the absence and presence of prazosin ($0.1 \mu\text{M}$; $n = 5$). Data are presented as mean \pm SEM. * denotes $P < 0.05$ from control; two-way ANOVA. *Data contributed by Paul Kerr, Stephanie Lunn and Michael Chen.*

3.3.3 9-Phenanthrol limits nerve-evoked vasoconstriction in a dose-dependent manner without acting at IK_{Ca} channels

Increases in perfusion pressure were measured in response to electrical stimulations over a range of frequencies from 1-40 Hz in the absence and presence of 9-phenanthrol at two different concentrations (5 μ M, 10 μ M; **Figure 3.3**). In the presence of 5 μ M 9-phenanthrol, pressure responses to the 15, 20, 30 and 40 Hz stimulations were significantly lower than control ($P < 0.05$). Upon increasing the concentration of 9-phenanthrol to 10 μ M, the responses decreased further, with significance from control at 15, 20, 30 and 40 Hz, and significance from 5 μ M 9-phenanthrol at 20, 30 and 40 Hz ($P < 0.05$). These results demonstrate that 9-phenanthrol limits nerve-evoked vasoconstriction in a dose-dependent manner.

Experimental concentrations of 9-phenanthrol vary from approximately 1 to 100 μ M throughout the literature; however, many researchers have used 10 μ M as it approximates the IC_{50} of 9-phenanthrol at TRPM4^{501,504,837,855,856,858,859}. Thus, from this point onward, 9-phenanthrol was applied at 10 μ M when used in single concentrations. Using the perfused mesenteric vascular bed, I next assessed whether activation of IK_{Ca} contributes to 9-phenanthrol's limitation of nerve-evoked vasoconstriction (**Figure 3.4**). Frequency-response curves were constructed in the absence of drugs, in the presence of 9-phenanthrol (10 μ M), and in the presence of 9-phenanthrol and the IK_{Ca} blocker NS6180 (1 μ M). Control responses were significantly higher than those in the presence of 9-phenanthrol with and without NS6180 ($P < 0.05$). Meanwhile, pressure responses were nearly identical between treatment with 9-phenanthrol alone and treatment with 9-phenanthrol + NS6180 ($P > 0.05$). Thus, blocking IK_{Ca} channels has no effect on the action of 9-phenanthrol in this preparation, suggesting that 9-phenanthrol's inhibition of constriction is not due to putative off-target activation of IK_{Ca} .

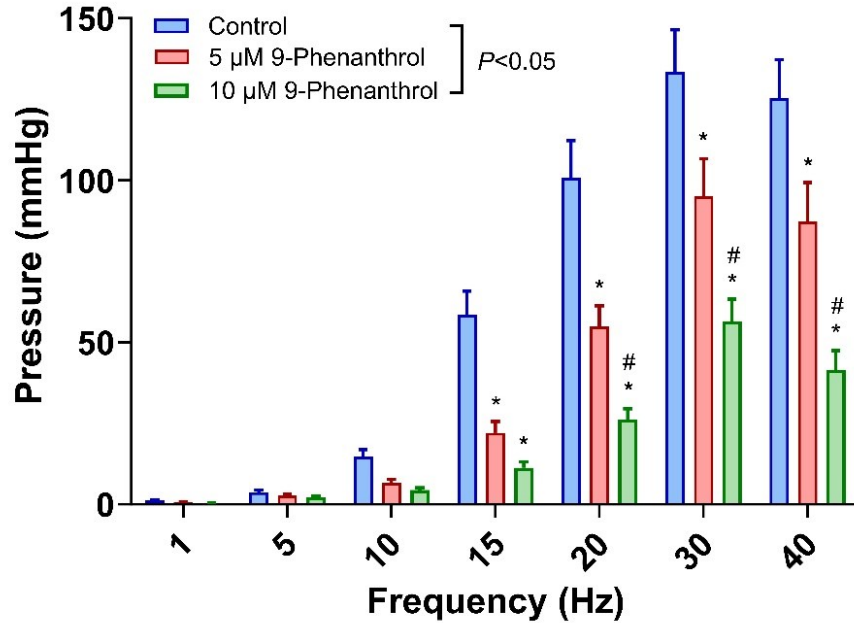


Figure 3.3: 9-Phenanthrol produces concentration-dependent inhibition of nerve-evoked vasoconstriction. Frequency-response relationships constructed using perfused mesenteric vascular beds from male Sprague-Dawley rats in the absence and presence of 9-phenanthrol (5 μM or 10 μM). Data are presented as mean \pm SEM ($n = 12$). * denotes $P < 0.05$ from control and # denotes $P < 0.05$ from 5 μM 9-phenanthrol; two-way ANOVA. *Data contributed by Nicholas Fialka and Michal Shaposhnikov.*

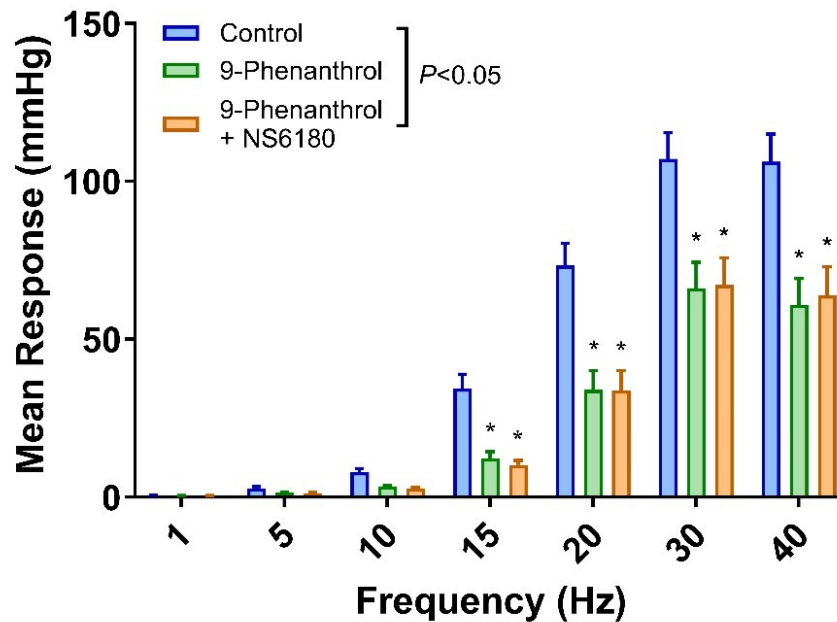


Figure 3.4: Inhibition of nerve-evoked vasoconstriction by 9-phenanthrol is not mediated by IK_{Ca} . Frequency-response relationships constructed using perfused mesenteric vascular beds from male Sprague-Dawley rats in the absence and presence of 9-phenanthrol (10 μM) and NS6180 (1 μM). Data are presented as mean \pm SEM ($n = 5$). * denotes $P < 0.05$ from control; two-way ANOVA.

A discrepancy exists between **Figures 3.3** and **3.4**: in **Figure 3.3**, 10 μM 9-phenanthrol induces a 58% reduction in the response at 30 Hz versus control, whereas in **Figure 3.4**, 10 μM 9-phenanthrol induces only a 38% reduction in the response at 30 Hz versus control. The cause for this is unclear; a possible explanation is that the sets of experiments were performed in different months, as seasonal changes in vascular function have been reported in the literature⁸⁶⁰⁻⁸⁶².

3.3.4 Characterization of pressure-evoked vasoconstriction in isolated mesenteric arteries using pressure myography

Pressure myography without luminal flow was characterized using isolated segments of fourth- to sixth-order mesenteric arteries from male Sprague-Dawley rats. Pressure-diameter relationships were constructed by measuring internal diameter of artery segments in response to ramps of intraluminal pressure from 20-120 mmHg in 20 mmHg increments. Myogenic reactivity was time-independent and not affected by a vehicle control of dimethyl sulfoxide (DMSO; **Figure 3.5a** and **b**). Under control conditions, arteries maintained their diameter across the range of pressures; replacing the bath of the myograph chamber with Ca^{2+} -free Krebs buffer revealed the passive diameter of the vessel at each pressure step. At an intraluminal pressure of 80 mmHg, mean diameters in successive time controls were $225.3 \pm 19.3 \mu\text{m}$ ($n = 6$), $226.2 \pm 18.4 \mu\text{m}$ ($n = 6$) and $202.4 \pm 18.1 \mu\text{m}$ ($n = 5$; **Figure 3.5a**; $P > 0.05$). Many of the pharmacological reagents in this research are dissolved in DMSO, thus a vehicle control was performed (**Figure 3.5b**). At the 80 mmHg pressure step, the mean arterial diameters before and after the addition of 20 μL of DMSO to the 7 mL myograph chamber (0.28 vol%) were $241.2 \pm 18.9 \mu\text{m}$ ($n = 4$) and $220.5 \pm 24.2 \mu\text{m}$ ($n = 4$; $P > 0.05$), respectively. Next, myogenic reactivity was shown to be endothelium-independent, as the pressure-diameter relationships constructed in endothelium-intact and endothelium-denuded arteries were very similar (**Figure 3.6**). No significant differences were observed in the active and passive diameters between endothelium-intact and -denuded arteries;

for example, at the 80 mmHg pressure step, the mean diameters of endothelium-intact and -denuded arteries were $230.4 \pm 13.4 \mu\text{m}$ ($n = 11$) and $233.5 \pm 10.7 \mu\text{m}$ ($n = 6$; $P > 0.05$; Student's t-test), respectively. The passive diameters in Ca^{2+} -free Krebs buffer were $322.9 \pm 12.7 \mu\text{m}$ ($n = 11$) and $310.7 \pm 8.0 \mu\text{m}$ ($n = 6$; $P > 0.05$; Student's t-test), respectively.

3.3.5 9-Phenanthrol abolishes myogenic tone without acting at IK_{Ca} channels

Segments of fourth- to sixth-order mesenteric arteries were isolated from male Sprague-Dawley rats and mounted on glass canulae in a pressure myograph. Pressure-diameter relationships were constructed by measuring the internal diameter of the artery in response to ramps of intraluminal pressure from 20-120 mmHg in 20 mmHg increments. Pressure ramps were performed in the absence and presence of 9-phenanthrol (10 μM), NS6180 (1 μM), and TRAM-34 (1 μM), and the passive diameter of the vessel was revealed by performing a pressure ramp in the absence of extracellular Ca^{2+} (**Figure 3.7**). Under control conditions, arteries demonstrated pressure-evoked vasoconstriction, wherein the active diameter was significantly lower than the passive diameter (Ca^{2+} -free) at intraluminal pressures of 60 mmHg and greater ($P < 0.05$, **Figure 3.7a**). The addition of 9-phenanthrol abolished pressure-evoked vasoconstriction, with no significant differences from passive diameter at any pressure step ($P > 0.05$). Subjecting vessels to either NS6180 (**Figure 3.7b**) or TRAM-34 (**Figure 3.7c**) in addition to 9-phenanthrol did not reverse the effect of 9-phenanthrol on pressure-evoked vasoconstriction. These data demonstrate that 9-phenanthrol abolishes myogenic vasoconstriction through an IK_{Ca} -independent mechanism.

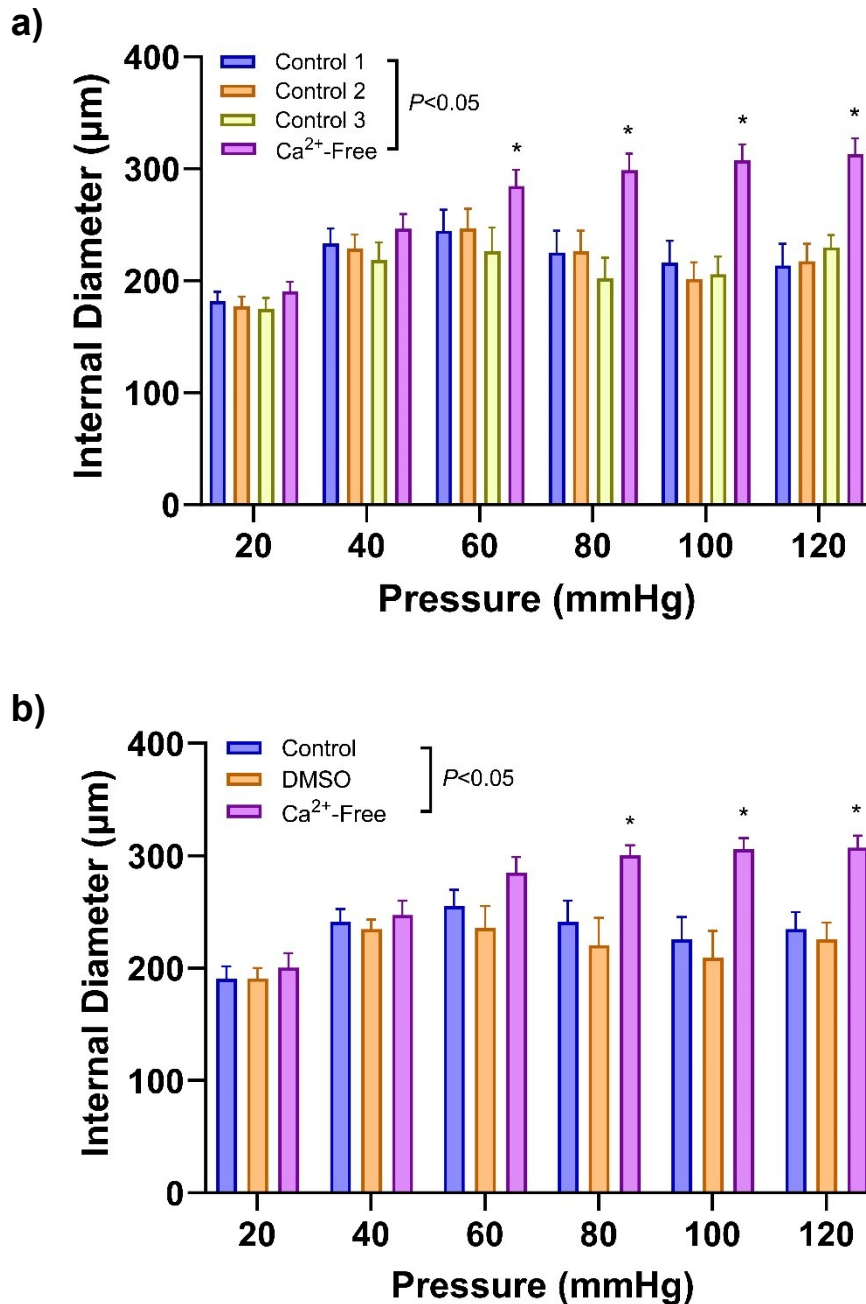


Figure 3.5: Myogenic reactivity of isolated rat mesenteric arteries is time-independent and is not affected by DMSO. Isolated third- and fourth-order mesenteric arteries from male Sprague-Dawley rats were mounted in a pressure myograph and used to construct pressure-diameter relationships. Diameter was measured over pressure ramps from 20-120 mmHg in 20 mmHg increments. Mean internal diameters in response to stepwise increases in intravascular pressure **a)** in time controls ($n = 5-6$) and **b)** before and after the addition of DMSO (0.28 vol%; $n = 4$). Data are presented as mean \pm SEM. * denotes $P < 0.05$ from control; two-way ANOVA. *Data contributed by Ran Wei.*

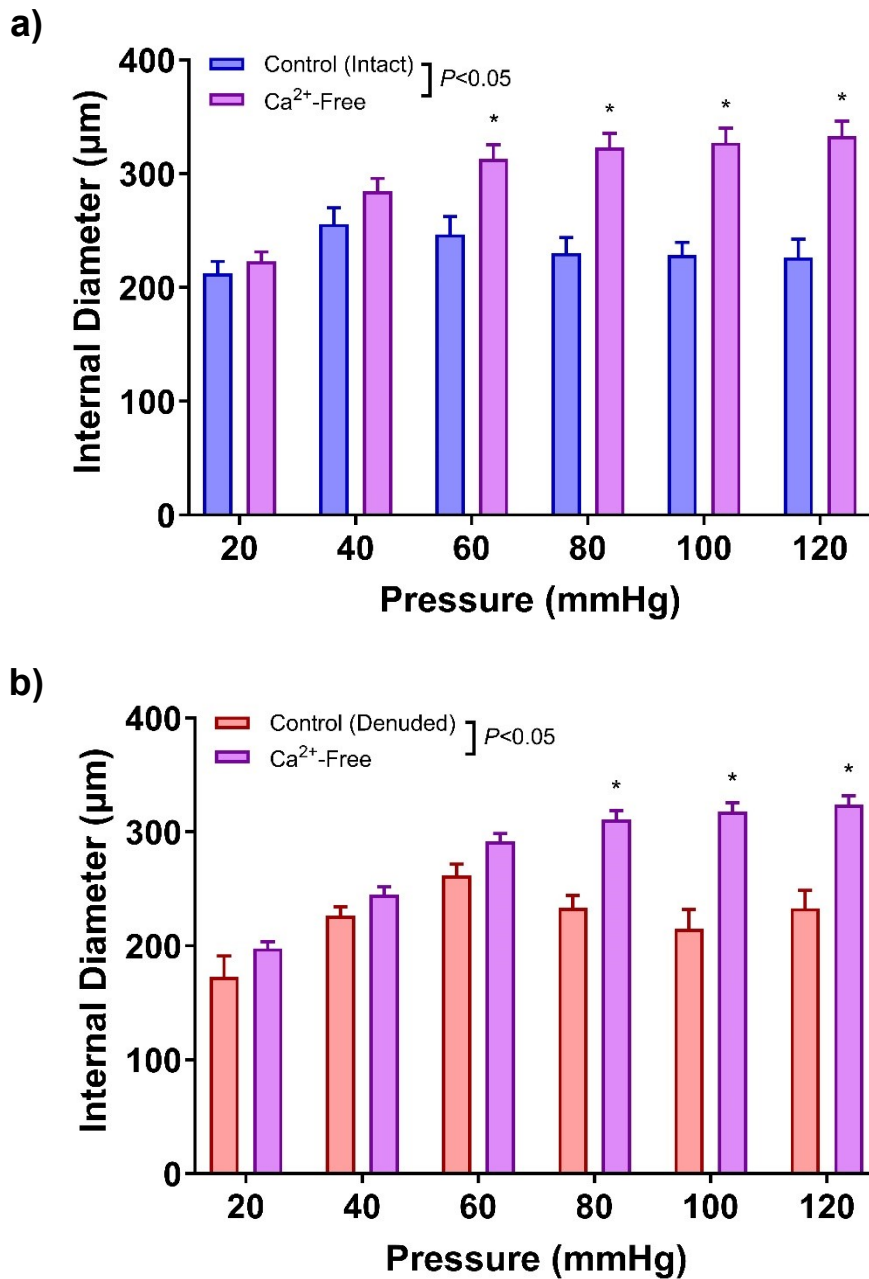


Figure 3.6: Myogenic reactivity of isolated rat mesenteric arteries is endothelium-independent. Isolated third- and fourth-order endothelium-intact and -denuded mesenteric arteries from male Sprague-Dawley rats were mounted in a pressure myograph and used to construct pressure-diameter relationships. Mean internal diameters in response to stepwise increases in intravascular pressure in **a)** endothelium-intact ($n = 11$) and **b)** endothelium-denuded ($n = 6$) arteries in the absence and presence of Ca^{2+} . Data are presented as mean \pm SEM. * denotes $P < 0.05$ from control; two-way ANOVA. *Data contributed by Ran Wei.*

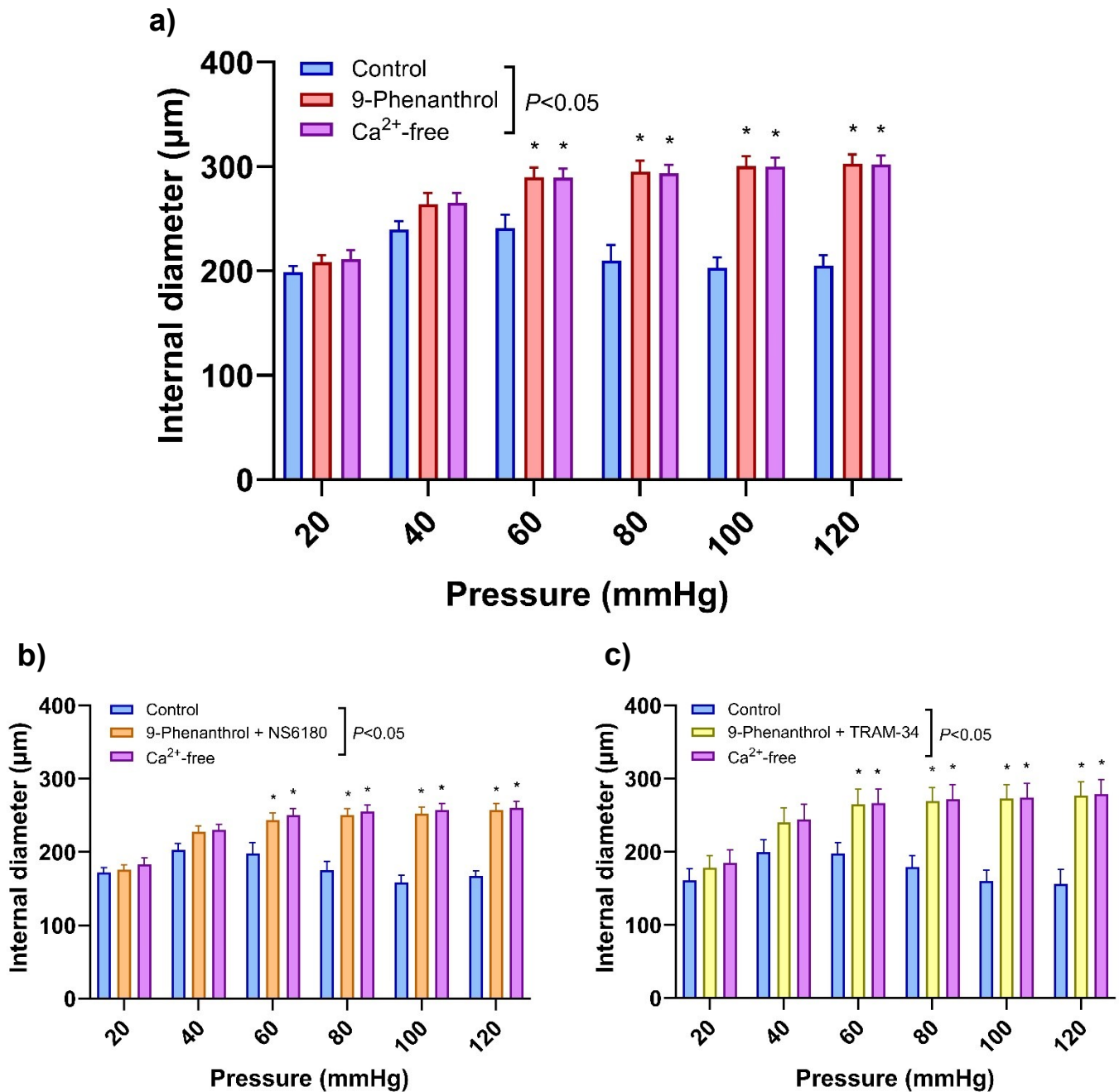


Figure 3.7: 9-Phenanthrol abolishes pressure-evoked vasoconstriction in isolated mesenteric arteries without acting at IK_{Ca} . Pressure myography was used to construct pressure-diameter relationships in isolated fourth- to sixth-order mesenteric arteries from male Sprague-Dawley rats. Pressure ramps were performed in the absence and presence of **a)** 9-phenanthrol (10 μ M; $n = 5$), **b)** 9-phenanthrol + NS6180 (1 μ M; $n = 7$), and **c)** 9-phenanthrol + TRAM-34 (1 μ M; $n = 5$). Data are presented as mean \pm SEM. * denotes $P < 0.05$ from control; two-way ANOVA.

3.3.6 9-Phenanthrol induces vasodilation without acting at IK_{Ca} channels

Segments of second- and third-order mesenteric arteries were isolated from male Sprague-Dawley rats and mounted in a wire myograph to measure isometric tension. Arteries were pre-constricted with either PE (3 μ M) or 5-HT (3 μ M) before cumulative concentration-response curves to 9-phenanthrol were constructed from 10 nM to 100 μ M in half-log concentrations, in the presence and absence of NS6180 (1 μ M; **Figure 3.8**). Upon pre-constriction with PE, vessels relaxed to 9-phenanthrol in a sigmoidal, concentration-dependent manner with a $\log EC_{50}$ of -6.31 ± 0.09 M ($n = 6$; **Figure 3.8a**). The addition of NS6180 produced no significant difference from control ($P > 0.05$). In vessels pre-constricted with 5-HT, 9-phenanthrol produced sigmoidal, concentration-dependent relaxation with a $\log EC_{50}$ of -7.11 ± 0.09 M ($n = 5$; **Figure 3.8b**). Again, the addition of NS6180 produced no significant difference from control ($P > 0.05$). However, the control 9-phenanthrol curve after pre-constriction to PE was significantly right-shifted versus the control 9-phenanthrol curve after pre-constriction to 5-HT ($P < 0.05$; two-way ANOVA). Taken together, these results suggest that 9-phenanthrol-induced vasorelaxation is not mediated by IK_{Ca} activation. However, the nature of the vasoconstrictor stimulus does significantly impact the $\log EC_{50}$ of 9-phenanthrol in isolated mesenteric arteries ($P < 0.05$; Student's t-test).

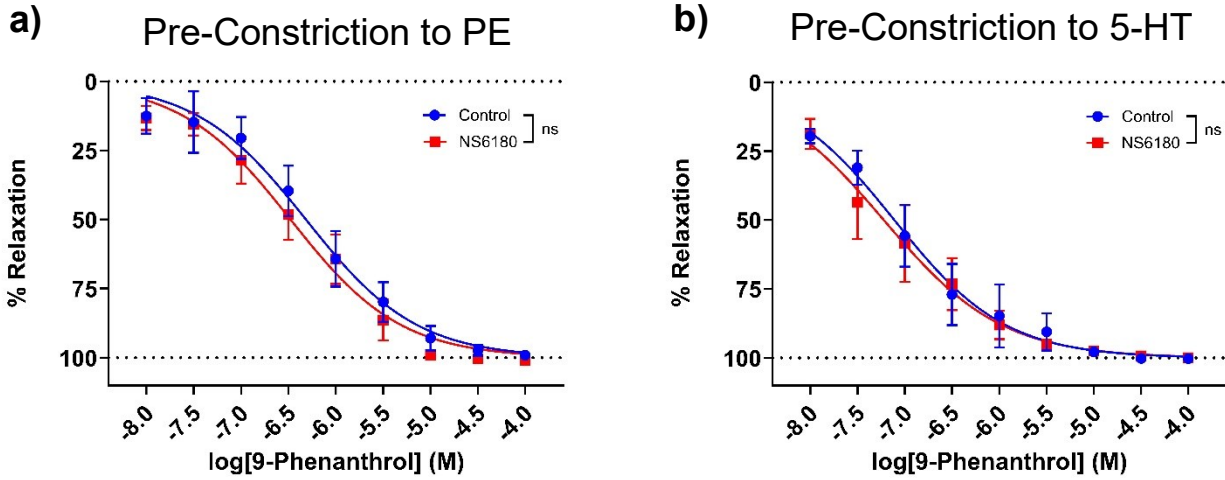


Figure 3.8: 9-Phenanthrol produces concentration-dependent relaxation of isolated mesenteric arteries. Wire myography was used to construct cumulative concentration-response curves to 9-phenanthrol in the absence and presence of NS6180 (1 μ M) using isolated second- and third-order mesenteric arteries from male Sprague-Dawley rats. 9-Phenanthrol was applied after pre-constriction to **a)** PE (3 μ M; $n = 6$) or **b)** 5-HT (3 μ M; $n = 5$). Data are presented as mean \pm SEM. $P > 0.05$; two-way ANOVA. *Data contributed by Alexia Maheux.*

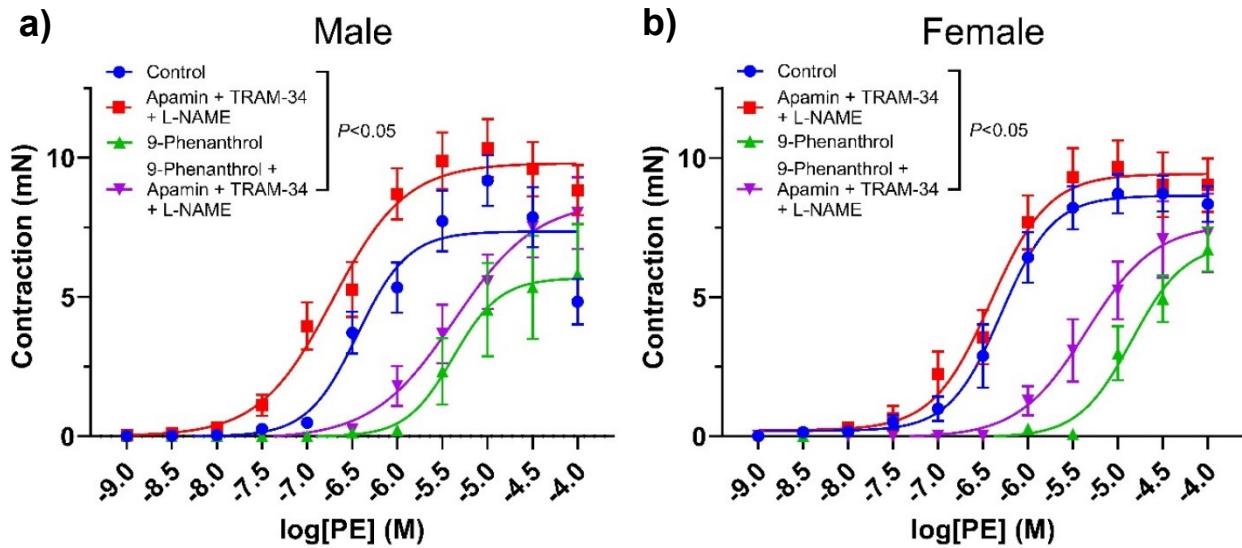


Figure 3.9: 9-Phenanthrol inhibits PE-induced vasoconstriction of isolated mesenteric arteries without affecting EDH or NO synthesis. Wire myography was used to construct cumulative concentration-response curves to PE in the absence and presence of 9-phenanthrol (10 μ M), apamin (50 nM), TRAM-34 (1 μ M), and L-NAME (100 μ M) using isolated second- and third-order mesenteric arteries from **a)** male ($n = 11-16$) and **b)** female ($n = 6-7$) Sprague-Dawley rats. Curves are unpaired and responses are expressed as magnitude of contraction (mN). Data are presented as mean \pm SEM. $P < 0.05$; two-way ANOVA. Significance between pairs of treatments at specific concentrations of PE were determined using Tukey's multiple comparisons, but omitted from graphs for clarity. *Data contributed by Sufyan Malik and Caleb McInroy.*

3.3.7 9-Phenanthrol limits phenylephrine-induced vasoconstriction

Second- and third-order mesenteric arteries from male and female Sprague-Dawley rats were mounted in a wire myograph and used to construct cumulative concentration-response curves to PE from 1 nM to 100 μ M in half-log concentrations, in the absence and presence of 9-phenanthrol (10 μ M), apamin (50 nM), TRAM-34 (1 μ M), and L-NAME (100 μ M; **Figure 3.9**). For this figure only, responses have not been normalized to maximum constrictions and are instead expressed as magnitude of constriction in mN. In both males (**Figure 3.9a**) and females (**Figure 3.9b**), there was overall significance of the drug treatment ($P < 0.05$); however, individual points of significance between groups using Tukey's multiple comparisons are omitted for clarity. In males, all three drug treatments were significantly different from control: administration of apamin + TRAM-34 + L-NAME caused significantly greater constriction than control, demonstrating that EDH and NO synthesis limit vasoconstriction to PE under control conditions. Conversely, administration of 9-phenanthrol alone or 9-phenanthrol + apamin + TRAM-34 + L-NAME caused significantly lower constriction than control ($P < 0.05$). The only pair of treatments with no significant differences were 9-phenanthrol alone and 9-phenanthrol + apamin + TRAM-34 + L-NAME ($P > 0.05$). These results suggest that 9-phenanthrol limits PE-induced vasoconstriction, and that EDH and NO synthesis do not meaningfully contribute to 9-phenanthrol's effect. These results were mostly duplicated in arteries from female rats, as either 9-phenanthrol alone or 9-phenanthrol + apamin + TRAM-34 + L-NAME caused significantly lower constriction than control ($P < 0.05$). Additionally, there was again no significant difference between constriction in the presence of 9-phenanthrol alone or 9-phenanthrol + apamin + TRAM-34 + L-NAME ($P > 0.05$), corroborating the idea that 9-phenanthrol does not act by enhancing EDH or NO synthesis. In contrast to the males, however, administration of apamin + TRAM-34 + L-NAME caused no increase from

control ($P>0.05$), suggesting a lower constitutive contribution of EDH and NO in females than in males.

I further investigated the mechanism of 9-phenanthrol's effect on PE-induced vasoconstriction by using mesenteric arteries from male Sprague-Dawley rats to construct cumulative concentration-response curves to PE in the absence and presence of 9-phenanthrol (10 μM), NS6180 (1 μM), and nifedipine (0.3 μM ; **Figure 3.10a**). Like in the previous experiment (**Figure 3.9a**), administration of 9-phenanthrol alone reduced contraction to PE by approximately 50% versus control at the highest concentrations of PE ($P<0.05$). Furthermore, administration of either NS6180 or nifedipine in addition to 9-phenanthrol did not reverse its effect. Applying NS6180 on top of 9-phenanthrol did not cause a significant difference in contraction versus 9-phenanthrol alone ($P>0.05$), showing that 9-phenanthrol's effect is not due to off-target activation of IK_{Ca} . The addition of nifedipine on top of 9-phenanthrol also did not cause a significant difference in contraction from 9-phenanthrol alone ($P>0.05$). Thus, once TRPM4 is blocked, blocking LTCCs produces no further inhibition of PE-induced contraction. This suggests that TRPM4 may be wholly responsible for the SMC depolarization which activates LTCCs. The actions of nifedipine alone were also assessed in mesenteric arteries from male rats: PE curves were constructed in the absence and presence of nifedipine (0.3 μM ; **Figure 3.10b**). Contraction in the presence of nifedipine alone was significantly reduced from control at PE concentrations $\geq 1 \mu\text{M}$ ($P<0.05$). Therefore, inhibition of LTCCs significantly limited PE-induced contraction. Of particular note is the fact that nifedipine alone reduced maximum vasoconstriction to $67.5 \pm 5.8\%$ of control maximum ($n = 5$; **Figure 3.10b**), and 9-phenanthrol alone reduced maximum vasoconstriction to $41.2 \pm 16.7\%$ of control maximum ($n = 6$; **Figure 3.10a**). Although these data sets cannot be directly compared, as they were performed in arteries from two separate groups of

male Sprague-Dawley rats, 9-phenanthrol appears to cause a greater inhibition of constriction than nifedipine. Together, these data suggest that blocking TRPM4 with 9-phenanthrol abolishes depolarization-dependent contraction, whereas blocking LTCCs with nifedipine only partially blocks depolarization-dependent contraction. Thus, there appears to be a component of depolarization-dependent Ca^{2+} -entry which is not mediated by LTCCs.

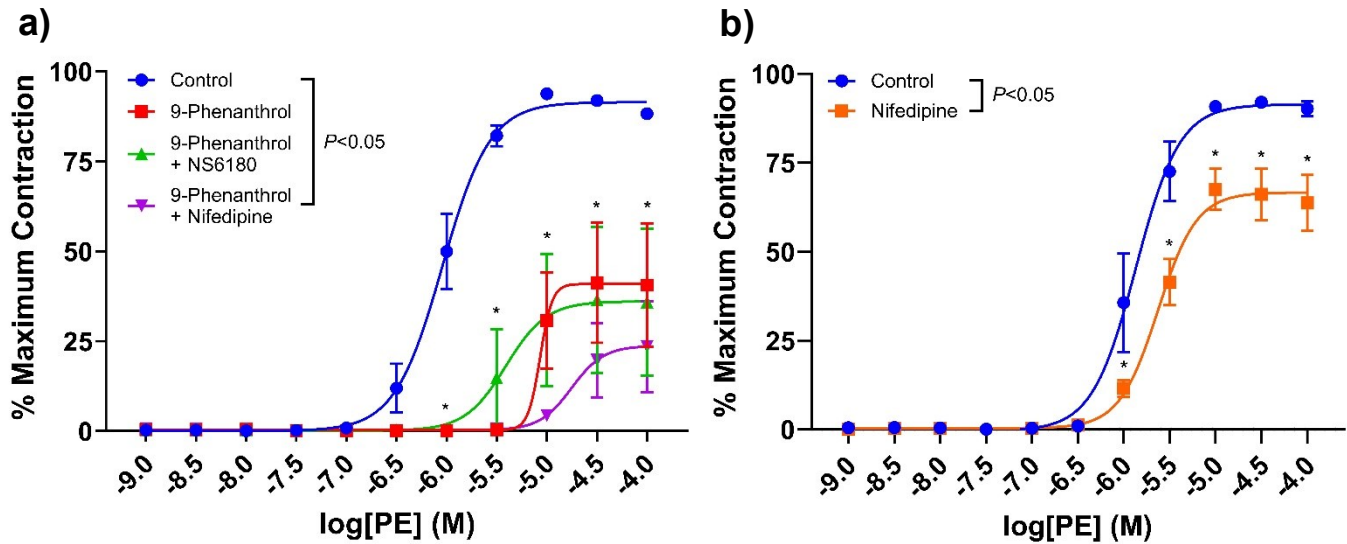


Figure 3.10: 9-Phenanthrol inhibits depolarization-dependent contraction to PE in an IK_{Ca} -independent manner. Isolated second- and third-order mesenteric arteries from male Sprague-Dawley rats were mounted in a wire myograph and used to construct cumulative concentration-response curves to PE **a)** in the absence and presence of 9-phenanthrol (10 μM), NS6180 (1 μM), and nifedipine (0.3 μM ; $n = 5-6$). Concentration-response curves to PE were also performed **b)** in the absence and presence of nifedipine (0.3 μM ; $n = 5$). * denotes $P < 0.05$ from control; two-way ANOVA. Data are presented as mean \pm SEM.

3.4 Discussion

TRPM4 channels serve a crucial role in vasoconstriction by coupling IP_3 -induced Ca^{2+} release from the SR to depolarization and contraction of VSMCs^{214,215}. The putative selective TRPM4 blocker, 9-phenanthrol, has been used since its discovery in 2008 as a pharmacological tool for investigating the physiological function of TRPM4, and is still used for this purpose to date^{501,837,851-853}. The data presented in this chapter support the hypothesis that 9-phenanthrol is

selective for TRPM4 and demonstrate that TRPM4 is a major contributor to agonist- and pressure-evoked vasoconstriction in rat mesenteric resistance arteries.

Although the canonical mechanism of action of 9-phenanthrol is blockade of TRPM4, several studies have raised doubts about the selectivity of the drug. In particular, four recent studies propose problems with 9-phenanthrol as an experimental tool: Veress *et al.* (2018) suggest that it inhibits K_{IR} channels⁸⁵⁵, Arullampalam *et al.* (2021) suggest that it activates murine TRPM4 when applied intracellularly⁸⁶³, Burris *et al.* (2015) suggest that it inhibits the Cl_{Ca} channel TMEM16A⁸⁵⁶, and Garland *et al.* (2015) suggest that it activates IK_{Ca} channels⁸⁵⁷. The action of 9-phenanthrol at K_{IR} is contradicted by other studies describing no effect of 9-phenanthrol on global K^+ currents at concentrations under $100 \mu M$ ^{500,858}. Additionally, the study from Arullampalam *et al.* shows that 9-phenanthrol activates murine TRPM4, but not human TRPM4, when applied intracellularly⁸⁶³. Therefore, this property is species-dependent, and the authors did not examine 9-phenanthrol's effect on rat TRPM4. This result must be taken into consideration, but ultimately is not directly relevant to the present study. However, no evidence has emerged in contradiction of 9-phenanthrol's putative inhibition of TMEM16A or activation of IK_{Ca} . Unfortunately, the quaternary structures of TRPM4, IK_{Ca} , and TMEM16A in the presence of exogenous ligands have not been solved, thus the precise binding sites of respective modulators such as 9-phenanthrol, SKA-31, TMEM16A blocker 2-(4-chloro-2-methylphenoxy)-*N*-[(2-methoxyphenyl)methylideneamino]acetamide (Ani9)⁸⁶⁴⁻⁸⁶⁶, and TMEM16A activator 3,4,5-trimethoxy-*N*-(2-methoxyethyl)-*N*-(4-phenyl-2-thiazolyl)benzamide (E_{act})^{856,866-868} have not been fully elucidated. The binding of 9-phenanthrol to these channels cannot yet be predicted by modelling, therefore the interpretation of functional results is crucial. Throughout this section, I

will address how these two potential off-target mechanisms of 9-phenanthrol's action (i.e. inhibition of TMEM16A and activation of IK_{Ca}) affect the interpretation of my results.

In second- and third-order mesenteric arteries, whole-artery expression of TRPM4 channels was found by RT-qPCR to be significantly greater than expression of either TRPC6 or IK_{Ca} channels. This is consistent with previous reports of TRPM4 expression in both VSMCs^{333,341,501,503,869} and ECs^{302,870-872}. In addition to TRPM4 and IK_{Ca} , I chose to investigate TRPC6 expression due to reports that TRPC6 is a crucial mediator of mechanotransduction pathways, including myogenic vasoconstriction, despite not being a mechanosensor itself^{331,496,549,873}. Studies have shown that knocking down either TRPC6 or TRPM4 reduces myogenic tone by 80-90% in rat cerebral arteries^{332,341}, suggesting either synergistic or serial activation of the channels³⁴². More recently, Nemeth *et al.* (2020) demonstrated that myogenic tone was abolished in isolated middle cerebral arteries from a global, germline TRPC6 KO mouse⁸⁷⁴. It is important to note that all the available studies examining the role of TRPC6 in the myogenic response use cerebral arteries due to the difficulty of recording myogenic vasoconstriction in mesenteric arteries, as I will discuss later in this section. My data show that, in contrast to cerebral arteries, TRPC6 mRNA expression is negligible in mesenteric arteries. Therefore TRPC6 is not a significant contributor to pressure-evoked vasoconstriction in these arteries.

Throughout the following chapters, I will only use TRAM-34 for pharmacological inhibition of IK_{Ca} channels, but within this chapter I have used both TRAM-34 and NS6180. NS6180 was developed more recently than TRAM-34, and was originally thought to block IK_{Ca} with higher selectivity than TRAM-34⁶⁸³. Further study has revealed that NS6180 blocks IK_{Ca} with similar selectivity to TRAM-34, likely at the same binding site^{682,684,685}. Individual experiments

use either TRAM-34 or NS6180, and some experiments were replicated once with each inhibitor in order to assess both. I saw no difference in functional results between experiments using NS6180 and those using TRAM-34. My research, as well as the relevant literature, suggests that TRAM-34 and NS6180 can be used interchangeably^{314,683}.

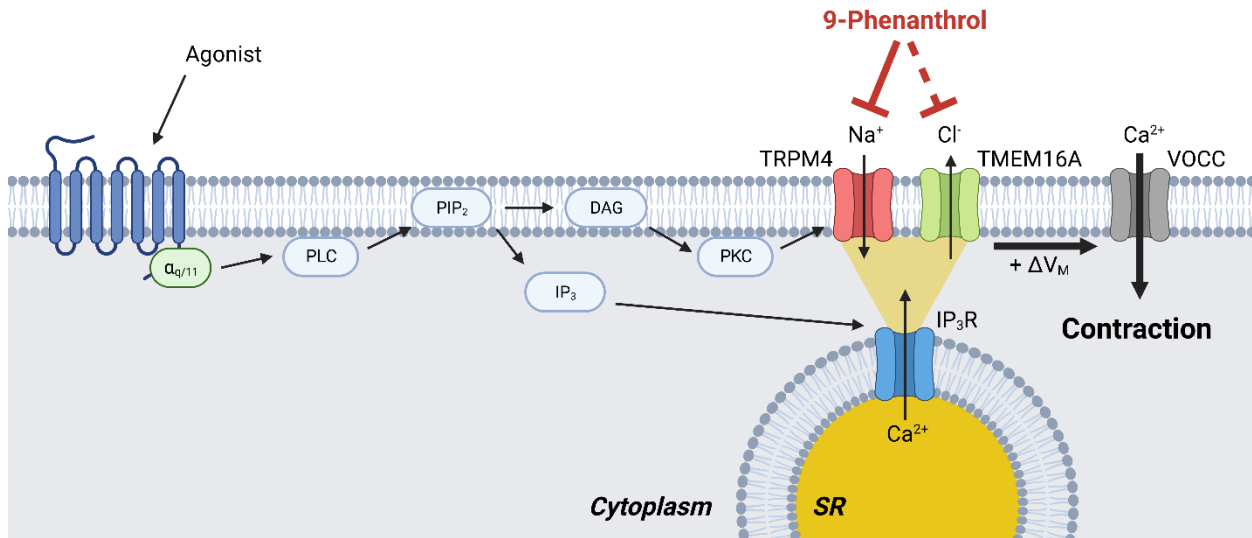


Figure 3.11: Schematic diagram of voltage-dependent vasoconstriction in a vascular smooth muscle cell. In response to $G_{q/11}$ PCR agonists such as NA, PE, or 5-HT, IP_3 production is increased, leading to Ca^{2+} release from the SR. Increased $[Ca^{2+}]_i$ activates TRPM4 and TMEM16A, leading to Na^+ influx and Cl^- efflux, respectively. These both cause depolarization of the membrane potential, activating VOCCs and initiating contraction. In addition to increased IP_3 production, the increase in DAG production activates PKC, which increases membrane translocation of TRPM4 to further increase contraction^{340,875}. 9-Phenanthrol has been characterized as a TRPM4 blocker, and has recently been identified as a putative TMEM16A blocker (adapted from Earley *et al.*, 2013)³⁴⁰.

I further examined the effect of 9-phenanthrol using the perfused rat mesenteric bed. This technique was characterized using prazosin to demonstrate that electric stimulus-evoked increases in perfusion pressure are mediated by the release of NA from perivascular nerves. Activation of α_1 -adrenoceptors on VSMCs by NA produces vasoconstriction with voltage-independent and -dependent components. α_1 -Adrenoceptors are $G_{q/11}$ PCRs, which means that their activation causes a PLC-mediated increase in DAG and IP_3 and subsequent Ca^{2+} release from the SR via IP_3 R; this is the voltage-independent component of vasoconstriction^{234,414}. Activation of α_1 -adrenoceptors

also causes depolarization of VSMCs, leading to the activation of VOCCs and enhanced influx of Ca^{2+} ; this is the voltage-dependent component of vasoconstriction^{267,492,876}. The proximal localization of plasmalemmal TRPM4 channels and SR membrane-bound IP_3Rs at SR-plasmalemmal junction points²¹⁴ allows TRPM4 to depolarize the cell in response to Ca^{2+} release from the SR^{215,500}, connecting the voltage-independent and voltage-dependent components of vasoconstriction (**Figure 3.11**). When applied in the perfused mesenteric bed, 9-phenanthrol produced a dose-dependent reduction in nerve-evoked vasoconstriction. Moreover, the effect of 9-phenanthrol was not affected by blocking IK_{Ca} with NS6180. These data clearly illustrate that 9-phenanthrol does not activate IK_{Ca} channels in the perfused mesenteric bed. Thus, 9-phenanthrol's inhibition of nerve-evoked vasoconstriction is attributable to blockade of TRPM4 and/or blockade of TMEM16A.

As discussed earlier, TRPM4 has been implicated as a crucial mediator of myogenic vasoconstriction. Using pressure myography, I found that 9-phenanthrol abolished myogenic vasoconstriction in isolated rat mesenteric arteries. Blockade of IK_{Ca} by either NS6180 or TRAM-34 caused no change and did not reverse the effect of 9-phenanthrol. This finding is consistent with previous studies in rat mesenteric, skeletal, and cerebral arteries wherein 9-phenanthrol abolished myogenic tone^{500,501}. Moreover, it was previously found that knocking down expression of TRPM4 using an antisense oligodeoxynucleotide reduced myogenic constriction of rat cerebral arteries by 70-85%⁵⁰². The authors showed that TRPM4 expression was reduced, but still present, in the rats receiving the antisense oligodeoxynucleotide, although expression was not quantified. The discrepancy between the studies, where 9-phenanthrol abolishes myogenic tone but TRPM4 knockdown leaves 15-30% myogenic tone is most likely due to the remaining expression level of TRPM4 after administering the antisense oligodeoxynucleotide.

Using wire myography, I found that 9-phenanthrol significantly inhibits the development of PE-induced tone in isolated mesenteric arteries. Seeing as PE is an agonist at α_1 -adrenoceptors, these results are consistent with the reduction of nerve-evoked vasoconstriction observed in the perfused mesenteric bed. Inhibiting SK_{Ca}, IK_{Ca} and eNOS with the well-characterized, selective inhibitors apamin, TRAM-34 and L-NAME, respectively, caused no significant difference in the response to 9-phenanthrol. These data further bolster the position that 9-phenanthrol is not producing its effects by activating IK_{Ca}. 9-Phenanthrol appears to inhibit PE-evoked depolarization of VSMCs without enhancing endothelium-dependent vasodilation. I also found that 9-phenanthrol produces concentration-dependent vasodilation in isolated mesenteric arteries. Interestingly, when arteries were pre-constricted with 3 μ M PE, the EC₅₀ of 9-phenanthrol was 490 nM (logEC₅₀ = -6.31 \pm 0.09 M; n = 6), whereas when arteries were pre-constricted with 3 μ M 5-HT, the EC₅₀ of 9-phenanthrol was relatively left-shifted at 78 nM (logEC₅₀ = -7.11 \pm 0.09 M; n = 5). In vascular smooth muscle, 5-HT produces vasoconstriction by activating G_{q/11}-coupled 5-HT_{2A} and 5-HT_{1B/1D} receptors^{153,314,877,878}, which initiates the same second messenger pathway as PE-induced vasoconstriction mediated by α_1 -adrenoceptors. It was unexpected that two agonists activating the same pathway would produce an order of magnitude difference in the EC₅₀ of 9-phenanthrol. This suggests that the relative contribution of voltage-independent and -dependent vasoconstriction varies depending on the vasoconstrictor stimulus. Sung *et al.* (2013) reported that nifedipine (1 μ M) inhibited 5-HT-induced vasoconstriction by over 70%⁸⁷⁹; in the present study I observed that nifedipine (0.3 μ M) inhibited PE-induced vasoconstriction by approximately 30%. These results cannot be directly compared due to the difference in nifedipine concentration used, but they indicate that voltage-dependent contraction may be a larger component of 5-HT-induced vasoconstriction than of PE-induced vasoconstriction. This hypothesis would need to be confirmed

in a future investigation, but if found to be true, it would be consistent with the left-shift I observed in the EC₅₀ of 9-phenanthrol in vessels pre-constricted to 5-HT versus PE.

Finally, using wire myography I also observed that 9-phenanthrol abolishes the depolarization-dependent component of PE-induced contraction in the VSMC. 9-Phenanthrol alone reduced PE-induced vasoconstriction by approximately 50%, and this did not significantly change in the presence of either NS6180 or nifedipine. The former demonstrates again that 9-phenanthrol's inhibition of contraction is not mediated by IK_{Ca} activation, whereas the latter demonstrates that blocking LTCCs with nifedipine produces no additional effect in the presence of 9-phenanthrol. This means that 9-phenanthrol abolishes the voltage-dependent component of PE-induced vasoconstriction. These data are congruent with whole-cell patch clamp recordings from Gonzales *et al.* (2010) showing that 9-phenanthrol hyperpolarizes VSMCs from rat cerebral arteries⁵⁰⁰. The same study also demonstrated that 9-phenanthrol does not directly inhibit VOCCs. Cerebral artery VSMCs were used for whole-cell patch clamping, and voltage-dependent Ca²⁺ currents (I_{Ca}) were elicited by clamping the voltage at -70 mV and stepping up to +30 mV. The authors found that I_{Ca} was identical in the absence and presence of 9-phenanthrol (30 μM). Taken with my finding that nifedipine produces no effect on top of 9-phenanthrol, this indicates that 9-phenanthrol abolishes PE-induced depolarization upstream of LTCCs. However, as I am comparing my results in mesenteric arteries with those from cerebral arteries, this requires further investigation in mesenteric arteries. Patch clamp recordings in mesenteric artery VSMCs would confirm whether or not G_{q/11}PCR agonist-induced depolarization is abolished by 9-phenanthrol.

In these wire myograph experiments I also observed that 9-phenanthrol alone inhibited PE-induced vasoconstriction to a greater extent than nifedipine alone. Thus, it appears LTCCs are not the only contributor to voltage-dependent vasoconstriction in rat mesenteric arteries. The most

obvious candidate for this mechanism is TTCCs, which are expressed alongside LTCCs in human and rodent resistance arteries^{273,275,286,287}. Nifedipine is a selective blocker of LTCCs, but can inhibit TTCCs at higher concentrations²⁹¹⁻²⁹³. The IC₅₀ values for nifedipine at LTCCs and TTCCs have been reported as 0.14-300 nM and 1.2 μM, respectively^{292,834}. In these experiments, I have applied nifedipine at a concentration of 0.3 μM as it is a literature-accepted concentration for the inhibition of LTCCs while minimizing effect on TTCCs^{266,834,835}. Thus, I would expect that TTCCs would not be inhibited in the presence of nifedipine, but would be inactive in the presence of 9-phenanthrol due to the abolishment of depolarization. This could be the mechanism underlying the difference between PE-evoked constriction with nifedipine and with 9-phenanthrol. To investigate this mechanism in future, I would propose using mibefradil or 3,3'-diindolylmethane derivatives^{286,294} as pharmacological tools to inhibit TTCCs and assess their contribution to PE-evoked vasoconstriction.

My data clearly establish that 9-phenanthrol's inhibition of vasoconstriction is not mediated by IK_{Ca} activation, in opposition to the findings of Garland *et al.* (2015)⁸⁵⁷. They observed that blockade of IK_{Ca} by TRAM-34 reversed the effects of 9-phenanthrol, whereas I observed that neither TRAM-34 nor NS6180 altered the effects of 9-phenanthrol. Garland *et al.* conclude that there is no evidence for a functional role of TRPM4 in mesenteric arteries. I propose this may be due in part to their use of non-myogenically active mesenteric arteries. Historically, there is a very limited body of literature investigating myogenic pressure-evoked vasoconstriction in mesenteric arteries. Instead, most *ex vivo* studies of myogenic reactivity use other resistance arteries, including cerebral^{202,332,466,490,492,494,500,880-883}, skeletal muscle^{501,811,883,884}, and renal arteries^{477,883,885}. Several older studies report that mesenteric arteries display little to no spontaneous development of myogenic tone^{886,887}, or that they only develop pressure-evoked

vasoconstriction in the presence of α_1 -adrenoreceptor agonists such as PE^{888,889}. However, more recent studies have found that it is possible for isolated mesenteric arteries to display myogenic tone in the pressure myograph^{229,289,849,885,890,891}. I and others in our lab have found that tissue handling may have a large impact on the development of myogenic tone in mesenteric arteries *in vitro*. Mesenteric vessels often require long equilibration periods (≥ 45 minutes) held at intraluminal pressures of 60-80 mmHg before spontaneously developing myogenic tone in the pressure myograph^{225,289,700,849}. Additionally, Sun *et al.* (1992) demonstrated that myogenic reactivity increases as vessel diameter decreases down the vascular tree of the mesenteric bed⁸⁹². First-order mesenteric arteries exhibited no myogenic tone, whereas second-, third-, and fourth-order mesenteric arteries exhibited myogenic tone of increasing magnitudes, with fourth-order arteries showing the largest pressure-induced decrease in diameter. Therefore, studying the myogenic response in mesenteric arteries necessitates using the smallest diameter arteries one is able to dissect without damaging: preferably fourth-order or smaller. Given the evidence that mediating myogenic reactivity may be the most prominent role of vascular TRPM4⁴⁶⁵, the use of non-myogenically active mesenteric arteries by Earley *et al.* (2015)⁸⁵⁷ provides little insight into the functional role of TRPM4 in mesenteric arteries. Furthermore, animal experiments suggest that mesenteric arteries exhibit myogenic reactivity *in vivo* to autoregulate blood flow^{491,893,894}. This casts doubt upon the physiological relevance of using myogenically inactive vessels. Conversely, my data suggest a pronounced role for TRPM4 in voltage-dependent vasoconstriction in mesenteric resistance arteries.

Although my data show that 9-phenanthrol does not activate IK_{Ca} , its putative effect as an inhibitor of TMEM16A as suggested by Burris *et al.* (2015) cannot be ruled out⁸⁵⁶. TMEM16A is expressed in VSMCs, including those from mesenteric arteries^{864,895-898}. In response to an increase

in $[Ca^{2+}]_i$, TMEM16A allows efflux of Cl^- ions from the cell, thereby causing depolarization²⁰². This means that blockade of TMEM16A and blockade of TRPM4 both produce inhibition of depolarization. Since both channels contribute to the voltage-dependent component of $G_{q/11}$ PCR-induced vasoconstriction by depolarizing the VSMC²⁰², the putative effect of 9-phenanthrol at TMEM16A would be disguised by its canonical effect at TRPM4. Notably, Heinze *et al.* (2014) reported that TMEM16A expression decreases down the vascular tree, with some expression in large mesenteric arteries, but very little expression in small mesenteric arteries⁸⁹⁸. Based upon this finding, I would hypothesize that TMEM16A is not a major contributor to voltage-dependent vasoconstriction in my experiments, regardless of whether or not 9-phenanthrol acts at the channel. Nevertheless, further experiments are required in order to assess both the contribution of TMEM16A to agonist-, nerve- and pressure-evoked vasoconstriction in mesenteric arteries, and 9-phenanthrol's putative inhibition of TMEM16A. The functional contribution of TMEM16A inhibition to 9-phenanthrol's effect would be more difficult to parse than the functional contribution of IK_{Ca} activation, but could potentially be investigated by incubating arteries with a TMEM16A activator such as E_{act} before administering 9-phenanthrol.

In summary, these data demonstrate that TRPM4 is a crucial mediator of agonist-, nerve- and pressure-evoked vasoconstriction in rat mesenteric resistance arteries. Applied with 9-phenanthrol, IK_{Ca} blockers NS6180 and TRAM-34 produced no effect, supporting the hypothesis that 9-phenanthrol does not activate IK_{Ca} . Additionally, nifedipine did not alter the effect of 9-phenanthrol, indicating that 9-phenanthrol abolishes agonist-evoked depolarization in VSMCs. If 9-phenanthrol is selective for TRPM4, this suggests that TRPM4 may be the sole mediator of depolarization in mesenteric artery smooth muscle. Conversely, it is possible that the effect of 9-phenanthrol is in part due to inhibition of TMEM16A. Further investigation is necessary to

determine whether TMEM16A has a functional role in smooth muscle depolarization in these arteries.

Chapter 4: Characterization of cardiovascular function in a novel Cx40 knockout rat

4.1 Introduction

Interendothelial and myoendothelial GJs are essential for the coordination of endothelium-dependent vasodilation (see §1.5). GJ channels (reviewed by Pogoda *et al.*, 2019)⁷³¹ are composed of two hemichannels or connexons, one from each of the coupled cells. Each connexon is made of six connexins, which are a large family of 4TM proteins containing cytoplasmic N- and C-termini. GJ channels create continuity in the cytosol of adjacent cells, allowing for the conduction of membrane potential with unitary conductances that vary depending on the Cx subtypes present. Additionally, GJ channels have relatively large pore diameters, and generally allow the passage of many vasoactive small molecules including Ca^{2+} , IP_3 , cAMP, cGMP, ATP, NAD^+ , and prostaglandins⁷⁵⁸⁻⁷⁶⁰.

Cx subtypes vary in the length of their C-terminal domain, and are named according to their molecular weights. Four Cx subtypes are expressed in the cardiovascular system: ECs express Cx37, Cx40, and to a lesser extent Cx43, whereas VSMCs express Cx43 and Cx45^{731,735,762}. Throughout the literature, the detection of endothelial Cx37 and/or Cx40 at interendothelial GJs and/or MEGJs varies depending on the species and the tissue (reviewed by Welsh *et al.*, 2018)⁷⁶². In small resistance arteries from rats and humans, Cx37 and Cx40 have been demonstrated to localize in ECs both at lateral cell borders and in MEPs, indicating their presence in interendothelial and myoendothelial GJs, respectively^{690,697,740,762,899-904}. Concurrently, electron microscopy studies have demonstrated that the number of MEPs connecting the endothelium to the media increases as vessel diameter decreases down the vascular tree^{671,735}. This is consistent with functional evidence demonstrating that the relative contribution of EDH versus NO

production to endothelium-dependent vasodilation also increases as vessel diameter decreases^{631,670}.

The role of GJ channels in vascular function was first investigated using classical GJ inhibitors such as heptanol, carbenoxolone and 18 α / β -glycyrrhetic acid⁹⁰⁵⁻⁹⁰⁷. These are non-selective agents which uncouple GJ channels via mechanisms of action that have not been fully elucidated. It is unclear whether these agents directly block hemichannels; however, they have been shown to be reversible allosteric modulators that reduce both the GJ pore diameter and spacing between channels⁹⁰⁸⁻⁹¹¹. Heptanol in particular is reported to uncouple GJs in a mechanism dependent upon its insertion into the plasmalemma where it reduces membrane fluidity; hence, pre-loading the plasmalemma of rat cardiomyocytes with a cholesterol analogue reverses the effect of heptanol⁹¹⁰. Although they are still used, these agents cannot distinguish the roles of individual Cxs, and they have been shown to exhibit non-junctional effects on ion currents, $[Ca^{2+}]_i$, and mitochondrial membrane potential^{906,912}.

More recently, two major experimental tools have facilitated investigation of the roles of specific Cx subtypes in vascular function: inhibitory Cx-mimetic peptides, and mouse knockout models. Cx-mimetic peptides are short peptides with sequence homology to the extracellular or intracellular domains of specific Cxs (reviewed by King *et al.*, 2021)⁹¹³. These peptides include Gap21, Gap26 and Gap27, which were originally designed against Cx32 and Cx43 for the purpose of producing anti-Cx antibodies, which were found to be ineffective GJ blockers^{914,915}. However, the peptides themselves were subsequently shown to inhibit GJ-mediated intercellular communication^{913,916,917}. Peptides selective for other Cxs were developed by altering the amino acid sequences of Gap26 and Gap27; this produced peptides including ^{37,40}Gap26, ⁴⁰Gap27 and ^{37,43}Gap27, targeted to Cx37, Cx40 and Cx43^{913,918}. ⁴⁰Gap27 inhibits Cx40 GJs without affecting

Cx37 or Cx43^{918,919}; however, the mechanism of action is still unclear, though several hypotheses exist. There is no current evidence that Gap26/27 causes disassembly of docked GJ channels⁹¹⁷, thus leaving two main models: 1) Gap26/27 may bind to the extracellular loops of hemichannels in order to prevent conduction and docking, resulting in decreased channel formation due to the high turnover of GJs, or 2) Gap26/27 may alter channel gating by allosterically decreasing the opening of hemichannels, even in the fully assembled GJ channel^{916,917}. Evidence of the reversibility of this blockade in cultured ECs supports the latter model over the former⁹²⁰. Regardless, the selectivity of these peptides has been called into question, due to the high concentrations ($\geq 100 \mu\text{M}$) and long incubation times ($\geq 1 \text{ h}$) required for maximal blockade of GJs^{901,903,917,921-925}, suggesting off-target effects. To this end, Wang *et al.* (2012) demonstrated that at a concentration of 1 mM, there is no difference between blockade of hemichannels by the active Gap26/27 and a control peptide with a scrambled sequence⁹²⁶.

Mouse germline knockouts of both Cx37 and Cx40 have been developed, although the Cx37 knockout mouse is less well-studied. The phenotypic changes in the Cx37 knockout mouse are largely non-vascular, including polyuria and polydipsia due to an associated decrease in renal expression of aquaporin 2⁷⁷⁷, and female infertility due to abnormal oocyte development^{774,927,928}. In these mice, blood vessel development and systemic blood pressure are unaffected^{776,779,929}. Conversely, Cx40 knockout mice exhibit impaired endothelial modulation of vascular diameter. Knockout of Cx40, but not Cx37, impairs upstream conduction of ACh- or bradykinin-induced endothelium-dependent vasodilation in cremaster arteries^{764,765}. Moreover, Brasen *et al.* (2018) found that vasodilation due to EDH was impaired in isolated renal arteries from Cx40 knockout mice⁶⁶¹. The Cx40 knockout mouse exhibits several other phenotypic changes in cardiovascular

function, including elevated systemic blood pressure, cardiac hypertrophy, and decreased eNOS expression in vessels such as the aorta and renal artery^{661,766,767}.

Until recently, only mouse models of Cx knockouts have been available. Due to their small size, physiological assays in mouse blood vessels are restricted to the use of large elastic arteries such as the aorta, rather than resistance arteries. In contrast, resistance arteries from rats such as mesenteric and cerebral arteries are easily accessible and large enough for fine dissection in physiological techniques such as wire and pressure myography. Our research group received a novel strain of Cx40 knockout rats as a gift from collaborator Dr. William Cupples; this has allowed me to perform functional experiments assessing the physiological role of Cx40 in the modulation of resistance artery diameter, which was not previously possible in mouse models. Thus, I have tested the hypothesis that *the Cx40 knockout rat will demonstrate impaired endothelial modulation of arterial diameter relative to the wild-type rat.*

4.2 Methods

A full description of methods is provided in **Chapter 2**. As stated in §2.2, experiments in this chapter use Cx40^{+/+} (wild-type or WT), Cx40^{+/-} (heterozygous or HET), and Cx40^{-/-} (knock-out or KO) rats bred from the WKY-Gja5^{em1Mcwi} mutant strain.

4.3 Results

4.3.1 Cx40 KO does not upregulate relative mRNA expression of Cx37 and Cx43

I have characterized the expression profile of endothelial Cxs in WT, HET and KO rats bred from the WKY-Gja5^{em1Mcwi} mutant strain by measuring the relative levels of mRNA coding for Cx37, Cx40 and Cx43 by RT-qPCR in isolated second- and third-order mesenteric arteries from male and female rats (**Figure 4.1a** and **b**, respectively). Within each sex, no significant differences in relative levels of mRNA expression were observed between genotypes ($P > 0.05$).

This was also true of Cx40, which is appropriate for this KO model: the WKY-Gja5^{em1Mcwi} mutant possesses a point mutation introducing a premature stop codon in exon 1 of the Cx40-coding gene Gja5. This method does not affect transcription of Cx40, but abolishes translation of Cx40. These results therefore do not confirm the absence of Cx40, but instead confirm that mRNA expression of Cx37 and Cx43 is not upregulated by a compensatory mechanism.

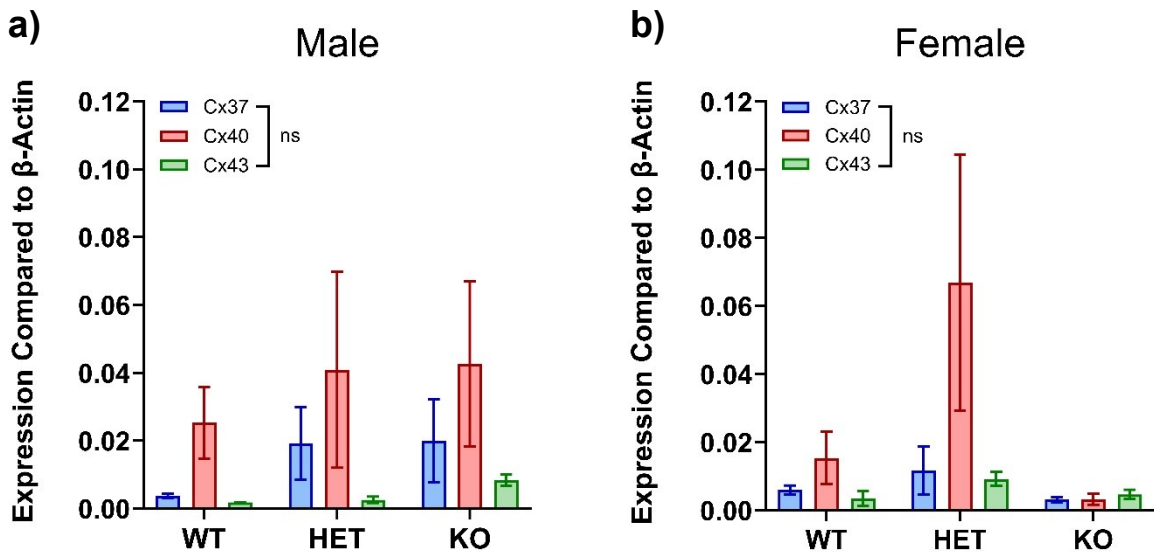
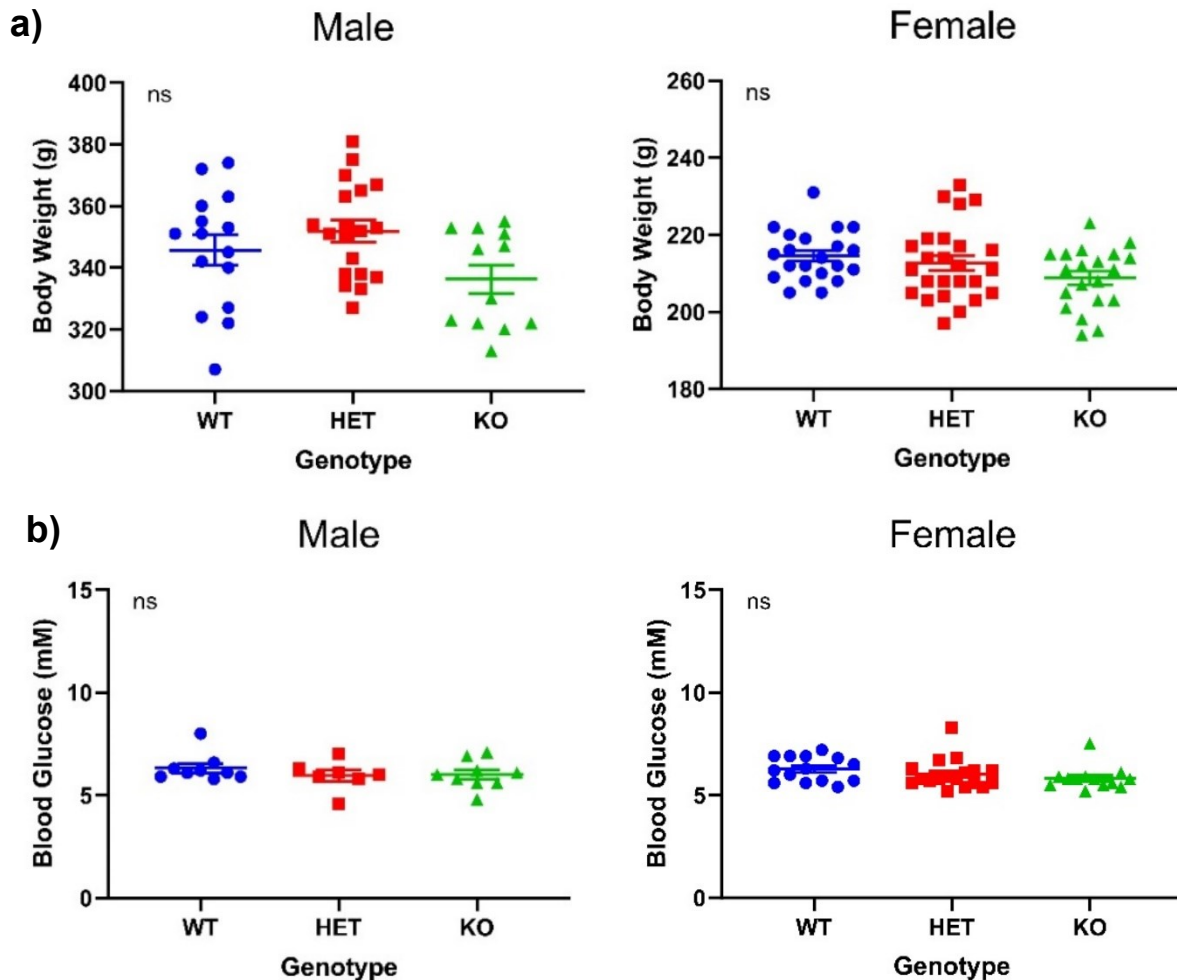


Figure 4.1: Relative mRNA expression of endothelial Cx subtypes is not altered across genotypes. Expression levels of mRNA coding for Cx37, Cx40 and Cx43 were determined using RT-qPCR and compared to mRNA of the reference gene *Actb*, coding for β -actin. mRNA was extracted from isolated second- and third-order mesenteric arteries from **a)** male ($n = 4-5$) and **b)** female ($n = 4$) WT, HET and KO rats. Arteries were taken from n different rats and measured in triplicate. Relative mRNA expression is expressed as $2^{-\Delta C_t}$, where $\Delta C_t = C_t(\text{gene}) - C_t(\text{Actb})$. $P > 0.05$; two-way ANOVA.

4.3.2 Genetic ablation of Cx40 produces hypertension and heart enlargement

In order to characterize the cardiovascular system of the Cx40 KO rat model, I first assessed gross phenotypic changes in the metabolic and hemodynamic properties of 6-month-old male and female WT, HET and KO rats. Within each sex, no significant differences in body weight were observed between genotypes ($P > 0.05$, **Figure 4.2a**). Random blood glucose was also unaffected by genotype ($P > 0.05$, **Figure 4.2b**). Next, systemic BP was measured by tail cuff plethysmography. Both male and female KO rats exhibited an increase in systolic BP that was

statistically significant from both WT and HET rats within each sex ($P < 0.05$, **Figure 4.2c**). In males, the mean systolic BP of KO rats (154.2 ± 3.5 mmHg; $n = 6$) was approximately 40 mmHg greater than that of either WT rats (112.8 ± 5.2 mmHg; $n = 6$) or HET rats (116.7 ± 7.8 mmHg; $n = 6$). This difference was also observed in females, wherein mean systolic BPs of WT, HET and KO rats were 106.3 ± 4.7 mmHg ($n = 6$), 118.7 ± 6.3 mmHg ($n = 7$) and 148.8 ± 6.4 mmHg ($n = 6$), respectively. No differences were observed in heart rate between genotypes ($P > 0.05$; data not shown). Finally, wet weights of kidneys and hearts were measured upon excision and expressed relative to body weight (**Figure 4.2d** and **e**). Within each sex, no significant difference was observed in relative kidney weight between genotypes ($P > 0.05$), but KO rats of both sexes showed a significant increase in relative heart weight versus WT and HET rats ($P < 0.05$).



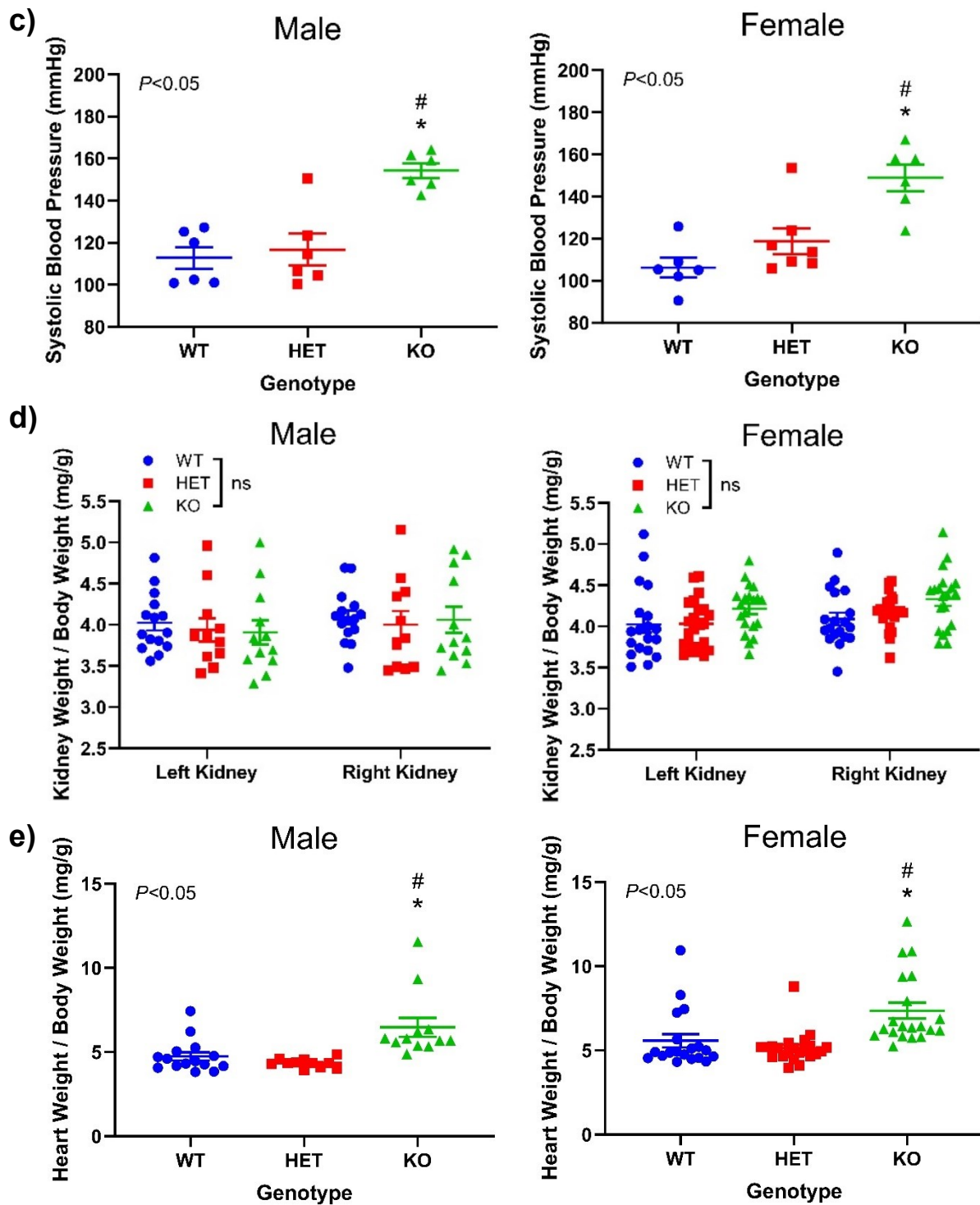


Figure 4.2: Genetic ablation of Cx40 causes increased systolic blood pressure and heart mass in male and female rats. Gross metabolic and hemodynamic characteristics of male and female WT, HET, and KO rats were measured at six months of age, including **a**) body weight ($n = 12-25$), **b**) random blood glucose ($n = 7-18$), **c**) systolic blood pressure ($n = 6-7$), **d**) left and right kidney weight ($n = 11-22$), and **e**) heart weight ($n = 11-22$). Data are presented as mean \pm SEM. * denotes $P < 0.05$ from WT and # denotes $P < 0.05$ from HET; one-way ANOVA. Tail cuff plethysmography performed by Jad Julian-Rachid.

4.3.3 Genetic ablation of Cx40 enhances nerve-evoked vasoconstriction in the rat perfused mesenteric vascular bed

In order to characterize the effect of Cx40 ablation on the physiological function of resistance arteries, I recorded responses in perfusion pressure to nerve-evoked vasoconstriction in the perfused mesenteric vascular beds of male and female WT, HET and KO rats. Frequency-response relationships from 1 to 40 Hz were constructed in the absence and presence of the SK_{Ca} inhibitor apamin (50 nM), the IK_{Ca} inhibitor TRAM-34 (1 μM) and the eNOS inhibitor L-NAME (100 μM). Treatments with apamin + TRAM-34, as well as apamin + TRAM-34 + L-NAME produced statistically significant increases in nerve-evoked vasoconstriction versus control in all genotype-sex groups ($P < 0.05$, **Figures 4.3** and **4.4**). Within each genotype-sex group, treatment with apamin + TRAM-34 increased pressure responses to 30 and 40 Hz stimulations by approximately 150% versus control. This suggests that the contribution of EDH to inhibition of vasoconstriction is unaffected in the absence of Cx40. The further increase in pressure responses in the presence of apamin + TRAM-34 + L-NAME suggests that the NO pathway is unaffected as well. Comparing the same data across genotypes (**Figure 4.5**) shows that mesenteric beds from male and female KO rats exhibit a statistically significant two-fold increase in pressure response to 15, 20, 30 and 40 Hz electrical stimulations versus WT and HET ($P < 0.05$, **Figure 4.5a** and **d**). With the addition of apamin + TRAM-34, the KO again exhibits a two-fold larger response than WT at 30 and 40 Hz ($P < 0.05$, **Figure 4.5b** and **e**). The addition of all three inhibitors still produces two-fold increases in the KO response at lower frequencies (e.g. 15 Hz), but the difference shrinks to approximately 1.25-fold at 30 and 40 Hz ($P < 0.05$, **Figure 4.5c** and **f**). This could suggest an impaired, but still significant, contribution of NO production to inhibition of vasoconstriction in the absence of Cx40.

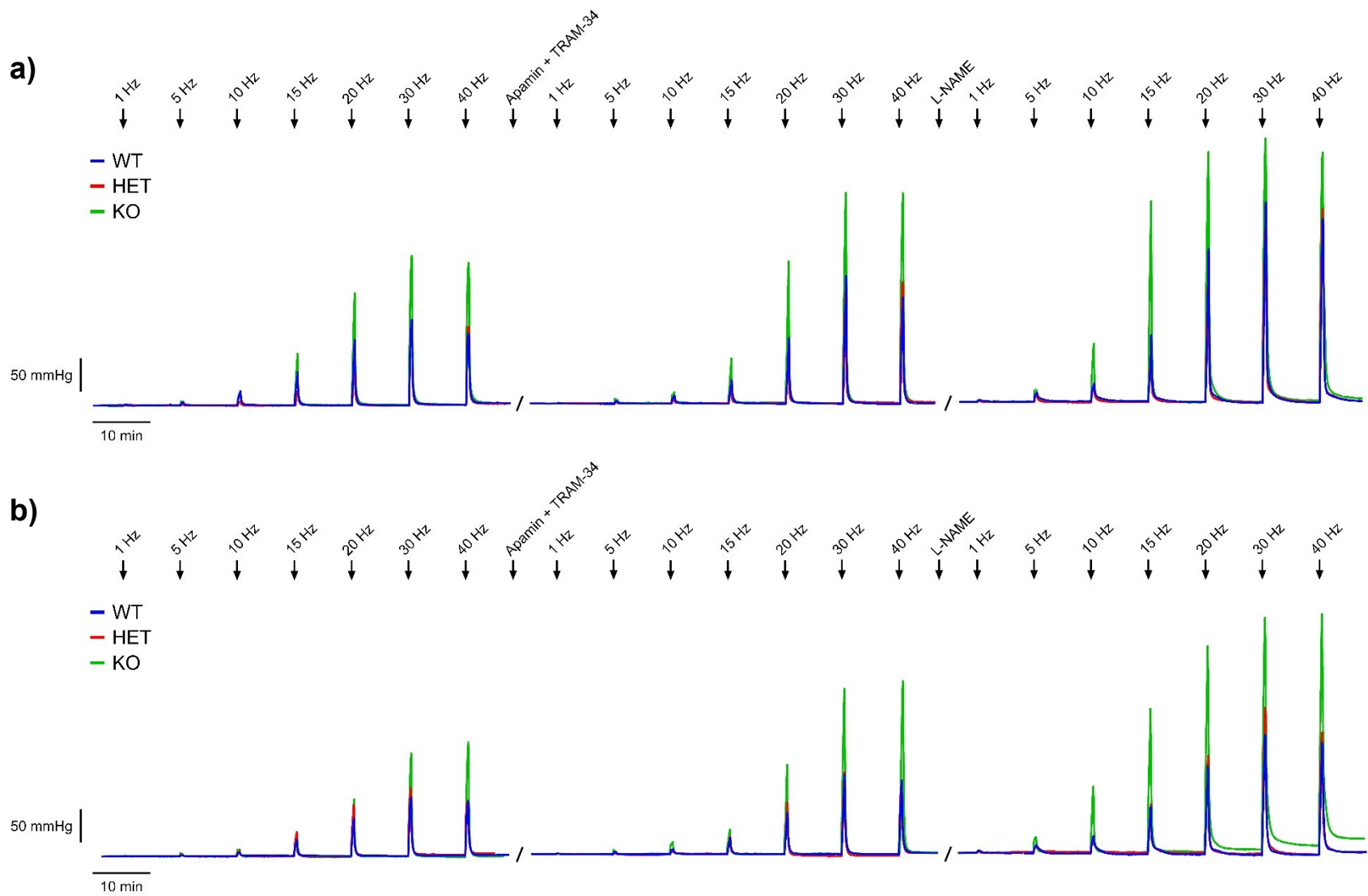


Figure 4.3: Representative traces of nerve-evoked vasoconstriction in the rat perfused mesenteric vascular bed. Frequency-response relationships constructed in endothelium-intact mesenteric vascular beds from **a)** male and **b)** female WT, HET and KO rats. The first relationship is in the absence of inhibitors; the second relationship is in the presence of apamin (50 nM) and TRAM-34 (1 μ M); the third relationship is in the presence of apamin, TRAM-34 and L-NAME (100 μ M).

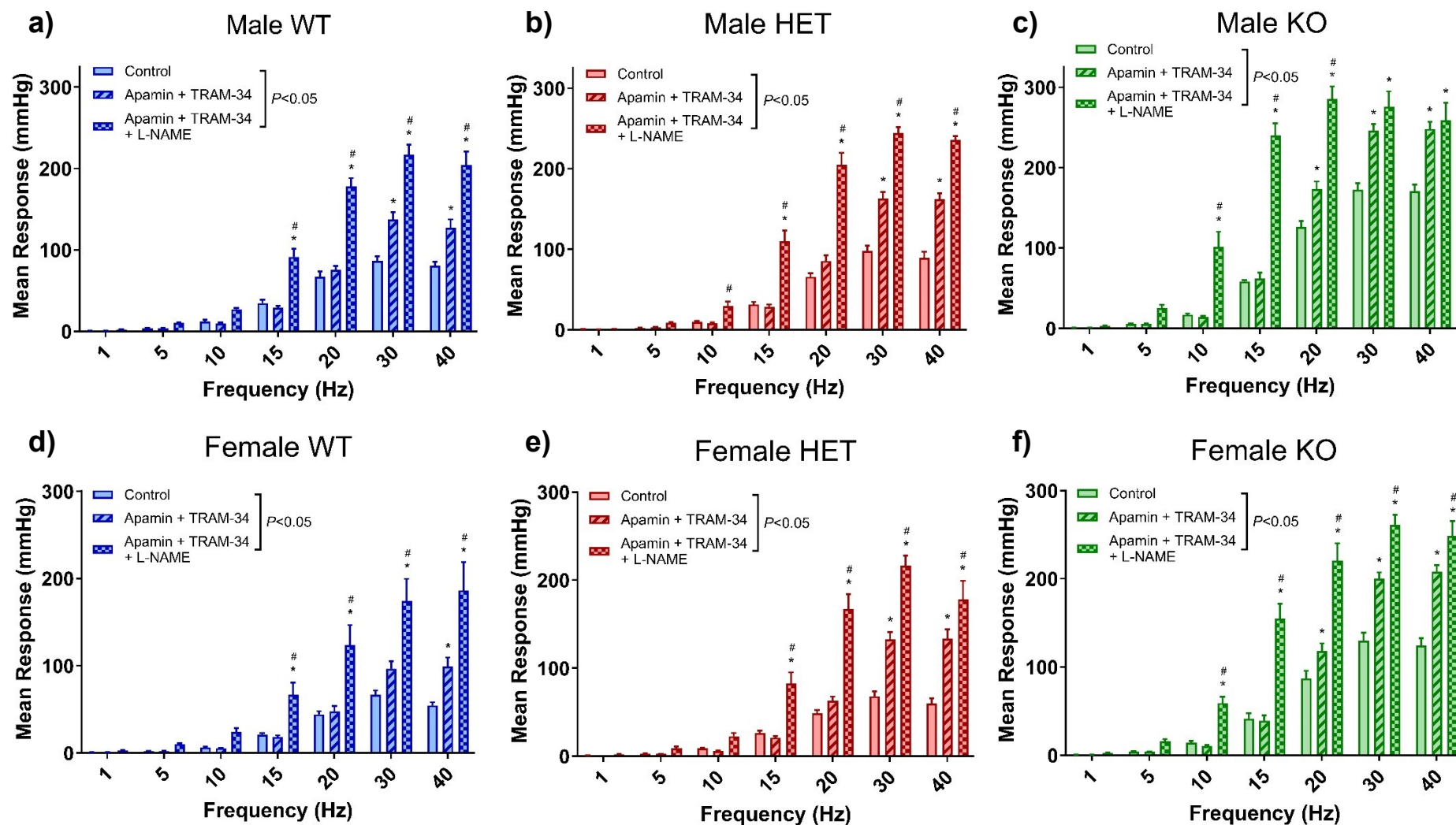


Figure 4.4: EDH and NO synthesis are significant contributors to inhibition of nerve-evoked vasoconstriction in perfused mesenteric vascular beds from Cx40 WT, HET and KO rats. Frequency-response relationships constructed in the absence and presence of apamin (50 nM), TRAM-34 (1 μ M) and L-NAME (100 μ M) using endothelium-intact mesenteric vascular beds from male **a)** WT ($n = 6$), **b)** HET ($n = 6$), and **c)** KO ($n = 7$) rats, and female **d)** WT ($n = 6$), **e)** HET ($n = 6$), and **f)** KO ($n = 6$) rats. Data are presented as mean \pm SEM. * denotes $P < 0.05$ from control and # denotes $P < 0.05$ from Apamin + TRAM-34; two-way ANOVA.

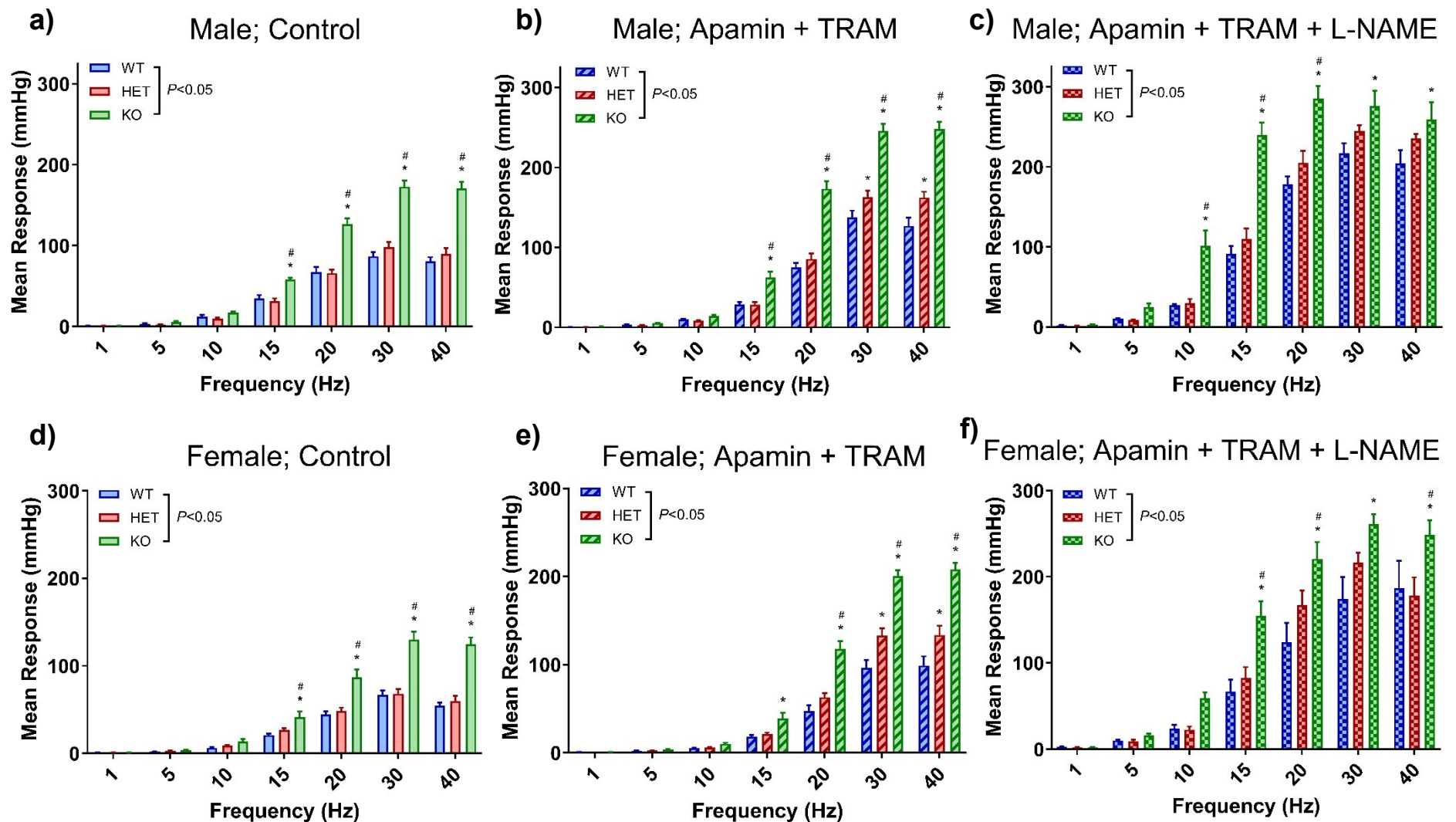


Figure 4.5: Genetic ablation of Cx40 enhances nerve-evoked vasoconstriction in the rat perfused mesenteric vascular bed. Unpaired frequency-response relationships of perfused mesenteric vascular beds from male (a, b, and c) and female (d, e, and f) WT ($n = 6$), HET ($n = 6$) and KO ($n = 6-7$) rats compared across genotypes within each drug treatment. Beds were perfused in the absence of drugs (a and d), in the presence of apamin (50 nM) and TRAM-34 (1 μ M; b and e), or in the presence of apamin, TRAM-34 and L-NAME (100 μ M; c and f). Data are presented as mean \pm SEM. * denotes $P < 0.05$ from WT and # denotes $P < 0.05$ from HET; two-way ANOVA.

The role of the endothelium in nerve-evoked vasoconstriction was investigated by perfusing endothelium-denuded mesenteric beds from each genotype-sex group. Within each group, the addition of apamin + TRAM-34 + L-NAME had no effect on stimulus-evoked responses ($P>0.05$, **Figure 4.6**), indicating that the potentiation of nerve-evoked vasoconstriction by these inhibitors (**Figures 4.4 and 4.5**) was due to their actions at EC targets rather than neuronal or SMC targets. Interestingly, when compared across genotypes, nerve-evoked vasoconstriction in the endothelium-denuded beds from male and female KO rats produced significantly higher responses than those in endothelium-denuded beds from WT and HET rats ($P<0.05$, **Figure 4.7**). This comparison is shown in the absence of inhibitors, but responses in KO beds remained significantly higher than WT and HET in the presence of apamin + TRAM-34 or apamin + TRAM-34 + L-NAME (data not shown). At the 30 and 40 Hz stimulations, endothelium-intact mesenteric beds from male KO rats exhibited approximately 200% higher pressure responses than male WT rats (**Figure 4.5a**); in endothelium-denuded beds, the male KO responses at 30 and 40 Hz were only 140% higher than those in male WT rats. (**Figure 4.7a**). In females, endothelium-intact beds from KO rats produced responses approximately 200% higher than WT rats to 30 and 40 Hz stimulations (**Figure 4.5d**), whereas endothelium-denuded beds from KO rats produced responses 250% higher than WT rats to 30 and 40 Hz stimulations (**Figure 4.7b**). These results suggest that the increased nerve-evoked vasoconstriction observed in the Cx40 KO is at least partially due to endothelium-independent mechanisms, which could involve changes in smooth muscle function.

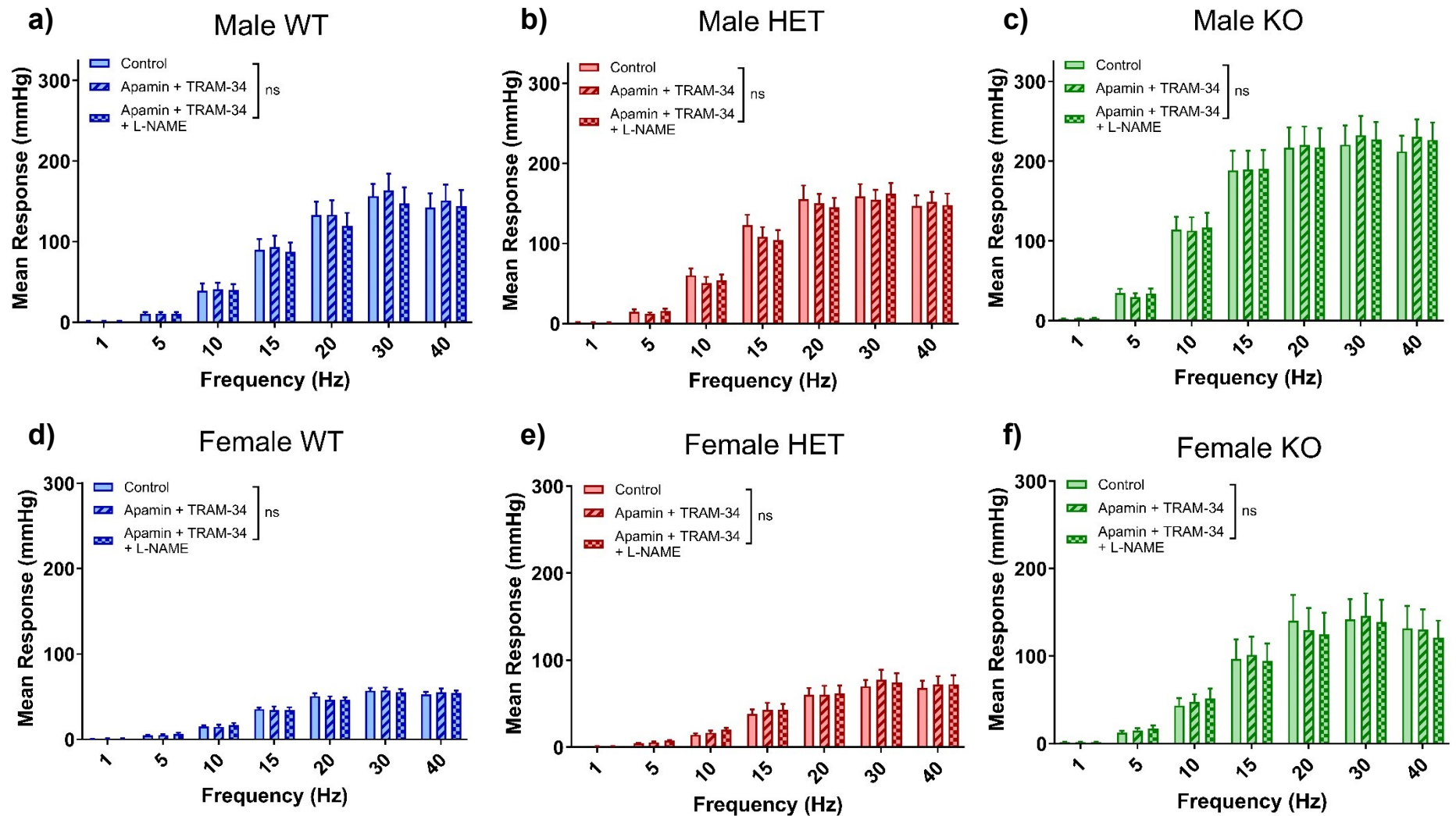


Figure 4.6: Removal of endothelium abolishes the effects of apamin, TRAM-34 and L-NAME but not the effect of Cx40 ablation in the rat perfused mesenteric vascular bed. Frequency-response relationships constructed in the absence and presence of apamin (50 nM), TRAM-34 (1 μ M) and L-NAME (100 μ M) using endothelium-denuded mesenteric vascular beds from male **a)** WT ($n = 6$), **b)** HET ($n = 6$), and **c)** KO ($n = 6$) rats, and female **d)** WT ($n = 6$), **e)** HET ($n = 6$), and **f)** KO ($n = 6$) rats. Data are presented as mean \pm SEM. $P > 0.05$; two-way ANOVA.

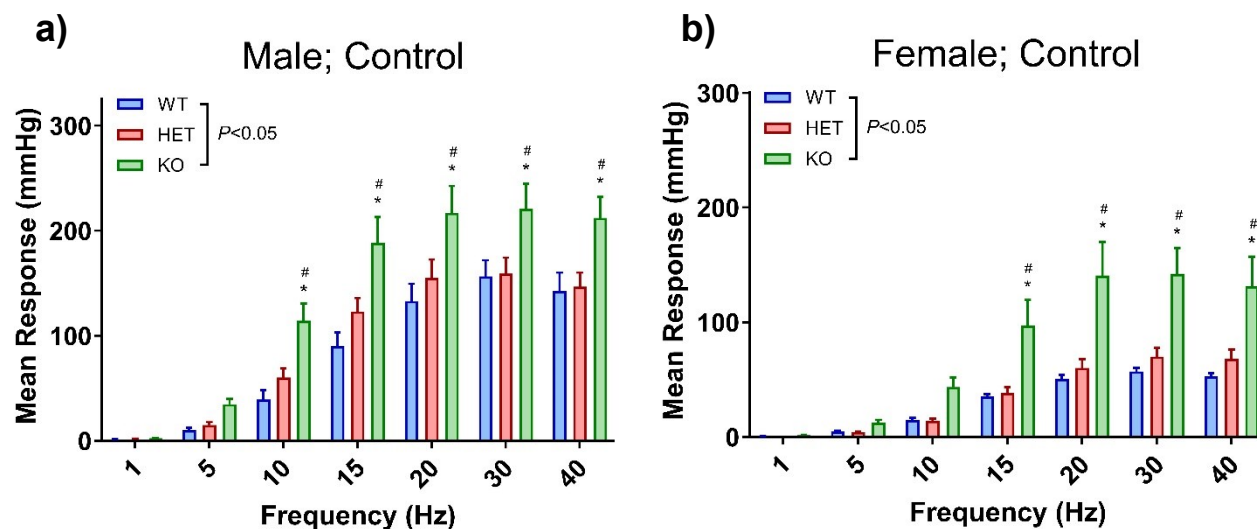


Figure 4.7: Perfused mesenteric vascular beds from Cx40 KO rats maintain a significant increase in nerve-evoked pressure responses versus WT and HET rats upon removal of endothelium. Unpaired frequency-response relationships of endothelium-denuded perfused mesenteric vascular beds from **a)** male and **b)** female WT ($n = 6$), HET ($n = 6$) and KO ($n = 6$) rats compared across genotypes in the absence of pharmacological inhibitors. Data are presented as mean \pm SEM. * denotes $P < 0.05$ from WT and # denotes $P < 0.05$ from HET; two-way ANOVA.

These data have also been analysed comparing the responses between the endothelium-intact and -denuded beds within each genotype-sex group (**Figure 4.8**). In this analysis, a notable sex-difference arises, wherein removing the endothelium produces significantly higher responses in beds from male rats ($P < 0.05$, **Figure 4.8a, b and c**), while no difference is produced in beds from female rats ($P > 0.05$, **Figure 4.8d, e and f**). The mechanism underlying this sex-difference is unclear but may involve differential production and secretion of endothelium-derived factors in males and females with higher relative production of vasodilatory factors versus vasoconstrictive factors in males than in females.

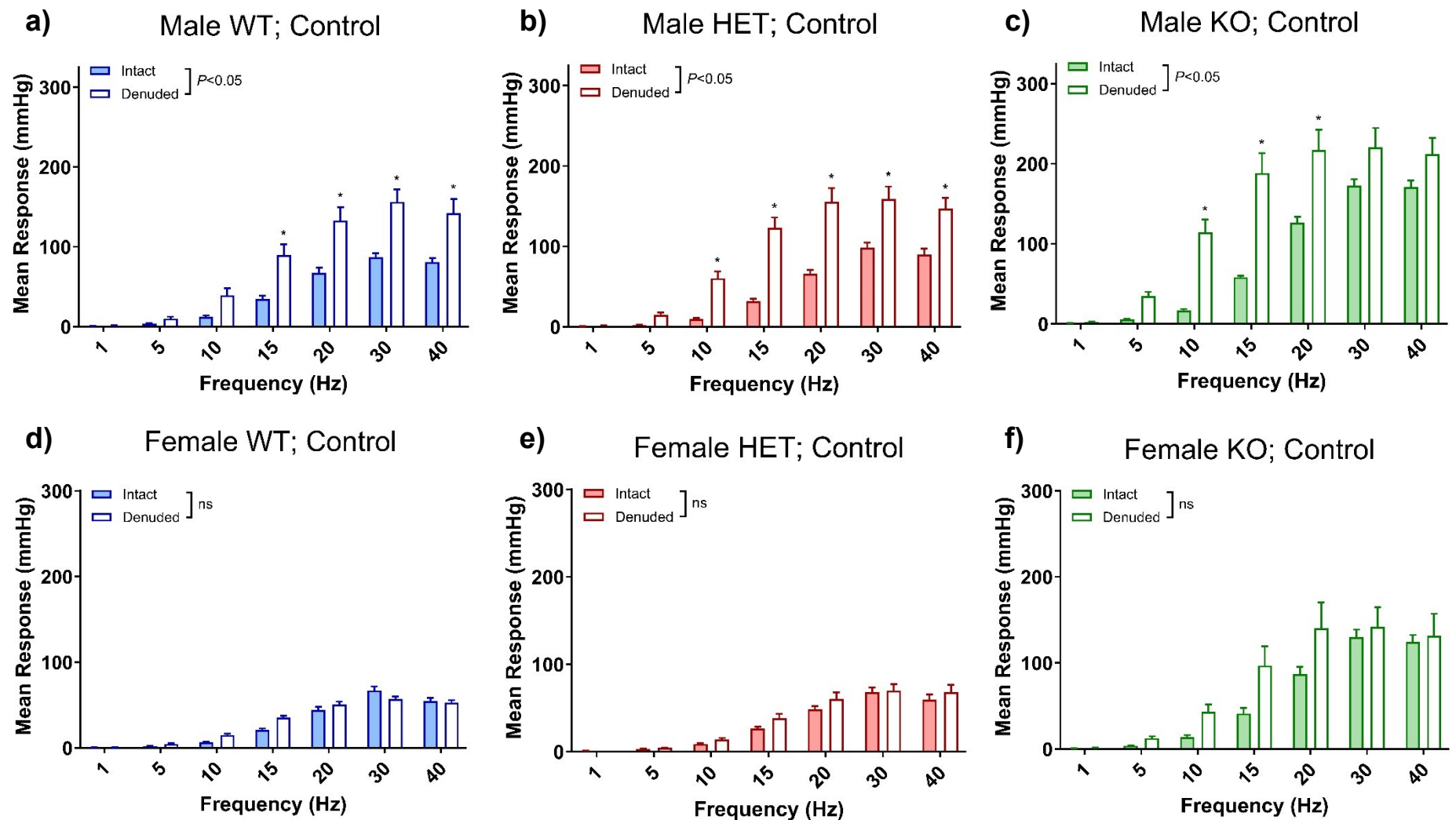


Figure 4.8: Removal of endothelium in the perfused mesenteric vascular bed enhances pressure responses in beds from males but not from females. Unpaired frequency-response relationships of endothelium-intact and -denuded perfused mesenteric vascular beds in the absence of pharmacological inhibitors. Male **a)** WT ($n = 6$), **b)** HET ($n = 6$), and **c)** KO ($n = 6-7$) rats; * denotes $P < 0.05$ from endothelium-intact; two-way ANOVA. Female **d)** WT ($n = 6$), **e)** HET ($n = 6$), and **f)** KO ($n = 6$) rats; $P > 0.05$; two-way ANOVA. Data are presented as mean \pm SEM.

4.3.4 Genetic ablation of Cx40 does not affect myogenic reactivity in isolated mesenteric arteries

Pressure myography was used to examine the role of Cx40 in the development of myogenic tone in isolated fourth- to sixth-order mesenteric arteries. Representative traces of internal diameter in response to changes in intraluminal pressure have been provided (**Figure 4.9**). Arteries from male and female WT, HET and KO rats all exhibited myogenic constriction, whereby the active diameter in the presence of Ca^{2+} was significantly lower than the passive diameter in the absence of Ca^{2+} ($P < 0.05$, **Figure 4.10**). Some genotype-sex groups (i.e. male WT, female WT and female KO; **Figure 4.10a, d and f**, respectively) exhibited potentiation of myogenic vasoconstriction in the presence of apamin + TRAM-34 + L-NAME. The observation that inhibiting SK_{Ca} , IK_{Ca} and eNOS, respectively, enhances myogenic vasoconstriction was in contrast to the lack of effect of endothelial removal on myogenic vasoconstriction (**§3.3.5**). This discrepancy has been previously observed in other animal models by our lab and others⁹³⁰⁻⁹³², and has prompted the hypothesis that endothelial removal produces no net effect due to the endothelial release of both vasodilatory and vasoconstrictive factors. However, when compared across genotypes, no significant differences in the development of myogenic tone were observed between arteries from WT, HET and KO rats in either males or females in the absence or presence of apamin, TRAM-34 and L-NAME ($P > 0.05$, **Figure 4.11**). In order to compare uncoupled results across genotypes, these data are expressed as % myogenic tone (see **§2.5**), which is a standard reporting practice in the literature. These results suggest that Cx40 does not play a significant role in the myogenic response in rat mesenteric arteries.

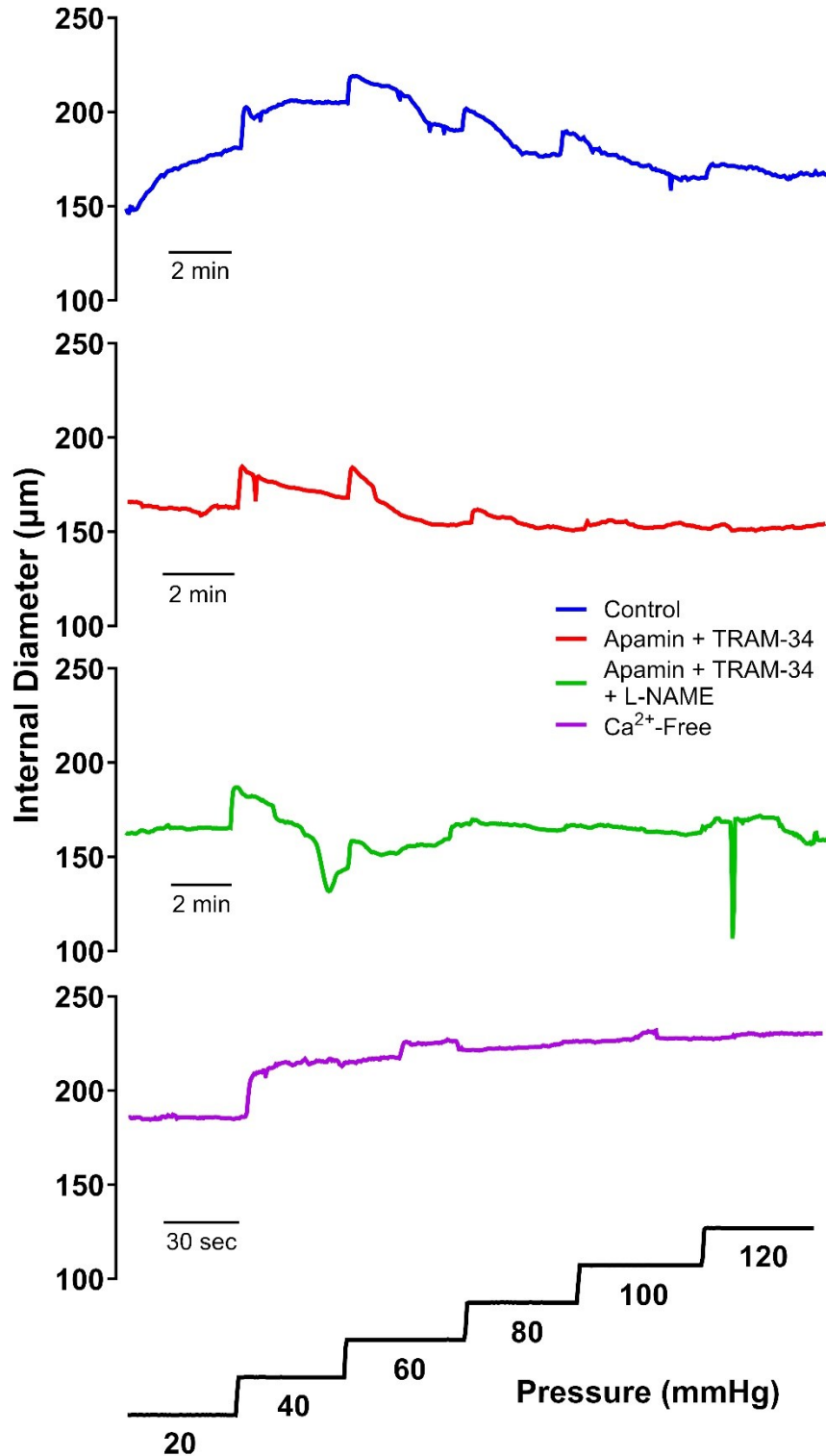


Figure 4.9: Representative trace of pressure-diameter relationships in an isolated mesenteric artery from a male WT rat. Pressure-diameter relationships constructed using pressure myography in an endothelium-intact segment of mesenteric artery from a male WT rat in the absence and presence of apamin (50 nM), TRAM-34 (1 μM), L-NAME (100 μM) and Ca²⁺.

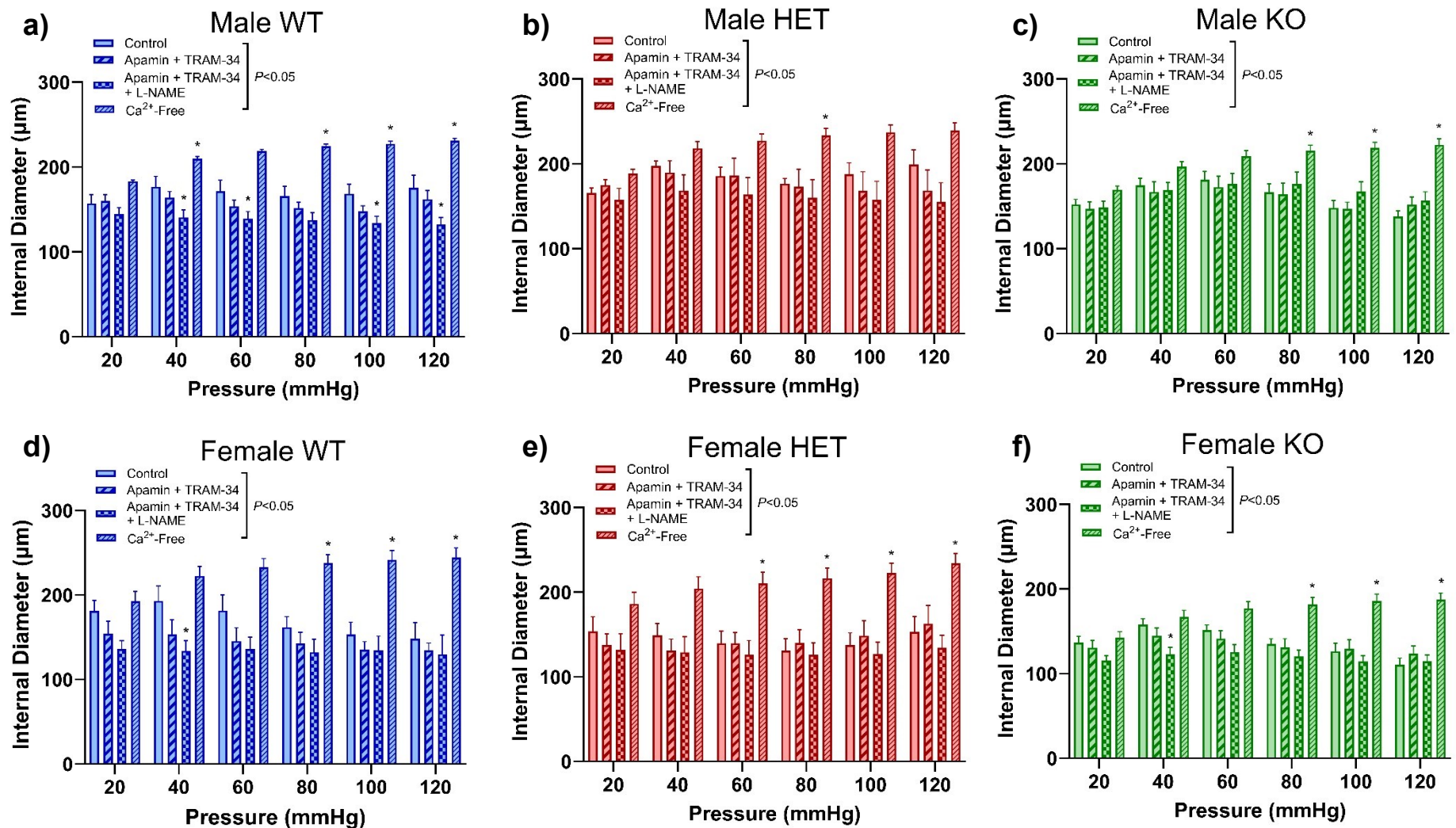


Figure 4.10: Pressure-evoked vasoconstriction occurs in isolated mesenteric arteries from Cx40 WT, HET and KO rats. Pressure myography was used to construct pressure-diameter relationships in the absence and presence of apamin (50 nM), TRAM-34 (1 μM) and L-NAME (100 μM) using isolated fourth- to sixth-order mesenteric arteries from male **a)** WT ($n = 6$), **b)** HET ($n = 6$), and **c)** KO ($n = 6$) rats, and female **d)** WT ($n = 6$), **e)** HET ($n = 8$), and **f)** KO ($n = 6$) rats. Data are presented as mean \pm SEM. * denotes $P < 0.05$ from control; two-way ANOVA.

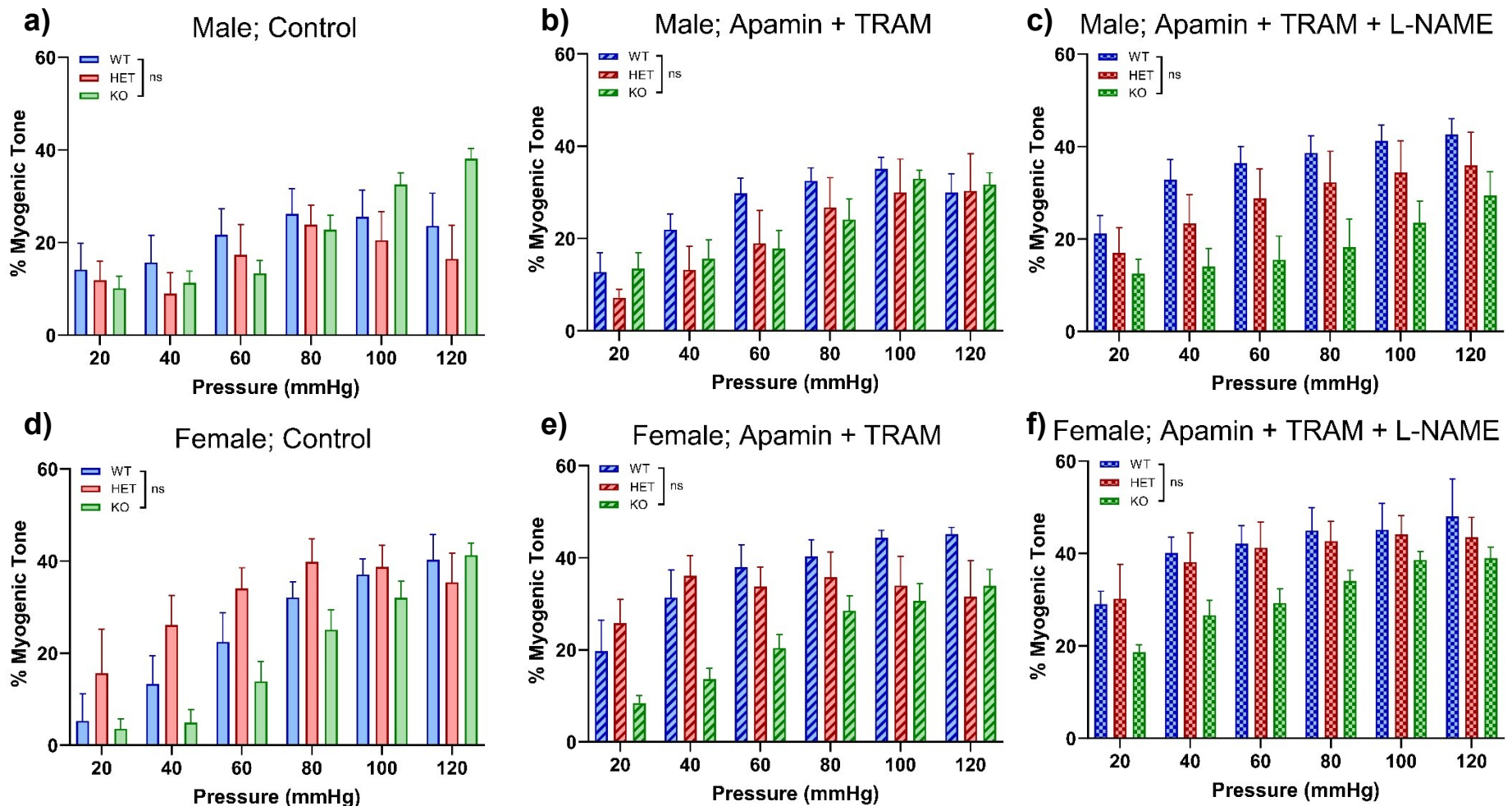


Figure 4.11: Myogenic response of isolated rat mesenteric arteries is not affected by genetic ablation of Cx40. Unpaired pressure-tone relationships of isolated fourth- to sixth-order mesenteric arteries from male (a, b, and c) and female (d, e, and f) WT ($n = 6$), HET ($n = 6-8$) and KO ($n = 6$) rats compared across genotypes within each drug treatment. Artery segments were mounted in a pressure myograph and subjected to stepwise pressure ramps in the absence of drugs (a and d), in the presence of apamin (50 nM) and TRAM-34 (1 μ M; b and e), or in the presence of apamin, TRAM-34 and L-NAME (100 μ M; c and f). Responses are expressed as % myogenic tone, which is the percentage difference in active diameter versus passive diameter at each pressure step. Data are presented as mean \pm SEM. $P > 0.05$; two-way ANOVA.

4.3.5 Genetic ablation of Cx40 enhances PE-induced vasoconstriction without affecting ACh-induced vasodilation in isolated rat mesenteric arteries

To investigate the role of Cx40 in endothelium-dependent vasodilation to ACh, isolated second and third order mesenteric arteries from male and female WT, HET and KO rats were assessed using wire myography. Vessel segments were pre-constricted with PE (3 μ M) before cumulative concentration-response curves to ACh were constructed in the presence and absence of apamin (50 nM), TRAM-34 (1 μ M) and L-NAME (100 μ M). The log of the EC₅₀ values for ACh in each treatment group were calculated (**Table 4.1**). All genotype-sex groups exhibited the lowest logEC₅₀ in the absence of inhibitors, and experienced similar increases in logEC₅₀ with the addition of EDH inhibitors apamin + TRAM-34, or the addition of eNOS inhibitor L-NAME. The presence of all three inhibitors caused a statistically significant increase in logEC₅₀ in all genotype-sex groups ($P < 0.05$; two-way ANOVA). Representative traces for control concentration-response curves to ACh in each genotype-sex group are provided (**Figure 4.12**).

logEC₅₀ (M) of ACh in isolated mesenteric arteries in the wire myograph				
Group	Control	Apamin + TRAM-34	L-NAME	Apamin + TRAM-34 + L-NAME
Male				
WT	-7.7 \pm 0.1	-7.1 \pm 0.1*	-7.3 \pm 0.3	-7.0 \pm 0.1*
HET	-7.4 \pm 0.1	-7.2 \pm 0.2	-7.4 \pm 0.2	-6.7 \pm 0.2*
KO	-8.1 \pm 0.1	-7.5 \pm 0.1	-7.4 \pm 0.1	-6.6 \pm 0.1*
Female				
WT	-7.7 \pm 0.1	-7.2 \pm 0.1*	-7.3 \pm 0.1	-6.6 \pm 0.1*
HET	-7.4 \pm 0.1	-7.2 \pm 0.1	-7.2 \pm 0.1	-6.7 \pm 0.1*
KO	-7.9 \pm 0.2	-7.4 \pm 0.1	-7.3 \pm 0.2*	-6.4 \pm 0.2*

Table 4.1: logEC₅₀ (M) values of ACh-induced vasodilation in isolated second- and third-order mesenteric arteries from male and female WT, HET, and KO rats using wire myography. Data are represented as mean \pm SEM ($n = 4-7$). Within each sex, overall effect of genotype was not significant ($P > 0.05$) but overall effect of drug treatment was significant ($P < 0.05$). * denotes $P < 0.05$ from the respective control within each group; two-way ANOVA. *Data contributed by Alexia Maheux, Brandon Truong and Sufyan Malik.*

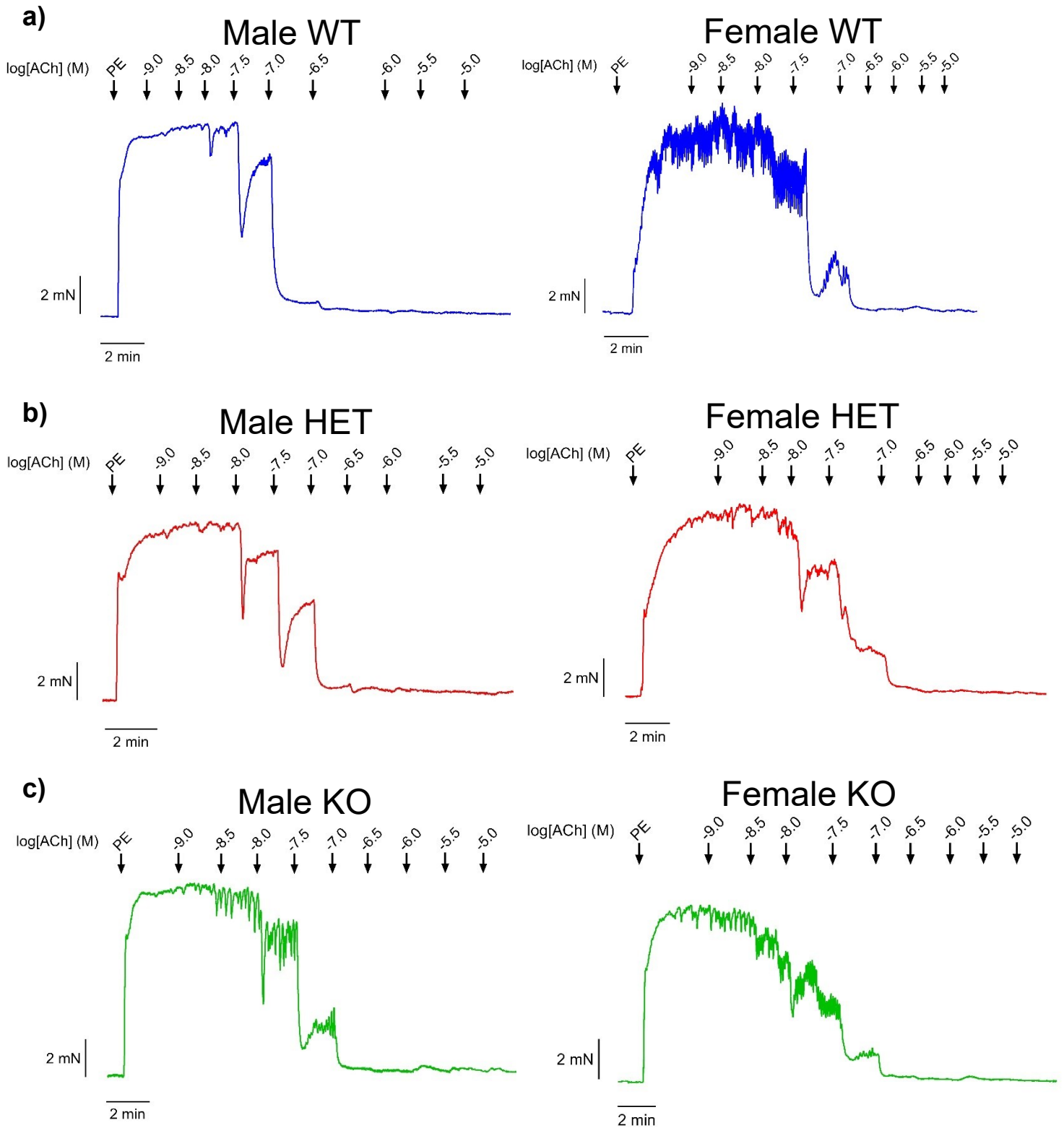


Figure 4.12: Representative traces of concentration-response curves to ACh in isolated mesenteric arteries from male and female WT, HET and KO rats. Concentration-response curves constructed using wire myography in endothelium-intact segments of second- and third-order mesenteric artery from male and female **a) WT**, **b) HET** and **c) KO** rats in the absence of drugs.

Isolated mesenteric arteries from all genotype-sex groups except for male HETs displayed statistically significant inhibition of ACh-induced vasodilation in the presence of apamin + TRAM-34 + L-NAME ($P < 0.05$, **Figures 4.13** and **4.14**). Together with the $\log EC_{50}$ values in **Table 4.1** which were unaffected by genotype ($P > 0.05$), these data suggest that ablation of Cx40 does not affect the contribution of either EDH or NO synthesis to ACh-evoked vasodilation. The significant increase in nerve-evoked vasoconstriction in KO versus WT rats observed in the perfused mesenteric bed (see **§4.3.3**) suggests that vasoconstriction may be enhanced in the absence of Cx40. Thus, agonist-induced tone was measured in mesenteric artery segments and compared between the genotypes within each sex (**Figure 4.15**). Cumulative concentration-response curves were constructed using the α_1 -adrenoceptor agonist PE and the TP agonist U46619. In both males and females, no differences were observed in the magnitude of PE-induced tone over a range of concentrations from 1 nM to 100 μ M ($P > 0.05$, **Figure 4.15a**). Conversely, in both sexes there was an overall statistical significance between the curves to U46619 ($P < 0.05$, **Figure 4.15b**). Multiple comparisons reveal that the male KO exhibited impaired vasoconstriction versus WT at U46619 concentrations of 0.3 and 1 μ M, whereas the female KO and HET exhibited impaired vasoconstriction versus WT at U46619 concentrations of 100 μ M, and $\geq 0.3 \mu$ M, respectively. The finding that knocking out Cx40 impaired U46619-induced vasoconstriction is in direct contrast with the observation of enhanced U46619-evoked vasoconstriction in isolated aortic rings from Cx40 KO mice in the literature⁷⁶⁶. Moreover, the lack of effect of Cx40 KO on PE-induced vasoconstriction is incongruous with the enhancement of nerve-evoked vasoconstriction observed in the perfused mesenteric vascular bed (**Figure 4.5**). The mechanisms underlying these discrepancies are unclear and may involve experimental differences between wire myography and tissue perfusion, such as the absence and presence of shear stress, respectively.

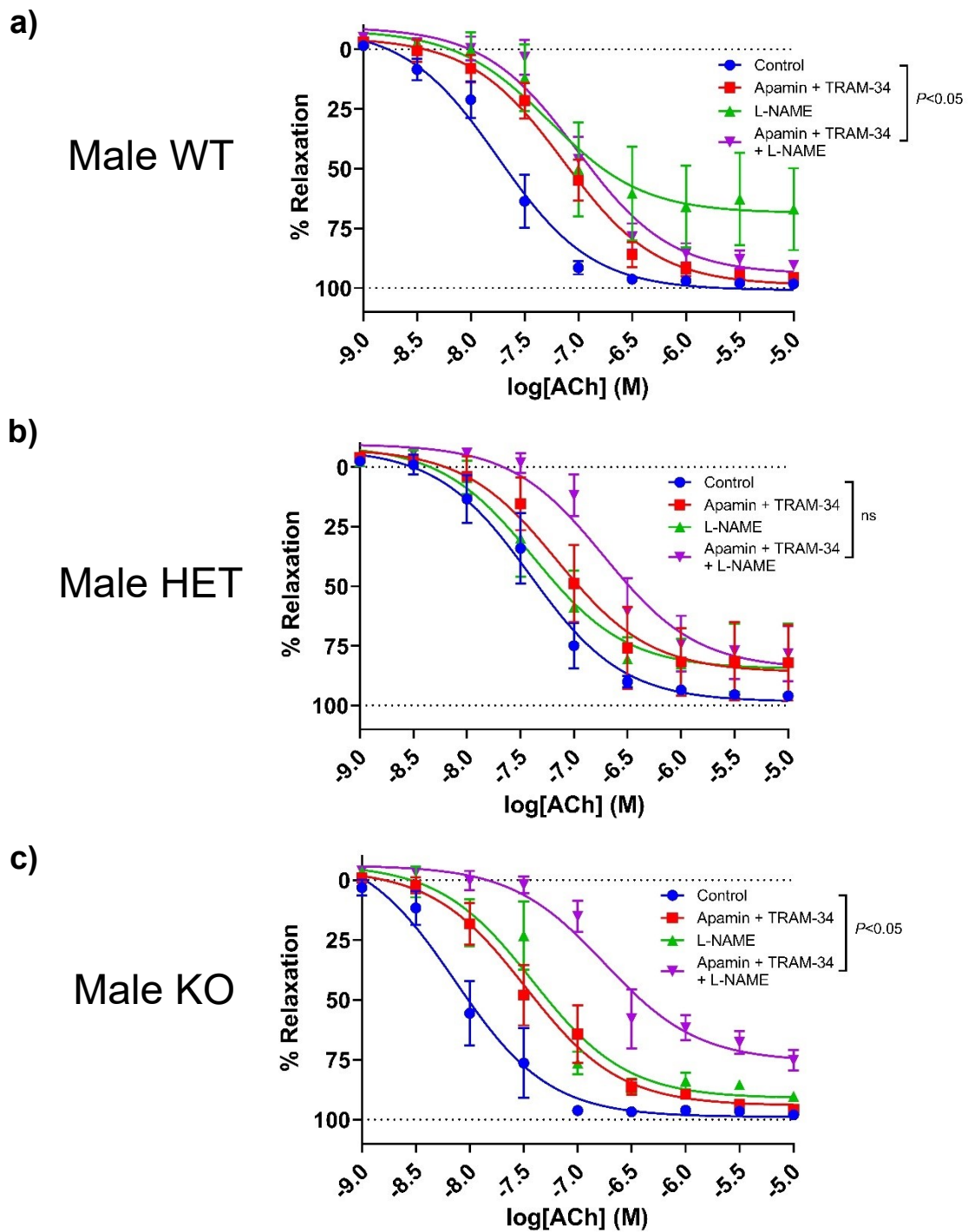


Figure 4.13: EDH and NO pathways both contribute to ACh-induced vasodilation in isolated mesenteric arteries from male WT, HET and KO rats. Wire myography was used to construct cumulative concentration-response curves to ACh in the absence and presence of apamin (50 nM), TRAM-34 (1 μ M) and L-NAME (100 μ M) using isolated second- and third-order mesenteric arteries from male **a)** WT ($n = 4-6$), **b)** HET ($n = 4-5$), and **c)** KO ($n = 3-4$) rats. Data are presented as mean \pm SEM. $P < 0.05$ was considered a significant difference between drug treatment data sets; two-way ANOVA. Data contributed by Alexia Maheux, Brandon Truong and Sufyan Malik.

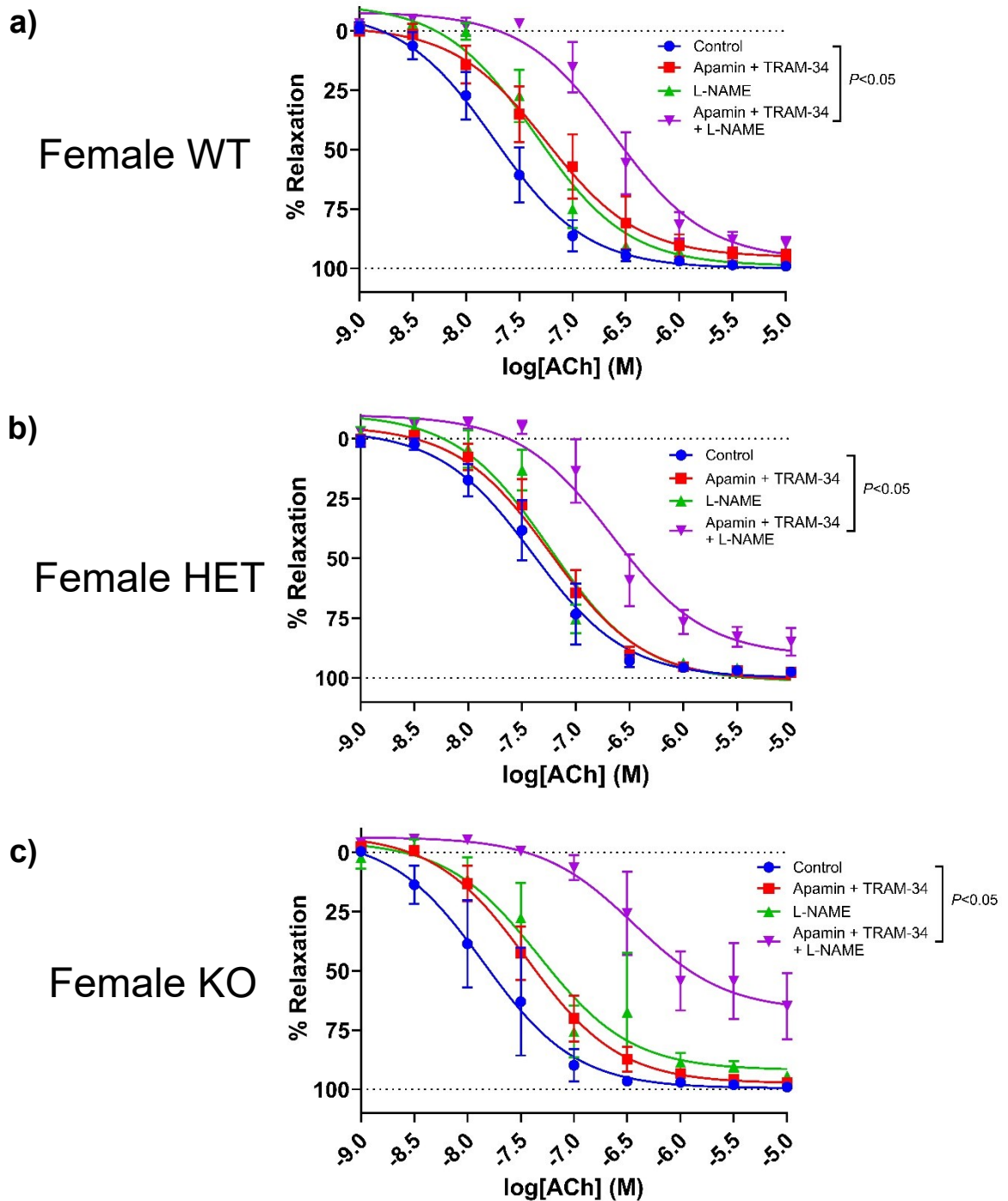


Figure 4.14: EDH and NO pathways both contribute to ACh-induced vasodilation in isolated mesenteric arteries from female WT, HET and KO rats. Wire myography was used to construct cumulative concentration-response curves to ACh in the absence and presence of apamin (50 nM), TRAM-34 (1 μ M) and L-NAME (100 μ M) using isolated second- and third-order mesenteric arteries from female **a**) WT ($n = 4-7$), **b**) HET ($n = 4-6$), and **c**) KO ($n = 4$) rats. Data are presented as mean \pm SEM. $P < 0.05$ was considered a significant difference between drug treatment data sets; two-way ANOVA. Data contributed by Alexia Maheux, Brandon Truong and Sufyan Malik.

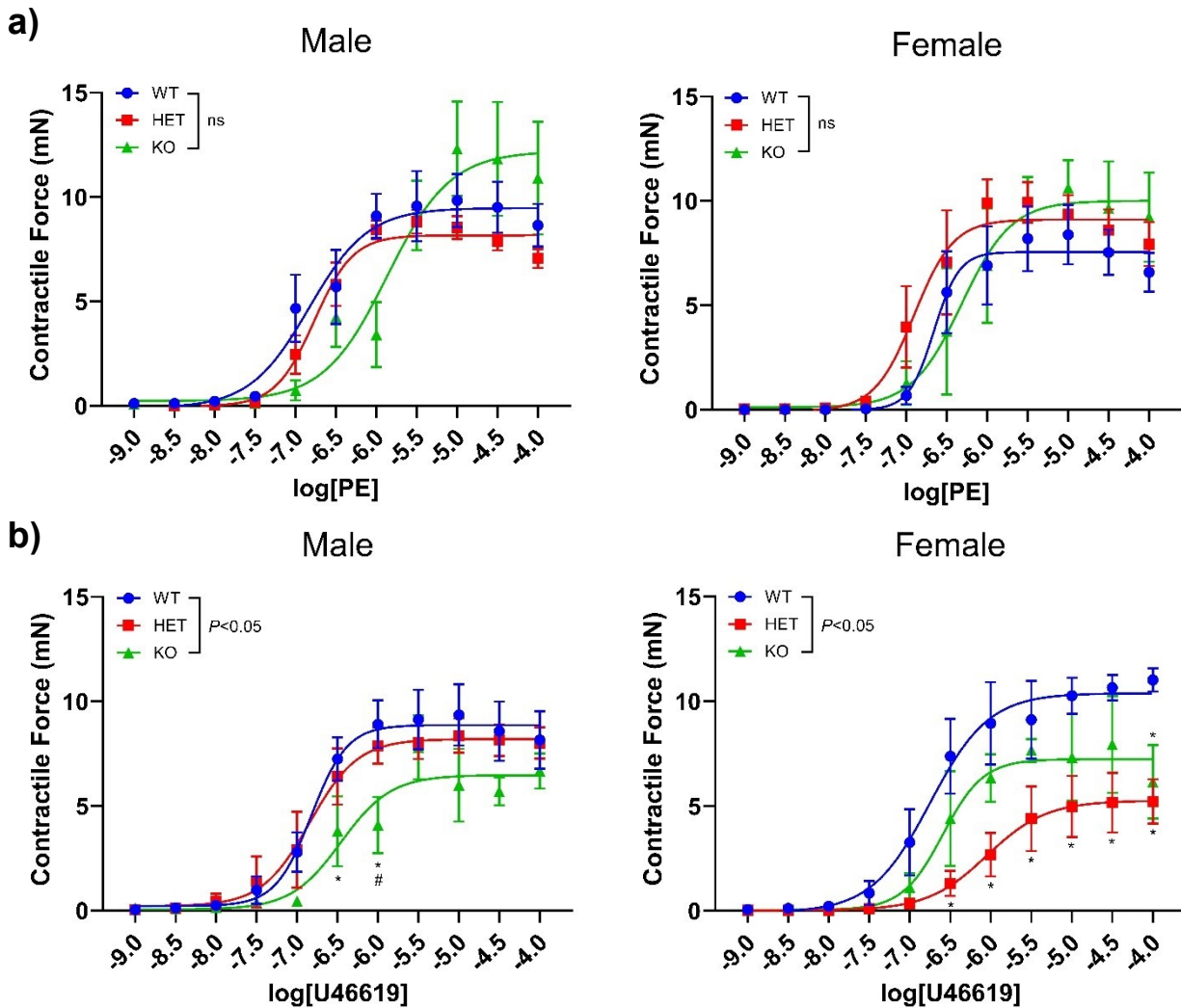


Figure 4.15: U46619-induced, but not PE-induced tone is impaired in isolated mesenteric arteries from male KO and female HET and KO rats. The isolated second- and third-order mesenteric arteries from male and female WT, HET and KO rats ($n = 4-7$) were mounted in a wire myograph and used to construct cumulative concentration-response curves to **a)** PE and **b)** U46619 (1 nM to 100 μ M). Data are presented as mean \pm SEM. * denotes $P < 0.05$ from WT and # denotes $P < 0.05$ from HET; two-way ANOVA. *Data contributed by Sufyan Malik and Caleb McInroy.*

4.3.6 Genetic ablation of Cx40 impairs post-ischemic functional recovery in the Langendorff-perfused rat heart

The putative cardioprotective role of Cx40 in ischemia/reperfusion injury was investigated using the Langendorff isolated heart perfusion. Hearts from male and female WT, HET and KO rats were perfused for a 30 minute equilibration period before the induction of global no-flow ischemia. Ischemia was maintained for 15 minutes followed by a 45 minute period of aerobic

reperfusion. LVDP was calculated as the difference between systolic and end-diastolic pressure, and two-way ANOVA was performed separately for pre- and post-ischemia (i.e. differences in LVDP between genotypes were assessed using two-way ANOVA for all pre-ischemic timepoints, then differences in LVDP between genotypes were assessed using a second two-way ANOVA for all post-ischemic timepoints). In both males and females, the overall effect of genotype was found to be statistically significant by two-way ANOVA ($P < 0.05$, **Figure 4.16**). Multiple comparisons revealed no specific timepoints at which the LVDP of the male KO heart was significantly impaired versus WT or HET (**Figure 4.16a**), but the LVDP of the female KO heart was significantly impaired versus WT at $t = 70$ min, 85 min and 90 min ($P < 0.05$, **Figure 4.16b**). This finding may be attributable to the increased heart mass observed in male and female KO rats (**Figure 4.2e**) but further investigation is required in order to establish a causal relationship.

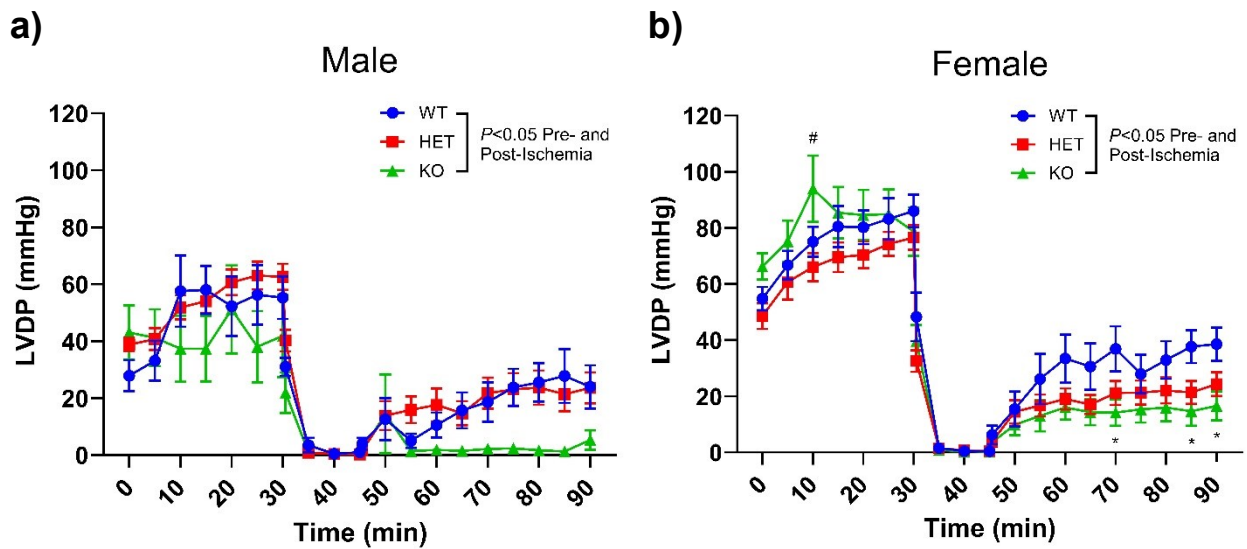


Figure 4.16: Post-ischemic functional recovery is impaired in Langendorff-perfused hearts from male and female KO rats. Hearts were excised from **a)** male WT ($n = 7$), HET ($n = 23$) and KO ($n = 5$) and **b)** female WT ($n = 15$), HET ($n = 24$) and KO ($n = 11$) rats and perfused in Langendorff mode. Global no-flow ischemia was induced at the 30 min. timepoint and flow was reinstated at the 45 min. timepoint. Data are presented as mean \pm SEM. * denotes $P < 0.05$ from WT and # denotes $P < 0.05$ from HET; two-way ANOVA. *Data contributed by Caleb McInroy.*

4.4 Discussion

The data presented in this chapter demonstrate that the genetic ablation of Cx40 in rats produces a distinct and pathological vascular phenotype. This is consistent with the patterns of Cx expression established in the literature. Of the three Cx subtypes expressed by ECs (i.e. Cx37, Cx40 and Cx43), Cx37 and Cx40 are mostly restricted to the cardiovascular system. Conversely, Cx43 is the most ubiquitously expressed Cx subtype in mammals, expressed by a wide variety of cell types throughout the body^{933,934}. Cx43 is the earliest GJ protein to be transcribed in mammalian embryonic development⁹³⁵⁻⁹³⁷, and it follows that a global KO of Cx43 results in neonatal lethality^{938,939}. The other two endothelial Cxs, Cx37 and Cx40, each have corresponding viable KO animal models, but phenotypic evidence in the Cx37 KO mouse indicates that Cx37 likely has a larger role in the control of vasculogenesis than the control of resistance artery diameter^{764,775,776,778}. Cx40 KO mice, on the other hand, show elevated systemic blood pressure, impaired EDH in isolated arteries and impaired conduction of endothelium-dependent vasodilation, as discussed previously (§4.1). Under physiological conditions, Cx40 is expressed in few tissues outside of the vascular endothelium. It is well established that Cx40 is expressed by vascular ECs and by atrial cardiomyocytes^{762,796,940}. Evidence exists to support the expression of Cx40 in cortical and spinal neurons; however, this has only been observed in early stages of neuronal development⁹⁴¹⁻⁹⁴⁴ or after the induction of traumatic brain injury⁹⁴⁵⁻⁹⁴⁷. Neuronal Cx40 expression ceases in later stages of cell differentiation, and is not detectable during normal post-natal development or adulthood^{942,948}. A few studies report Cx40 expression in other cell types such as intestinal smooth muscle^{949,950}, but most reports of Cx40 expression in other organs were found upon closer inspection to be restricted to the vascular endothelium within those organs⁹⁵¹⁻

⁹⁵⁴. Taken together, these findings suggest that any changes observed in the Cx40 KO rat versus the WT are attributable to altered vascular function.

The WKY-Gja5^{em1M^{cwi}} mutant strain used in this research was produced by introducing a 1-bp substitution into exon 1 (c.25G>T)⁸⁰³, resulting in a premature stop codon in place of Glu9^{804,805}. Using this method to induce a KO does not alter transcription, but makes translation of the functional 356 aa peptide impossible. Thus, the detection of mRNA coding for Cx40 was expected in arteries from all three genotypes, including the KO rats. This was supported by my results: using RT-qPCR, I observed no significant differences in relative expression levels of mRNA coding for Cx37, Cx40 or Cx43 between the three genotypes. Although this does not confirm the absence of Cx40, it illustrates that the other endothelial Cxs are not subject to compensatory upregulation in the HET or KO rats. In 2023 the Cupples laboratory, from whom we received the WKY-Gja5^{em1M^{cwi}} strain, demonstrated the absence of Cx40 from ECs in the renal cortex using immunohistochemical staining⁹⁵⁵. Replicating this experiment in isolated mesenteric resistance arteries is necessary to confirm the absence of functional Cx40 in the EC plasma membrane and is a future direction for this research. Similarly, protein expression levels of Cx40 and the other vascular Cxs should be measured using Western blotting.

I observed two major changes in the hemodynamic phenotype of the Cx40 KO rat: an increase in systolic blood pressure of approximately 40 mmHg in both males and females, and an increased in the relative weight of the heart. These observations are consistent with reports from Cx40 KO mice, which also experience elevated systemic blood pressure and enlargement of the heart⁷⁶⁷. Measuring the wet weight of an organ and normalizing it to body weight is a literature-accepted method for measuring tissue growth which is still used to date^{767,897,956-958}. However, this method cannot distinguish between hypertrophic and hyperplastic growth. Novielli-Kuntz *et al.*

(2019) found by weighing hearts that Cx40 KO mice exhibit an increase in heart weight relative to WT controls; the authors then used agglutinin staining to measure cardiomyocyte cross-sectional area in left atria and ventricles⁷⁶⁷. They demonstrate that the Cx40 KO mouse exhibits hypertrophic growth of both atrial and ventricular myocytes. This is notable due to the fact that in adult mammals, Cx40 is expressed in atrial cardiomyocytes but not ventricular cardiomyocytes^{793,959,960}. These results suggest that cardiac hypertrophy is not likely a direct consequence of the absence of Cx40 in the cardiomyocytes, and is more likely an indirect result of changes in vascular function. Visualising the cross-sectional area of the atrial and ventricular cardiomyocytes, as well as measuring the thickness of the left ventricular wall must be performed in the Cx40 rat to confirm that the heart enlargement in the present study is due to hypertrophy. However, the observation of cardiac hypertrophy in the Cx40 KO mouse indicates that this is a reasonable prediction.

Under normal circumstances, Cx40 has been detected in both interendothelial and myoendothelial GJs⁷⁶²; therefore, the absence of Cx40 was expected to impact both the conducted vasomotor response and EDH, respectively^{731,961}. The techniques used in this research cannot measure the vascular conducted response, so the research in this chapter instead focuses on the effect of the KO on EDH and the implications for overall vascular function. In order to determine whether endothelium-dependent vasodilation is impaired in the absence of Cx40, I assessed the function of resistance arteries using the perfused mesenteric vascular bed, and pressure and wire myography in isolated mesenteric arteries. Due to the evidence that ablation of Cx40 may impair EDH⁶⁶¹, I used the selective SK_{Ca} and IK_{Ca} blockers apamin and TRAM-34, respectively, in order to reveal the relative contribution of EDH to vasodilation in arteries from WT, HET and KO rats. Despite the fact that NO has been shown to easily diffuse through plasma membranes, there is

some evidence from Cx40 KO mice indicating that the NO pathway of vasodilation may also be affected by the ablation of Cx40. For example, the Cx40 KO mouse showed decreased expression of eNOS in aortic ECs⁷⁶⁶. Moreover, Figueroa *et al.* (2013) reported that Cx expression was necessary for the entry of extracellular NO into HeLa cells, rather than diffusion alone⁹⁶². Thus, I also assessed the contribution of NO production to vasodilation in arteries from WT, HET and KO rats using the eNOS inhibitor L-NAME.

Using the perfused mesenteric bed, I measured responses in perfusion pressure to electrical field stimulation of perivascular nerves. In the absence of any pharmacological tools, beds from KO rats exhibited significantly higher nerve-evoked vasoconstriction (approximately 200%) than those from either WT or HET rats. I expected that if EDH is impaired in the absence of Cx40, inhibiting EDH with apamin and TRAM-34 should increase nerve-evoked vasoconstriction in the WT but have no effect in the KO. In opposition to this prediction, I observed that the addition of apamin and TRAM-34 produced a proportionate increase in nerve-evoked vasoconstriction in all six genotype-sex groups. This key result demonstrates that in mesenteric resistance arteries, EDH is at least partially independent of Cx40. The addition of the eNOS inhibitor L-NAME on top of apamin and TRAM-34 produced a further increase in nerve-evoked pressure responses in all six genotype-sex groups, demonstrating that the NO pathway is also independent of Cx40. Thus, EDH and NO production both contribute to the limitation of nerve-evoked vasoconstriction regardless of whether or not Cx40 is present. The lack of effect on EDH may be explained by some reports that Cx40 is less abundant than Cx37 in MEGJs^{697,963}; it is possible that only Cx37 may be necessary for MEGJ function.

I next investigated the role of the endothelium in nerve-evoked vasoconstriction by removing the endothelial cell layer of the mesenteric bed using 0.5% Triton X-100. The effects of

apamin, TRAM-34 and L-NAME were abolished in the endothelium-denuded beds, which confirms that the endothelium was properly removed. Notably, removal of the endothelium did not reverse the enhancement of nerve-evoked responses in beds from KO rats. Endothelium-denuded mesenteric beds from male KO rats produced pressure responses 140% higher than those from male WT rats, while endothelium-denuded mesenteric beds from female KO rats produced responses 250% higher than those from female WT rats. These data indicate that the enhancement of vasoconstriction in mesenteric beds from KO rats was at least partially due to an endothelium-independent mechanism. This means that, despite the fact that Cx40 is not expressed by VSMCs, the genetic ablation of Cx40 must cause a change in smooth muscle function.

I also investigated the effect of knocking out Cx40 on myogenic reactivity, which is a crucial aspect of physiological vascular function. Myogenic tone is well-understood to be an endothelium-independent function of vascular smooth muscle^{700,880,884}; however, the results from the perfused mesenteric bed indicate that vessels from Cx40 KO rats counterintuitively display an endothelium-independent increase in nerve-evoked vasoconstriction. This led me to predict that isolated mesenteric arteries would display a similar increase in pressure-evoked vasoconstriction. However, this was not observed. Within each sex, Cx40 genotype had no significant effect on myogenic reactivity. Comparing this finding with previous literature in the Cx40 KO mouse is difficult, as only two research groups have investigated myogenic tone in the KO mouse^{768,964}. Jacobsen and Sorensen (2015) observed that myogenic reactivity was somewhat enhanced in perfused renal afferent arterioles from KO mice⁷⁶⁸. They suggest that arteries from KO mice develop myogenic tone at lower pressures than those from WT mice; however, they state that the baseline diameter of WT arteries was significantly larger than the baseline diameter of KO arteries, and did not present the normalized myogenic tone to account for this. Conversely, Chaston *et al.*

(2013) found using pressure myography in isolated mesenteric arteries that vessels from Cx40 KO mice exhibited significantly less myogenic tone than those from WT mice⁹⁶⁴. Using the current rat model, my observation of no significant effect in either direction lands between the previous two studies in mice.

Both vasoconstriction and endothelium-dependent vasodilation were further assessed using wire myography of isolated mesenteric arteries. Previous reports from Cx40 KO mice show impaired ACh-evoked vasorelaxation in isolated segments of aorta⁷⁶⁶ and renal artery⁶⁶¹, as well as enhanced vasoconstriction elicited by the thromboxane A₂ (TP) receptor agonist U46619⁷⁶⁶. In contrast, mesenteric arteries from the current rat model exhibited no effect of Cx40 genotype upon either ACh-evoked vasorelaxation, or PE-evoked vasoconstriction. Using apamin, TRAM-34 and L-NAME to inhibit SK_{Ca}, IK_{Ca} and eNOS, respectively, revealed that the relative contributions of EDH and NO production to vasorelaxation were unaffected by the ablation of Cx40. Interestingly, U46619-evoked vasoconstriction was impaired, rather than enhanced, in vessels from male KO rats versus vessels from male WT rats, and in vessels from female KO and HET rats versus vessels from female WT rats.

I also investigated the role of Cx40 in ischemia/reperfusion injury using the Langendorff heart perfusion. The expression of Cx40 in atrial cardiomyocytes is well documented^{792,793}, and has been shown in mouse models to be cardioprotective. Morel *et al.* (2014) found that an EC-specific deletion of Cx40 in mice produced greater infarct size and greater leukocyte infiltration after ischemia/reperfusion in Langendorff-perfused hearts⁸⁰⁰. Deletion of Cx40 also exacerbates ischemia/reperfusion injury in the vasculature: Fang *et al.* (2013) induced hindlimb ischemia by ligating the femoral artery and found that tissue perfusion and survival were compromised and leukocyte infiltration were increased in the Cx40 KO mouse⁹⁶⁵. My results align with the literature

and support a cardioprotective role of Cx40 in ischemia/reperfusion injury. I observed a statistically significant impairment of post-ischemic LVDP in hearts from KO rats. It is possible that this result is a consequence of the heart enlargement observed in the KO rats. However, using the Langendorff heart perfusion, it is impossible to determine whether the enlarged heart causes impaired recovery from ischemia, or whether they are concurrent but independent phenomena. Nevertheless, I suspect that the former is more likely, due the fact that Cx40 is not expressed in ventricular cardiomyocytes in adult mammals^{792,793}.

Considering all these data, the most prominent positive results in the Cx40 KO rat are a ~40 mmHg increase in systemic BP, an increase in relative mass of the heart, and an increase in nerve-evoked vasoconstriction that was at least partially endothelium-independent. These findings illustrate a crucial physiological role of Cx40, and lay out a clear path for future research: investigating the underlying change to smooth muscle function in the absence of Cx40. The previous literature in Cx40 KO mice provide some clues to which mechanisms may be responsible for the altered smooth muscle phenotype.

The most prominent factor which may explain these deleterious effects is the dysfunction of juxtaglomerular cells in the absence of Cx40. Also called renin-producing cells, juxtaglomerular cells are a specialized type of renal vascular cell found in the wall of the renal afferent arteriole at the entrance to the glomerulus^{966,967}. These cells are responsible for the synthesis of renin, a protease enzyme central to the control of systemic BP and fluid-electrolyte homeostasis as part of the renin-angiotensin-aldosterone system (RAAS)^{968,969}. Renin hydrolyzes angiotensinogen to convert it into angiotensin I, which is further converted by angiotensin-converting enzyme (ACE) into angiotensin II. Angiotensin II precipitates vasoconstriction directly by acting at the AT₁R, a G_{q/11}PCR, on VSMCs thereby increasing systemic BP⁹⁷⁰. Juxtaglomerular cells are

mechanosensitive, and regulate renin release by sensing and responding to changes in perfusion pressure (reviewed by Yamaguchi *et al.*, 2023)⁹⁶⁷. High perfusion pressure increases shear stress-induced Ca^{2+} entry, which in turn suppresses renin secretion; whereas low perfusion pressure, especially in conditions such as hypotension, dehydration, or hemorrhaging, stimulates renin secretion in order to rescue systemic BP^{967,968,971,972}. Crucially, juxtaglomerular cells are also one of the only cell types other than ECs to express Cx40⁹⁷³⁻⁹⁷⁶. Cx40 is the main Cx subtype expressed by juxtaglomerular cells^{975,976}, and is necessary for their electrical and structural coupling to both ECs and VSMCs^{977,978}. Wagner *et al.* (2010) found in the Cx40 KO mouse that in the absence of Cx40 the juxtaglomerular cells are displaced from the afferent arteriole wall, both abolishing their ability to directly sense intraarterial pressure and inhibiting the pressure-mediated negative regulation of renin synthesis and secretion usually exerted by adjacent ECs⁹⁷⁸. Thus, the absence of pressure-induced Ca^{2+} entry into juxtaglomerular cells results in the disinhibition of renin synthesis and secretion, leading to hyperreninemia and hypertension^{967,978,979}. This is now considered to be the mechanism underlying the hypertension observed in the Cx40 mouse⁹⁷⁹, based on several key pieces of evidence. Wagner *et al.* (2010) generated mice with either EC-specific or juxtaglomerular cell-specific deletion of Cx40, and observed that the juxtaglomerular cell-specific deletion of Cx40 produced hypertension, whereas the EC-specific deletion did not⁹⁷⁸. The hypertension of Cx40 KO mice was also found to be insensitive to dietary salt intake, but was fully reversed by administering RAAS inhibitors such as the ACE-inhibitor ramipril or the AT₁R antagonist candesartan⁹⁷⁴. Additionally, Cx40 and AT₁R double KO mice were found to be normotensive⁹⁸⁰.

The RAAS mechanism of hypertension has not yet been investigated in the Cx40 KO rat used in the present study. However, studies have confirmed that Cx40 is highly expressed in

juxtaglomerular cells in WKY rats^{981,982}, upon which the WKY-Gja5^{em1Mewi} strain is based. Thus, it is logical to hypothesize that the same disruption of the juxtaglomerular apparatus underlies the hypertension observed in this study. Future research should involve measuring plasma renin levels in all six genotype-sex groups, as well as immunohistochemical staining to determine whether the juxtaglomerular cells are ectopically localized as occurs in the Cx40 KO mouse⁹⁷⁸. Another useful experiment would be the administration of a non-selective GJ inhibitor such as carbenoxolone or 18 α / β -glycyrrhetic acid in the perfused mesenteric vascular bed. If the GJ inhibitor mimicked the results from the KO rat in the WT rat, this would demonstrate that the absence of Cx40 is directly responsible for the increase in nerve-evoked vasoconstriction; otherwise, this would demonstrate that the chronic, systemic consequences of knocking out Cx40 are responsible.

Hyperreninemia also serves as a putative explanation for the impairment of U46619-evoked vasoconstriction observed in arteries from KO rats using wire myography. Angiotensin II has been shown to stimulate the production of thromboxane A₂ from arachidonic acid by COX-1/2 and thromboxane synthase^{983,984}. Furthermore, the action of thromboxane A₂ at TP has also been established as a necessary contributor to angiotensin II-dependent hypertension^{985,986}. TP, like many other GPCRs, has been shown to undergo agonist-induced desensitization and internalization⁹⁸⁷⁻⁹⁹⁰. The impairment of TP agonist-induced vasoconstriction in the Cx40 rat warrants investigation of cell surface TP expression and total TP content in mesenteric arteries, as well as the measurement of plasma eicosanoids.

The increase in plasma levels of angiotensin II cannot directly explain the enhancement of vasoconstriction in the perfused mesenteric vascular bed. The mesenteric bed is flushed to remove blood then perfused with Krebs buffer, meaning that no renin or angiotensin II is present in the system. Therefore, the endothelium-independent increase in nerve-evoked vasoconstriction in

beds from KO rats must be due to a change in VSMC function. This could either be a direct effect of knocking out Cx40, or it could be an effect of chronic hyperreninemia. The latter of these options is corroborated by evidence that several animal models of systemic hypertension are accompanied by an increase in expression and/or activity of LTCCs in VSMCs^{270,271,991-995}. In particular, Pesic *et al.* (2004) demonstrated a causal relationship between intramural pressure and VSMC expression of LTCCs²⁷⁰. The authors banded rat aortae between the origins of the left and right renal arteries in order to elevate BP in the right renal artery without altering BP in the left. Western blot analyses detected a 3.25-fold increase in expression of α_{1C} (the pore-forming subunit of Cav1.2) in right renal arteries versus left renal arteries. They further demonstrated that isolated renal arteries from control rats displayed an increase in α_{1C} expression after being cultured in a depolarizing high $[K^+]$ medium. The two-kidney one-clip model used by Pesic *et al.* has been shown elsewhere to increase renin secretion in the affected kidney⁹⁹⁶. Meanwhile, another group found that rats infused with angiotensin II for 28 days displayed increased LTCC activity in isolated cerebral arteries, but showed no change in channel expression⁹⁹³. Taken together, these studies indicate that increased expression and/or activity of LTCCs in VSMCs could potentially occur in the Cx40 KO rat, and would align with the results I obtained in the perfused mesenteric vascular bed. Future experiments should assess whether α_{1C} expression is increased at both the mRNA and protein level, and whether I_{Ca} in VSMCs is increased using electrophysiological recording. Nevertheless, this line of investigation would be insufficient to explain all of my results. As a counterexample, I observed no effect of the Cx40 KO on myogenic tone in isolated mesenteric arteries; if LTCCs are upregulated in VSMCs in the Cx40 KO rat, then I would expect to have seen an enhancement of myogenic tone based upon the positive correlation between LTCC expression and myogenic vasoconstriction demonstrated in the literature^{995,997,998}.

Impairment of the conducted vasomotor response may also contribute to enhanced vasoconstriction in the perfused bed. Interendothelial GJs are mostly composed of Cx40^{697,739,900,963}. It has been proposed that the conducted vasomotor response not only allows for the control of arterial diameter upstream from a stimulus, but also allows active membrane processes to amplify the hyperpolarization as it is conducted. Studies have found that hyperpolarization conducted along the vascular EC layer decays at a slower rate than would be expected of passive conduction^{662,770}. It is possible that interendothelial conduction contributes to the limitation of nerve-evoked vasoconstriction in the perfused mesenteric vascular bed, and that the absence of Cx40 impairs this amplification of hyperpolarization. This could account for the finding that enhanced vasoconstriction occurs not only in the endothelium-denuded bed, but in the endothelium-intact bed as well. In order to investigate this in future experiments, I would measure the conducted vasomotor response in isolated resistance arteries using pressure myography combined with a pneumatic ejector as described in the literature^{765,999-1002}. Based on the literature, I hypothesize that arteries from the KO rat would show impaired conduction of endothelium-dependent vasodilation (such as to ACh or bradykinin) but would not show any change in conduction of endothelium-independent vasodilation (such as to pinacidil or adenosine)^{764,765,1003}.

Another putative explanation which would align with my results is the disruption of mechanotransduction in the absence of Cx40. In the present study, enhanced vasoconstriction was only observed in the perfused mesenteric vascular bed, and not in the pressure or wire myograph. This discrepancy was particularly surprising, since both nerve- and PE-evoked vasoconstriction are mediated by α_1 -adrenoceptor agonism. The most obvious difference between these assays is that the perfused mesenteric vascular bed is the only one to incorporate shear stress, which is a physiologically relevant vasodilatory stimulus^{691,695}. As I have discussed previously,

mechanosensation in the vasculature is not fully understood, and is thought to be the sum of functions of many different protein structures including the extracellular matrix, integrins, cytoskeleton proteins, and mechanosensitive ion channels (reviewed by Davis *et al.*, 2023)⁴⁹⁵. It is unclear if Cx40 is directly involved in mechanosensation, but studies have demonstrated that Cx40 is at least indirectly linked to mechanosensation¹⁰⁰⁴. I have previously discussed that Cx40 is necessary for the detection of BP by juxtaglomerular cells; however, Cxs have been associated with mechanosensation elsewhere in the vasculature as well. Shear stress is a regulator of Cx expression and distribution in ECs, and has been shown to alter both mRNA and protein expression of Cx40, albeit with contradictory results. Shear stress has been shown to upregulate Cx40 in cultured human aortic ECs¹⁰⁰⁵ and HUVECs¹⁰⁰⁶, but has also been shown to downregulate Cx40 in cultured rat aortic ECs¹⁰⁰⁷. In human coronary artery ECs co-cultured with SMCs, low shear stress (5 dyn/cm²) downregulated Cx40 versus no-flow controls, but higher shear stress (12 dyn/cm²) maintained the same expression level of Cx40 versus no-flow¹⁰⁰⁸. Moreover, knockdown of Cx40 with siRNA causes a morphological change to ECs and they become elongated in shape, which may affect their function¹⁰⁰⁵. These data do not create a clear illustration of Cx40's role in mechanotransduction, but nevertheless suggest that Cx40 expression and mechanotransduction are closely related. Mechanotransduction is not only a property of vascular ECs and juxtaglomerular cells, but of VSMCs as well⁴⁹⁵, which could account for the endothelium-independent component of the response I observed in the perfused mesenteric vascular bed. In order to investigate the role of Cx40 in mechanotransduction, I propose using electrophysiological recording of EC and VSMC membrane potential in endothelium-intact and -denuded isolated mesenteric arteries from WT, HET and KO rats in the presence and absence of shear stress (as described previously^{546,700}). If any differences in shear stress-induced V_M were observed, I would then measure mRNA and

protein levels of the most prominent proteins involved in mechanotransduction including Piezo1, TRPV4, TRPC6 and TRPM4⁴⁹⁵ to determine whether ablation of Cx40 affects expression of these channels.

The other major difference between nerve- and PE-evoked vasoconstriction is that nerve-evoked vasoconstriction is not solely mediated by α_1 -adrenoceptor agonism. In addition to releasing NA, sympathetic nerves co-release ATP and NPY, which act as vasoconstrictors at P2X and Y receptors, respectively^{367,368}. The only evidence of Cx40's involvement in this process suggests that Cx40 may be required for α_1 -adrenoceptor signalling in the kidney, and that pharmacological inhibition of Cx40 attenuates PE-evoked vasoconstriction in the glomerulus¹⁰⁰⁹. This is opposite to what I observed, wherein knocking out Cx40 greatly enhanced nerve-evoked vasoconstriction and had no effect on PE-evoked vasoconstriction.

In summary, the data presented in this chapter support the hypothesis that the Cx40 KO rat experiences impaired endothelial modulation of resistance artery diameter in addition to the large endothelium-independent component of the observed effects. Cx40 is necessary in the maintenance of normal cardiovascular function, as rats lacking Cx40 experience pronounced hypertension and enlargement of the heart. Additionally, nerve-evoked vasoconstriction is greatly enhanced in the absence of Cx40, indicating that Cx40 is an important contributor to the physiological control of resistance artery diameter and therefore tissue blood flow and arterial BP.

Chapter 5: Genetic ablation of Cx40 decreases the magnitude of vascular dysfunction incurred in mild hypercaloric challenge

5.1 Introduction

CVD is the global leading cause of death, and is a prevalent comorbidity of metabolic disease states such as T2DM (see §1.1.1). The data presented in **Chapter 4** demonstrate that Cx40 serves a crucial physiological role in cardiovascular function, particularly in the maintenance of systemic blood pressure and the limitation of vasoconstriction in resistance arteries. Within this chapter, I will investigate the role of Cx40 in cardiovascular pathophysiology and the development of CVD.

T2DM is characterized by hyperglycemia and hyperinsulinemia, both of which increase NOX expression and activity in ECs³¹. This in turn increases oxidative stress within ECs, leading to the uncoupling of eNOS, decreased bioavailability of NO, and ultimately impaired endothelium-dependent vasodilation^{16,31}. The inability of the endothelium to perform its physiological role in the maintenance of vascular tone is called endothelial dysfunction. Endothelial dysfunction is accepted to be an early factor driving the development of atherosclerotic CVD, occurring before the development of the diagnostic features of T2DM^{473,1010-1013}.

The phenotypic changes in endothelial dysfunction also include changes in GJ expression and activity. Over the past two decades, many studies have established that vascular gap junctional communication is altered in disease states including diabetes mellitus, hypertension, and atherosclerosis (reviewed by Brisset *et al.*, 2009; and Leybaert *et al.*, 2017)^{917,1014}. However, the nature of these changes varies depending upon the disease or disease model, and the type and location of affected arteries. One of the first studies to examine pathophysiological changes in connexin function used a rat model of renovascular hypertension⁹⁸¹. The left renal artery of the rat was clipped to induce renin-dependent hypertension; in response, the authors found increased

mRNA and protein expression of Cx40 in both kidneys, particularly in the juxtaglomerular cells and endothelium of the afferent arteriole. Similarly, a later study by Zhang *et al.* (2005) found in mice that streptozotocin (STZ)-induced diabetes (analogous to T1DM) was accompanied by an increase in Cx37 expression in the glomerulus and an increase in Cx40 expression in the renal afferent arteriole⁹⁷⁵.

Conversely, outside of the renal vasculature, CVD is mostly characterized by downregulation of endothelial Cx40 and Cx37 rather than upregulation. One of the earliest studies concerning connexin regulation in diabetes observed that cultured rat microvascular ECs subjected to hyperglycemia exhibited downregulation in Cx43, but no change in expression of Cx37 or Cx40¹⁰¹⁵. However, animal studies using *in vivo* models such as STZ-induced diabetes soon followed, with most reporting that Cx40 and/or Cx37 are downregulated in CVD¹⁰¹⁶⁻¹⁰¹⁸. Makino *et al.* (2008) found that STZ-induced diabetes in mice was accompanied by decreased protein expression of both Cx37 and Cx40 in coronary artery ECs¹⁰¹⁷. The authors also found that inhibition of Cx40 by ⁴⁰Gap27 (300 μ M) abolished endothelium-dependent relaxation to ACh in diabetic vessels, but a much larger concentration (600 μ M) was necessary to see partial inhibition in control vessels. These data demonstrate that a decrease in the population and possibly activity of Cx40 contributes to endothelial dysfunction in diabetes. The same research group later demonstrated that increased *O*-linked N-acetylglucosamine protein modification of Cx40 may underlie its downregulation in diabetes¹⁰¹⁸. Furthermore, evidence shows that conduction of vasoconstrictor responses has been shown to be impaired in cremaster arterioles from STZ-induced diabetic mice versus control mice¹⁰¹⁹.

Cx37 and Cx40 are also downregulated in models of T2DM. Young *et al.* (2008) showed that the Zucker obese rat experienced a significant decrease in mRNA and protein levels of Cx37

and Cx40, but not Cx43, in mesenteric arteries¹⁰²⁰. In 2016, Takahashi *et al.* reported that high-fat diet (HFD)-fed mice were more susceptible to the induction of atrial arrhythmia, and simultaneously showed that Cx40 expression was greatly decreased in atrial cardiomyocytes¹⁰²¹. HFD has also been found to cause downregulation of atrial Cx40 and Cx43 in rats⁷⁷². Most recently, in 2021 Si *et al.* reported that Cx40 protein expression in coronary artery ECs is significantly decreased in mice receiving single-dose STZ followed by HFD⁷⁹⁹. The authors also found that T2DM was associated with decreased expression of human antigen R (HuR), an RNA-binding protein responsible for regulating the expression and stability of mRNAs of many genes, including *Gja5*, which encodes Cx40^{799,1022}. Correspondingly, they observed lower levels of *Gja5* mRNA binding to HuR, and suggest that the decrease in HuR expression is likely to underlie the decrease in Cx40 expression observed in T2DM.

Alterations in connexin expression have also been implicated in the etiologies of other forms of CVD^{917,1014,1023,1024}. In a mouse model of atherosclerosis, endothelial cells covering atherosclerotic plaques were found to stop expressing Cx37 and Cx40 in favour of upregulated Cx43¹⁰²⁵. A high cholesterol diet-induced model of hyperlipidemia in mice has also shown to decrease expression of Cx37 and Cx40 in aortic ECs, with the notable finding that treatment with simvastatin rescues expression of Cx37 but not Cx40¹⁰²⁶. In a similar manner, induction of generalized inflammation by i.p. injection of lipopolysaccharide greatly reduced Cx37 and Cx40 expression in aortic endothelium of mice¹⁰²⁷. Oral L-NAME-induced hypertension was also found to reduce aortic endothelial connexin expression in rats; however, only Cx37 and Cx43, but not Cx40, were reduced¹⁰²⁸. Even aging, which itself increases the risk of CVD, has been found to be associated with decreased expression of all three endothelial connexins in the rat aorta¹⁰²⁹.

In addition to pathophysiological changes in connexin expression, there is some evidence for changes in connexin activity via posttranslational modification^{762,917}. The conductance of Cx40-containing hemichannels is increased by PKA-mediated phosphorylation at the C-terminus of Cx40¹⁰³⁰⁻¹⁰³². Low levels of ROS activate PKA, whereas high levels of ROS, as are characteristic of many disease states, have been shown to decrease PKA activity^{1031,1033}. Thus, high ROS production leads to decreased phosphorylation of Cx40, thereby increasing the resistance of interendothelial coupling⁷⁶². This link has been demonstrated in the contexts of ischemia/reperfusion injury and sepsis, wherein elevated ROS production leads to a decrease in Cx40 conductance^{1031,1034-1036}.

From the literature, it is clear that alterations in endothelial Cx40 correlate with endothelial dysfunction in CVD. In most arteries, CVD is associated with a decrease in Cx40 expression and activity, which bolsters the case for a cardioprotective role of Cx40. However, it is unclear whether the downregulation of Cx40 is a contributor to CVD, or simply a consequence of CVD. I aim to elucidate the role of Cx40 in the onset of T2DM by using a mildly hypercaloric HFD model analogous to prediabetes in humans. The diet used in this research is based on a formulation by our collaborator Dr. Ahmed El-Yazbi for the purpose of studying the onset of endothelial dysfunction before the establishment of T2DM or obesity^{473,818,819}. In this chapter, I apply the mild hypercaloric challenge as a stressor to the novel Cx40 KO rat. I hypothesize that *the Cx40 KO rat is more susceptible to endothelial dysfunction than the WT rat, and will therefore incur a greater magnitude of arterial functional impairment when subjected to a mild hypercaloric challenge.*

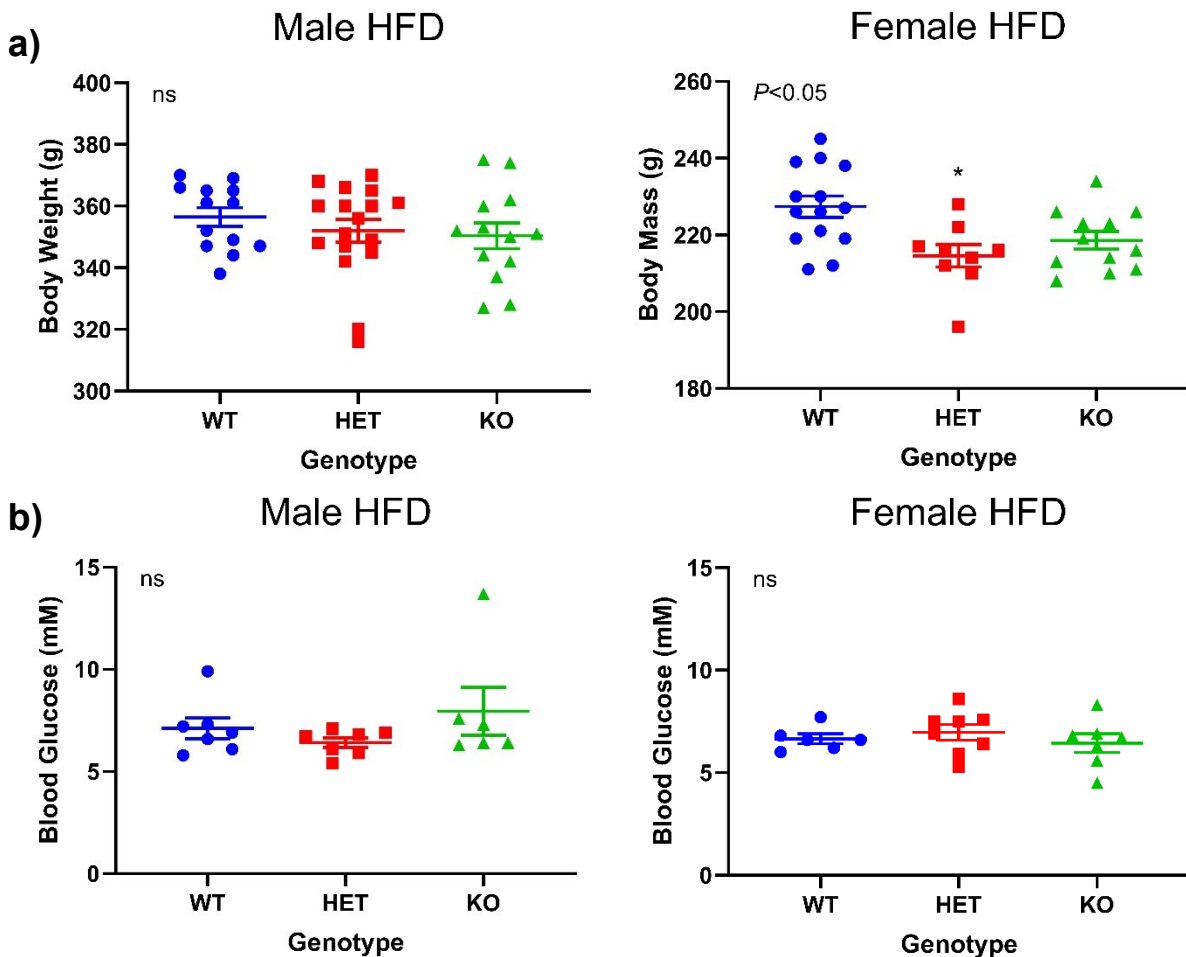
5.2 Methods

A full description of methods is provided in **Chapter 2**. As stated in §2.2, experiments in this chapter use Cx40^{+/+} (wild-type or WT), Cx40^{+/-} (heterozygous or HET), and Cx40^{-/-} (knock-out or KO) rats bred from the WKY-Gja5^{em1M_{cwi}} mutant strain.

5.3 Results

5.3.1 Hypercaloric challenge does not affect Cx40 KO-induced hypertension or heart enlargement

In order to investigate the cardiovascular impact of mild hypercaloric challenge in the Cx40 KO rat model, male and female WT, HET and KO rats were fed with HFD from 3 months of age until euthanasia at 6 months of age. I first assessed gross phenotypic changes in the metabolic and hemodynamic properties of the rats (**Figure 5.1**). As in the control diet (CD)-fed rats from the previous chapter (§4.3.2), no significant differences in body weight were observed between genotypes in male rats ($P>0.05$, **Figure 5.1a**). However, HFD-fed female HET rats were



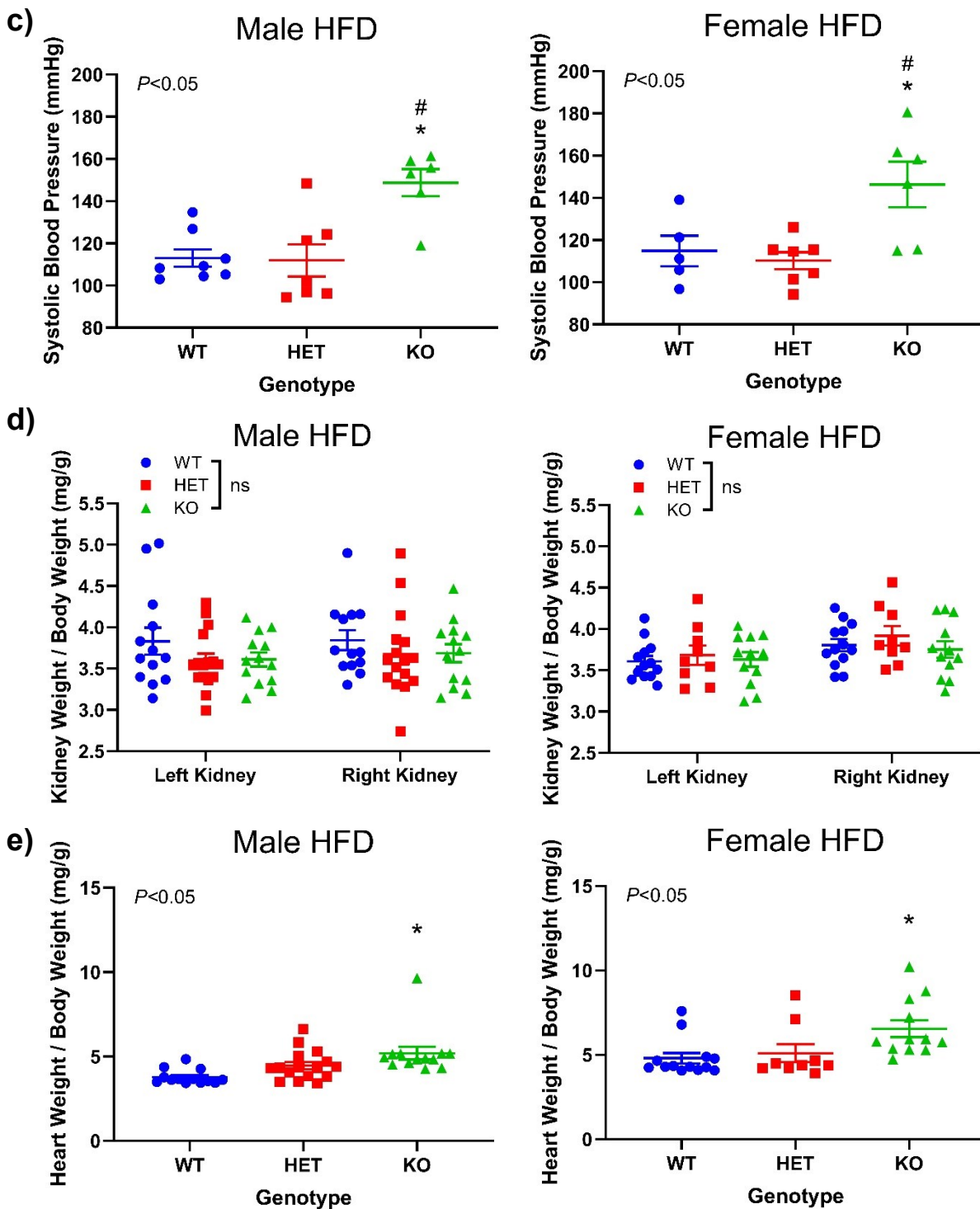
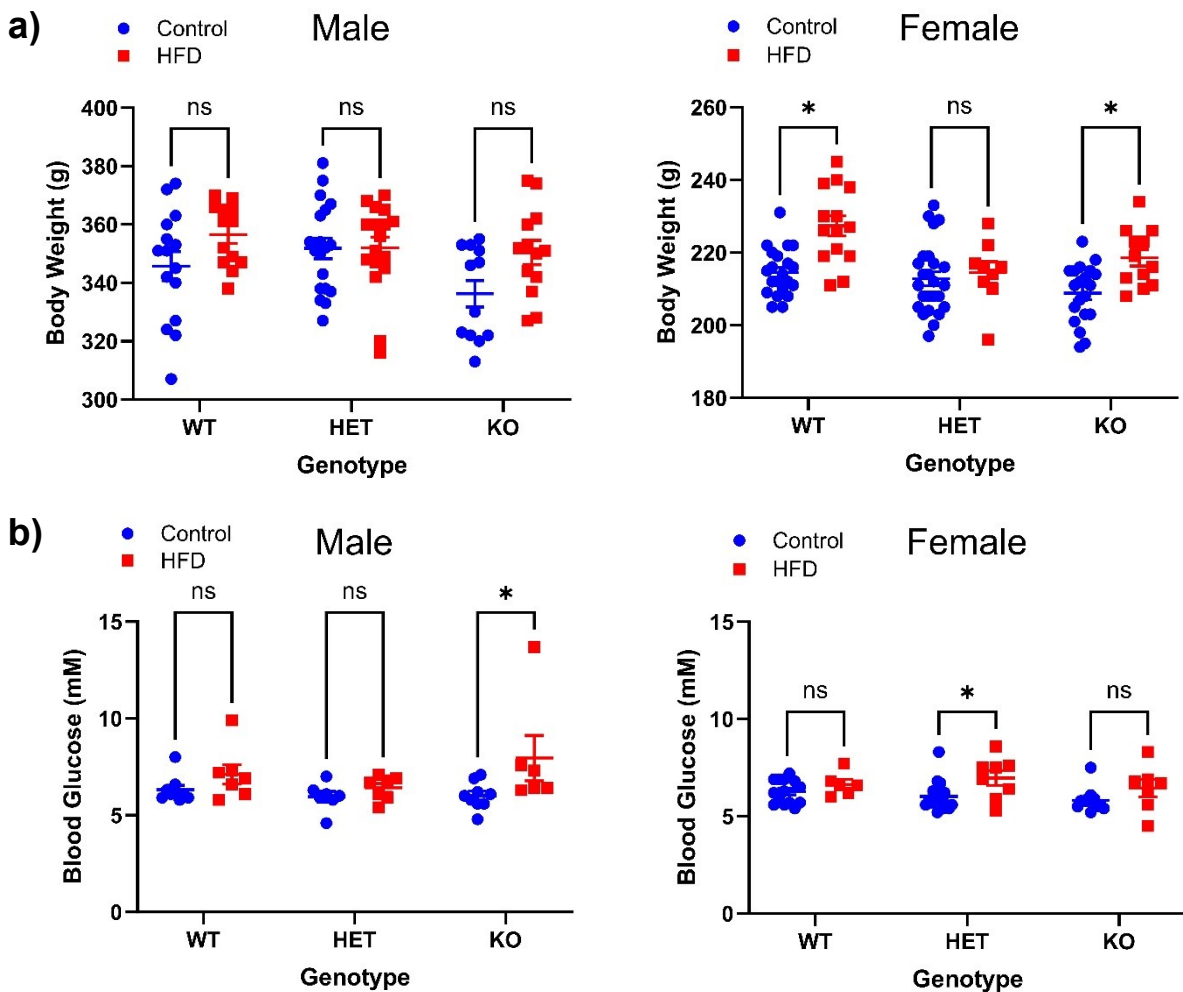


Figure 5.1: HFD does not alter Cx40 KO-induced increase in systolic blood pressure and heart mass. Gross metabolic and hemodynamic characteristics of HFD-fed male and female WT, HET, and KO rats were measured at six months of age after 12 weeks of HFD feeding, including **a**) body weight ($n = 9-17$), **b**) random blood glucose ($n = 6-8$), **c**) systolic blood pressure ($n = 5-8$), **d**) left and right kidney weight ($n = 9-16$), and **e**) heart weight ($n = 9-16$). Data are presented as mean \pm SEM. * denotes $P < 0.05$ from WT and # denotes $P < 0.05$ from HET; one-way ANOVA. Tail cuff plethysmography performed by Jad Julian-Rachid.

significantly smaller than HFD-fed female WT rats with a mean difference of 12.8 ± 3.9 g ($n = 9-14$). Within each sex, random blood glucose was unaffected by genotype ($P > 0.05$, **Figure 5.1b**). The increase in systemic BP observed in the CD-fed KO rats was also preserved in the HFD-fed rats. HFD-fed KO rats exhibited a statistically significant increase in systolic BP versus HFD-fed WT and HET rats within each sex ($P < 0.05$, **Figure 5.1c**). In males and females, the mean systolic BP of HFD-fed KO rats (148.8 ± 6.4 mmHg, $n = 6$ and 146.3 ± 10.8 mmHg, $n = 6$, respectively) was approximately 35 mmHg greater than that of either HFD-fed WT rats (113.1 ± 4.1 mmHg, $n = 8$ and 114.8 ± 7.2 mmHg, $n = 5$, respectively) or HET rats (111.9 ± 7.6 mmHg, $n = 7$ and 110.2 ± 4.1 mmHg, $n = 7$, respectively). No differences were observed in heart rate between genotypes ($P > 0.05$; data not shown). Finally, wet weights of kidneys and hearts were measured upon excision and expressed relative to body weight (and e). Like the CD-fed rats, no significant difference was observed in relative kidney weight between genotypes of HFD-fed rats ($P > 0.05$, **Figure 5.1d**). Hearts from HFD-fed KO rats of both sexes were enlarged versus those from HFD-fed WTs ($P < 0.05$), but were not significantly larger than those from HFD-fed HETs ($P > 0.05$, **Figure 5.1e**).

Next, I have compared these biometric data from the HFD-fed rats (**Figure 5.2**) to the corresponding data from the CD-fed rats (§4.3.2). HFD-fed male WT, HET and KO rats experienced no significant change in body weight versus CD-fed controls. In contrast, HFD-fed female WT and KO rats both experienced a statistically significant increase in body weight versus controls ($+12.8 \pm 3.0$ g, $n = 14-21$ and $+9.7 \pm 3.1$ g, $n = 12-20$, respectively; $P < 0.05$) whereas HFD-fed HETs did not ($P > 0.05$, **Figure 5.2a**). The HFD did not affect random blood glucose in most genotype-sex groups ($P > 0.05$), except for male KO rats and female HET rats, which experienced significant increases versus control ($P < 0.05$, **Figure 5.2b**). Next, I observed that HFD had no significant effect on systolic BP in any of the genotype-sex groups ($P > 0.05$, **Figure 5.2c**).

Although I have shown that the HFD-fed male KO still experienced significant heart enlargement versus the HFD-fed male WT, comparing across the diets shows a significantly greater heart weight in the CD-fed male KO than in the HFD-fed male KO ($P < 0.05$, **Figure 5.2d**). Finally, HFD was found to have no effect on kidney weight in the male rats ($P > 0.05$, **Figure 5.2e**). Surprisingly, in all genotypes, HFD-fed female rats had significantly smaller relative kidney weight than CD-fed female rats ($P < 0.05$). Additionally, this effect was still present when accounting for changes in body weight by comparing the absolute weight of the kidneys (**Figure B1, Appendix B**).



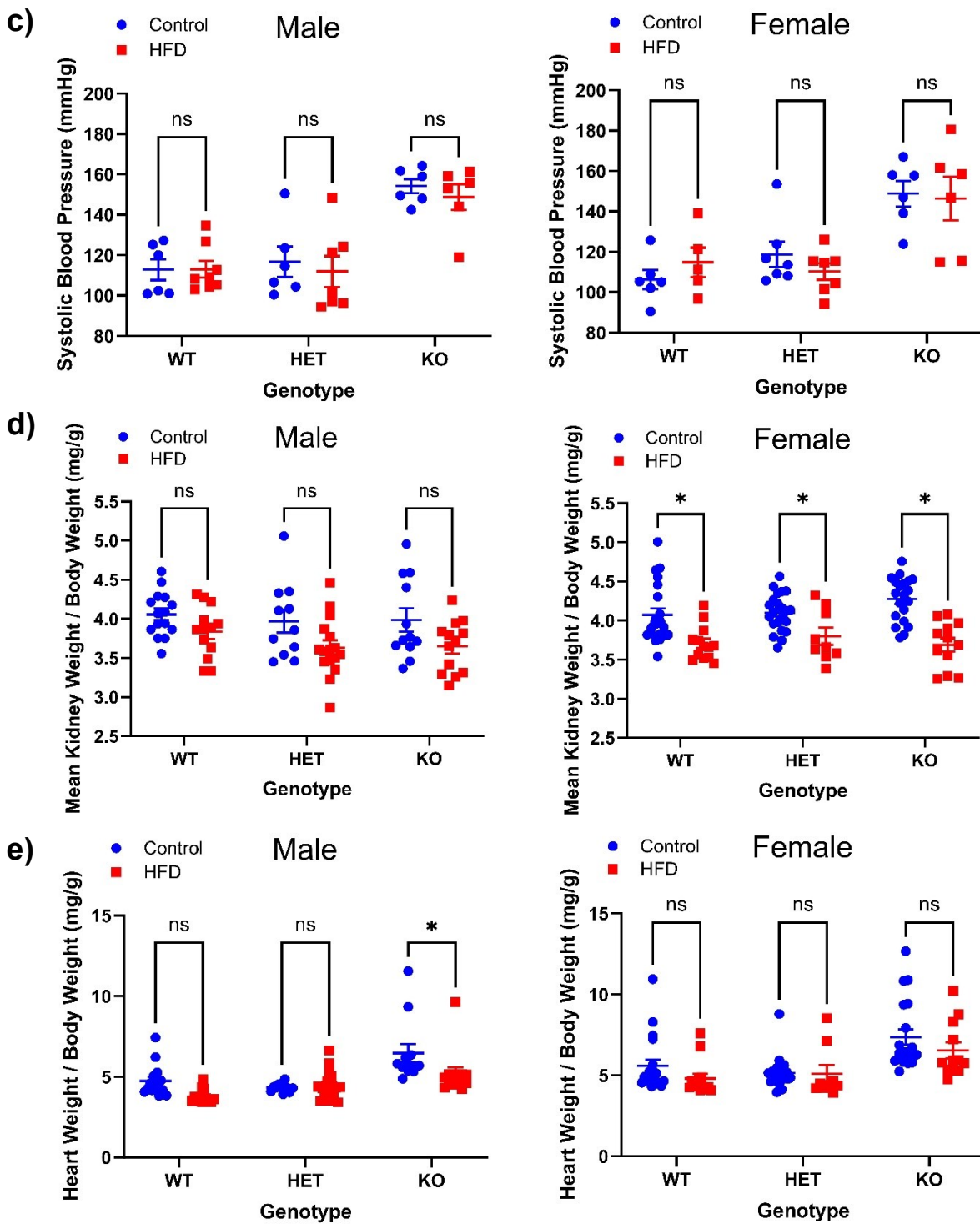


Figure 5.2: Comparisons of phenotypic changes between control and HFD-fed rats. Gross metabolic and hemodynamic characteristics of control and HFD-fed male and female WT, HET, and KO rats were compared on the basis of diet within each genotype-sex group. **a)** body weight ($n = 9-25$), **b)** random blood glucose ($n = 6-18$), **c)** systolic blood pressure ($n = 5-8$), **d)** mean kidney weight ($n = 9-22$), and **e)** heart weight ($n = 9-22$). Data are presented as mean \pm SEM. * denotes $P < 0.05$ from control diet; two-way ANOVA with Šidák's multiple comparison tests. *Tail cuff plethysmography performed by Jad Julian-Rachid.*

5.3.2 Hypercaloric challenge enhances nerve-evoked vasoconstriction but does not impair EDH or NO production

Next I aimed to characterize the effect of hypercaloric challenge on the physiological function of resistance arteries in the Cx40 KO rat model. Using the same methods and experimental parameters as in the CD-fed rats (§4.3.3), I recorded responses in perfusion pressure to nerve-evoked vasoconstriction in the perfused mesenteric vascular beds of HFD-fed male and female WT, HET and KO rats. Frequency-response relationships from 1 to 40 Hz were constructed in the absence and presence of the SK_{Ca} inhibitor apamin (50 nM), the IK_{Ca} inhibitor TRAM-34 (1 μM) and the eNOS inhibitor L-NAME (100 μM). The administration of apamin + TRAM-34 and apamin + TRAM-34 + L-NAME produced statistically significant increases in nerve-evoked vasoconstriction in all genotype-sex groups ($P < 0.05$, **Figure 5.3**). Similarly to the CD-fed rats, treatment with apamin + TRAM-34 produced an increase in pressure responses only at the highest frequencies (20-40 Hz). This increase was proportionally larger in WT beds than in KO beds: at 30 Hz, apamin + TRAM-34 caused a 165% increase in the HFD-fed WT response, but only a 130% increase in the HFD-fed KO response. In females, these increases were 160% and 150%, respectively. This may indicate that HFD reduces the contribution of EDH to inhibition of vasoconstriction in the absence of Cx40. Administering apamin + TRAM-34 + L-NAME produces increases in nerve-evoked vasoconstriction at frequencies as low as 10 Hz, with a disproportionately high increase in the HFD-fed KO beds from both sexes. At higher frequencies of stimulation, the responses in the presence of all three inhibitors reach a tissue maximum in each genotype-sex group and become indistinguishable from the responses in the presence of apamin + TRAM-34, particularly in the HFD-fed KO beds.

Comparing across genotypes (**Figure 5.4**) reveals that mesenteric beds from HFD-fed male and female KO rats exhibit a statistically significant increase in pressure responses versus HFD-

fed WT and HET beginning at 15 Hz stimulations in the males and 20 Hz in the females ($P < 0.05$, **Figure 5.4a** and **d**). In the CD-fed rats, this increase was approximately 200%, but is noticeably smaller in the HFD-fed rats (~165% in males and ~135% in females). The increased pressure responses in the HFD-fed KO beds versus the HFD-fed WT and HET beds are maintained after the addition of apamin + TRAM-34 or apamin + TRAM-34 + L-NAME ($P < 0.05$, **Figure 5.4b**, **c**, **e** and **f**). Notably, in the presence of all three inhibitors, the HFD-fed male KO displays a left-shifted frequency response curve versus HFD-fed male WT and HET, but no longer displays an increase in the maximum response. At 30 Hz, the KO is no longer significant versus the WT, and at 40 Hz, the KO is not significant versus either the WT or HET ($P > 0.05$, **Figure 5.4c**). A similar phenomenon occurs in the female beds, where the frequency-response curve in the HFD-fed KO is left-shifted but does not display an increased maximum response versus the HFD-fed WT (**Figure 5.4f**).

Finally, in order to directly assess the effect of the hypercaloric challenge, the data in beds from HFD-fed rats have been compared with the corresponding data in beds from CD-fed rats (**Figures 5.5**, **5.6** and **5.7**). In beds from male rats, HFD had no significant effect on nerve-evoked vasoconstriction in HET rats ($P > 0.05$, **Figure 5.6a**, **b** and **c**) but increased responses in WT and KO rats ($P < 0.05$, **Figures 5.5a**, **b** and **c** and **5.7a**, **b** and **c**). In beds from female rats, divisions based upon genotype were less clear, but notably reveal no significant differences in the presence of apamin + TRAM-34 + L-NAME ($P > 0.05$, **Figures 5.5f**, **5.6f** and **5.7f**). This indicates that in beds from female rats, HFD had no effect on the combined contribution of EDH and NO production.

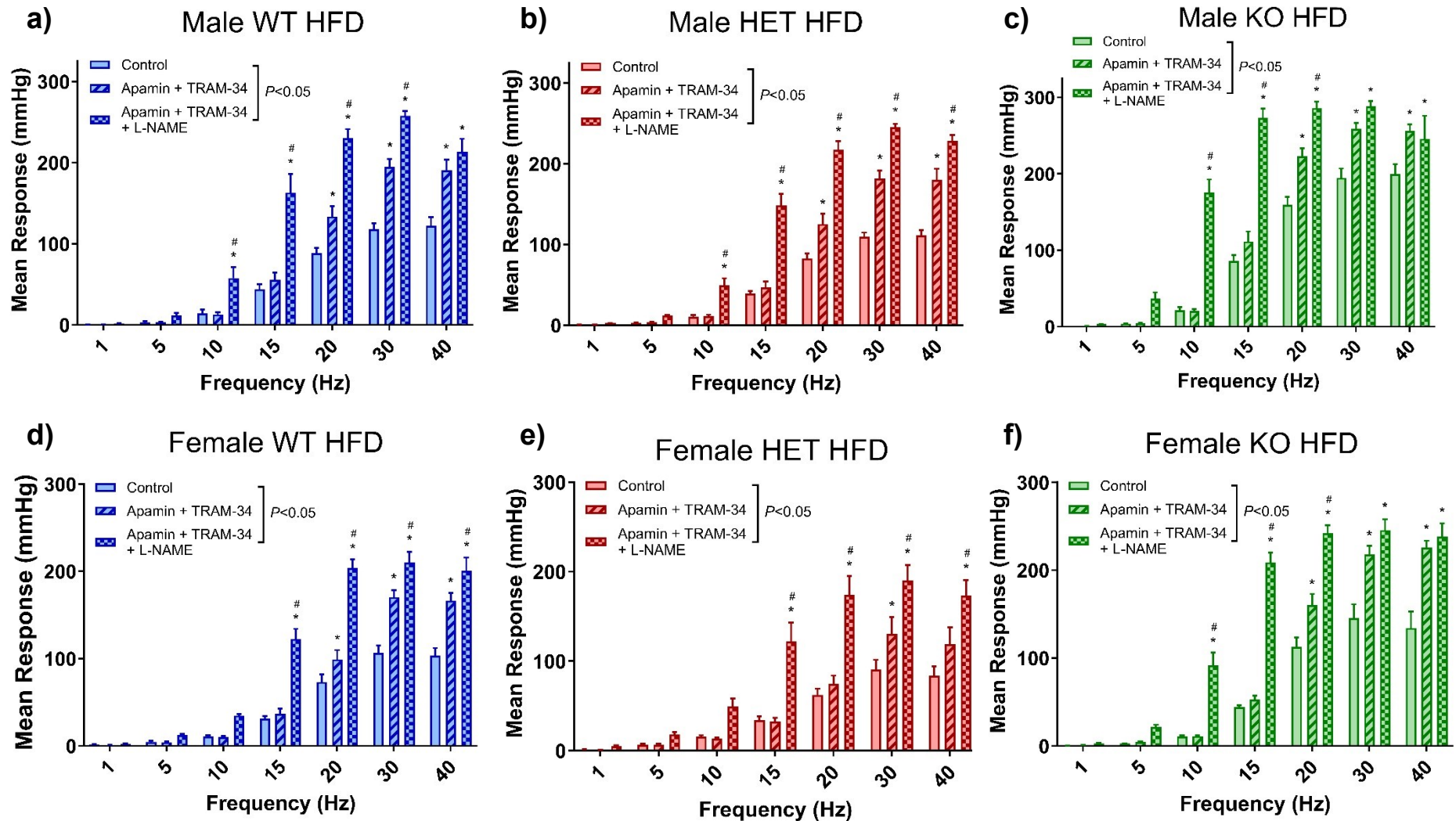


Figure 5.3: HFD does not impair contribution of EDH and NO synthesis to inhibition of nerve-evoked vasoconstriction in perfused mesenteric vascular beds from Cx40 WT, HET and KO rats. Frequency-response relationships constructed in the absence and presence of apamin (50 nM), TRAM-34 (1 μ M) and L-NAME (100 μ M) using endothelium-intact mesenteric vascular beds from HFD-fed male **a)** WT ($n = 6$), **b)** HET ($n = 9$), and **c)** KO ($n = 7$) rats, and female **d)** WT ($n = 7$), **e)** HET ($n = 6$), and **f)** KO ($n = 6$) rats. Data are presented as mean \pm SEM. * denotes $P < 0.05$ from control and # denotes $P < 0.05$ from Apamin + TRAM-34; two-way ANOVA.

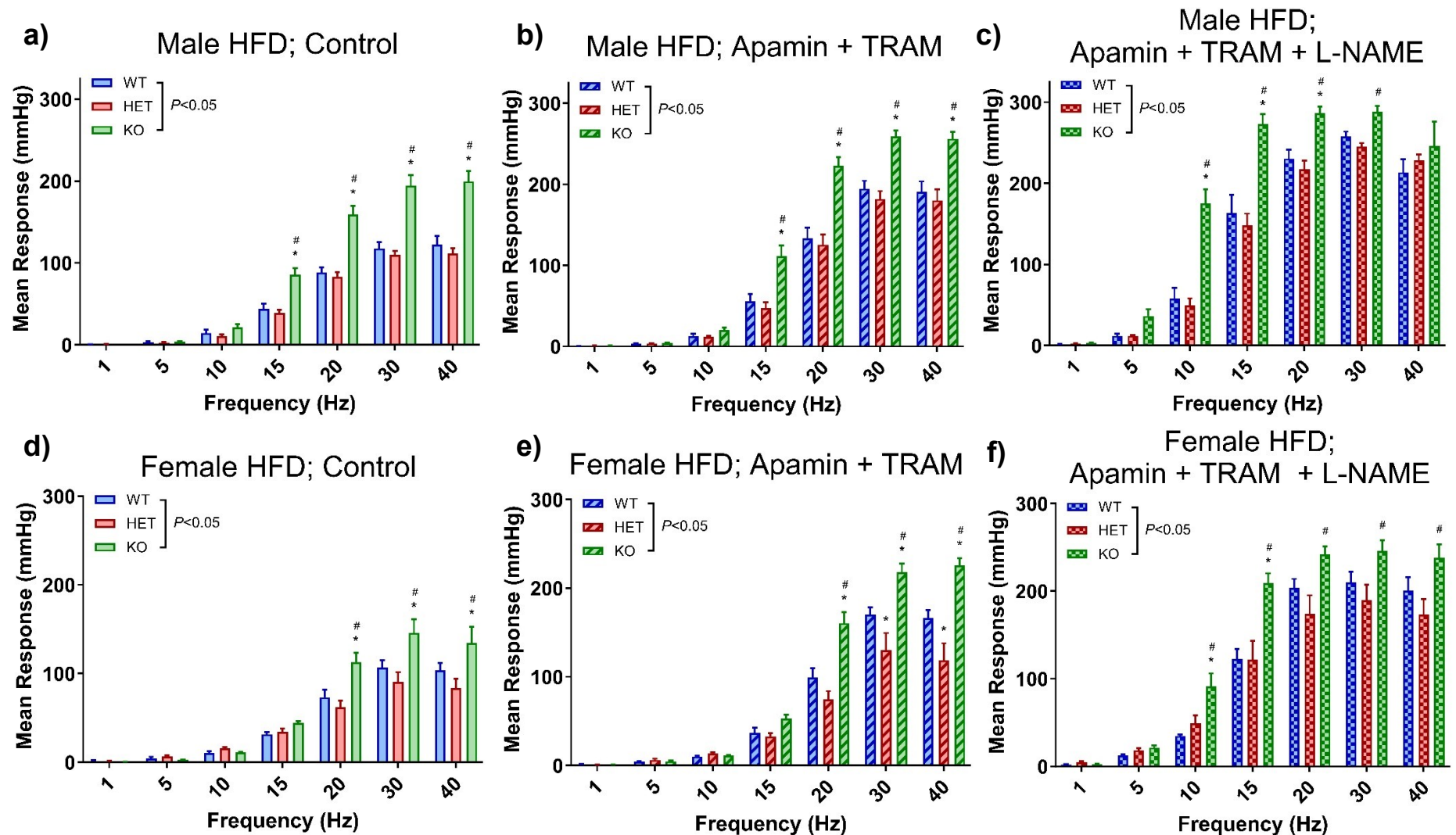


Figure 5.4: Genetic ablation of Cx40 enhances nerve-evoked vasoconstriction in the perfused mesenteric vascular bed from HFD-fed rats. Unpaired frequency-response relationships of perfused mesenteric vascular beds from HFD-fed male (a, b, and c) and female (d, e, and f) WT ($n = 6-7$), HET ($n = 6-9$) and KO ($n = 6-7$) rats compared across genotypes within each drug treatment. Beds were perfused in the absence of drugs (a and d), in the presence of apamin (50 nM) and TRAM-34 (1 μ M; b and e), or in the presence of apamin, TRAM-34 and L-NAME (100 μ M; c and f). Data are presented as mean \pm SEM. * denotes $P < 0.05$ from WT and # denotes $P < 0.05$ from HET; two-way ANOVA.

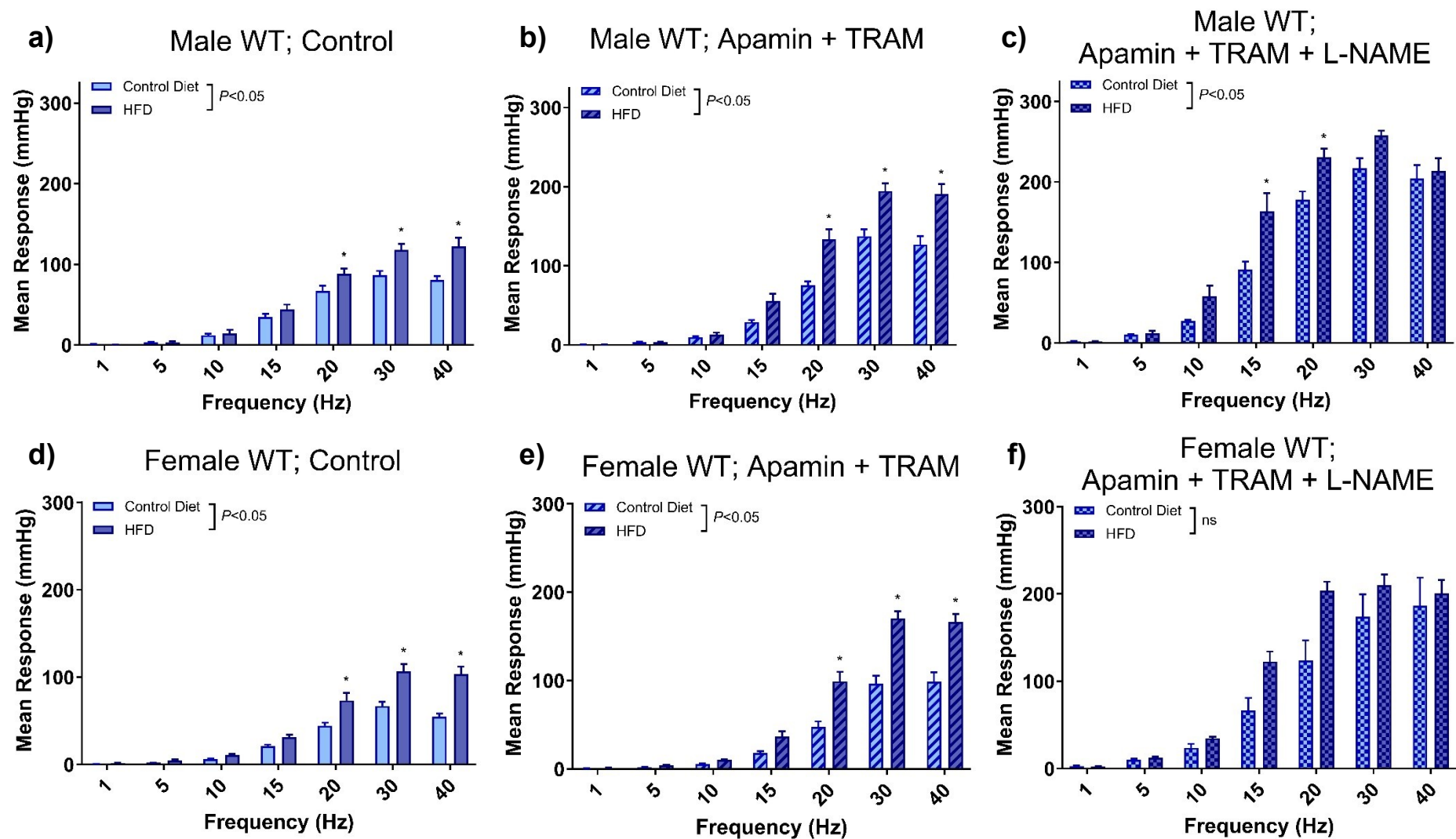


Figure 5.5: HFD significantly enhances nerve-evoked vasoconstriction in perfused mesenteric vascular beds from Cx40 WT rats. Unpaired frequency-response relationships of perfused mesenteric vascular beds from control and HFD-fed male ($n = 6$; **a**, **b**, and **c**) and female ($n = 6-7$; **d**, **e**, and **f**) WT rats in the absence and presence of apamin (50 nM), TRAM-34 (1 μ M) and L-NAME (100 μ M). Data are presented as mean \pm SEM. * denotes $P < 0.05$ from control; two-way ANOVA.

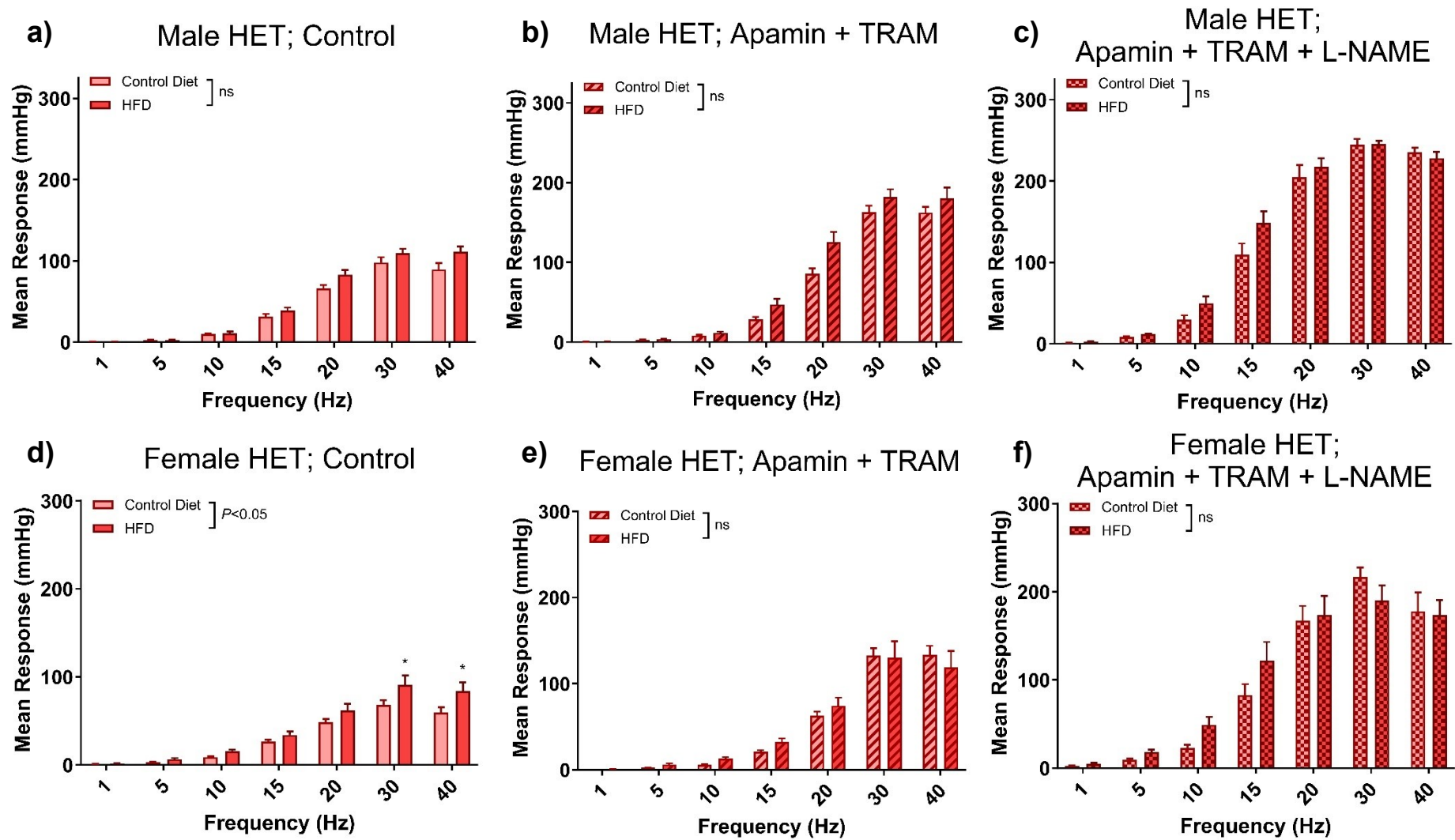


Figure 5.6: HFD significantly enhances nerve-evoked vasoconstriction in perfused mesenteric vascular beds from female, but not male Cx40 HET rats. Unpaired frequency-response relationships of perfused mesenteric vascular beds from control and HFD-fed male ($n = 6-9$; **a**, **b**, and **c**) and female ($n = 6$; **d**, **e**, and **f**) HET rats in the absence and presence of apamin (50 nM), TRAM-34 (1 μ M) and L-NAME (100 μ M). Data are presented as mean \pm SEM. * denotes $P < 0.05$ from control; two-way ANOVA.

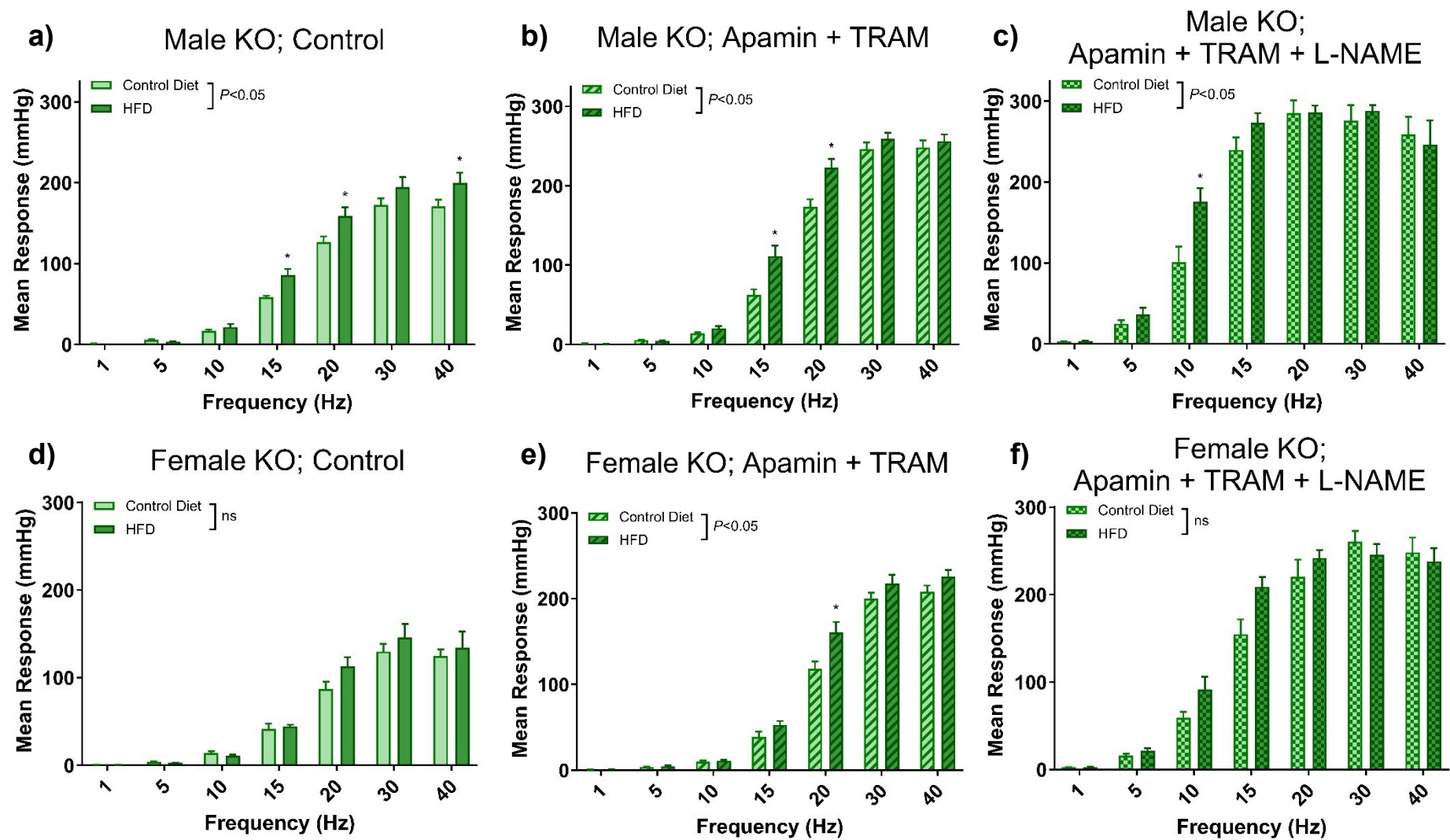


Figure 5.7: HFD significantly enhances nerve-evoked vasoconstriction in perfused mesenteric vascular beds from Cx40 KO rats. Unpaired frequency-response relationships of perfused mesenteric vascular beds from control and HFD-fed male ($n = 7$; **a**, **b**, and **c**) and female ($n = 6$; **d**, **e**, and **f**) KO rats in the absence and presence of apamin (50 nM), TRAM-34 (1 μ M) and L-NAME (100 μ M). Data are presented as mean \pm SEM. * denotes $P < 0.05$ from control; two-way ANOVA.

5.3.3 Mild hypercaloric challenge does not affect myogenic reactivity in isolated mesenteric arteries

Pressure myography was used to examine the effect of HFD on the development of myogenic tone in fourth- to sixth-order mesenteric arteries isolated from Cx40 WT, HET and KO rats. Arteries from HFD-fed male and female WT, HET and KO rats all exhibited myogenic constriction that was statistically significant from their passive diameter in the absence of Ca^{2+} ($P < 0.05$, **Figure 5.8**). In order to examine the effect of the hypercaloric challenge, these data were expressed as % myogenic tone (see §2.5) and compared to myogenic tone data in arteries from CD-fed rats. In the absence of apamin, TRAM-34 or L-NAME, HFD had no effect on myogenic tone in any of the genotype-sex groups ($P > 0.05$, **Figure 5.9**). For the sake of clarity, data in the presence of apamin + TRAM-34 or apamin + TRAM-34 + L-NAME have not been included, but HFD was still found to have no significant effect in the presence of these treatments ($P > 0.05$, data not shown). These results suggest that the myogenic response is not affected during early metabolic strain and development of endothelial dysfunction.

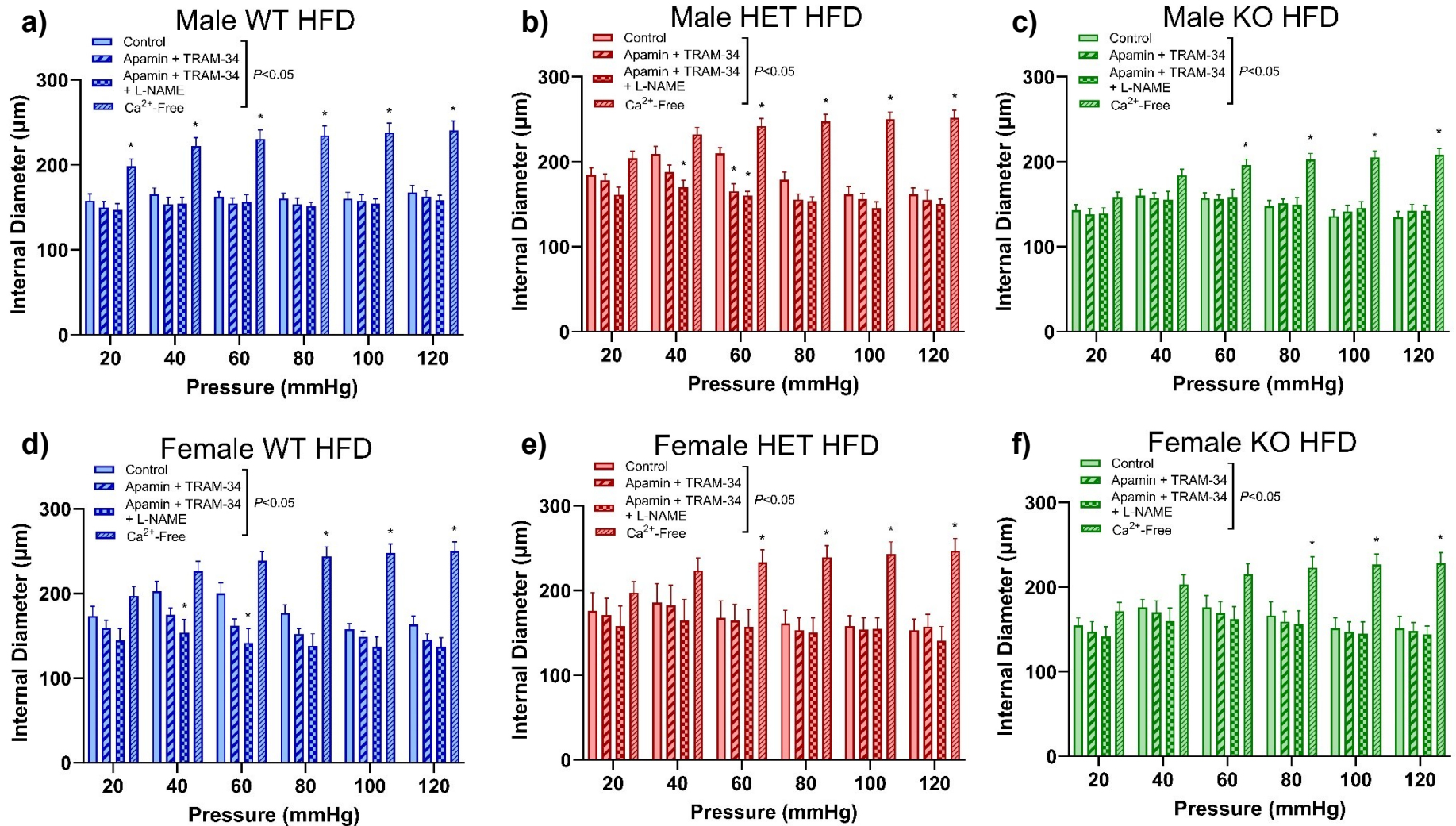


Figure 5.8: Pressure-evoked vasoconstriction occurs in isolated mesenteric arteries from HFD-fed Cx40 WT, HET and KO rats. Pressure myography was used to construct pressure-diameter relationships in the absence and presence of apamin (50 nM), TRAM-34 (1 μM) and L-NAME (100 μM) using isolated fourth- to sixth-order mesenteric arteries from male **a)** WT ($n = 7$), **b)** HET ($n = 8$), and **c)** KO ($n = 6$) rats, and female **d)** WT ($n = 7$), **e)** HET ($n = 6$), and **f)** KO ($n = 6$) rats. Data are presented as mean \pm SEM. * denotes $P < 0.05$ from control; two-way ANOVA.

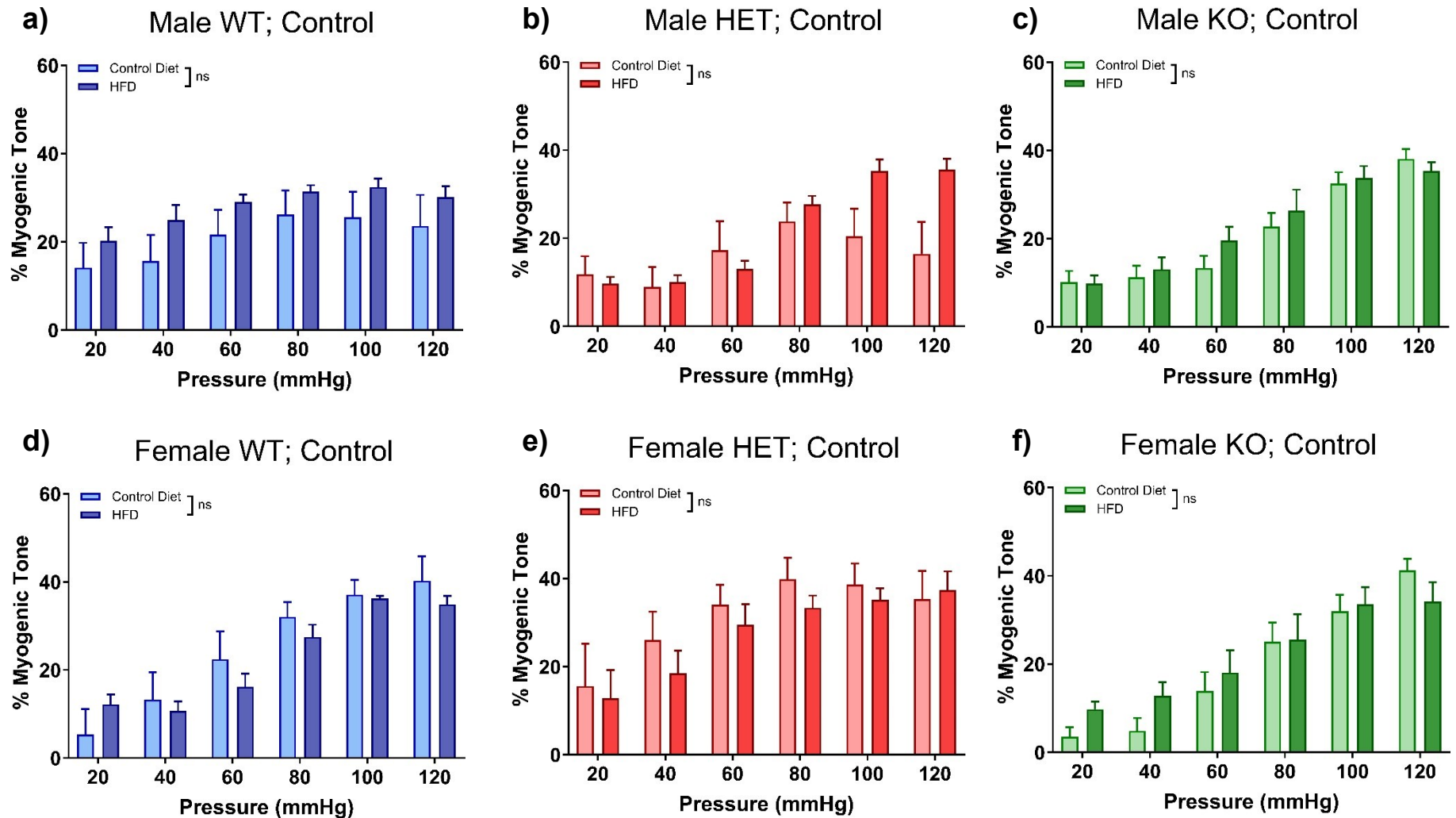


Figure 5.9: Myogenic response of isolated rat mesenteric arteries is not affected by HFD. Unpaired pressure-tone relationships of isolated fourth- to sixth-order mesenteric arteries from male **a)** WT ($n = 6-7$), **b)** HET ($n = 6-8$), and **c)** KO ($n = 6$) rats, and female **d)** WT ($n = 6-7$), **e)** HET ($n = 6-8$), and **f)** KO ($n = 6$) rats in the absence of drugs compared across diet within each genotype. Responses are expressed as % myogenic tone, which is the percentage difference in active diameter versus passive diameter at each pressure step. Data are presented as mean \pm SEM. $P > 0.05$; two-way ANOVA.

5.3.4 HFD enhances post-ischemic functional recovery in the Langendorff-perfused rat heart

The effect of HFD on ischemia/reperfusion injury in hearts from Cx40 WT, HET and KO rats was investigated using the Langendorff isolated heart perfusion. Hearts from HFD-fed male and female WT, HET and KO rats were perfused using the same parameters as in the previous chapter (§4.3.6): 30 minutes pre-ischemic equilibration, 15 minutes global no-flow ischemia and 45 minutes aerobic reperfusion. LVDP was calculated as the difference between systolic and end-diastolic pressure, and two-way ANOVA was performed in two separate analyses; once for all pre-ischemic timepoints and once for all post-ischemic timepoints. The overall effect of genotype was not statistically significant in either pre- or post-ischemia in HFD-fed male hearts, but was significant in both pre- and post-ischemia in females ($P > 0.05$ and $P < 0.05$, **Figure 5.10a** and **b**, respectively). In the previous chapter, the effect of genotype was found to be significant in CD-fed males (**Figure 4.16**); this suggests that HFD rescues post-ischemic recovery in the male KO.

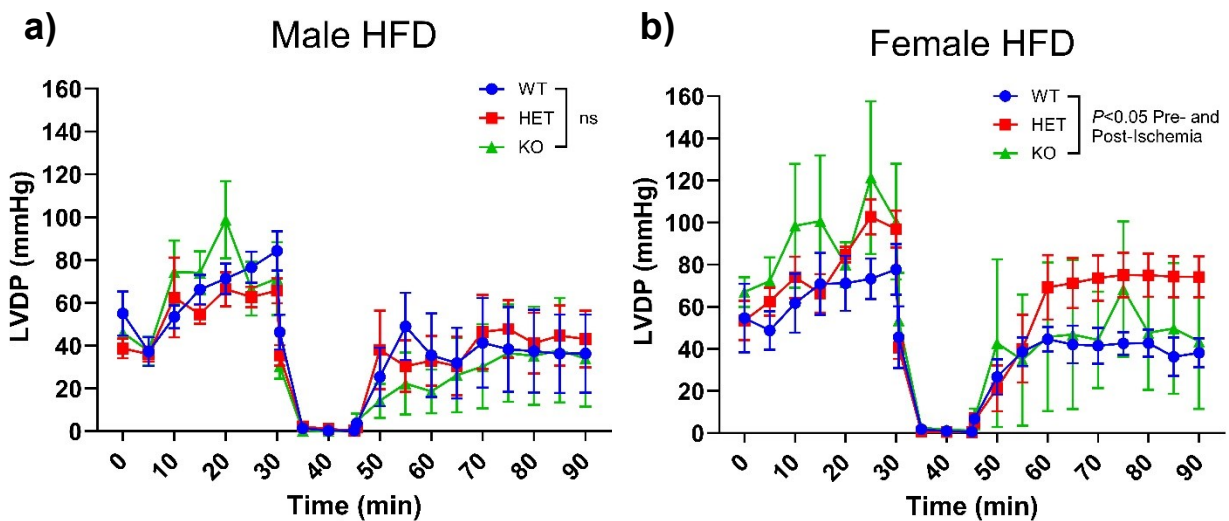


Figure 5.10: Post-ischemic functional recovery in Langendorff-perfused hearts from HFD-fed male and female rats. Hearts were excised from HFD-fed **a)** male WT ($n = 8$), HET ($n = 6$) and KO ($n = 6$) and **b)** female WT ($n = 6$), HET ($n = 6$) and KO ($n = 5$) rats and perfused in Langendorff mode. Global no-flow ischemia was induced at the 30 min. timepoint and flow was reinstated at the 45 min. timepoint. Data are presented as mean \pm SEM. P values represent overall effect of genotype; two-way ANOVA. *Data contributed by Caleb McInroy.*

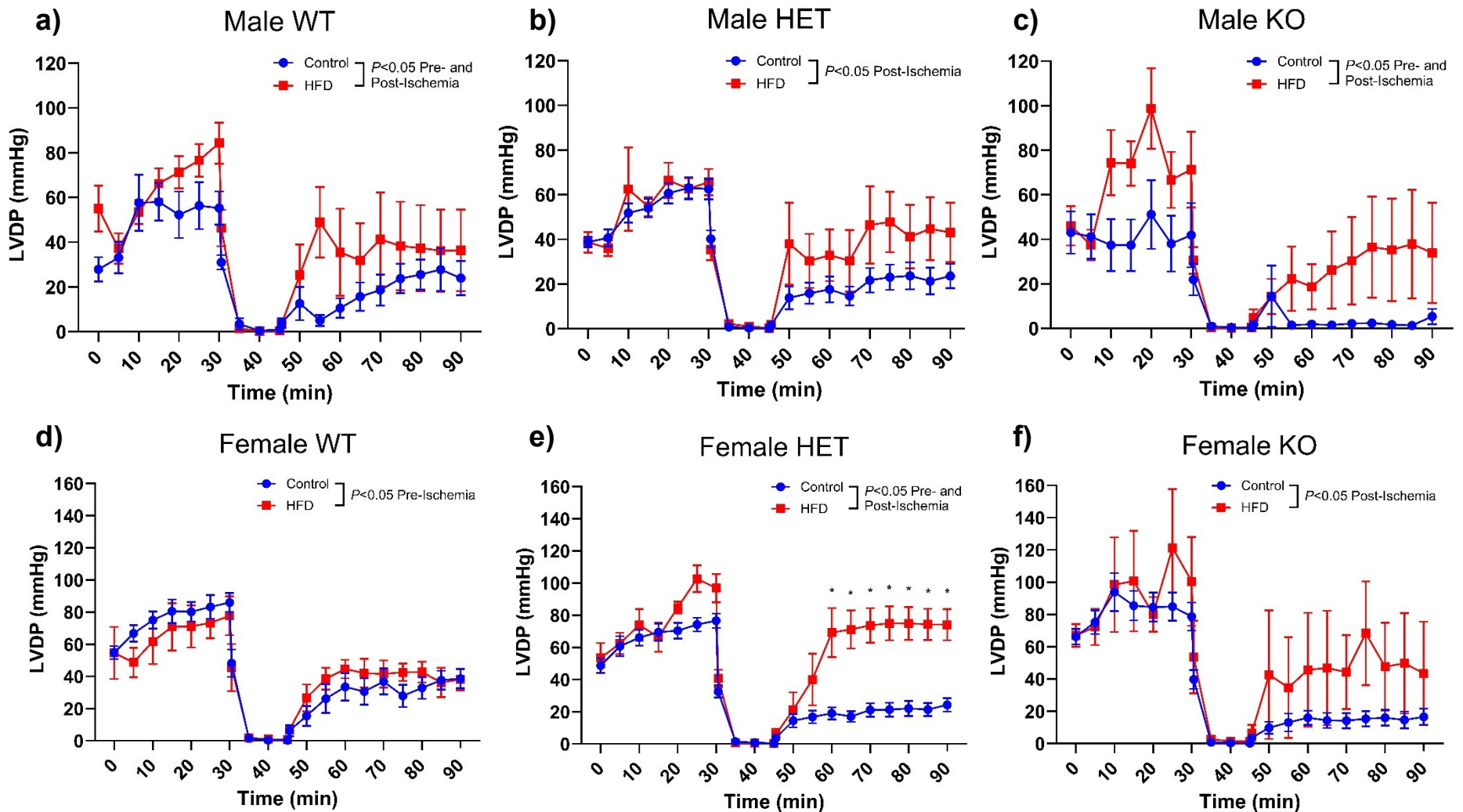


Figure 5.11: HFD enhances post-ischemic functional recovery in Langendorff perfused rat hearts. Hearts were excised from CD- and HFD-fed **a)** male WT ($n = 7-8$), HET ($n = 6-23$) and KO ($n = 5-6$) and **b)** female WT ($n = 6-15$), HET ($n = 6-24$) and KO ($n = 5-11$) rats and perfused in Langendorff mode. Global no-flow ischemia was induced at the 30 min. timepoint and flow was reinstated at the 45 min. timepoint. Data are presented as mean \pm SEM. * denotes $P < 0.05$ from control; two-way ANOVA. *Data contributed by Caleb McInroy.*

Next, the data from HFD-fed rat hearts was directly compared with the data previously collected in CD-fed rat hearts. HFD caused significant differences in LVDP in every genotype-sex group: HFD significantly enhanced post-ischemic recovery in hearts from male WT, HET and KO, and female HET and KO rats ($P < 0.05$, **Figure 5.11a, b, c, e, and f**, respectively). This effect was most pronounced in the female HET rats, though the reason for this is unclear and requires further investigation. In the female HETs, HFD produced a high-magnitude increase in post-ischemic LVDP of approximately 50 mmHg.

5.4 Discussion

The data presented in this chapter do not support the hypothesis that genetic ablation of Cx40 makes rats more susceptible to cardiovascular damage by a mild hypercaloric challenge. Contrarily, my results from functional assays suggest that the damage incurred by the KO rat is either the same or lesser magnitude than the damage incurred by the WT rat. These results are particularly significant due not only to the novelty of the WKY-Gja5^{em1Mcwi} mutant strain, but also due to the mild HFD formulation. Throughout the history of rodent models of HFD-induced obesity, a wide range of diet formulations have been used experimentally, usually with a fat content between 30% and 78% of the total metabolizable energy (cf. standard laboratory rodent diets usually contain 10-15% kcal from fat)^{1037,1038}. Toward the high end of this range, the clinical relevance becomes questionable, as diets that exceed 35% kcal from fat are considered obesogenic in humans¹⁰³⁹. This has led the attention of researchers toward the more representative “Western diet”, which usually comprises 40-45% kcal from fat and a low protein : carbohydrate ratio^{1037,1040-1042}. The HFD in the current study has a fat content slightly below this range at 39.1% kcal from fat, and was formulated with the goal to be non-obesogenic within a 12 week time course in order to model prediabetes in rodents rather than obesity and T2DM⁸¹⁸. The purpose of this research was

thus to examine how endothelial dysfunction develops in response to a metabolic challenge, and determine whether Cx40 is involved in this mechanism.

I first assessed the impact of HFD on body weight and hemodynamic phenotype. HFD did not cause a significant increase in body weight or BP in any of the male rats, nor did it cause an increase in random blood glucose in male WTs, which is consistent with observations in male Sprague-Dawley rats by Dr. El-Yazbi's group^{473,818}. However, HFD was found to cause a significant increase in body weight in female WT and KO rats. This aligns with sex-differences in the development of obesity described in the literature: in many HFD studies, female rodents exhibit obesity after a shorter time course than is required to observe obesity in males¹⁰³⁷. Additionally, random blood glucose was significantly increased in two genotype-sex groups: male KOs and female HETs. The underlying cause of this observation is unclear; however, future experiments should involve the measurement of fasting blood glucose, plasma insulin and serum cholesterol levels in order to more fully understand the hemodynamic changes produced by HFD. In most other metrics, the major cardiovascular changes observed in the KO versus the WT rats were preserved in the HFD-fed KO rats.

Interestingly, the relative weights of the kidneys were found to be smaller in the HFD-fed female rats than in the CD-fed female rats. Most HFD studies in the literature show increased kidney weight due to renal hypertrophy^{1043,1044}, but more recently a moderate HFD (45% kcal from fat) has been shown by Sánchez-Navarro *et al.* (2021) to decrease the relative weight of the kidneys in male mice¹⁰⁴⁵. Nevertheless, the authors demonstrate that the absolute weight of the kidneys were not smaller in the HFD-fed mice, rather that an increase in body weight led to a decrease in the ratio of kidney weight to body weight. In the present study, the absolute weight of the kidneys in HFD-fed female WT and KO rats was found to be significantly smaller than those in CD-fed

female WT and KO rats, and no difference was found in HETs. This occurred despite the rats being age-matched and the HFD-fed female rats exhibiting an equal or larger body weight than their CD-fed counterparts. Despite the evidence that HFD treatments may cause renal hypertrophy, other studies have instead observed tubular necrosis, shrinkage of glomeruli and a decrease in total renal volume in response to diets high in saturated fat^{1046,1047}. Renal injury in obesity is well-described, and involves the deregulation of cytokine production in adipose tissue, leading to overproduction of inflammatory cytokines such as interleukin-1 β (IL-1 β), interleukin-6 (IL-6) and tumor necrosis factor- α (TNF- α ; reviewed by Castro *et al.*, 2021)¹⁰⁴⁸. Increased renal inflammation ultimately leads to increased glomerular permeability, fibrosis and glomerulosclerosis. This may explain why HFD-fed female WT and KO rats exhibited a significant increase in body weight, and were the only groups to exhibit decreased absolute mass of the kidneys. This constitutes a future line of investigation, and would require the measurement of inflammatory cytokine production in renal and adipose tissue, as well as markers of renal injury such as urinary levels of creatinine and HSP72¹⁰⁴⁵.

I next assessed the function of resistance arteries in the perfused mesenteric vascular bed, revealing that HFD causes an increase in nerve-evoked vasoconstriction in vessels from all six genotype-sex groups except male HET rats. Moreover, HFD did not appear to affect the contribution of either EDH or NO production to the limitation of nerve-evoked vasoconstriction, as apamin + TRAM-34 and apamin + TRAM-34 + L-NAME produced a large, statistically significant increase in pressure responses in all genotype-sex groups. The only caveat being that in beds from HFD-fed KO rats, apamin + TRAM-34 + L-NAME did not increase the magnitude of the response to high-frequency stimulations versus beds from HFD-fed WT and HET rats, but instead left-shifted the frequency-response curve. These results do not support the hypothesis that

HFD causes a greater magnitude of endothelial dysfunction in the absence of Cx40; in fact, beds from WT rats appeared to incur the greatest impact of HFD, as they showed the greatest number of significantly increased responses (**Figures 5.5, 5.6 and 5.7**). Considering these results together, I propose two major underlying mechanisms which require further investigation: an increase in ROS production in the vasculature of the HFD-fed rat, and increased involvement of the RAAS.

Increased metabolic demand and resultant oxidative stress such as occurs in the vasculature during prediabetes or T2DM is well understood to increase the production of ROS by mechanisms including leakage from the mitochondrial electron transport chain and the upregulation of NOX enzymes (reviewed by Di Marco *et al.*, 2015)¹⁰⁴⁹. Increased ROS levels in turn promote inflammation by mechanisms including the activation of nuclear factor κ B (NF- κ B) by ONOO⁻ to increase transcription of pro-inflammatory cytokines^{1050,1051}. Oxidative stress and inflammation are interrelated and feed into one another; recruited inflammatory immune cells increase the local metabolic demand and contribute to ROS production¹⁰⁵². Using their HFD formulation upon which mine was based, Dr. El-Yazbi's group observed increased production of O₂⁻ and several inflammatory mediators including transforming growth factor (TGF)- β 1, IL-1 β , and CD68 by staining and Western blots in both aortic tissue and perivascular adipose tissue (PVAT)^{473,818}. Increased O₂⁻ production increases levels of ONOO⁻, which in turn uncouples eNOS to produce more O₂⁻ in a positive feedback loop⁶¹⁵. ONOO⁻ has been demonstrated to cause structural damage to vascular cells¹⁰⁵³⁻¹⁰⁵⁶ and also contributes to enhanced vasoconstriction by several mechanisms (**Figure 5.12**). Foremost of these mechanisms, ONOO⁻ inhibits the synthesis of the vasodilator PGI₂¹⁰⁵⁷, and inhibits NO signalling through PKG¹⁰⁵⁸. In addition to these mechanisms, Dr. El-Yazbi's group found that enhanced PE-evoked vasoconstriction in arteries from HFD-fed rats was associated with an increase in expression of ROCK, thereby enhancing Ca²⁺ sensitization⁴⁷³.

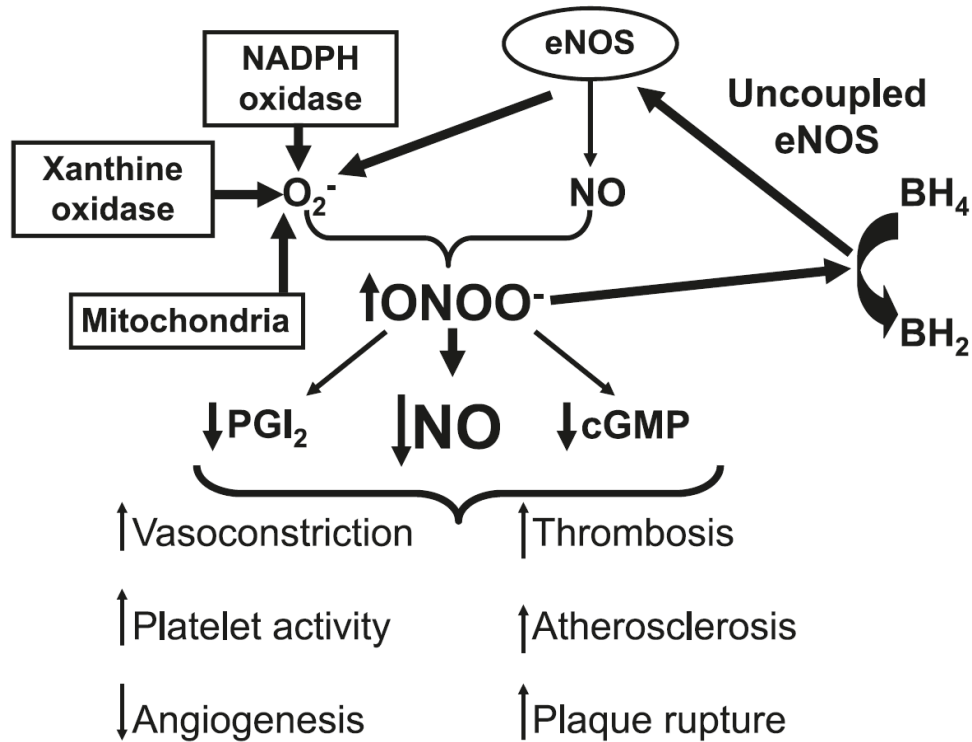


Figure 5.12: Schematic diagram illustrating the formation of $ONOO^-$ and its role in vascular dysfunction. Increased production of O_2^- in conditions of oxidative stress leads to the formation of $ONOO^-$ and decreased bioavailability of NO. $ONOO^-$ subsequently elicits deleterious effects including uncoupling eNOS, and enhanced vasoconstriction, platelet activity, and atherosclerosis (from Kerr *et al.*, 2012)⁶¹⁵.

Taking the data from Dr. El-Yazbi's group (Elkhatib *et al.* 2019)⁴⁷³ into consideration with my own, I suspect that increased ROS production is a major contributor to the HFD-induced increase in nerve-evoked vasoconstriction observed in the perfused mesenteric vascular bed. Our laboratory has previously combined DHE visualization of O_2^- with pressure myography in order to continuously and simultaneously record O_2^- and arterial diameter in real time⁷¹¹. In future experiments, I propose using this method in order to measure O_2^- production in response to PE-evoked vasoconstriction in isolated mesenteric arteries from CD- and HFD-fed rats. I hypothesize that both baseline and PE-evoked O_2^- levels are greater in arteries from HFD-fed rats than those from CD-fed rats. Furthermore, if increased ROS generation is a major contributor to these functional results, then enhanced vasoconstriction would be expected to be partially rescued by

adding superoxide dismutase⁸¹⁸ or phosphodiesterase-5-inhibitors¹⁰⁵³. These experiments should be accompanied by the serological and immunohistochemical analysis for ROS and inflammatory markers performed by Elkhatib *et al.* (2019) in order to confirm that vascular inflammation occurs in these rats. This would also elucidate whether there is any difference in O₂⁻ production or inflammation between the Cx40 genotypes, in both the CD- and HFD-fed rats. Si *et al.* (2021) recently observed that ablation of Cx40 in cultured human cardiac ECs exhibited an increase in O₂⁻ versus control as measured by DHE staining, although the authors were unable to explain this relationship⁷⁹⁹. This finding suggests the possibility that increased ROS production contributes to the enhanced vasoconstriction in the CD-fed KO versus the CD-fed WT observed in the previous chapter (§4.3.3).

Interrelated with the increase in ROS production, the other putative contributor to the HFD-induced enhancement in nerve-evoked vasoconstriction involves dysregulation of the RAAS. In the previous chapter, I discussed the literature showing that ablation of Cx40 in mice impairs baroreception in the renal juxtaglomerular cells, resulting in hyperreninemia (§4.4). There is evidence in the literature to suggest that obesity stimulates the RAAS in a similar manner. White adipose tissue has been shown to express angiotensinogen and ACE, and possibly renin, though the latter has not yet been confirmed to be expressed at the protein level¹⁰⁵⁹⁻¹⁰⁶⁴. This capacity of adipose tissue has been described as a “local adipose RAAS” in the literature^{1065,1066}. Obesity has been shown to increase expression and secretion of adipose-derived angiotensinogen in animal models and human patients^{1060,1063}. HFD-fed dogs were similarly shown to incur high plasma renin levels¹⁰⁶⁷. Angiotensin II has also been found to exert positive feedback, acting at the AT₁R to stimulate further production of adipose-derived angiotensinogen¹⁰⁵⁹. Obesity does not only stimulate the local adipose RAAS, but the intrarenal RAAS as well. For example, cultured human

proximal tubule cells treated with saturated fatty acids showed increased expression of angiotensinogen, renin, and AT₁R¹⁰⁶⁸. Not only does obesity cause this stimulation of RAAS, but RAAS activity may be necessary for diet-induced weight gain: angiotensinogen KO mice were found to gain less weight than WT mice in both control and HFD-fed groups¹⁰⁶².

In the context of the present study, this is potentially a useful model for understanding my results. As previously stated, hyperreninemia has been observed in Cx40 mice, but not confirmed in the Cx40 KO rat. However, if this is the case, then the ablation of Cx40 and the mild hypercaloric HFD may share this major mechanism. This is congruent with my results, wherein I saw the largest effect of HFD on WT rats. In the KO rat, the RAAS is likely already hyperactive, leaving less capacity to be further stimulated by the hypercaloric challenge. In order to investigate this hypothesis, plasma renin and angiotensin II levels should be measured in CD- and HFD-fed rats of all genotype-sex groups.

Arguably the most surprising result from the present study was the observation that mild HFD improved recovery of LVDP after myocardial ischemia in all genotype-sex groups except female WT. Dietary fatty acids are the predominant oxidative substrate of mitochondria in cardiomyocytes, and dependence upon fatty acid oxidation increases during post-ischemic reperfusion^{1069,1070}. In obesity, high plasma concentrations of fatty acids lead to an increase in fatty acid uptake by cardiomyocytes, and a subsequent increase in fatty acid oxidation¹⁰⁷¹. The accumulation of fatty acids stored as triglycerides eventually leads to oxidative stress, mitochondrial dysfunction on the cellular level, and cardiac dysfunction on the organ level (reviewed by Lopaschuk *et al.*, 2010)¹⁰⁷⁰. HFD protocols in the literature vary over a wide range of diet compositions and feeding timelines, and can be either obesogenic or non-obesogenic; consequently, the reported effects of HFD on ischemia/reperfusion injury vary greatly as well. For

example, Littlejohns *et al.* (2014) found that isolated hearts from mice fed a non-obesogenic HFD were significantly more susceptible to ischemia/reperfusion injury than controls, with a significantly greater infarct size after a 40 minute ischemic period¹⁰⁷². The authors' HFD comprised 45% calories from fat and was administered over 22 weeks, which is a slightly higher fat content than the current study (cf. 39.3%), and a feeding timeline nearly twice as long. Contrarily, Insete *et al.* (2019) found that isolated hearts from mice fed an obesogenic HFD incurred a significantly smaller infarct size than controls after a 20 minute ischemic period¹⁰⁷³. Thus, there is a mixture of evidence for cardioprotective¹⁰⁷³⁻¹⁰⁷⁵ and deleterious^{1072,1076-1078} effects of HFD in animal studies.

It has also been suggested that the relative amounts of dietary saturated and monounsaturated fats versus polyunsaturated fats is more influential on experimental outcomes than simply the total fat content of the diet¹⁰⁷⁹. Detailed compositional information is often unreported in HFD studies and may be a crucial factor in the apparently contradictory findings in the literature. Regardless, my results suggest that the mild HFD model is cardioprotective. Not only did HFD improve post-ischemic recovery of LVDP, but the heart enlargement observed in male KO rats was present but significantly reduced in HFD-fed versus CD-fed rats. A putative mechanism for this protection may involve an HFD-induced increase in plasma levels of fatty acids large enough to support the heart's metabolic demand during ischemia, but not large enough to precipitate heart failure. Further investigation should examine this hypothesis by shortening or lengthening the feeding timeline of the mild HFD; it is possible that administration of the mild HFD for longer than 12 weeks might produce heart failure rather than cardioprotection. Serological analysis of plasma fatty acids, triglycerides and cholesterol should also be performed in order to more completely characterize this model.

Taken together, the results in this chapter do not support the hypothesis that genetic ablation of Cx40 makes rats more vulnerable to metabolic stress in a mild HFD. Instead, these results suggest that the absence of Cx40 may lessen the extent of HFD-induced endothelial dysfunction. These data also indicate that there is likely some overlap in the mechanisms of vascular dysfunction produced by Cx40 ablation and HFD, particularly through hyperactivation of the RAAS.

Chapter 6: General discussion and future directions

6.1 General discussion

The modulation of resistance artery diameter is a multi-factorial process that is crucial for controlling tissue perfusion in response to changes in energetic demand, and ultimately maintaining systemic BP. This process is dependent upon the coordinated actions of ECs, VSMCs and perivascular nerves in response to chemical and mechanical stimuli. In turn, this coordination is mediated by chemical and electrical signalling between cells, and the crosstalk between chemical and electrical pathways. Thus, a large number of ion channels are involved in the electrical control of VSMC membrane potential, and subsequently the control of smooth muscle contraction. In this thesis, I have investigated the role of two of these ion channels in the modulation of resistance artery diameter: TRPM4 in VSMCs, and Cx40-containing GJ channels in ECs.

Since the discovery of myogenic reactivity over one hundred years ago⁴⁷⁴, great research interest has been devoted to unraveling the mechanism by which blood vessels detect and respond to changes in intramural pressure^{465,495}. A large body of evidence suggests that TRPM4 has a prominent role in vascular mechanosensation, regardless of whether or not it is directly mechanosensitive. This includes findings that suppression of TRPM4 expression inhibits the development of myogenic tone in rat cerebral arteries⁵⁰². However, much of the evidence for the role of TRPM4 in pressure-evoked vasoconstriction comes from experiments conducted using the pharmacological TRPM4 inhibitor 9-phenanthrol^{500,501}, which has recently come under scrutiny for putative off-target effects. In particular, it has been suggested 9-phenanthrol's inhibition of pressure-evoked vasoconstriction may be at least partially attributable to activation of IK_{Ca} channels⁸⁵⁷. Thus, I examined the role of TRPM4 in vasoconstriction evoked both by intramural

pressure and other stimuli, and investigated 9-phenanthrol's mechanism of action using functional assays.

In **Chapter 3** I first demonstrated that mRNA coding for TRPM4 is highly expressed in mesenteric arteries, especially compared to expression of mRNA coding for TRPC6, another candidate for mediating pressure-evoked Ca^{2+} influx in VSMCs^{331,332}. I then showed that 9-phenanthrol inhibits nerve-evoked vasoconstriction in a dose-dependent manner. The additional presence of the pharmacological IK_{Ca} inhibitor NS6180 did not affect 9-phenanthrol's inhibition of nerve-evoked vasoconstriction, indicating that this effect of 9-phenanthrol is not mediated by IK_{Ca} activation. Using pressure myography, I demonstrated that 9-phenanthrol abolishes myogenic vasoconstriction. This effect was similarly unaffected by IK_{Ca} inhibitors TRAM-34 and NS6180. In addition to nerve- and pressure-evoked vasoconstriction, I used wire myography to show that 9-phenanthrol produces concentration-dependent vasorelaxation after pre-constriction to either PE or 5-HT. This effect was again unaffected in the presence of NS6180, indicating no involvement of IK_{Ca} activation. Although these data do not rule out the possibility of off-target effects of 9-phenanthrol at other channels such as TMEM16⁸⁵⁶, my findings contradict IK_{Ca} activation as a mechanism of action for 9-phenanthrol.

Using wire myography, I also demonstrated that 9-phenanthrol inhibits PE-evoked vasoconstriction. The concentration-response relationship of PE in the presence of 9-phenanthrol was significantly lower than control, but not significantly different to the concentration-response relationship of PE in the presence of 9-phenanthrol + apamin + TRAM-34 + L-NAME. This demonstrated that the effect of 9-phenanthrol is not attributable to enhancement of EDH or NO production. Finally, I showed that 9-phenanthrol's inhibition of PE-evoked vasoconstriction was not significantly altered by the addition of the LTCC-blocker nifedipine. This result suggests that

9-phenanthrol alone is able to abolish the depolarization-dependent component of vasoconstriction; thus TRPM4 is necessary for depolarization-dependent contraction in VSMCs.

I next explored the role of the endothelial GJ protein Cx40 in the modulation of resistance artery diameter. In this research I used the novel Cx40 KO rat to compare cardiovascular function in the presence and absence of Cx40. These data, presented in **Chapter 4**, clearly establish a crucial role of Cx40 in cardiovascular physiology. I found that germline, global KO of Cx40 produces hypertension and heart enlargement in both male and female rats. In the perfused mesenteric vascular bed, Cx40 KO was shown to cause a high-magnitude increase in nerve-evoked vasoconstriction. The addition of apamin + TRAM-34 and apamin + TRAM-34 + L-NAME produced proportionate increases in nerve-evoked pressure responses in all genotypes, illustrating that the component mechanisms of endothelium-dependent vasodilation, EDH and NO production, were unaffected by the global absence of Cx40. The Cx40 KO-associated increase in nerve-evoked vasoconstriction was found to be partially preserved in males and fully preserved in females after the removal of the endothelium. This key result illustrated that genetic ablation of Cx40 not only affects endothelial function, but produces deleterious effects on smooth muscle function as well. Interestingly, I also found that in beds from male WT, HET and KO rats nerve-evoked pressure responses in endothelium-denuded beds were significantly higher than those in endothelium-intact beds, whereas in beds from female WT, HET and KO rats no difference was observed. This observation may be due to reported sex-based differences in eicosanoid production by ECs¹⁰⁸⁰⁻¹⁰⁸³, and differences in the EC response to sex hormones^{1084,1085} which become apparent after the removal of the endothelium. However, this is speculative and requires further research.

I also demonstrated using pressure myography that Cx40 has no impact on the development of the myogenic response in isolated mesenteric arteries. Additionally, wire myography revealed

that the contributions of EDH and NO production to ACh-evoked vasodilation in isolated arteries is unaffected by the global absence of Cx40. PE-evoked vasoconstriction was also unaffected by the absence of Cx40. However, tone induced by the TP agonist U46619 was significantly impaired in isolated mesenteric arteries from male KO and female HET and KO rats. This is consistent with literature reports of hyperreninemia in Cx40 KO mice^{974,977,978,980,1086} and could be explained by agonist induced desensitization and internalization of TP⁹⁸⁷⁻⁹⁹⁰; however, this has yet to be investigated and is a direction for future research. Finally, I showed that isolated hearts from Cx40 KO rats are less resistant to ischemia/reperfusion injury, which aligns with literature in the Cx40 KO mouse⁸⁰⁰. The mechanism underlying this result is unclear and may involve cardiac hypertrophy⁷⁶⁷ and/or the impairment of intercellular conduction in the His bundle and Purkinje fibers lacking Cx40⁷⁹¹. Regardless, these data together demonstrate that Cx40 is a necessary component of normal cardiovascular function.

In order to better understand this protective role of Cx40, I applied a mild HFD to the current rat model in order to assess whether Cx40 is protective in the face of metabolic challenge. Thus, in **Chapter 5** I assessed the cardiovascular effects of feeding male and female Cx40 WT, HET and KO rats a HFD (39.3% kcal from fat) for 12 weeks. The HFD protocol was found to be non-obesogenic in males, but obesogenic in female WTs and KOs. The KO-induced hypertension and heart enlargement observed in **Chapter 4** were preserved in the HFD-fed rats. A surprising decrease in kidney mass was observed in female rats, and may indicate sex-linked kidney damage induced by the HFD.

In the perfused mesenteric vascular bed, the effects of apamin, TRAM-34 and L-NAME on nerve-evoked pressure responses observed in CD-fed rats were preserved in HFD-fed rats. Comparing the results between CD-fed and HFD-fed rats within each genotype showed that

responses in HFD-fed male WT rats were significantly higher than those in CD-fed rats in the absence and presence of apamin + TRAM-34 or apamin + TRAM-34 + L-NAME. The same was observed in female WT rats, except that the addition of L-NAME produced responses in the HFD-fed bed that were not significantly different from the CD-fed bed. This indicates that HFD may impair endothelial NO production in the female WT. Overall, HFD had the greatest effect of nerve-evoked vasoconstriction in male and female WT rats, which may suggest an overlap between the deleterious mechanisms of Cx40 ablation and mild HFD.

Finally, I demonstrated that mild HFD counterintuitively enhanced the tolerance of isolated hearts to ischemia/reperfusion injury in all genotype-sex groups except female WT. It is difficult to directly compare these results to findings in the literature due to the extremely variable nature of HFD models and Langendorff heart perfusion protocols. HFD studies in the literature differ greatly in nutrient composition and feeding timeline, and Langendorff protocols differ in the length time of the ischemia and reperfusion periods. My results align with a portion of the literature which describes a cardioprotective effect of increased dietary fat in the context of ischemia/reperfusion¹⁰⁷³⁻¹⁰⁷⁵.

In conclusion, the data presented in this thesis illustrate crucial roles for both TRPM4 and Cx40 in the maintenance and regulation of arterial diameter and systemic blood pressure. I have presented several lines of evidence to support the hypothesis that these ion channels are necessary for the intercellular coordination of ECs and VSMCs to finely control arterial diameter in response to various physiological stimuli.

6.2 Future directions

The data presented in this thesis draw attention to several potential avenues for future research such as:

Investigating whether the functional effects of 9-phenanthrol are mediated by action at TMEM16A. My data in **Chapter 3** contradict the putative action of 9-phenanthrol as an activator of IK_{Ca} , but do not rule out its putative action as a TMEM16A inhibitor. This could be investigated by conducting functional experiments with 9-phenanthrol in the presence of known small-molecule TMEM16A activators (e.g. E_{act}) and inhibitors (e.g. Ani9)⁸⁶⁶.

Investigating the effect of genetic ablation of Cx40 on the conducted vasomotor response. As Cx40 is present in interendothelial GJs, it is an important mediator of the vascular conduction of membrane potential. Thus, the conducted vasomotor response is expected to be impaired or abolished in arteries from the Cx40 KO rat. This can be examined using pressure myography coupled with a pneumatic pressure ejector as described in the literature^{765,999-1002}.

Determining the contribution of ROS production to cardiovascular changes in the CD- and HFD-fed Cx40 KO rat. Evidence suggests that the absence of Cx40 creates oxidative stress in ECs⁷⁹⁹ and this may contribute to the vascular dysfunction observed in the Cx40 KO rat. Thus, interendothelial GJs may have a role in preventing overproduction of O_2^- . Moreover, oxidative stress is well-understood to underlie vascular dysfunction in T2DM¹⁰⁴⁹. It would be beneficial to investigate whether or not the absence of Cx40 exacerbates HFD-induced oxidative stress in ECs, especially given evidence that T2DM is associated with a downregulation of Cx40^{799,1020,1021}.

Investigating the effect of age in the CD- and HFD-fed Cx40 KO rat. The absolute and relative expression of endothelial Cxs has been shown to change with age¹⁰²⁹. Therefore, measuring vascular function and the expression of Cx subtypes other than Cx40 in the Cx40 KO rat at a range of ages would provide a more complete understanding of the role of Cx40 in physiological and pathophysiological cardiovascular function. Additionally, manipulating the

timeline of the HFD protocol provide more insight into the chronology of prediabetes and the development of endothelial dysfunction.

References

1. Grundy D. Principles and standards for reporting animal experiments in The Journal of Physiology and Experimental Physiology. *Exp Physiol.* 2015; 100(7): 755-758.
2. World Health Organization. *Cardiovascular diseases (CVDs)*, <[https://www.who.int/en/news-room/fact-sheets/detail/cardiovascular-diseases-\(cvds\)](https://www.who.int/en/news-room/fact-sheets/detail/cardiovascular-diseases-(cvds))> (2021).
3. Regensteiner JG, Golden S, Huebschmann AG, Barrett-Connor E, Chang AY, Chyun D, Fox CS, Kim C, Mehta N, Reckelhoff JF, Reusch JE, Rexrode KM, Sumner AE, Welty FK, Wenger NK, Anton B. Sex differences in the cardiovascular consequences of diabetes mellitus: a scientific statement from the American Heart Association. *Circulation.* 2015; 132(25): 2424-2447.
4. Anderson TJ, Gregoire J, Hegele RA, Couture P, Mancini GB, McPherson R, Francis GA, Poirier P, Lau DC, Grover S, Genest J, Jr., Carpentier AC, Dufour R, Gupta M, Ward R, Leiter LA, Lonn E, Ng DS, Pearson GJ, Yates GM, Stone JA, Ur E. 2012 update of the Canadian Cardiovascular Society guidelines for the diagnosis and treatment of dyslipidemia for the prevention of cardiovascular disease in the adult. *Can J Cardiol.* 2013; 29(2): 151-167.
5. Xu G, Liu B, Sun Y, Du Y, Snetselaar LG, Hu FB, Bao W. Prevalence of diagnosed type 1 and type 2 diabetes among US adults in 2016 and 2017: population based study. *Bmj.* 2018; 362: k1497.
6. Knowler WC, Barrett-Connor E, Fowler SE, Hamman RF, Lachin JM, Walker EA, Nathan DM. Reduction in the incidence of type 2 diabetes with lifestyle intervention or metformin. *N Engl J Med.* 2002; 346(6): 393-403.
7. Mulvany MJ, Aalkjær C. Structure and function of small arteries. *Physiol Rev.* 1990; 70(4): 921-961.
8. Rhodin JAG. Architecture of the vessel wall in *Handbook of Physiology, The Cardiovascular System*. Vol. 2 (eds Bohr DF, Somlyo AD, Sparks HV) Ch. 1, 1-31 (American Physiological Society, 1980).
9. Martinez-Lemus LA. The dynamic structure of arterioles. *Basic Clin Pharmacol Toxicol.* 2012; 110(1): 5-11.
10. Medical B. Medical gallery of Blausen medical 2014. *WikiJournal of Medicine.* 2014; 1(2): 1-79.
11. Smaje L, Zweifach BW, Intaglietta M. Micropressures and capillary filtration coefficients in single vessels of the cremaster muscle of the rat. *Microvasc Res.* 1970; 2(1): 96-110.
12. Schiffrin EL. The endothelium of resistance arteries: physiology and role in hypertension. *Prostaglandins Leukot Essent Fatty Acids.* 1996; 54(1): 17-25.
13. Triggle CR, Samuel SM, Ravishankar S, Marei I, Arunachalam G, Ding H. The endothelium: influencing vascular smooth muscle in many ways. *Can J Physiol Pharmacol.* 2012; 90(6): 713-738.
14. Kerr PM, Tam R, Ondrusova K, Mittal R, Narang D, Tran CH, Welsh DG, Plane F. Endothelial feedback and the myoendothelial projection. *Microcirculation.* 2012; 19(5): 416-422.
15. Barton M. The discovery of endothelium-dependent contraction: the legacy of Paul M. Vanhoutte. *Pharmacol Res.* 2011; 63(6): 455-462.

16. Vanhoutte PM, Shimokawa H, Feletou M, Tang EH. Endothelial dysfunction and vascular disease – a 30th anniversary update. *Acta Physiol (Oxf)*. 2017; 219(1): 22-96.
17. Barton M, Haudenschild CC. Endothelium and atherogenesis: endothelial therapy revisited. *J Cardiovasc Pharmacol*. 2001; 38 Suppl 2: S23-25.
18. Pfister SL, Gauthier KM, Campbell WB. Vascular pharmacology of epoxyeicosatrienoic acids. *Adv Pharmacol*. 2010; 60: 27-59.
19. Naß J, Terglane J, Gerke V. Weibel Palade bodies: unique secretory organelles of endothelial cells that control blood vessel homeostasis. *Front Cell Dev Biol*. 2021; 9: 813995.
20. Eliceiri BP, Paul R, Schwartzberg PL, Hood JD, Leng J, Cheresh DA. Selective requirement for Src kinases during VEGF-induced angiogenesis and vascular permeability. *Mol Cell*. 1999; 4(6): 915-924.
21. Fischer C, Schneider M, Carmeliet P. Principles and therapeutic implications of angiogenesis, vasculogenesis and arteriogenesis. *Handb Exp Pharmacol*. 2006;(176 Pt 2): 157-212.
22. Oosthuysen B, Moons L, Storkebaum E, Beck H, Nuyens D, Brusselmans K, Van Dorpe J, Hellings P, Gorselink M, Heymans S, Theilmeier G, Dewerchin M, Laudenbach V, Vermynen P, Raat H, Acker T, Vleminckx V, Van Den Bosch L, Cashman N, Fujisawa H, Drost MR, Sciot R, Bruyninckx F, Hicklin DJ, Ince C, Gressens P, Lupu F, Plate KH, Robberecht W, Herbert JM, Collen D, Carmeliet P. Deletion of the hypoxia-response element in the vascular endothelial growth factor promoter causes motor neuron degeneration. *Nat Genet*. 2001; 28(2): 131-138.
23. Cossutta M, Darche M, Carpentier G, Houpe C, Ponzio M, Raineri F, Vallée B, Gilles ME, Villain D, Picard E, Casari C, Denis C, Paques M, Courty J, Cascone I. Weibel-Palade bodies orchestrate pericytes during angiogenesis. *Arterioscler Thromb Vasc Biol*. 2019; 39(9): 1843-1858.
24. Félétou M. Integrated Systems Physiology: from Molecule to Function to Disease in *The Endothelium: Part 1: Multiple Functions of the Endothelial Cells-Focus on Endothelium-Derived Vasoactive Mediators*. (Morgan & Claypool Life Sciences Publishers, 2011).
25. Libby P, Sukhova G, Lee RT, Liao JK. Molecular biology of atherosclerosis. *Int J Cardiol*. 1997; 62 Suppl 2: S23-29.
26. Ross R. Atherosclerosis — an inflammatory disease. *N Engl J Med*. 1999; 340(2): 115-126.
27. Schächinger V, Britten MB, Zeiher AM. Prognostic impact of coronary vasodilator dysfunction on adverse long-term outcome of coronary heart disease. *Circulation*. 2000; 101(16): 1899-1906.
28. Suwaidi JA, Hamasaki S, Higano ST, Nishimura RA, Holmes DR, Jr., Lerman A. Long-term follow-up of patients with mild coronary artery disease and endothelial dysfunction. *Circulation*. 2000; 101(9): 948-954.
29. Heitzer T, Schlinzig T, Krohn K, Meinertz T, Münzel T. Endothelial dysfunction, oxidative stress, and risk of cardiovascular events in patients with coronary artery disease. *Circulation*. 2001; 104(22): 2673-2678.
30. Werner N, Nickenig G. Influence of cardiovascular risk factors on endothelial progenitor cells: limitations for therapy? *Arterioscler Thromb Vasc Biol*. 2006; 26(2): 257-266.
31. Meza CA, La Favor JD, Kim DH, Hickner RC. Endothelial dysfunction: is there a hyperglycemia-induced imbalance of NOX and NOS? *Int J Mol Sci*. 2019; 20(15).

32. Avogaro A, Albiero M, Menegazzo L, de Kreutzenberg S, Fadini GP. Endothelial dysfunction in diabetes: the role of reparatory mechanisms. *Diabetes Care*. 2011; 34 Suppl 2: S285-290.
33. Pfitzner J. Poiseuille and his law. *Anaesthesia*. 1976; 31(2): 273-275.
34. Zhang JXJ, Hoshino K. Microfluidics and micro total analytical systems in *Molecular Sensors and Nanodevices*. (eds Zhang JXJ, Hoshino K) Ch. 3, 103-168 (William Andrew Publishing, 2014).
35. Ostadfar A. Fluid mechanics and biofluids principles in *Biofluid Mechanics: Principles and Applications*. Ch. 1, 1-60 (Academic Press, 2016).
36. Sweeney HL, Hammers DW. Muscle contraction. *Cold Spring Harb Perspect Biol*. 2018; 10(2).
37. Kuo IY, Ehrlich BE. Signaling in muscle contraction. *Cold Spring Harb Perspect Biol*. 2015; 7(2): a006023.
38. Filo RS, Bohr DF, Ruegg JC. Glycerinated skeletal and smooth muscle: calcium and magnesium dependence. *Science*. 1965; 147(3665): 1581-1583.
39. Rayment I, Holden HM, Whittaker M, Yohn CB, Lorenz M, Holmes KC, Milligan RA. Structure of the actin-myosin complex and its implications for muscle contraction. *Science*. 1993; 261(5117): 58-65.
40. Seow CY. Myosin crossbridge, contractile unit, and the mechanism of contraction in airway smooth muscle: a mechanical engineer's perspective. *J Eng Sci Med Diagn Ther*. 2019; 2(1): 0108041-0108046.
41. Squire JM. Muscle filament structure and muscle contraction. *Annual Review of Biophysics and Bioengineering*. 1975; 4(1): 137-163.
42. Knöll R, Hoshijima M, Chien KR. Z-line proteins: implications for additional functions. *European Heart Journal Supplements*. 2002; 4(suppl_I): I13-I17.
43. Bárány K, Bárány M. Myosin light chains in *Biochemistry of Smooth Muscle Contraction*. (ed Bárány M) Ch. 2, 21-35 (Academic Press, 1996).
44. Wang L, Chitano P, Seow CY. Filament evanescence of myosin II and smooth muscle function. *J Gen Physiol*. 2021; 153(3).
45. Sweeney HL, Holzbaur ELF. Motor proteins. *Cold Spring Harb Perspect Biol*. 2018; 10(5).
46. Kim J-H, Lee L-K, Lee W-D, Lee J-U, Kim M-Y, Kim I-H, Choi B-R, Yang S-M, Jeon H-J, Lee T-H, Kwak T-Y, Kim B, Kim J. A review of signal transduction in mechanisms of smooth muscle contraction and its relevance for specialized physical therapy. *Journal of Physical Therapy Science*. 2013; 25(1): 129-141.
47. Zhang J, Herrera AM, Paré PD, Seow CY. Dense-body aggregates as plastic structures supporting tension in smooth muscle cells. *Am J Physiol Lung Cell Mol Physiol*. 2010; 299(5): L631-638.
48. Herrera AM, McParland BE, Bienkowska A, Tait R, Paré PD, Seow CY. 'Sarcomeres' of smooth muscle: functional characteristics and ultrastructural evidence. *J Cell Sci*. 2005; 118(Pt 11): 2381-2392.
49. Kargacin GJ, Cooke PH, Abramson SB, Fay FS. Periodic organization of the contractile apparatus in smooth muscle revealed by the motion of dense bodies in single cells. *J Cell Biol*. 1989; 108(4): 1465-1475.

50. Guilford WH, Dupuis DE, Kennedy G, Wu J, Patlak JB, Warshaw DM. Smooth muscle and skeletal muscle myosins produce similar unitary forces and displacements in the laser trap. *Biophys J*. 1997; 72(3): 1006-1021.
51. Harris DE, Warshaw DM. Smooth and skeletal muscle actin are mechanically indistinguishable in the in vitro motility assay. *Circ Res*. 1993; 72(1): 219-224.
52. Hinssen H, D'Haese J, Small JV, Sobieszek A. Mode of filament assembly of myosins from muscle and nonmuscle cells. *J Ultrastruct Res*. 1978; 64(3): 282-302.
53. Geiger B, Dutton AH, Tokuyasu KT, Singer SJ. Immunoelectron microscope studies of membrane-microfilament interactions: distributions of alpha-actinin, tropomyosin, and vinculin in intestinal epithelial brush border and chicken gizzard smooth muscle cells. *J Cell Biol*. 1981; 91(3 Pt 1): 614-628.
54. Walsh MP. The Ayerst Award Lecture 1990. Calcium-dependent mechanisms of regulation of smooth muscle contraction. *Biochem Cell Biol*. 1991; 69(12): 771-800.
55. Chou RG, Stromer MH, Robson RM, Huiatt TW. Substructure of cytoplasmic dense bodies and changes in distribution of desmin and alpha-actinin in developing smooth muscle cells. *Cell Motil Cytoskeleton*. 1994; 29(3): 204-214.
56. Aguilar HN, Mitchell BF. Physiological pathways and molecular mechanisms regulating uterine contractility. *Hum Reprod Update*. 2010; 16(6): 725-744.
57. Small JV. Geometry of actin-membrane attachments in the smooth muscle cell: the localisations of vinculin and alpha-actinin. *Embo j*. 1985; 4(1): 45-49.
58. Schmid E, Osborn M, Rungger-Brändle E, Gabbiani G, Weber K, Franke WW. Distribution of vimentin and desmin filaments in smooth muscle tissue of mammalian and avian aorta. *Exp Cell Res*. 1982; 137(2): 329-340.
59. Stromer MH, Bendayan M. Arrangement of desmin intermediate filaments in smooth muscle cells as shown by high-resolution immunocytochemistry. *Cell Motil Cytoskeleton*. 1988; 11(2): 117-125.
60. Webb RC. Smooth muscle contraction and relaxation. *Adv Physiol Educ*. 2003; 27(1-4): 201-206.
61. Ghosh D, Syed AU, Prada MP, Nystoriak MA, Santana LF, Nieves-Cintrón M, Navedo MF. Calcium channels in vascular smooth muscle. *Adv Pharmacol*. 2017; 78: 49-87.
62. Johnson JD, Snyder C, Walsh M, Flynn M. Effects of myosin light chain kinase and peptides on Ca²⁺ exchange with the N- and C-terminal Ca²⁺ binding sites of calmodulin. *J Biol Chem*. 1996; 271(2): 761-767.
63. Kamm KE, Stull JT. Dedicated myosin light chain kinases with diverse cellular functions. *J Biol Chem*. 2001; 276(7): 4527-4530.
64. Krueger JK, Zhi G, Stull JT, Trehwella J. Neutron-scattering studies reveal further details of the Ca²⁺/calmodulin-dependent activation mechanism of myosin light chain kinase. *Biochemistry*. 1998; 37(40): 13997-14004.
65. Persechini A, Yano K, Stemmer PM. Ca²⁺ binding and energy coupling in the calmodulin-myosin light chain kinase complex. *J Biol Chem*. 2000; 275(6): 4199-4204.
66. Padre RC, Stull JT. Functional assembly of fragments from bisected smooth muscle myosin light chain kinase. *J Biol Chem*. 2000; 275(35): 26665-26673.
67. Allen BG, Walsh MP. The biochemical basis of the regulation of smooth-muscle contraction. *Trends Biochem Sci*. 1994; 19(9): 362-368.
68. Perrie WT, Smillie LB, Perry SB. A phosphorylated light-chain component of myosin from skeletal muscle. *Biochem J*. 1973; 135(1): 151-164.

69. Ikebe M, Hartshorne DJ, Elzinga M. Identification, phosphorylation, and dephosphorylation of a second site for myosin light chain kinase on the 20,000-dalton light chain of smooth muscle myosin. *J Biol Chem*. 1986; 261(1): 36-39.
70. Ikebe M, Hartshorne DJ, Elzinga M. Phosphorylation of the 20,000-dalton light chain of smooth muscle myosin by the calcium-activated, phospholipid-dependent protein kinase. Phosphorylation sites and effects of phosphorylation. *J Biol Chem*. 1987; 262(20): 9569-9573.
71. Brozovich FV, Nicholson CJ, Degen CV, Gao YZ, Aggarwal M, Morgan KG. Mechanisms of vascular smooth muscle contraction and the basis for pharmacologic treatment of smooth muscle disorders. *Pharmacol Rev*. 2016; 68(2): 476-532.
72. Raeymaekers L, Wuytack F. Ca²⁺ pumps in smooth muscle cells. *J Muscle Res Cell Motil*. 1993; 14(2): 141-157.
73. Erdödi F, Ito M, Hartshorne DJ. Myosin light chain phosphatase in *Biochemistry of Smooth Muscle Contraction*. (ed Bárány M) Ch. 10, 131-142 (Academic Press, 1996).
74. Shirazi A, Iizuka K, Fadden P, Mosse C, Somlyo AP, Somlyo AV, Haystead TA. Purification and characterization of the mammalian myosin light chain phosphatase holoenzyme. The differential effects of the holoenzyme and its subunits on smooth muscle. *J Biol Chem*. 1994; 269(50): 31598-31606.
75. Lodish HF, Berk A, Zipursky SL, Matsudaira P, Baltimore D, Darnell J. *Molecular cell biology*. 4th ed. edn, (W.H. Freeman, 2000).
76. Lehman W, Denault D, Marston S. The caldesmon content of vertebrate smooth muscle. *Biochim Biophys Acta*. 1993; 1203(1): 53-59.
77. Smith CW, Marston SB. Disassembly and reconstitution of the Ca²⁺-sensitive thin filaments of vascular smooth muscle. *FEBS Lett*. 1985; 184(1): 115-119.
78. Marston SB, Lehman W. Caldesmon is a Ca²⁺-regulatory component of native smooth-muscle thin filaments. *Biochem J*. 1985; 231(3): 517-522.
79. Rozenblum GT, Gimona M. Calponins: adaptable modular regulators of the actin cytoskeleton. *Int J Biochem Cell Biol*. 2008; 40(10): 1990-1995.
80. Winder SJ, Allen BG, Clément-Chomienne O, Walsh MP. Regulation of smooth muscle actin-myosin interaction and force by calponin. *Acta Physiol Scand*. 1998; 164(4): 415-426.
81. Ngai PK, Walsh MP. Inhibition of smooth muscle actin-activated myosin Mg²⁺-ATPase activity by caldesmon. *J Biol Chem*. 1984; 259(22): 13656-13659.
82. Lash JA, Sellers JR, Hathaway DR. The effects of caldesmon on smooth muscle heavy actomeromyosin ATPase activity and binding of heavy meromyosin to actin. *J Biol Chem*. 1986; 261(34): 16155-16160.
83. Alahyan M, Webb MR, Marston SB, El-Mezgueldi M. The mechanism of smooth muscle caldesmon-tropomyosin inhibition of the elementary steps of the actomyosin ATPase. *J Biol Chem*. 2006; 281(28): 19433-19448.
84. Gunning P, O'Neill G, Hardeman E. Tropomyosin-based regulation of the actin cytoskeleton in time and space. *Physiol Rev*. 2008; 88(1): 1-35.
85. Chalovich JM, Lutz E, Baxley T, Schroeter MM. Acrylodan-labeled smooth muscle tropomyosin reports differences in the effects of troponin and caldesmon in the transition from the active state to the inactive state. *Biochemistry*. 2011; 50(27): 6093-6101.

86. Wang CL, Wang LW, Xu SA, Lu RC, Saavedra-Alanis V, Bryan J. Localization of the calmodulin- and the actin-binding sites of caldesmon. *J Biol Chem.* 1991; 266(14): 9166-9172.
87. Sobue K, Morimoto K, Inui M, Kanda K, Kakiuchi S. Control of actin-myosin interaction of gizzard smooth muscle by calmodulin-and caldesmonlinked flip-flop mechanism. *Biomedical Research.* 1982; 3(2): 188-196.
88. Gerthoffer WT, Yamboliev IA, Shearer M, Pohl J, Haynes R, Dang S, Sato K, Sellers JR. Activation of MAP kinases and phosphorylation of caldesmon in canine colonic smooth muscle. *J Physiol.* 1996; 495: 597-609.
89. Ngai PK, Walsh MP. The effects of phosphorylation of smooth-muscle caldesmon. *Biochem J.* 1987; 244(2): 417-425.
90. Scott-Woo GC, Sutherland C, Walsh MP. Kinase activity associated with caldesmon is Ca²⁺/calmodulin-dependent kinase II. *Biochem J.* 1990; 268(2): 367-370.
91. Tanaka T, Ohta H, Kanda K, Tanaka T, Hidaka H, Sobue K. Phosphorylation of high-M_r caldesmon by protein kinase C modulates the regulatory function of this protein on the interaction between actin and myosin. *Eur J Biochem.* 1990; 188(3): 495-500.
92. Winder SJ, Walsh MP. Smooth muscle calponin. Inhibition of actomyosin MgATPase and regulation by phosphorylation. *J Biol Chem.* 1990; 265(17): 10148-10155.
93. Hodgkinson JL, Marston SB, Craig R, Vibert P, Lehman W. Three-dimensional image reconstruction of reconstituted smooth muscle thin filaments: effects of caldesmon. *Biophys J.* 1997; 72(6): 2398-2404.
94. Gallant C, Appel S, Graceffa P, Leavis P, Lin JJ, Gunning PW, Schevzov G, Chaponnier C, DeGnore J, Lehman W, Morgan KG. Tropomyosin variants describe distinct functional subcellular domains in differentiated vascular smooth muscle cells. *Am J Physiol Cell Physiol.* 2011; 300(6): C1356-1365.
95. Hartshorne DJ. Biochemistry of the contractile process in smooth muscle in *Physiology of the gastrointestinal tract.* (ed Johnson LR) Ch. 13, 423-482 (Raven Press, 1987).
96. Moran CM, Garriock RJ, Miller MK, Heimark RL, Gregorio CC, Krieg PA. Expression of the fast twitch troponin complex, fTnT, fTnI and fTnC, in vascular smooth muscle. *Cell Motil Cytoskeleton.* 2008; 65(8): 652-661.
97. Takeya K, Kathol I, Sutherland C, Wang X, Loutzenhiser R, Walsh MP. Expression of troponin subunits in the rat renal afferent arteriole. *IUBMB Life.* 2019; 71(10): 1475-1481.
98. Kim HR, Appel S, Vetterkind S, Gangopadhyay SS, Morgan KG. Smooth muscle signalling pathways in health and disease. *J Cell Mol Med.* 2008; 12(6a): 2165-2180.
99. Saddouk FZ, Ginnan R, Singer HA. Ca²⁺/Calmodulin-dependent protein kinase II in vascular smooth muscle. *Adv Pharmacol.* 2017; 78: 171-202.
100. DeVries G, Fraser ED, Walsh MP. Protein kinase C from chicken gizzard: characterization and detection of an inhibitor and endogenous substrates. *Biochem Cell Biol.* 1989; 67(6): 260-270.
101. Schaefer M. Protein Kinase C in *xPharm: The Comprehensive Pharmacology Reference.* (eds Enna SJ, Bylund DB) 1-4 (Elsevier, 2007).
102. Grange JJ, Baca-Regen LM, Nollendorfs AJ, Persidsky Y, Sudan DL, Baxter BT. Protein kinase C isoforms in human aortic smooth muscle cells. *J Vasc Surg.* 1998; 27(5): 919-926; discussion 926-917.

103. Ito M, Okamoto R, Ito H, Zhe Y, Dohi K. Regulation of myosin light-chain phosphorylation and its roles in cardiovascular physiology and pathophysiology. *Hypertens Res.* 2022; 45(1): 40-52.
104. Eto M, Katsuki S, Ohashi M, Miyagawa Y, Tanaka Y, Takeya K, Kitazawa T. Possible roles of N- and C-terminal unstructured tails of CPI-17 in regulating Ca²⁺ sensitization force of smooth muscle. *J Smooth Muscle Res.* 2022; 58(0): 22-33.
105. Schworer CM, Colbran RJ, Keefer JR, Soderling TR. Ca²⁺/calmodulin-dependent protein kinase II. Identification of a regulatory autophosphorylation site adjacent to the inhibitory and calmodulin-binding domains. *J Biol Chem.* 1988; 263(27): 13486-13489.
106. Perrino BA. Regulation of gastrointestinal motility by Ca²⁺/calmodulin-stimulated protein kinase II. *Archives of Biochemistry and Biophysics.* 2011; 510(2): 174-181.
107. Tansey MG, Word RA, Hidaka H, Singer HA, Schworer CM, Kamm KE, Stull JT. Phosphorylation of myosin light chain kinase by the multifunctional calmodulin-dependent protein kinase II in smooth muscle cells. *J Biol Chem.* 1992; 267(18): 12511-12516.
108. Kim I, Je HD, Gallant C, Zhan Q, Riper DV, Badwey JA, Singer HA, Morgan KG. Ca²⁺-calmodulin-dependent protein kinase II-dependent activation of contractility in ferret aorta. *J Physiol.* 2000; 526 Pt 2(Pt 2): 367-374.
109. Rokolya A, Singer HA. Inhibition of CaM kinase II activation and force maintenance by KN-93 in arterial smooth muscle. *Am J Physiol Cell Physiol.* 2000; 278(3): C537-545.
110. Billaud M, Lohman AW, Johnstone SR, Biwer LA, Mutchler S, Isakson BE. Regulation of cellular communication by signaling microdomains in the blood vessel wall. *Pharmacol Rev.* 2014; 66(2): 513-569.
111. ZhuGe R, Tuft RA, Fogarty KE, Bellve K, Fay FS, Walsh JV, Jr. The influence of sarcoplasmic reticulum Ca²⁺ concentration on Ca²⁺ sparks and spontaneous transient outward currents in single smooth muscle cells. *J Gen Physiol.* 1999; 113(2): 215-228.
112. Wray S, Burdyga T. Sarcoplasmic reticulum function in smooth muscle. *Physiological Reviews.* 2010; 90(1): 113-178.
113. Allbritton NL, Meyer T, Stryer L. Range of messenger action of calcium ion and inositol 1,4,5-trisphosphate. *Science.* 1992; 258(5089): 1812-1815.
114. Kargacin GJ. Calcium signaling in restricted diffusion spaces. *Biophys J.* 1994; 67(1): 262-272.
115. Amberg GC, Navedo MF. Calcium dynamics in vascular smooth muscle. *Microcirculation.* 2013; 20(4): 281-289.
116. McCarron JG, Olson ML, Chalmers S. Mitochondrial regulation of cytosolic Ca²⁺ signals in smooth muscle. *Pflugers Arch.* 2012; 464(1): 51-62.
117. Berridge MJ. Smooth muscle cell calcium activation mechanisms. *J Physiol.* 2008; 586(21): 5047-5061.
118. Devine CE, Somlyo AV, Somlyo AP. Sarcoplasmic reticulum and mitochondria as cation accumulation sites in smooth muscle. *Philos Trans R Soc Lond B Biol Sci.* 1973; 265(867): 17-23.
119. Tribe RM, Borin ML, Blaustein MP. Functionally and spatially distinct Ca²⁺ stores are revealed in cultured vascular smooth muscle cells. *Proc Natl Acad Sci U S A.* 1994; 91(13): 5908-5912.
120. Somlyo AP, Somlyo AV. Flash photolysis studies of excitation-contraction coupling, regulation, and contraction in smooth muscle. *Annu Rev Physiol.* 1990; 52: 857-874.

121. Somlyo AP, Himpens B. Cell calcium and its regulation in smooth muscle. *Faseb j.* 1989; 3(11): 2266-2276.
122. Liu Z, Khalil RA. Evolving mechanisms of vascular smooth muscle contraction highlight key targets in vascular disease. *Biochem Pharmacol.* 2018; 153: 91-122.
123. Gabella G. Structure of smooth muscles in *Smooth Muscle: An Assessment of Current Knowledge.* (eds Bülbring E, Brading AF, Jones AW, Tomita T) Ch. 1, 1-46 (Edward Arnold Publishers, 1981).
124. Devine CE, Somlyo AV, Somlyo AP. Sarcoplasmic reticulum and excitation-contraction coupling in mammalian smooth muscles. *J Cell Biol.* 1972; 52(3): 690-718.
125. Bond M, Kitazawa T, Somlyo AP, Somlyo AV. Release and recycling of calcium by the sarcoplasmic reticulum in guinea-pig portal vein smooth muscle. *J Physiol.* 1984; 355: 677-695.
126. Mironneau C, Mironneau J, Savineau JP. Maintained contractions of rat uterine smooth muscle incubated in a Ca^{2+} -free solution. *Br J Pharmacol.* 1984; 82(3): 735-743.
127. Ross R, Klebanoff SJ. Fine structural changes in uterine smooth muscle and fibroblasts in response to estrogen. *J Cell Biol.* 1967; 32(1): 155-167.
128. Phillippe M, Saunders T, Basa A. Intracellular mechanisms underlying prostaglandin $\text{F}2\alpha$ -stimulated phasic myometrial contractions. *Am J Physiol.* 1997; 273(4): E665-673.
129. Golovina VA, Blaustein MP. Spatially and functionally distinct Ca^{2+} stores in sarcoplasmic and endoplasmic reticulum. *Science.* 1997; 275(5306): 1643-1648.
130. Shmygol A, Wray S. Functional architecture of the SR calcium store in uterine smooth muscle. *Cell Calcium.* 2004; 35(6): 501-508.
131. Young RC, Mathur SP. Focal sarcoplasmic reticulum calcium stores and diffuse inositol 1,4,5-trisphosphate and ryanodine receptors in human myometrium. *Cell Calcium.* 1999; 26(1-2): 69-75.
132. Gordienko DV, Greenwood IA, Bolton TB. Direct visualization of sarcoplasmic reticulum regions discharging Ca^{2+} sparks in vascular myocytes. *Cell Calcium.* 2001; 29(1): 13-28.
133. Steenbergen JM, Fay FS. The quantal nature of calcium release to caffeine in single smooth muscle cells results from activation of the sarcoplasmic reticulum Ca^{2+} -ATPase. *J Biol Chem.* 1996; 271(4): 1821-1824.
134. Puskin JS, Gunter TE, Gunter KK, Russell PR. Evidence for more than one Ca^{2+} transport mechanism in mitochondria. *Biochemistry.* 1976; 15(17): 3834-3842.
135. Somlyo AP, Somlyo AV. The sarcoplasmic reticulum: then and now. *Novartis Found Symp.* 2002; 246: 258-268; discussion 268-271, 272-256.
136. Yamamoto H, van Breemen C. Ca^{2+} compartments in saponin-skinned cultured vascular smooth muscle cells. *J Gen Physiol.* 1986; 87(3): 369-389.
137. Horikawa Y, Goel A, Somlyo AP, Somlyo AV. Mitochondrial calcium in relaxed and tetanized myocardium. *Biophys J.* 1998; 74(3): 1579-1590.
138. Dulhunty AF, Pouliquin P. What we don't know about the structure of ryanodine receptor calcium release channels. *Clin Exp Pharmacol Physiol.* 2003; 30(10): 713-723.
139. Laporte R, Hui A, Laher I. Pharmacological modulation of sarcoplasmic reticulum function in smooth muscle. *Pharmacol Rev.* 2004; 56(4): 439-513.
140. Narayanan D, Adebisi A, Jaggar JH. Inositol trisphosphate receptors in smooth muscle cells. *Am J Physiol Heart Circ Physiol.* 2012; 302(11): H2190-2210.

141. Foskett JK, White C, Cheung KH, Mak DO. Inositol trisphosphate receptor Ca^{2+} release channels. *Physiol Rev.* 2007; 87(2): 593-658.
142. Südhof TC, Newton CL, Archer BT, 3rd, Ushkaryov YA, Mignery GA. Structure of a novel InsP_3 receptor. *Embo j.* 1991; 10(11): 3199-3206.
143. Mignery GA, Südhof TC, Takei K, De Camilli P. Putative receptor for inositol 1,4,5-trisphosphate similar to ryanodine receptor. *Nature.* 1989; 342(6246): 192-195.
144. Maranto AR. Primary structure, ligand binding, and localization of the human type 3 inositol 1,4,5-trisphosphate receptor expressed in intestinal epithelium. *J Biol Chem.* 1994; 269(2): 1222-1230.
145. Furuichi T, Yoshikawa S, Miyawaki A, Wada K, Maeda N, Mikoshiba K. Primary structure and functional expression of the inositol 1,4,5-trisphosphate-binding protein P_{400} . *Nature.* 1989; 342(6245): 32-38.
146. Blondel O, Takeda J, Janssen H, Seino S, Bell GI. Sequence and functional characterization of a third inositol trisphosphate receptor subtype, IP3R-3, expressed in pancreatic islets, kidney, gastrointestinal tract, and other tissues. *J Biol Chem.* 1993; 268(15): 11356-11363.
147. Wojcikiewicz RJ, Luo SG. Differences among type I, II, and III inositol-1,4,5-trisphosphate receptors in ligand-binding affinity influence the sensitivity of calcium stores to inositol-1,4,5-trisphosphate. *Mol Pharmacol.* 1998; 53(4): 656-662.
148. Newton CL, Mignery GA, Südhof TC. Co-expression in vertebrate tissues and cell lines of multiple inositol 1,4,5-trisphosphate (InsP_3) receptors with distinct affinities for InsP_3 . *J Biol Chem.* 1994; 269(46): 28613-28619.
149. Grayson TH, Haddock RE, Murray TP, Wojcikiewicz RJ, Hill CE. Inositol 1,4,5-trisphosphate receptor subtypes are differentially distributed between smooth muscle and endothelial layers of rat arteries. *Cell Calcium.* 2004; 36(6): 447-458.
150. Zhao G, Adebisi A, Blaskova E, Xi Q, Jaggar JH. Type 1 inositol 1,4,5-trisphosphate receptors mediate UTP-induced cation currents, Ca^{2+} signals, and vasoconstriction in cerebral arteries. *Am J Physiol Cell Physiol.* 2008; 295(5): C1376-1384.
151. Zhou H, Nakamura T, Matsumoto N, Hisatsune C, Mizutani A, Iesaki T, Daida H, Mikoshiba K. Predominant role of type 1 IP_3 receptor in aortic vascular muscle contraction. *Biochem Biophys Res Commun.* 2008; 369(1): 213-219.
152. Kadamur G, Ross EM. Mammalian phospholipase C. *Annu Rev Physiol.* 2013; 75: 127-154.
153. Kovács A, Hársing LG, Jr., Szénási G. Vasoconstrictor 5-HT receptors in the smooth muscle of the rat middle cerebral artery. *Eur J Pharmacol.* 2012; 689(1-3): 160-164.
154. Eglen RM, Whiting RL. Heterogeneity of vascular muscarinic receptors. *J Auton Pharmacol.* 1990; 10(4): 233-245.
155. Schmitz EA, Takahashi H, Karakas E. Structural basis for activation and gating of IP_3 receptors. *Nat Commun.* 2022; 13(1): 1408.
156. Arige V, Terry LE, Wagner LE, 2nd, Malik S, Baker MR, Fan G, Joseph SK, Serysheva, II, Yule DI. Functional determination of calcium-binding sites required for the activation of inositol 1,4,5-trisphosphate receptors. *Proc Natl Acad Sci U S A.* 2022; 119(39): e2209267119.
157. Alzayady KJ, Wang L, Chandrasekhar R, Wagner LE, 2nd, Van Petegem F, Yule DI. Defining the stoichiometry of inositol 1,4,5-trisphosphate binding required to initiate Ca^{2+} release. *Sci Signal.* 2016; 9(422): ra35.

158. Chandrasekhar R, Alzayady KJ, Wagner LE, 2nd, Yule DI. Unique regulatory properties of heterotetrameric inositol 1,4,5-trisphosphate receptors revealed by studying concatenated receptor constructs. *J Biol Chem*. 2016; 291(10): 4846-4860.
159. Bezprozvanny I, Watras J, Ehrlich BE. Bell-shaped calcium-response curves of Ins(1,4,5)P₃- and calcium-gated channels from endoplasmic reticulum of cerebellum. *Nature*. 1991; 351(6329): 751-754.
160. Finch EA, Turner TJ, Goldin SM. Calcium as a coagonist of inositol 1,4,5-trisphosphate-induced calcium release. *Science*. 1991; 252(5004): 443-446.
161. Finch EA, Turner TJ, Goldin SM. Subsecond kinetics of inositol 1,4,5-trisphosphate-induced calcium release reveal rapid potentiation and subsequent inactivation by calcium. *Ann N Y Acad Sci*. 1991; 635: 400-403.
162. Iino M. Biphasic Ca²⁺ dependence of inositol 1,4,5-trisphosphate-induced Ca release in smooth muscle cells of the guinea pig taenia caeci. *J Gen Physiol*. 1990; 95(6): 1103-1122.
163. Iino M. Calcium dependent inositol trisphosphate-induced calcium release in the guinea-pig taenia caeci. *Biochem Biophys Res Commun*. 1987; 142(1): 47-52.
164. Melville Z, Dridi H, Yuan Q, Reiken S, Wronska A, Liu Y, Clarke OB, Marks AR. A drug and ATP binding site in type 1 ryanodine receptor. *Structure*. 2022; 30(7): 1025-1034.e1024.
165. Efremov RG, Leitner A, Aebersold R, Raunser S. Architecture and conformational switch mechanism of the ryanodine receptor. *Nature*. 2015; 517(7532): 39-43.
166. Zalk R, Clarke OB, des Georges A, Grassucci RA, Reiken S, Mancina F, Hendrickson WA, Frank J, Marks AR. Structure of a mammalian ryanodine receptor. *Nature*. 2015; 517(7532): 44-49.
167. Marx SO, Reiken S, Hisamatsu Y, Jayaraman T, Burkhoff D, Rosemblyt N, Marks AR. PKA phosphorylation dissociates FKBP12.6 from the calcium release channel (ryanodine receptor): defective regulation in failing hearts. *Cell*. 2000; 101(4): 365-376.
168. Lanner JT, Georgiou DK, Joshi AD, Hamilton SL. Ryanodine receptors: structure, expression, molecular details, and function in calcium release. *Cold Spring Harb Perspect Biol*. 2010; 2(11): a003996.
169. MacKenzie AE, Korneluk RG, Zorzato F, Fujii J, Phillips M, Iles D, Wieringa B, Leblond S, Bailly J, Willard HF, et al. The human ryanodine receptor gene: its mapping to 19q13.1, placement in a chromosome 19 linkage group, and exclusion as the gene causing myotonic dystrophy. *Am J Hum Genet*. 1990; 46(6): 1082-1089.
170. Trask B, Fertitta A, Christensen M, Youngblom J, Bergmann A, Copeland A, de Jong P, Mohrenweiser H, Olsen A, Carrano A, et al. Fluorescence in situ hybridization mapping of human chromosome 19: cytogenetic band location of 540 cosmids and 70 genes or DNA markers. *Genomics*. 1993; 15(1): 133-145.
171. Otsu K, Fujii J, Periasamy M, Difilippantonio M, Uppender M, Ward DC, MacLennan DH. Chromosome mapping of five human cardiac and skeletal muscle sarcoplasmic reticulum protein genes. *Genomics*. 1993; 17(2): 507-509.
172. Sorrentino V, Giannini G, Malzac P, Mattei MG. Localization of a novel ryanodine receptor gene (RYR3) to human chromosome 15q14-q15 by in situ hybridization. *Genomics*. 1993; 18(1): 163-165.
173. Vaithianathan T, Narayanan D, Asuncion-Chin MT, Jeyakumar LH, Liu J, Fleischer S, Jaggar JH, Dopico AM. Subtype identification and functional characterization of

- ryanodine receptors in rat cerebral artery myocytes. *Am J Physiol Cell Physiol*. 2010; 299(2): C264-278.
174. Zheng YM, Wang QS, Liu QH, Rathore R, Yadav V, Wang YX. Heterogeneous gene expression and functional activity of ryanodine receptors in resistance and conduit pulmonary as well as mesenteric artery smooth muscle cells. *J Vasc Res*. 2008; 45(6): 469-479.
 175. Kaßmann M, Szijártó IA, García-Prieto CF, Fan G, Schleifenbaum J, Anistan YM, Tabeling C, Shi Y, le Noble F, Witzentrath M, Huang Y, Markó L, Nelson MT, Gollasch M. Role of ryanodine type 2 receptors in elementary Ca²⁺ signaling in arteries and vascular adaptive responses. *J Am Heart Assoc*. 2019; 8(9): e010090.
 176. Chen YS, Van Petegem F. Structural and functional conservation of the activating Ca²⁺ binding site in inositol 1,4,5-trisphosphate and ryanodine receptors. *Cell Calcium*. 2022; 108: 102671.
 177. Laver DR. Regulation of the RyR channel gating by Ca²⁺ and Mg²⁺. *Biophys Rev*. 2018; 10(4): 1087-1095.
 178. Ching LL, Williams AJ, Sitsapesan R. Evidence for Ca²⁺ activation and inactivation sites on the luminal side of the cardiac ryanodine receptor complex. *Circ Res*. 2000; 87(3): 201-206.
 179. Laver DR, Roden LD, Ahern GP, Eager KR, Junankar PR, Dulhunty AF. Cytoplasmic Ca²⁺ inhibits the ryanodine receptor from cardiac muscle. *J Membr Biol*. 1995; 147(1): 7-22.
 180. Ma R, Haji-Ghassemi O, Ma D, Jiang H, Lin L, Yao L, Samurkas A, Li Y, Wang Y, Cao P, Wu S, Zhang Y, Murayama T, Moussian B, Van Petegem F, Yuchi Z. Structural basis for diamide modulation of ryanodine receptor. *Nat Chem Biol*. 2020; 16(11): 1246-1254.
 181. Lau K, Chan MM, Van Petegem F. Lobe-specific calmodulin binding to different ryanodine receptor isoforms. *Biochemistry*. 2014; 53(5): 932-946.
 182. Buck E, Zimanyi I, Abramson JJ, Pessah IN. Ryanodine stabilizes multiple conformational states of the skeletal muscle calcium release channel. *J Biol Chem*. 1992; 267(33): 23560-23567.
 183. Fessenden JD, Chen L, Wang Y, Paolini C, Franzini-Armstrong C, Allen PD, Pessah IN. Ryanodine receptor point mutant E4032A reveals an allosteric interaction with ryanodine. *Proc Natl Acad Sci U S A*. 2001; 98(5): 2865-2870.
 184. Lai FA, Misra M, Xu L, Smith HA, Meissner G. The ryanodine receptor-Ca²⁺ release channel complex of skeletal muscle sarcoplasmic reticulum. Evidence for a cooperatively coupled, negatively charged homotetramer. *J Biol Chem*. 1989; 264(28): 16776-16785.
 185. Meissner G. The structural basis of ryanodine receptor ion channel function. *J Gen Physiol*. 2017; 149(12): 1065-1089.
 186. Ngo VA, Perissinotti LL, Miranda W, Chen SRW, Noskov SY. Mapping ryanodine binding sites in the pore cavity of ryanodine receptors. *Biophys J*. 2017; 112(8): 1645-1653.
 187. Ottolini M, Hong K, Sonkusare SK. Calcium signals that determine vascular resistance. *Wiley Interdiscip Rev Syst Biol Med*. 2019; 11(5): e1448.
 188. Cheng H, Lederer WJ. Calcium sparks. *Physiol Rev*. 2008; 88(4): 1491-1545.
 189. Loesser KE, Castellani L, Franzini-Armstrong C. Dispositions of junctional feet in muscles of invertebrates. *J Muscle Res Cell Motil*. 1992; 13(2): 161-173.

190. Lesh RE, Nixon GF, Fleischer S, Airey JA, Somlyo AP, Somlyo AV. Localization of ryanodine receptors in smooth muscle. *Circ Res*. 1998; 82(2): 175-185.
191. Moore ED, Voigt T, Kobayashi YM, Isenberg G, Fay FS, Gallitelli MF, Franzini-Armstrong C. Organization of Ca²⁺ release units in excitable smooth muscle of the guinea-pig urinary bladder. *Biophys J*. 2004; 87(3): 1836-1847.
192. Yang XR, Lin MJ, Yip KP, Jeyakumar LH, Fleischer S, Leung GP, Sham JS. Multiple ryanodine receptor subtypes and heterogeneous ryanodine receptor-gated Ca²⁺ stores in pulmonary arterial smooth muscle cells. *Am J Physiol Lung Cell Mol Physiol*. 2005; 289(2): L338-348.
193. Gollasch M, Wellman GC, Knot HJ, Jaggar JH, Damon DH, Bonev AD, Nelson MT. Ontogeny of local sarcoplasmic reticulum Ca²⁺ signals in cerebral arteries: Ca²⁺ sparks as elementary physiological events. *Circ Res*. 1998; 83(11): 1104-1114.
194. Bonev AD, Jaggar JH, Rubart M, Nelson MT. Activators of protein kinase C decrease Ca²⁺ spark frequency in smooth muscle cells from cerebral arteries. *Am J Physiol*. 1997; 273(6): C2090-2095.
195. Pérez GJ, Bonev AD, Patlak JB, Nelson MT. Functional coupling of ryanodine receptors to K_{Ca} channels in smooth muscle cells from rat cerebral arteries. *J Gen Physiol*. 1999; 113(2): 229-238.
196. Nelson MT, Cheng H, Rubart M, Santana LF, Bonev AD, Knot HJ, Lederer WJ. Relaxation of arterial smooth muscle by calcium sparks. *Science*. 1995; 270(5236): 633-637.
197. Hogg RC, Wang Q, Large WA. Time course of spontaneous calcium-activated chloride currents in smooth muscle cells from the rabbit portal vein. *J Physiol*. 1993; 464: 15-31.
198. Saleh SN, Greenwood IA. Activation of chloride currents in murine portal vein smooth muscle cells by membrane depolarization involves intracellular calcium release. *Am J Physiol Cell Physiol*. 2005; 288(1): C122-131.
199. Hogg RC, Wang Q, Helliwell RM, Large WA. Properties of spontaneous inward currents in rabbit pulmonary artery smooth muscle cells. *Pflugers Arch*. 1993; 425(3-4): 233-240.
200. Zhou JG, Ren JL, Qiu QY, He H, Guan YY. Regulation of intracellular Cl⁻ concentration through volume-regulated ClC-3 chloride channels in A10 vascular smooth muscle cells. *J Biol Chem*. 2005; 280(8): 7301-7308.
201. Bulley S, Jaggar JH. Cl⁻ channels in smooth muscle cells. *Pflugers Arch*. 2014; 466(5): 861-872.
202. Bulley S, Neeb ZP, Burris SK, Bannister JP, Thomas-Gatewood CM, Jangsangthong W, Jaggar JH. TMEM16A/ANO1 channels contribute to the myogenic response in cerebral arteries. *Circ Res*. 2012; 111(8): 1027-1036.
203. Leblanc N, Ledoux J, Saleh S, Sanguinetti A, Angermann J, O'Driscoll K, Britton F, Perrino BA, Greenwood IA. Regulation of calcium-activated chloride channels in smooth muscle cells: a complex picture is emerging. *Can J Physiol Pharmacol*. 2005; 83(7): 541-556.
204. Matchkov VV, Boedtker DM, Aalkjaer C. The role of Ca²⁺ activated Cl⁻ channels in blood pressure control. *Curr Opin Pharmacol*. 2015; 21: 127-137.
205. ZhuGe R, Sims SM, Tuft RA, Fogarty KE, Walsh JV, Jr. Ca²⁺ sparks activate K⁺ and Cl⁻ channels, resulting in spontaneous transient currents in guinea-pig tracheal myocytes. *J Physiol*. 1998; 513 (Pt 3)(Pt 3): 711-718.

206. Jaggar JH, Porter VA, Lederer WJ, Nelson MT. Calcium sparks in smooth muscle. *Am J Physiol Cell Physiol.* 2000; 278(2): C235-256.
207. Bootman MD, Berridge MJ. Subcellular Ca²⁺ signals underlying waves and graded responses in HeLa cells. *Curr Biol.* 1996; 6(7): 855-865.
208. Tovey SC, de Smet P, Lipp P, Thomas D, Young KW, Missiaen L, De Smedt H, Parys JB, Berridge MJ, Thuring J, Holmes A, Bootman MD. Calcium puffs are generic InsP₃-activated elementary calcium signals and are downregulated by prolonged hormonal stimulation to inhibit cellular calcium responses. *J Cell Sci.* 2001; 114(Pt 22): 3979-3989.
209. Parker I, Smith IF. Recording single-channel activity of inositol trisphosphate receptors in intact cells with a microscope, not a patch clamp. *J Gen Physiol.* 2010; 136(2): 119-127.
210. Burdyga TV, Taggart MJ, Crichton C, Smith GL, Wray S. The mechanism of Ca²⁺ release from the SR of permeabilised guinea-pig and rat ureteric smooth muscle. *Biochim Biophys Acta.* 1998; 1402(1): 109-114.
211. Boittin FX, Coussin F, Morel JL, Halet G, Macrez N, Mironneau J. Ca²⁺ signals mediated by Ins(1,4,5)P₃-gated channels in rat ureteric myocytes. *Biochem J.* 2000; 349(Pt 1): 323-332.
212. Bayguinov O, Hagen B, Bonev AD, Nelson MT, Sanders KM. Intracellular calcium events activated by ATP in murine colonic myocytes. *Am J Physiol Cell Physiol.* 2000; 279(1): C126-135.
213. Olson ML, Chalmers S, McCarron JG. Mitochondrial Ca²⁺ uptake increases Ca²⁺ release from inositol 1,4,5-trisphosphate receptor clusters in smooth muscle cells. *J Biol Chem.* 2010; 285(3): 2040-2050.
214. Gonzales AL, Earley S. Endogenous cytosolic Ca²⁺ buffering is necessary for TRPM4 activity in cerebral artery smooth muscle cells. *Cell Calcium.* 2012; 51(1): 82-93.
215. Gonzales AL, Amberg GC, Earley S. Ca²⁺ release from the sarcoplasmic reticulum is required for sustained TRPM4 activity in cerebral artery smooth muscle cells. *Am J Physiol Cell Physiol.* 2010; 299(2): C279-288.
216. Gordienko DV, Bolton TB. Crosstalk between ryanodine receptors and IP₃ receptors as a factor shaping spontaneous Ca²⁺-release events in rabbit portal vein myocytes. *J Physiol.* 2002; 542(Pt 3): 743-762.
217. Hajnóczky G, Thomas AP. Minimal requirements for calcium oscillations driven by the IP₃ receptor. *Embo j.* 1997; 16(12): 3533-3543.
218. Lechleiter JD, Clapham DE. Molecular mechanisms of intracellular calcium excitability in *X. laevis* oocytes. *Cell.* 1992; 69(2): 283-294.
219. Marchant J, Callamaras N, Parker I. Initiation of IP₃-mediated Ca²⁺ waves in *Xenopus* oocytes. *Embo j.* 1999; 18(19): 5285-5299.
220. Bootman MD, Berridge MJ, Lipp P. Cooking with calcium: the recipes for composing global signals from elementary events. *Cell.* 1997; 91(3): 367-373.
221. Iino M, Kasai H, Yamazawa T. Visualization of neural control of intracellular Ca²⁺ concentration in single vascular smooth muscle cells in situ. *Embo j.* 1994; 13(21): 5026-5031.
222. Hill-Eubanks DC, Werner ME, Heppner TJ, Nelson MT. Calcium signaling in smooth muscle. *Cold Spring Harb Perspect Biol.* 2011; 3(9): a004549.
223. Stevens RJ, Weinert JS, Publicover NG. Visualization of origins and propagation of excitation in canine gastric smooth muscle. *Am J Physiol.* 1999; 277(3): C448-460.

224. Hamada H, Damron DS, Hong SJ, Van Wagoner DR, Murray PA. Phenylephrine-induced Ca^{2+} oscillations in canine pulmonary artery smooth muscle cells. *Circ Res.* 1997; 81(5): 812-823.
225. Miriel VA, Mauban JR, Blaustein MP, Wier WG. Local and cellular Ca^{2+} transients in smooth muscle of pressurized rat resistance arteries during myogenic and agonist stimulation. *J Physiol.* 1999; 518 (Pt 3)(Pt 3): 815-824.
226. Kasai Y, Yamazawa T, Sakurai T, Taketani Y, Iino M. Endothelium-dependent frequency modulation of Ca^{2+} signalling in individual vascular smooth muscle cells of the rat. *J Physiol.* 1997; 504 (Pt 2)(Pt 2): 349-357.
227. Peng H, Matchkov V, Ivarsen A, Aalkjær C, Nilsson H. Hypothesis for the initiation of vasomotion. *Circ Res.* 2001; 88(8): 810-815.
228. Jaggar JH. Intravascular pressure regulates local and global Ca^{2+} signaling in cerebral artery smooth muscle cells. *Am J Physiol Cell Physiol.* 2001; 281(2): C439-448.
229. Zacharia J, Zhang J, Wier WG. Ca^{2+} signaling in mouse mesenteric small arteries: myogenic tone and adrenergic vasoconstriction. *Am J Physiol Heart Circ Physiol.* 2007; 292(3): H1523-1532.
230. Jaggar JH, Nelson MT. Differential regulation of Ca^{2+} sparks and Ca^{2+} waves by UTP in rat cerebral artery smooth muscle cells. *Am J Physiol Cell Physiol.* 2000; 279(5): C1528-1539.
231. Boittin FX, Macrez N, Halet G, Mironneau J. Norepinephrine-induced Ca^{2+} waves depend on InsP_3 and ryanodine receptor activation in vascular myocytes. *Am J Physiol.* 1999; 277(1): C139-151.
232. Ruehlmann DO, Lee CH, Poburko D, van Breemen C. Asynchronous Ca^{2+} waves in intact venous smooth muscle. *Circ Res.* 2000; 86(4): E72-79.
233. Heppner TJ, Bonev AD, Santana LF, Nelson MT. Alkaline pH shifts Ca^{2+} sparks to Ca^{2+} waves in smooth muscle cells of pressurized cerebral arteries. *Am J Physiol Heart Circ Physiol.* 2002; 283(6): H2169-2176.
234. Lamont C, Wier WG. Different roles of ryanodine receptors and inositol (1,4,5)-trisphosphate receptors in adrenergically stimulated contractions of small arteries. *Am J Physiol Heart Circ Physiol.* 2004; 287(2): H617-625.
235. Stewart M, Needham M, Bankhead P, Gardiner TA, Scholfield CN, Curtis TM, McGeown JG. Feedback via Ca^{2+} -activated ion channels modulates endothelin 1 signaling in retinal arteriolar smooth muscle. *Invest Ophthalmol Vis Sci.* 2012; 53(6): 3059-3066.
236. Westcott EB, Goodwin EL, Segal SS, Jackson WF. Function and expression of ryanodine receptors and inositol 1,4,5-trisphosphate receptors in smooth muscle cells of murine feed arteries and arterioles. *J Physiol.* 2012; 590(8): 1849-1869.
237. Mufti RE, Brett SE, Tran CH, Abd El-Rahman R, Anfinogenova Y, El-Yazbi A, Cole WC, Jones PP, Chen SR, Welsh DG. Intravascular pressure augments cerebral arterial constriction by inducing voltage-insensitive Ca^{2+} waves. *J Physiol.* 2010; 588(Pt 20): 3983-4005.
238. Intaglietta M. Arteriolar vasomotion: implications for tissue ischemia. *Blood Vessels.* 1991; 28 Suppl 1: 1-7.
239. Griffith TM. Temporal chaos in the microcirculation. *Cardiovasc Res.* 1996; 31(3): 342-358.

240. Catterall WA. Voltage-gated calcium channels. *Cold Spring Harb Perspect Biol.* 2011; 3(8): a003947.
241. Harraz OF, Welsh DG. T-type Ca²⁺ channels in cerebral arteries: approaches, hypotheses, and speculation. *Microcirculation.* 2013; 20(4): 299-306.
242. Carbone E, Lux HD. A low voltage-activated, fully inactivating Ca channel in vertebrate sensory neurones. *Nature.* 1984; 310(5977): 501-502.
243. Boll W, Lux HD. Action of organic antagonists on neuronal calcium currents. *Neurosci Lett.* 1985; 56(3): 335-339.
244. Zamponi GW, Striessnig J, Koschak A, Dolphin AC. The physiology, pathology, and pharmacology of voltage-gated calcium channels and their future therapeutic potential. *Pharmacol Rev.* 2015; 67(4): 821-870.
245. Lipkind GM, Fozzard HA. Modeling of the outer vestibule and selectivity filter of the L-type Ca²⁺ channel. *Biochemistry.* 2001; 40(23): 6786-6794.
246. Zhu J, Qiu H, Guo W. Probing ion binding in the selectivity filter of the Ca_v1.1 channel with molecular dynamics. *Biophys J.* 2023; 122(3): 496-505.
247. Tuluc P, Yarov-Yarovoy V, Benedetti B, Flucher BE. Molecular interactions in the voltage sensor controlling gating properties of Cav calcium channels. *Structure.* 2016; 24(2): 261-271.
248. Bezanilla F. The voltage sensor in voltage-dependent ion channels. *Physiol Rev.* 2000; 80(2): 555-592.
249. Fernández-Quintero ML, El Ghaleb Y, Tuluc P, Campiglio M, Liedl KR, Flucher BE. Structural determinants of voltage-gating properties in calcium channels. *Elife.* 2021; 10.
250. Pantazis A, Savalli N, Sigg D, Neely A, Olcese R. Functional heterogeneity of the four voltage sensors of a human L-type calcium channel. *Proc Natl Acad Sci U S A.* 2014; 111(51): 18381-18386.
251. Catterall WA, Perez-Reyes E, Snutch TP, Striessnig J. International Union of Pharmacology. XLVIII. Nomenclature and structure-function relationships of voltage-gated calcium channels. *Pharmacol Rev.* 2005; 57(4): 411-425.
252. Perez-Reyes E, Schneider T. Molecular biology of calcium channels. *Kidney Int.* 1995; 48(4): 1111-1124.
253. Servili E, Trus M, Maayan D, Atlas D. β-Subunit of the voltage-gated Ca²⁺ channel Cav1.2 drives signaling to the nucleus via H-Ras. *Proc Natl Acad Sci U S A.* 2018; 115(37): E8624-e8633.
254. Pragnell M, De Waard M, Mori Y, Tanabe T, Snutch TP, Campbell KP. Calcium channel β-subunit binds to a conserved motif in the I-II cytoplasmic linker of the α₁-subunit. *Nature.* 1994; 368(6466): 67-70.
255. Dolphin AC. β subunits of voltage-gated calcium channels. *J Bioenerg Biomembr.* 2003; 35(6): 599-620.
256. Hofmann F, Flockerzi V, Kahl S, Wegener JW. L-type Cav1.2 calcium channels: from in vitro findings to in vivo function. *Physiol Rev.* 2014; 94(1): 303-326.
257. Davies A, Kadurin I, Alvarez-Laviada A, Douglas L, Nieto-Rostro M, Bauer CS, Pratt WS, Dolphin AC. The α_{2δ} subunits of voltage-gated calcium channels form GPI-anchored proteins, a posttranslational modification essential for function. *Proc Natl Acad Sci U S A.* 2010; 107(4): 1654-1659.
258. Chen Y, Wu Q, Jin Z, Qin Y, Meng F, Zhao G. Review of voltage-gated calcium channel α_{2δ} subunit ligands for the treatment of chronic neuropathic pain and insight into

- structure-activity relationship (SAR) by pharmacophore modeling. *Curr Med Chem*. 2022; 29(30): 5097-5112.
259. Gong HC, Hang J, Kohler W, Li L, Su TZ. Tissue-specific expression and gabapentin-binding properties of calcium channel $\alpha_2\delta$ subunit subtypes. *J Membr Biol*. 2001; 184(1): 35-43.
 260. Jay SD, Ellis SB, McCue AF, Williams ME, Vedvick TS, Harpold MM, Campbell KP. Primary structure of the γ subunit of the DHP-sensitive calcium channel from skeletal muscle. *Science*. 1990; 248(4954): 490-492.
 261. Cheng X, Liu J, Asuncion-Chin M, Blaskova E, Bannister JP, Dopico AM, Jaggar JH. A novel Cav1.2 N terminus expressed in smooth muscle cells of resistance size arteries modifies channel regulation by auxiliary subunits. *J Biol Chem*. 2007; 282(40): 29211-29221.
 262. Bannister JP, Thomas-Gatewood CM, Neeb ZP, Adebisi A, Cheng X, Jaggar JH. Cav1.2 channel N-terminal splice variants modulate functional surface expression in resistance size artery smooth muscle cells. *J Biol Chem*. 2011; 286(17): 15058-15066.
 263. Bartels P, Yu D, Huang H, Hu Z, Herzig S, Soong TW. Alternative splicing at N terminus and domain I modulates Cav1.2 inactivation and surface expression. *Biophys J*. 2018; 114(9): 2095-2106.
 264. Tang ZZ, Hong X, Wang J, Soong TW. Signature combinatorial splicing profiles of rat cardiac- and smooth-muscle Cav1.2 channels with distinct biophysical properties. *Cell Calcium*. 2007; 41(5): 417-428.
 265. Smirnov SV, Aaronson PI. Ca^{2+} currents in single myocytes from human mesenteric arteries: evidence for a physiological role of L-type channels. *J Physiol*. 1992; 457: 455-475.
 266. Morel N, Buryi V, Feron O, Gomez JP, Christen MO, Godfraind T. The action of calcium channel blockers on recombinant L-type calcium channel α_1 -subunits. *Br J Pharmacol*. 1998; 125(5): 1005-1012.
 267. Moosmang S, Schulla V, Welling A, Feil R, Feil S, Wegener JW, Hofmann F, Klugbauer N. Dominant role of smooth muscle L-type calcium channel Cav1.2 for blood pressure regulation. *Embo j*. 2003; 22(22): 6027-6034.
 268. Hirehallur SD, Haworth ST, Leming JT, Chang J, Hernandez G, Gordon JB, Rusch NJ. Upregulation of vascular calcium channels in neonatal piglets with hypoxia-induced pulmonary hypertension. *Am J Physiol Lung Cell Mol Physiol*. 2008; 295(5): L915-924.
 269. Kharade SV, Sonkusare SK, Srivastava AK, Thakali KM, Fletcher TW, Rhee SW, Rusch NJ. The β_3 subunit contributes to vascular calcium channel upregulation and hypertension in angiotensin II-infused C57BL/6 mice. *Hypertension*. 2013; 61(1): 137-142.
 270. Pesic A, Madden JA, Pesic M, Rusch NJ. High blood pressure upregulates arterial L-type Ca^{2+} channels: is membrane depolarization the signal? *Circ Res*. 2004; 94(10): e97-104.
 271. Pratt PF, Bonnet S, Ludwig LM, Bonnet P, Rusch NJ. Upregulation of L-type Ca^{2+} channels in mesenteric and skeletal arteries of SHR. *Hypertension*. 2002; 40(2): 214-219.
 272. Ruiz-Velasco V, Mayer MB, Inscho EW, Hymel LJ. Modulation of dihydropyridine receptors in vascular smooth muscle cells by membrane potential and cell proliferation. *Eur J Pharmacol*. 1994; 268(3): 311-318.

273. Gustafsson F, Andreassen D, Salomonsson M, Jensen BL, Holstein-Rathlou N. Conducted vasoconstriction in rat mesenteric arterioles: role for dihydropyridine-insensitive Ca^{2+} channels. *Am J Physiol Heart Circ Physiol*. 2001; 280(2): H582-590.
274. Andreassen D, Friis UG, Uhrenholt TR, Jensen BL, Skøtt O, Hansen PB. Coexpression of voltage-dependent calcium channels $\text{Cav}1.2$, $2.1a$, and $2.1b$ in vascular myocytes. *Hypertension*. 2006; 47(4): 735-741.
275. Ball CJ, Wilson DP, Turner SP, Saint DA, Beltrame JF. Heterogeneity of L- and T-channels in the vasculature: rationale for the efficacy of combined L- and T-blockade. *Hypertension*. 2009; 53(4): 654-660.
276. Jensen LJ, Salomonsson M, Jensen BL, Holstein-Rathlou NH. Depolarization-induced calcium influx in rat mesenteric small arterioles is mediated exclusively via mibefradil-sensitive calcium channels. *Br J Pharmacol*. 2004; 142(4): 709-718.
277. Walsh CP, Davies A, Butcher AJ, Dolphin AC, Kitmitto A. Three-dimensional structure of $\text{Cav}3.1$: comparison with the cardiac L-type voltage-gated calcium channel monomer architecture. *J Biol Chem*. 2009; 284(33): 22310-22321.
278. Lacinová L, Klugbauer N. Modulation of gating currents of the $\text{Cav}3.1$ calcium channel by $\alpha_2\delta_{2a}$ and γ_5 subunits. *Arch Biochem Biophys*. 2004; 425(2): 207-213.
279. Arteaga-Tlecuitl R, Sanchez-Sandoval AL, Ramirez-Cordero BE, Rosendo-Pineda MJ, Vaca L, Gomora JC. Increase of $\text{Cav}3$ channel activity induced by HVA β_{1b} -subunit is not mediated by a physical interaction. *BMC Res Notes*. 2018; 11(1): 810.
280. Thompson WR, Majid AS, Czymmek KJ, Ruff AL, García J, Duncan RL, Farach-Carson MC. Association of the $\alpha_2\delta_1$ subunit with $\text{Cav}3.2$ enhances membrane expression and regulates mechanically induced ATP release in MLO-Y4 osteocytes. *J Bone Miner Res*. 2011; 26(9): 2125-2139.
281. Dubel SJ, Altier C, Chaumont S, Lory P, Bourinet E, Nargeot J. Plasma membrane expression of T-type calcium channel α_1 subunits is modulated by high voltage-activated auxiliary subunits. *J Biol Chem*. 2004; 279(28): 29263-29269.
282. Lacinová L, Klugbauer N, Hofmann F. Absence of modulation of the expressed calcium channel α_{1G} subunit by $\alpha_2\delta$ subunits. *J Physiol*. 1999; 516 (Pt 3)(Pt 3): 639-645.
283. Wyatt CN, Page KM, Berrow NS, Brice NL, Dolphin AC. The effect of overexpression of auxiliary Ca^{2+} channel subunits on native Ca^{2+} channel currents in undifferentiated mammalian NG108-15 cells. *J Physiol*. 1998; 510 (Pt 2)(Pt 2): 347-360.
284. Strube C. Absence of regulation of the T-type calcium current by $\text{Cav}1.1$, β_{1a} and γ_1 dihydropyridine receptor subunits in skeletal muscle cells. *Pflugers Arch*. 2008; 455(5): 921-927.
285. Cottrell GS, Soubrane CH, Hounshell JA, Lin H, Owenson V, Rigby M, Cox PJ, Barker BS, Ottolini M, Ince S, Bauer CC, Perez-Reyes E, Patel MK, Stevens EB, Stephens GJ. CACHD1 is an $\alpha_2\delta$ -like protein that modulates $\text{Cav}3$ voltage-gated calcium channel activity. *J Neurosci*. 2018; 38(43): 9186-9201.
286. Jensen LJ, Holstein-Rathlou NH. Is there a role for T-type Ca^{2+} channels in regulation of vasomotor tone in mesenteric arterioles? *Can J Physiol Pharmacol*. 2009; 87(1): 8-20.
287. Harraz OF, Visser F, Brett SE, Goldman D, Zechariah A, Hashad AM, Menon BK, Watson T, Starreveld Y, Welsh DG. $\text{Cav}1.2/\text{Cav}3.x$ channels mediate divergent vasomotor responses in human cerebral arteries. *J Gen Physiol*. 2015; 145(5): 405-418.
288. Björling K, Morita H, Olsen MF, Prodan A, Hansen PB, Lory P, Holstein-Rathlou NH, Jensen LJ. Myogenic tone is impaired at low arterial pressure in mice deficient in the

- low-voltage-activated Cav3.1 T-type Ca²⁺ channel. *Acta Physiol (Oxf)*. 2013; 207(4): 709-720.
289. Mikkelsen MF, Björling K, Jensen LJ. Age-dependent impact of Cav3.2 T-type calcium channel deletion on myogenic tone and flow-mediated vasodilatation in small arteries. *J Physiol*. 2016; 594(20): 5881-5898.
290. Harraz OF, Brett SE, Zechariah A, Romero M, Puglisi JL, Wilson SM, Welsh DG. Genetic ablation of Cav3.2 channels enhances the arterial myogenic response by modulating the RyR-BK_{Ca} axis. *Arterioscler Thromb Vasc Biol*. 2015; 35(8): 1843-1851.
291. Harraz OF, Welsh DG. Protein kinase A regulation of T-type Ca²⁺ channels in rat cerebral arterial smooth muscle. *J Cell Sci*. 2013; 126(Pt 13): 2944-2954.
292. Lee TS, Kaku T, Takebayashi S, Uchino T, Miyamoto S, Hadama T, Perez-Reyes E, Ono K. Actions of mibefradil, efonidipine and nifedipine block of recombinant T- and L-type Ca²⁺ channels with distinct inhibitory mechanisms. *Pharmacology*. 2006; 78(1): 11-20.
293. Akaike N, Kanaide H, Kuga T, Nakamura M, Sadoshima J, Tomoike H. Low-voltage-activated calcium current in rat aorta smooth muscle cells in primary culture. *J Physiol*. 1989; 416: 141-160.
294. Wang D, Neupane P, Ragnarsson L, Capon RJ, Lewis RJ. Diindolylmethane derivatives: new selective blockers for T-type calcium channels. *Membranes (Basel)*. 2022; 12(8).
295. Earley S, Brayden JE. Transient receptor potential channels in the vasculature. *Physiol Rev*. 2015; 95(2): 645-690.
296. Samanta A, Hughes TET, Moiseenkova-Bell VY. Transient Receptor Potential (TRP) Channels in *Membrane Protein Complexes: Structure and Function*. (eds Harris JR, Boekema EJ) Ch. 6, 141-165 (Springer Singapore, 2018).
297. Yildirim E, Dietrich A, Birnbaumer L. The mouse C-type transient receptor potential 2 (TRPC2) channel: alternative splicing and calmodulin binding to its N terminus. *Proc Natl Acad Sci U S A*. 2003; 100(5): 2220-2225.
298. Liao M, Cao E, Julius D, Cheng Y. Structure of the TRPV1 ion channel determined by electron cryo-microscopy. *Nature*. 2013; 504(7478): 107-112.
299. Singh AK, McGoldrick LL, Saotome K, Sobolevsky AI. X-ray crystallography of TRP channels. *Channels (Austin)*. 2018; 12(1): 137-152.
300. Yue Z, Xie J, Yu AS, Stock J, Du J, Yue L. Role of TRP channels in the cardiovascular system. *Am J Physiol Heart Circ Physiol*. 2015; 308(3): H157-182.
301. Hofmann T, Chubanov V, Gudermann T, Montell C. TRPM5 is a voltage-modulated and Ca²⁺-activated monovalent selective cation channel. *Curr Biol*. 2003; 13(13): 1153-1158.
302. Nilius B, Prenen J, Droogmans G, Voets T, Vennekens R, Freichel M, Wissenbach U, Flockerzi V. Voltage dependence of the Ca²⁺-activated cation channel TRPM4. *J Biol Chem*. 2003; 278(33): 30813-30820.
303. Matta JA, Ahern GP. Voltage is a partial activator of rat thermosensitive TRP channels. *J Physiol*. 2007; 585(Pt 2): 469-482.
304. Brauchi S, Orio P. Voltage sensing in thermo-TRP channels. *Adv Exp Med Biol*. 2011; 704: 517-530.
305. Seebohm G, Schreiber JA. Beyond hot and spicy: TRPV channels and their pharmacological modulation. *Cell Physiol Biochem*. 2021; 55(S3): 108-130.
306. Nilius B, Talavera K, Owsianik G, Prenen J, Droogmans G, Voets T. Gating of TRP channels: a voltage connection? *J Physiol*. 2005; 567(Pt 1): 35-44.

307. Montell C, Rubin GM. Molecular characterization of the *Drosophila* *trp* locus: a putative integral membrane protein required for phototransduction. *Neuron*. 1989; 2(4): 1313-1323.
308. Nadezhdin KD, Talyzina IA, Parthasarathy A, Neuberger A, Zhang DX, Sobolevsky AI. Structure of human TRPV4 in complex with GTPase RhoA. *Nature Communications*. 2023; 14(1): 3733.
309. Deng Z, Paknejad N, Maksaev G, Sala-Rabanal M, Nichols CG, Hite RK, Yuan P. Cryo-EM and X-ray structures of TRPV4 reveal insight into ion permeation and gating mechanisms. *Nat Struct Mol Biol*. 2018; 25(3): 252-260.
310. Saotome K, Singh AK, Yelshanskaya MV, Sobolevsky AI. Crystal structure of the epithelial calcium channel TRPV6. *Nature*. 2016; 534(7608): 506-511.
311. Valente P, García-Sanz N, Gomis A, Fernández-Carvajal A, Fernández-Ballester G, Viana F, Belmonte C, Ferrer-Montiel A. Identification of molecular determinants of channel gating in the transient receptor potential box of vanilloid receptor I. *Faseb j*. 2008; 22(9): 3298-3309.
312. Garcia-Elias A, Berna-Erro A, Rubio-Moscardo F, Pardo-Pastor C, Mrkonjić S, Sepúlveda RV, Vicente R, González-Nilo F, Valverde MA. Interaction between the Linker, Pre-S1, and TRP Domains Determines Folding, Assembly, and Trafficking of TRPV Channels. *Structure*. 2015; 23(8): 1404-1413.
313. Gregorio-Teruel L, Valente P, González-Ros JM, Fernández-Ballester G, Ferrer-Montiel A. Mutation of I696 and W697 in the TRP box of vanilloid receptor subtype I modulates allosteric channel activation. *J Gen Physiol*. 2014; 143(3): 361-375.
314. Tykocki NR, Boerman EM, Jackson WF. Smooth muscle ion channels and regulation of vascular tone in resistance arteries and arterioles. *Compr Physiol*. 2017; 7(2): 485-581.
315. Chen X, Yang D, Ma S, He H, Luo Z, Feng X, Cao T, Ma L, Yan Z, Liu D, Tepel M, Zhu Z. Increased rhythmicity in hypertensive arterial smooth muscle is linked to transient receptor potential canonical channels. *J Cell Mol Med*. 2010; 14(10): 2483-2494.
316. Dietrich A, Chubanov V, Kalwa H, Rost BR, Gudermann T. Cation channels of the transient receptor potential superfamily: their role in physiological and pathophysiological processes of smooth muscle cells. *Pharmacol Ther*. 2006; 112(3): 744-760.
317. Strübing C, Krapivinsky G, Krapivinsky L, Clapham DE. Formation of novel TRPC channels by complex subunit interactions in embryonic brain. *J Biol Chem*. 2003; 278(40): 39014-39019.
318. Strübing C, Krapivinsky G, Krapivinsky L, Clapham DE. TRPC1 and TRPC5 form a novel cation channel in mammalian brain. *Neuron*. 2001; 29(3): 645-655.
319. Ma X, Cheng KT, Wong CO, O'Neil RG, Birnbaumer L, Ambudkar IS, Yao X. Heteromeric TRPV4-C1 channels contribute to store-operated Ca²⁺ entry in vascular endothelial cells. *Cell Calcium*. 2011; 50(6): 502-509.
320. Hofmann T, Obukhov AG, Schaefer M, Harteneck C, Gudermann T, Schultz G. Direct activation of human TRPC6 and TRPC3 channels by diacylglycerol. *Nature*. 1999; 397(6716): 259-263.
321. Fan C, Choi W, Sun W, Du J, Lü W. Structure of the human lipid-gated cation channel TRPC3. *Elife*. 2018; 7.

322. Erkan-Candag H, Clarke A, Tiapko O, Gsell MA, Stockner T, Groschner K. Diacylglycerols interact with the L2 lipidation site in TRPC3 to induce a sensitized channel state. *EMBO Rep.* 2022; 23(7): e54276.
323. Erkan-Candag H, Krivic D, Gsell MAF, Aleksanyan M, Stockner T, Dimova R, Tiapko O, Groschner K. Characterization of DAG binding to TRPC channels by target-dependent cis-trans isomerization of OptoDARg. *Biomolecules.* 2022; 12(6).
324. Kanki H, Kinoshita M, Akaike A, Satoh M, Mori Y, Kaneko S. Activation of inositol 1,4,5-trisphosphate receptor is essential for the opening of mouse TRP5 channels. *Mol Pharmacol.* 2001; 60(5): 989-998.
325. Schaefer M, Plant TD, Obukhov AG, Hofmann T, Gudermann T, Schultz G. Receptor-mediated regulation of the nonselective cation channels TRPC4 and TRPC5. *J Biol Chem.* 2000; 275(23): 17517-17526.
326. Tang J, Lin Y, Zhang Z, Tikunova S, Birnbaumer L, Zhu MX. Identification of common binding sites for calmodulin and inositol 1,4,5-trisphosphate receptors on the carboxyl termini of trp channels. *J Biol Chem.* 2001; 276(24): 21303-21310.
327. Xi Q, Adebisi A, Zhao G, Chapman KE, Waters CM, Hassid A, Jaggar JH. IP₃ constricts cerebral arteries via IP₃ receptor-mediated TRPC3 channel activation and independently of sarcoplasmic reticulum Ca²⁺ release. *Circ Res.* 2008; 102(9): 1118-1126.
328. Adebisi A, Zhao G, Narayanan D, Thomas-Gatewood CM, Bannister JP, Jaggar JH. Isoform-selective physical coupling of TRPC3 channels to IP₃ receptors in smooth muscle cells regulates arterial contractility. *Circ Res.* 2010; 106(10): 1603-1612.
329. Adebisi A, Thomas-Gatewood CM, Leo MD, Kidd MW, Neeb ZP, Jaggar JH. An elevation in physical coupling of type 1 inositol 1,4,5-trisphosphate (IP₃) receptors to transient receptor potential 3 (TRPC3) channels constricts mesenteric arteries in genetic hypertension. *Hypertension.* 2012; 60(5): 1213-1219.
330. Hartmann J, Dragicevic E, Adelsberger H, Henning HA, Sumser M, Abramowitz J, Blum R, Dietrich A, Freichel M, Flockerzi V, Birnbaumer L, Konnerth A. TRPC3 channels are required for synaptic transmission and motor coordination. *Neuron.* 2008; 59(3): 392-398.
331. Spassova MA, Hewavitharana T, Xu W, Soboloff J, Gill DL. A common mechanism underlies stretch activation and receptor activation of TRPC6 channels. *Proc Natl Acad Sci U S A.* 2006; 103(44): 16586-16591.
332. Welsh DG, Morielli AD, Nelson MT, Brayden JE. Transient receptor potential channels regulate myogenic tone of resistance arteries. *Circ Res.* 2002; 90(3): 248-250.
333. Yang XR, Lin MJ, McIntosh LS, Sham JS. Functional expression of transient receptor potential melastatin- and vanilloid-related channels in pulmonary arterial and aortic smooth muscle. *Am J Physiol Lung Cell Mol Physiol.* 2006; 290(6): L1267-1276.
334. Zhang Q, Cao Y, Luo Q, Wang P, Shi P, Song C, E M, Ren J, Fu B, Sun H. The transient receptor potential vanilloid-3 regulates hypoxia-mediated pulmonary artery smooth muscle cells proliferation via PI3K/AKT signaling pathway. *Cell Prolif.* 2018; 51(3): e12436.
335. Voets T, Prenen J, Vriens J, Watanabe H, Janssens A, Wissenbach U, Bödding M, Droogmans G, Nilius B. Molecular determinants of permeation through the cation channel TRPV4. *J Biol Chem.* 2002; 277(37): 33704-33710.

336. Mercado J, Baylie R, Navedo MF, Yuan C, Scott JD, Nelson MT, Brayden JE, Santana LF. Local control of TRPV4 channels by AKAP150-targeted PKC in arterial smooth muscle. *J Gen Physiol.* 2014; 143(5): 559-575.
337. Tajada S, Moreno CM, O'Dwyer S, Woods S, Sato D, Navedo MF, Santana LF. Distance constraints on activation of TRPV4 channels by AKAP150-bound PKC α in arterial myocytes. *J Gen Physiol.* 2017; 149(6): 639-659.
338. Chen YL, Daneva Z, Kuppusamy M, Ottolini M, Baker TM, Klimentova E, Shah SA, Sokolowski JD, Park MS, Sonkusare SK. Novel smooth muscle Ca²⁺-signaling nanodomains in blood pressure regulation. *Circulation.* 2022; 146(7): 548-564.
339. Zholos A, Johnson C, Burdyga T, Melanaphy D. TRPM channels in the vasculature. *Adv Exp Med Biol.* 2011; 704: 707-729.
340. Earley S. TRPM4 channels in smooth muscle function. *Pflugers Arch.* 2013; 465(9): 1223-1231.
341. Earley S, Waldron BJ, Brayden JE. Critical role for transient receptor potential channel TRPM4 in myogenic constriction of cerebral arteries. *Circ Res.* 2004; 95(9): 922-929.
342. Gonzales AL, Yang Y, Sullivan MN, Sanders L, Dabertrand F, Hill-Eubanks DC, Nelson MT, Earley S. A PLC γ 1-dependent, force-sensitive signaling network in the myogenic constriction of cerebral arteries. *Sci Signal.* 2014; 7(327): ra49.
343. Xiong S, Wang B, Lin S, Zhang H, Li Y, Wei X, Cui Y, Wei X, Lu Z, Gao P, Li L, Zhao Z, Liu D, Zhu Z. Activation of transient receptor potential melastatin subtype 8 attenuates cold-induced hypertension through ameliorating vascular mitochondrial dysfunction. *J Am Heart Assoc.* 2017; 6(8).
344. Johnson CD, Melanaphy D, Purse A, Stokesberry SA, Dickson P, Zholos AV. Transient receptor potential melastatin 8 channel involvement in the regulation of vascular tone. *Am J Physiol Heart Circ Physiol.* 2009; 296(6): H1868-1877.
345. Melanaphy D, Johnson CD, Kustov MV, Watson CA, Borysova L, Burdyga TV, Zholos AV. Ion channel mechanisms of rat tail artery contraction-relaxation by menthol involving, respectively, TRPM8 activation and L-type Ca²⁺ channel inhibition. *Am J Physiol Heart Circ Physiol.* 2016; 311(6): H1416-h1430.
346. Sun J, Yang T, Wang P, Ma S, Zhu Z, Pu Y, Li L, Zhao Y, Xiong S, Liu D, Zhu Z. Activation of cold-sensing transient receptor potential melastatin subtype 8 antagonizes vasoconstriction and hypertension through attenuating RhoA/Rho kinase pathway. *Hypertension.* 2014; 63(6): 1354-1363.
347. Silva DF, Wenceslau CF, McCarthy CG, Szasz T, Ogbi S, Webb RC. TRPM8 channel activation triggers relaxation of pudendal artery with increased sensitivity in the hypertensive rats. *Pharmacol Res.* 2019; 147: 104329.
348. Fedinec AL, Liu J, Zhang R, Harsono M, Pourcyrous M, Parfenova H. The cold receptor TRPM8 activation leads to attenuation of endothelium-dependent cerebral vascular functions during head cooling. *J Cereb Blood Flow Metab.* 2021; 41(11): 2897-2906.
349. Huang F, Ni M, Zhang JM, Li DJ, Shen FM. TRPM8 downregulation by angiotensin II in vascular smooth muscle cells is involved in hypertension. *Mol Med Rep.* 2017; 15(4): 1900-1908.
350. Ralevic V, Dunn WR. Purinergic transmission in blood vessels. *Auton Neurosci.* 2015; 191: 48-66.
351. Burnstock G, Ralevic V. Purinergic signaling and blood vessels in health and disease. *Pharmacol Rev.* 2014; 66(1): 102-192.

352. Mitchell C, Syed NI, Tengah A, Gurney AM, Kennedy C. Identification of contractile P2Y1, P2Y6, and P2Y12 receptors in rat intrapulmonary artery using selective ligands. *J Pharmacol Exp Ther*. 2012; 343(3): 755-762.
353. Wilson C, Dryer SE. A mutation in TRPC6 channels abolishes their activation by hypoosmotic stretch but does not affect activation by diacylglycerol or G protein signaling cascades. *Am J Physiol Renal Physiol*. 2014; 306(9): F1018-1025.
354. North RA. Molecular physiology of P2X receptors. *Physiol Rev*. 2002; 82(4): 1013-1067.
355. Kawate T, Michel JC, Birdsong WT, Gouaux E. Crystal structure of the ATP-gated P2X(4) ion channel in the closed state. *Nature*. 2009; 460(7255): 592-598.
356. Li M, Kawate T, Silberberg SD, Swartz KJ. Pore-opening mechanism in trimeric P2X receptor channels. *Nat Commun*. 2010; 1(4): 44.
357. Gitterman DP, Evans RJ. Properties of P2X and P2Y receptors are dependent on artery diameter in the rat mesenteric bed. *Br J Pharmacol*. 2000; 131(8): 1561-1568.
358. Harhun MI, Sukhanova K, Gordienko D, Dyskina Y. Molecular identification of P2X receptors in vascular smooth muscle cells from rat anterior, posterior, and basilar arteries. *Pharmacol Rep*. 2015; 67(6): 1055-1060.
359. Phillips JK, Hill CE. Neuroreceptor mRNA expression in the rat mesenteric artery develops independently of innervation. *Int J Dev Neurosci*. 1999; 17(4): 377-386.
360. Nichols CM, Povstyan OV, Albert AP, Gordienko DV, Khan O, Vasilikostas G, Khong TK, Wan A, Reddy M, Harhun MI. Vascular smooth muscle cells from small human omental arteries express P2X1 and P2X4 receptor subunits. *Purinergic Signal*. 2014; 10(4): 565-572.
361. Valdecantos P, Briones R, Moya P, Germain A, Huidobro-Toro JP. Pharmacological identification of P2X₁, P2X₄ and P2X₇ nucleotide receptors in the smooth muscles of human umbilical cord and chorionic blood vessels. *Placenta*. 2003; 24(1): 17-26.
362. Lewis CJ, Evans RJ. P2X receptor immunoreactivity in different arteries from the femoral, pulmonary, cerebral, coronary and renal circulations. *J Vasc Res*. 2001; 38(4): 332-340.
363. Nicke A, Kerschensteiner D, Soto F. Biochemical and functional evidence for heteromeric assembly of P2X1 and P2X4 subunits. *J Neurochem*. 2005; 92(4): 925-933.
364. Harhun MI, Povstyan OV, Albert AP, Nichols CM. ATP-evoked sustained vasoconstrictions mediated by heteromeric P2X1/4 receptors in cerebral arteries. *Stroke*. 2014; 45(8): 2444-2450.
365. Sukhanova KY, Harhun MI, Bouryi VA, Gordienko DV. Mechanisms of [Ca²⁺]_i elevation following P2X receptor activation in the guinea-pig small mesenteric artery myocytes. *Pharmacol Rep*. 2013; 65(1): 152-163.
366. Sukhanova KY, Thugorka OM, Bouryi VA, Harhun MI, Gordienko DV. Mechanisms of the sarcoplasmic reticulum Ca²⁺ release induced by P2X receptor activation in mesenteric artery myocytes. *Pharmacol Rep*. 2014; 66(3): 363-372.
367. Sheng Y, Zhu L. The crosstalk between autonomic nervous system and blood vessels. *Int J Physiol Pathophysiol Pharmacol*. 2018; 10(1): 17-28.
368. Burnstock G. The fifth Heymans memorial lecture - Ghent, February 17, 1990. Co-transmission. *Arch Int Pharmacodyn Ther*. 1990; 304: 7-33.
369. Hansen MA, Dutton JL, Balcar VJ, Barden JA, Bennett MR. P_{2X} (purinergic) receptor distributions in rat blood vessels. *J Auton Nerv Syst*. 1999; 75(2-3): 147-155.

370. Rummery NM, Brock JA, Pakdeechote P, Ralevic V, Dunn WR. ATP is the predominant sympathetic neurotransmitter in rat mesenteric arteries at high pressure. *J Physiol*. 2007; 582(Pt 2): 745-754.
371. Osmond DA, Inscho EW. P2X₁ receptor blockade inhibits whole kidney autoregulation of renal blood flow in vivo. *Am J Physiol Renal Physiol*. 2010; 298(6): F1360-1368.
372. Ralevic V, Burnstock G. Postjunctional synergism of noradrenaline and adenosine 5'-triphosphate in the mesenteric arterial bed of the rat. *Eur J Pharmacol*. 1990; 175(3): 291-299.
373. Brock JA, Yeoh M, McLachlan EM. Enhanced neurally evoked responses and inhibition of norepinephrine reuptake in rat mesenteric arteries after spinal transection. *Am J Physiol Heart Circ Physiol*. 2006; 290(1): H398-405.
374. Hoth M, Penner R. Depletion of intracellular calcium stores activates a calcium current in mast cells. *Nature*. 1992; 355(6358): 353-356.
375. Feske S, Gwack Y, Prakriya M, Srikanth S, Puppel SH, Tanasa B, Hogan PG, Lewis RS, Daly M, Rao A. A mutation in Orai1 causes immune deficiency by abrogating CRAC channel function. *Nature*. 2006; 441(7090): 179-185.
376. Zhang SL, Yeromin AV, Zhang XH, Yu Y, Safrina O, Penna A, Roos J, Stauderman KA, Cahalan MD. Genome-wide RNAi screen of Ca²⁺ influx identifies genes that regulate Ca²⁺ release-activated Ca²⁺ channel activity. *Proc Natl Acad Sci U S A*. 2006; 103(24): 9357-9362.
377. Vig M, Peinelt C, Beck A, Koomoa DL, Rabah D, Koblan-Huberson M, Kraft S, Turner H, Fleig A, Penner R, Kinet JP. CRACM1 is a plasma membrane protein essential for store-operated Ca²⁺ entry. *Science*. 2006; 312(5777): 1220-1223.
378. Yeung PS, Yamashita M, Prakriya M. Molecular basis of allosteric Orai1 channel activation by STIM1. *J Physiol*. 2020; 598(9): 1707-1723.
379. Sallinger M, Berlansky S, Frischauf I. Orai channels: key players in Ca²⁺ homeostasis. *Curr Opin Physiol*. 2020; 17: 42-49.
380. Hou X, Pedi L, Diver MM, Long SB. Crystal structure of the calcium release-activated calcium channel Orai. *Science*. 2012; 338(6112): 1308-1313.
381. Yoast RE, Emrich SM, Zhang X, Xin P, Johnson MT, Fike AJ, Walter V, Hempel N, Yule DI, Sneyd J, Gill DL, Trebak M. The native ORAI channel trio underlies the diversity of Ca²⁺ signaling events. *Nat Commun*. 2020; 11(1): 2444.
382. Hou X, Outhwaite IR, Pedi L, Long SB. Cryo-EM structure of the calcium release-activated calcium channel Orai in an open conformation. *Elife*. 2020; 9.
383. Zhang X, Xin P, Yoast RE, Emrich SM, Johnson MT, Pathak T, Benson JC, Azimi I, Gill DL, Monteith GR, Trebak M. Distinct pharmacological profiles of ORAI1, ORAI2, and ORAI3 channels. *Cell Calcium*. 2020; 91: 102281.
384. Baryshnikov SG, Pulina MV, Zulian A, Linde CI, Golovina VA. Orai1, a critical component of store-operated Ca²⁺ entry, is functionally associated with Na⁺/Ca²⁺ exchanger and plasma membrane Ca²⁺ pump in proliferating human arterial myocytes. *Am J Physiol Cell Physiol*. 2009; 297(5): C1103-1112.
385. Fernandez RA, Wan J, Song S, Smith KA, Gu Y, Tauseef M, Tang H, Makino A, Mehta D, Yuan JX. Upregulated expression of STIM2, TRPC6, and Orai2 contributes to the transition of pulmonary arterial smooth muscle cells from a contractile to proliferative phenotype. *Am J Physiol Cell Physiol*. 2015; 308(8): C581-593.

386. Potier M, Gonzalez JC, Motiani RK, Abdullaev IF, Bisailon JM, Singer HA, Trebak M. Evidence for STIM1- and Orai1-dependent store-operated calcium influx through I_{CRAC} in vascular smooth muscle cells: role in proliferation and migration. *Faseb j.* 2009; 23(8): 2425-2437.
387. Li J, McKeown L, Ojelabi O, Stacey M, Foster R, O'Regan D, Porter KE, Beech DJ. Nanomolar potency and selectivity of a Ca²⁺ release-activated Ca²⁺ channel inhibitor against store-operated Ca²⁺ entry and migration of vascular smooth muscle cells. *Br J Pharmacol.* 2011; 164(2): 382-393.
388. Mancarella S, Potireddy S, Wang Y, Gao H, Gandhirajan RK, Autieri M, Scalia R, Cheng Z, Wang H, Madesh M, Houser SR, Gill DL. Targeted STIM deletion impairs calcium homeostasis, NFAT activation, and growth of smooth muscle. *Faseb j.* 2013; 27(3): 893-906.
389. Oritani K, Kincade PW. Identification of stromal cell products that interact with pre-B cells. *J Cell Biol.* 1996; 134(3): 771-782.
390. Williams RT, Manji SS, Parker NJ, Hancock MS, Van Stekelenburg L, Eid JP, Senior PV, Kazenwadel JS, Shandala T, Saint R, Smith PJ, Dziadek MA. Identification and characterization of the STIM (stromal interaction molecule) gene family: coding for a novel class of transmembrane proteins. *Biochem J.* 2001; 357(Pt 3): 673-685.
391. Liou J, Kim ML, Heo WD, Jones JT, Myers JW, Ferrell JE, Jr., Meyer T. STIM is a Ca²⁺ sensor essential for Ca²⁺-store-depletion-triggered Ca²⁺ influx. *Curr Biol.* 2005; 15(13): 1235-1241.
392. Stathopoulos PB, Li GY, Plevin MJ, Ames JB, Ikura M. Stored Ca²⁺ depletion-induced oligomerization of stromal interaction molecule 1 (STIM1) via the EF-SAM region: An initiation mechanism for capacitive Ca²⁺ entry. *J Biol Chem.* 2006; 281(47): 35855-35862.
393. Novello MJ, Zhu J, Feng Q, Ikura M, Stathopoulos PB. Structural elements of stromal interaction molecule function. *Cell Calcium.* 2018; 73: 88-94.
394. Liou J, Fivaz M, Inoue T, Meyer T. Live-cell imaging reveals sequential oligomerization and local plasma membrane targeting of stromal interaction molecule 1 after Ca²⁺ store depletion. *Proc Natl Acad Sci U S A.* 2007; 104(22): 9301-9306.
395. Park CY, Hoover PJ, Mullins FM, Bachhawat P, Covington ED, Raunser S, Walz T, Garcia KC, Dolmetsch RE, Lewis RS. STIM1 clusters and activates CRAC channels via direct binding of a cytosolic domain to Orai1. *Cell.* 2009; 136(5): 876-890.
396. Yuan JP, Zeng W, Dorwart MR, Choi YJ, Worley PF, Muallem S. SOAR and the polybasic STIM1 domains gate and regulate Orai channels. *Nat Cell Biol.* 2009; 11(3): 337-343.
397. Gruszczynska-Biegala J, Pomorski P, Wisniewska MB, Kuznicki J. Differential roles for STIM1 and STIM2 in store-operated calcium entry in rat neurons. *PLoS One.* 2011; 6(4): e19285.
398. Brandman O, Liou J, Park WS, Meyer T. STIM2 is a feedback regulator that stabilizes basal cytosolic and endoplasmic reticulum Ca²⁺ levels. *Cell.* 2007; 131(7): 1327-1339.
399. Song MY, Makino A, Yuan JX. STIM2 contributes to enhanced store-operated Ca²⁺ entry in pulmonary artery smooth muscle cells from patients with idiopathic pulmonary arterial hypertension. *Pulm Circ.* 2011; 1(1): 84-94.

400. Berra-Romani R, Mazzocco-Spezia A, Pulina MV, Golovina VA. Ca²⁺ handling is altered when arterial myocytes progress from a contractile to a proliferative phenotype in culture. *Am J Physiol Cell Physiol*. 2008; 295(3): C779-790.
401. Johnson MT, Gudlur A, Zhang X, Xin P, Emrich SM, Yoast RE, Courjaret R, Nwokonko RM, Li W, Hempel N, Machaca K, Gill DL, Hogan PG, Trebak M. L-type Ca²⁺ channel blockers promote vascular remodeling through activation of STIM proteins. *Proc Natl Acad Sci U S A*. 2020; 117(29): 17369-17380.
402. Trebak M. STIM/Orai signalling complexes in vascular smooth muscle. *J Physiol*. 2012; 590(17): 4201-4208.
403. Ruhle B, Trebak M. Emerging roles for native Orai Ca²⁺ channels in cardiovascular disease. *Curr Top Membr*. 2013; 71: 209-235.
404. Zhang W, Halligan KE, Zhang X, Bisailon JM, Gonzalez-Cobos JC, Motiani RK, Hu G, Vincent PA, Zhou J, Barroso M, Singer HA, Matrougui K, Trebak M. Orai1-mediated I_{CRAC} is essential for neointima formation after vascular injury. *Circ Res*. 2011; 109(5): 534-542.
405. Krishnan V, Ali S, Gonzales AL, Thakore P, Griffin CS, Yamasaki E, Alvarado MG, Johnson MT, Trebak M, Earley S. STIM1-dependent peripheral coupling governs the contractility of vascular smooth muscle cells. *Elife*. 2022; 11.
406. Shuttleworth TJ. Orai Channels in *Studies of Epithelial Transporters and Ion Channels: Ion Channels and Transporters of Epithelia in Health and Disease*. Vol. 3 (eds Hamilton KL, Devor DC) Ch. 26, 1051-1079 (Springer International Publishing, 2020).
407. Mignen O, Thompson JL, Shuttleworth TJ. Both Orai1 and Orai3 are essential components of the arachidonate-regulated Ca²⁺-selective (ARC) channels. *J Physiol*. 2008; 586(1): 185-195.
408. Mignen O, Thompson JL, Shuttleworth TJ. The molecular architecture of the arachidonate-regulated Ca²⁺-selective ARC channel is a pentameric assembly of Orai1 and Orai3 subunits. *J Physiol*. 2009; 587(Pt 17): 4181-4197.
409. Zhang X, Zhang W, González-Cobos JC, Jardin I, Romanin C, Matrougui K, Trebak M. Complex role of STIM1 in the activation of store-independent Orai1/3 channels. *J Gen Physiol*. 2014; 143(3): 345-359.
410. Zhang X, González-Cobos JC, Schindl R, Muik M, Ruhle B, Motiani RK, Bisailon JM, Zhang W, Fahrner M, Barroso M, Matrougui K, Romanin C, Trebak M. Mechanisms of STIM1 activation of store-independent leukotriene C₄-regulated Ca²⁺ channels. *Mol Cell Biol*. 2013; 33(18): 3715-3723.
411. Kasakov L, Ellis J, Kirkpatrick K, Milner P, Burnstock G. Direct evidence for concomitant release of noradrenaline, adenosine 5'-triphosphate and neuropeptide Y from sympathetic nerve supplying the guinea-pig vas deferens. *J Auton Nerv Syst*. 1988; 22(1): 75-82.
412. Racchi H, Irrázabal MJ, Howard M, Morán S, Zalaquett R, Huidobro-Toro JP. Adenosine 5'-triphosphate and neuropeptide Y are co-transmitters in conjunction with noradrenaline in the human saphenous vein. *Br J Pharmacol*. 1999; 126(5): 1175-1185.
413. Donoso MV, Steiner M, Huidobro-Toro JP. BIBP 3226, suramin and prazosin identify neuropeptide Y, adenosine 5'-triphosphate and noradrenaline as sympathetic cotransmitters in the rat arterial mesenteric bed. *J Pharmacol Exp Ther*. 1997; 282(2): 691-698.

414. Zang WJ, Balke CW, Wier WG. Graded α_1 -adrenoceptor activation of arteries involves recruitment of smooth muscle cells to produce 'all or none' Ca^{2+} signals. *Cell Calcium*. 2001; 29(5): 327-334.
415. Wier WG, Zang WJ, Lamont C, Raina H. Sympathetic neurogenic Ca^{2+} signalling in rat arteries: ATP, noradrenaline and neuropeptide Y. *Exp Physiol*. 2009; 94(1): 31-37.
416. Tan CMJ, Green P, Tapoulal N, Lewandowski AJ, Leeson P, Herring N. The role of neuropeptide Y in cardiovascular health and disease. *Front Physiol*. 2018; 9: 1281.
417. Lamont C, Wier WG. Evoked and spontaneous purinergic junctional Ca^{2+} transients (jCaTs) in rat small arteries. *Circ Res*. 2002; 91(6): 454-456.
418. Lamont C, Vainorius E, Wier WG. Purinergic and adrenergic Ca^{2+} transients during neurogenic contractions of rat mesenteric small arteries. *J Physiol*. 2003; 549(Pt 3): 801-808.
419. Lamont C, Vial C, Evans RJ, Wier WG. P2X₁ receptors mediate sympathetic postjunctional Ca^{2+} transients in mesenteric small arteries. *Am J Physiol Heart Circ Physiol*. 2006; 291(6): H3106-3113.
420. Rubart M, Patlak JB, Nelson MT. Ca^{2+} currents in cerebral artery smooth muscle cells of rat at physiological Ca^{2+} concentrations. *J Gen Physiol*. 1996; 107(4): 459-472.
421. Nelson MT, Standen NB, Brayden JE, Worley JF, 3rd. Noradrenaline contracts arteries by activating voltage-dependent calcium channels. *Nature*. 1988; 336(6197): 382-385.
422. Navedo MF, Amberg GC, Votaw VS, Santana LF. Constitutively active L-type Ca^{2+} channels. *Proc Natl Acad Sci U S A*. 2005; 102(31): 11112-11117.
423. Amberg GC, Navedo MF, Nieves-Cintrón M, Molkentin JD, Santana LF. Calcium sparklets regulate local and global calcium in murine arterial smooth muscle. *J Physiol*. 2007; 579(Pt 1): 187-201.
424. Navedo MF, Nieves-Cintrón M, Amberg GC, Yuan C, Votaw VS, Lederer WJ, McKnight GS, Santana LF. AKAP150 is required for stuttering persistent Ca^{2+} sparklets and angiotensin II-induced hypertension. *Circ Res*. 2008; 102(2): e1-e11.
425. Navedo MF, Amberg GC, Nieves M, Molkentin JD, Santana LF. Mechanisms underlying heterogeneous Ca^{2+} sparklet activity in arterial smooth muscle. *J Gen Physiol*. 2006; 127(6): 611-622.
426. Guo Y, Bo T, Zhou X, Gao L, Wang Y, Zhao J. AKAP5 signaling complexes: focal points and functional properties. *Neuro Endocrinol Lett*. 2015; 36(1): 7-14.
427. Navedo MF, Hell JW. AKAP5 keeps L-type channels and NFAT on their toes. *Cell Rep*. 2014; 7(5): 1341-1342.
428. Martín-Aragón Baudel M, Flores-Tamez VA, Hong J, Reddy GR, Maillard P, Burns AE, Man KNM, Sasse KC, Ward SM, Catterall WA, Bers DM, Hell JW, Nieves-Cintrón M, Navedo MF. Spatiotemporal control of vascular Cav1.2 by $\alpha_1\text{C}$ S1928 phosphorylation. *Circ Res*. 2022; 131(12): 1018-1033.
429. Fu Y, Westenbroek RE, Scheuer T, Catterall WA. Phosphorylation sites required for regulation of cardiac calcium channels in the fight-or-flight response. *Proc Natl Acad Sci U S A*. 2013; 110(48): 19621-19626.
430. Oliveria SF, Dell'Acqua ML, Sather WA. AKAP79/150 anchoring of calcineurin controls neuronal L-type Ca^{2+} channel activity and nuclear signaling. *Neuron*. 2007; 55(2): 261-275.

431. Yang L, Liu G, Zakharov SI, Morrow JP, Rybin VO, Steinberg SF, Marx SO. Ser¹⁹²⁸ is a common site for Cav1.2 phosphorylation by protein kinase C isoforms. *J Biol Chem*. 2005; 280(1): 207-214.
432. Ishida Y, Kitayama K, Hanada K, Shibutani S, Nishizaki K, Kinjo T, Endo T, Suzuki A, Tateyama S, Nishizaki F, Sukekawa T, Tanaka M, Osanai T, Okumura K, Tomita H. Diltiazem inhibits coronary spasm via inhibition of Cav1.2 phosphorylation and protein kinase C activation in a mouse model of coronary spastic angina. *Int Heart J*. 2021; 62(4): 910-918.
433. Murphy JG, Sanderson JL, Gorski JA, Scott JD, Catterall WA, Sather WA, Dell'Acqua ML. AKAP-anchored PKA maintains neuronal L-type calcium channel activity and NFAT transcriptional signaling. *Cell Rep*. 2014; 7(5): 1577-1588.
434. Sonkusare SK, Dalsgaard T, Bonev AD, Hill-Eubanks DC, Kotlikoff MI, Scott JD, Santana LF, Nelson MT. AKAP150-dependent cooperative TRPV4 channel gating is central to endothelium-dependent vasodilation and is disrupted in hypertension. *Sci Signal*. 2014; 7(333): ra66.
435. Fan HC, Zhang X, McNaughton PA. Activation of the TRPV4 ion channel is enhanced by phosphorylation. *J Biol Chem*. 2009; 284(41): 27884-27891.
436. Himpens B, Casteels R. Different effects of depolarization and muscarinic stimulation on the Ca²⁺/force relationship during the contraction-relaxation cycle in the guinea pig ileum. *Pflugers Arch*. 1990; 416(1-2): 28-35.
437. Bradley AB, Morgan KG. Alterations in cytoplasmic calcium sensitivity during porcine coronary artery contractions as detected by aequorin. *J Physiol*. 1987; 385: 437-448.
438. DeFeo TT, Morgan KG. Calcium-force relationships as detected with aequorin in two different vascular smooth muscles of the ferret. *J Physiol*. 1985; 369: 269-282.
439. Yang Q, Hori M. Characterization of contractile machinery of vascular smooth muscles in hypertension. *Life (Basel)*. 2021; 11(7).
440. Dimopoulos GJ, Semba S, Kitazawa K, Eto M, Kitazawa T. Ca²⁺-dependent rapid Ca²⁺ sensitization of contraction in arterial smooth muscle. *Circ Res*. 2007; 100(1): 121-129.
441. Somlyo AP, Somlyo AV. Ca²⁺ sensitivity of smooth muscle and nonmuscle myosin II: modulated by G proteins, kinases, and myosin phosphatase. *Physiol Rev*. 2003; 83(4): 1325-1358.
442. Ringvold HC, Khalil RA. Protein kinase C as regulator of vascular smooth muscle function and potential target in vascular disorders. *Adv Pharmacol*. 2017; 78: 203-301.
443. Maruyama Y, Nishida M, Sugimoto Y, Tanabe S, Turner JH, Kozasa T, Wada T, Nagao T, Kurose H. G $\alpha_{12/13}$ mediates α_1 -adrenergic receptor-induced cardiac hypertrophy. *Circ Res*. 2002; 91(10): 961-969.
444. Yang YM, Kuen DS, Chung Y, Kurose H, Kim SG. G $\alpha_{12/13}$ signaling in metabolic diseases. *Exp Mol Med*. 2020; 52(6): 896-910.
445. Siehler S. G $\alpha_{12/13}$ -dependent signaling of G-protein-coupled receptors: disease context and impact on drug discovery. *Expert Opin Drug Discov*. 2007; 2(12): 1591-1604.
446. Riobo NA, Manning DR. Receptors coupled to heterotrimeric G proteins of the G12 family. *Trends Pharmacol Sci*. 2005; 26(3): 146-154.
447. Colicelli J. Human RAS superfamily proteins and related GTPases. *Sci STKE*. 2004; 2004(250): Re13.

448. Hart MJ, Jiang X, Kozasa T, Roscoe W, Singer WD, Gilman AG, Sternweis PC, Bollag G. Direct stimulation of the guanine nucleotide exchange activity of p115 RhoGEF by $G\alpha_{13}$. *Science*. 1998; 280(5372): 2112-2114.
449. Katoh H, Aoki J, Yamaguchi Y, Kitano Y, Ichikawa A, Negishi M. Constitutively active $G\alpha_{12}$, $G\alpha_{13}$, and $G\alpha_q$ induce Rho-dependent neurite retraction through different signaling pathways. *J Biol Chem*. 1998; 273(44): 28700-28707.
450. Majumdar M, Seasholtz TM, Buckmaster C, Toksoz D, Brown JH. A rho exchange factor mediates thrombin and $G\alpha_{12}$ -induced cytoskeletal responses. *J Biol Chem*. 1999; 274(38): 26815-26821.
451. Siehler S. Regulation of RhoGEF proteins by $G_{12/13}$ -coupled receptors. *Br J Pharmacol*. 2009; 158(1): 41-49.
452. Cherfils J, Zeghouf M. Regulation of small GTPases by GEFs, GAPs, and GDIs. *Physiol Rev*. 2013; 93(1): 269-309.
453. Amano M, Nakayama M, Kaibuchi K. Rho-kinase/ROCK: A key regulator of the cytoskeleton and cell polarity. *Cytoskeleton (Hoboken)*. 2010; 67(9): 545-554.
454. Feng J, Ito M, Ichikawa K, Isaka N, Nishikawa M, Hartshorne DJ, Nakano T. Inhibitory phosphorylation site for Rho-associated kinase on smooth muscle myosin phosphatase. *J Biol Chem*. 1999; 274(52): 37385-37390.
455. Khromov A, Choudhury N, Stevenson AS, Somlyo AV, Eto M. Phosphorylation-dependent autoinhibition of myosin light chain phosphatase accounts for Ca^{2+} sensitization force of smooth muscle contraction. *J Biol Chem*. 2009; 284(32): 21569-21579.
456. Niiro N, Koga Y, Ikebe M. Agonist-induced changes in the phosphorylation of the myosin-binding subunit of myosin light chain phosphatase and CPI17, two regulatory factors of myosin light chain phosphatase, in smooth muscle. *Biochem J*. 2003; 369(Pt 1): 117-128.
457. Kitazawa T, Eto M, Woodsome TP, Khalequzzaman M. Phosphorylation of the myosin phosphatase targeting subunit and CPI-17 during Ca^{2+} sensitization in rabbit smooth muscle. *J Physiol*. 2003; 546(Pt 3): 879-889.
458. Kitazawa T, Eto M, Woodsome TP, Brautigam DL. Agonists trigger G protein-mediated activation of the CPI-17 inhibitor phosphoprotein of myosin light chain phosphatase to enhance vascular smooth muscle contractility. *J Biol Chem*. 2000; 275(14): 9897-9900.
459. Kitazawa T, Kitazawa K. Size-dependent heterogeneity of contractile Ca^{2+} sensitization in rat arterial smooth muscle. *J Physiol*. 2012; 590(21): 5401-5423.
460. Murtada SI, Humphrey JD. Regional heterogeneity in the regulation of vasoconstriction in arteries and its role in vascular mechanics. *Adv Exp Med Biol*. 2018; 1097: 105-128.
461. Ratz PH, Berg KM, Urban NH, Miner AS. Regulation of smooth muscle calcium sensitivity: KCl as a calcium-sensitizing stimulus. *Am J Physiol Cell Physiol*. 2005; 288(4): C769-783.
462. Sakurada S, Takuwa N, Sugimoto N, Wang Y, Seto M, Sasaki Y, Takuwa Y. Ca^{2+} -dependent activation of Rho and Rho kinase in membrane depolarization-induced and receptor stimulation-induced vascular smooth muscle contraction. *Circ Res*. 2003; 93(6): 548-556.
463. Klemke RL, Cai S, Giannini AL, Gallagher PJ, de Lanerolle P, Cheresch DA. Regulation of cell motility by mitogen-activated protein kinase. *J Cell Biol*. 1997; 137(2): 481-492.

464. Moreno-Domínguez A, Colinas O, El-Yazbi A, Walsh EJ, Hill MA, Walsh MP, Cole WC. Ca²⁺ sensitization due to myosin light chain phosphatase inhibition and cytoskeletal reorganization in the myogenic response of skeletal muscle resistance arteries. *J Physiol.* 2013; 591(5): 1235-1250.
465. El-Yazbi AF, Abd-Elrahman KS. ROK and arteriolar myogenic tone generation: molecular evidence in health and disease. *Front Pharmacol.* 2017; 8: 87.
466. Lagaud G, Gaudreault N, Moore ED, Van Breemen C, Laher I. Pressure-dependent myogenic constriction of cerebral arteries occurs independently of voltage-dependent activation. *Am J Physiol Heart Circ Physiol.* 2002; 283(6): H2187-2195.
467. Behuliak M, Pintérová M, Bencze M, Petrová M, Líšková S, Karen P, Kuneš J, Vaněčková I, Zicha J. Ca²⁺ sensitization and Ca²⁺ entry in the control of blood pressure and adrenergic vasoconstriction in conscious Wistar-Kyoto and spontaneously hypertensive rats. *J Hypertens.* 2013; 31(10): 2025-2035.
468. Zicha J, Behuliak M, Pintérová M, Bencze M, Kuneš J, Vaněčková I. The interaction of calcium entry and calcium sensitization in the control of vascular tone and blood pressure of normotensive and hypertensive rats. *Physiol Res.* 2014; 63(Suppl 1): S19-27.
469. Wei X, Lan T, Zhou Y, Cheng J, Li P, Zeng X, Yang Y. Mechanism of α 1-adrenergic receptor-induced increased contraction of rat mesenteric artery in aging hypertension rats. *Gerontology.* 2021; 67(3): 323-337.
470. Behuliak M, Bencze M, Vaněčková I, Kuneš J, Zicha J. Basal and activated calcium sensitization mediated by RhoA/Rho kinase pathway in rats with genetic and salt hypertension. *Biomed Res Int.* 2017; 2017: 8029728.
471. Heaps CL, Bray JF, Parker JL. Enhanced KCl-mediated contractility and Ca²⁺ sensitization in porcine collateral-dependent coronary arteries persist after exercise training. *Am J Physiol Heart Circ Physiol.* 2020; 319(4): H915-h926.
472. Liou YM, Morgan KG. Redistribution of protein kinase C isoforms in association with vascular hypertrophy of rat aorta. *Am J Physiol.* 1994; 267(4 Pt 1): C980-989.
473. Elkhatib MAW, Mroueh A, Rafeh RW, Sleiman F, Fouad H, Saad EI, Fouda MA, Elgaddar O, Issa K, Eid AH, Eid AA, Abd-Elrahman KS, El-Yazbi AF. Amelioration of perivascular adipose inflammation reverses vascular dysfunction in a model of nonobese prediabetic metabolic challenge: potential role of antidiabetic drugs. *Transl Res.* 2019; 214: 121-143.
474. Bayliss WM. On the local reactions of the arterial wall to changes of internal pressure. *J Physiol.* 1902; 28(3): 220-231.
475. Davis MJ, Hill MA. Signaling mechanisms underlying the vascular myogenic response. *Physiol Rev.* 1999; 79(2): 387-423.
476. Davis MJ. Perspective: physiological role(s) of the vascular myogenic response. *Microcirculation.* 2012; 19(2): 99-114.
477. Loutzenhisser R, Bidani A, Chilton L. Renal myogenic response: kinetic attributes and physiological role. *Circ Res.* 2002; 90(12): 1316-1324.
478. Davis MJ. Myogenic response gradient in an arteriolar network. *Am J Physiol.* 1993; 264(6 Pt 2): H2168-2179.
479. Harder DR. Pressure-dependent membrane depolarization in cat middle cerebral artery. *Circ Res.* 1984; 55(2): 197-202.
480. Osol G, Halpern W. Myogenic properties of cerebral blood vessels from normotensive and hypertensive rats. *Am J Physiol.* 1985; 249(5 Pt 2): H914-921.

481. Jackson PA, Duling BR. Myogenic response and wall mechanics of arterioles. *Am J Physiol*. 1989; 257(4 Pt 2): H1147-1155.
482. Kuo L, Davis MJ, Chilian WM. Myogenic activity in isolated subepicardial and subendocardial coronary arterioles. *Am J Physiol*. 1988; 255(6 Pt 2): H1558-1562.
483. Hu XQ, Xiao D, Zhu R, Huang X, Yang S, Wilson SM, Zhang L. Chronic hypoxia suppresses pregnancy-induced upregulation of large-conductance Ca^{2+} -activated K^{+} channel activity in uterine arteries. *Hypertension*. 2012; 60(1): 214-222.
484. Sabe SA, Kononov MA, Bellam KG, Sodha N, Ehsan A, Jackson WF, Feng J, Sellke FW. Poorly controlled hypertension is associated with increased coronary myogenic tone in patients undergoing cardiac surgery with cardiopulmonary bypass. *J Thorac Cardiovasc Surg*. 2023; 165(6): e256-e267.
485. Hayashi K, Epstein M, Saruta T. Altered myogenic responsiveness of the renal microvasculature in experimental hypertension. *J Hypertens*. 1996; 14(12): 1387-1401.
486. Sauv e M, Hui SK, Dinh DD, Foltz WD, Momen A, Nedospasov SA, Offermanns S, Husain M, Kroetsch JT, Lidington D, Bolz SS. Tumor necrosis factor/sphingosine-1-phosphate signaling augments resistance artery myogenic tone in diabetes. *Diabetes*. 2016; 65(7): 1916-1928.
487. Belik J. The myogenic response of arterial vessels is increased in fetal pulmonary hypertension. *Pediatr Res*. 1995; 37(2): 196-201.
488. Haddock RE, Grayson TH, Morris MJ, Howitt L, Chadha PS, Sandow SL. Diet-induced obesity impairs endothelium-derived hyperpolarization via altered potassium channel signaling mechanisms. *PLoS One*. 2011; 6(1): e16423.
489. VanWijk MJ, Boer K, van der Meulen ET, Bleker OP, Spaan JA, VanBavel E. Resistance artery smooth muscle function in pregnancy and preeclampsia. *Am J Obstet Gynecol*. 2002; 186(1): 148-154.
490. Kold-Petersen H, Br ndum E, Nilsson H, Flyvbjerg A, Aalkjaer C. Impaired myogenic tone in isolated cerebral and coronary resistance arteries from the goto-kakizaki rat model of type 2 diabetes. *J Vasc Res*. 2012; 49(3): 267-278.
491. Burrows ME, Johnson PC. Diameter, wall tension, and flow in mesenteric arterioles during autoregulation. *Am J Physiol*. 1981; 241(6): H829-837.
492. Knot HJ, Nelson MT. Regulation of arterial diameter and wall $[Ca^{2+}]$ in cerebral arteries of rat by membrane potential and intravascular pressure. *J Physiol*. 1998; 508 (Pt 1): 199-209.
493. Zhang J, Berra-Romani R, Sinnegger-Brauns MJ, Striessnig J, Blaustein MP, Matteson DR. Role of $Ca_v1.2$ L-type Ca^{2+} channels in vascular tone: effects of nifedipine and Mg^{2+} . *Am J Physiol Heart Circ Physiol*. 2007; 292(1): H415-425.
494. Abd El-Rahman RR, Harraz OF, Brett SE, Anfinogenova Y, Mufti RE, Goldman D, Welsh DG. Identification of L- and T-type Ca^{2+} channels in rat cerebral arteries: role in myogenic tone development. *Am J Physiol Heart Circ Physiol*. 2013; 304(1): H58-71.
495. Davis MJ, Earley S, Li YS, Chien S. Vascular mechanotransduction. *Physiol Rev*. 2023; 103(2): 1247-1421.
496. Nikolaev YA, Cox CD, Ridone P, Rohde PR, Cordero-Morales JF, V squez V, Laver DR, Martinac B. Mammalian TRP ion channels are insensitive to membrane stretch. *J Cell Sci*. 2019; 132(23).
497. Swain SM, Liddle RA. Piezo1 acts upstream of TRPV4 to induce pathological changes in endothelial cells due to shear stress. *J Biol Chem*. 2021; 296: 100171.

498. Garcia-Elias A, Mrkonjic S, Pardo-Pastor C, Inada H, Hellmich UA, Rubio-Moscardó F, Plata C, Gaudet R, Vicente R, Valverde MA. Phosphatidylinositol-4,5-bisphosphate-dependent rearrangement of TRPV4 cytosolic tails enables channel activation by physiological stimuli. *Proc Natl Acad Sci U S A*. 2013; 110(23): 9553-9558.
499. Chen YL, Sonkusare SK. Endothelial TRPV4 channels and vasodilator reactivity. *Curr Top Membr*. 2020; 85: 89-117.
500. Gonzales AL, Garcia ZI, Amberg GC, Earley S. Pharmacological inhibition of TRPM4 hyperpolarizes vascular smooth muscle. *Am J Physiol Cell Physiol*. 2010; 299(5): C1195-1202.
501. Csípő T, Czikora Á, Fülöp G, Gulyás H, Rutkai I, Tóth EP, Pórszász R, Szalai A, Bölcskei K, Helyes Z, Pintér E, Papp Z, Ungvári Z, Tóth A. A central role for TRPM4 in Ca²⁺-signal amplification and vasoconstriction. *Int J Mol Sci*. 2022; 23(3).
502. Reading SA, Brayden JE. Central role of TRPM4 channels in cerebral blood flow regulation. *Stroke*. 2007; 38(8): 2322-2328.
503. Morita H, Honda A, Inoue R, Ito Y, Abe K, Nelson MT, Brayden JE. Membrane stretch-induced activation of a TRPM4-like nonselective cation channel in cerebral artery myocytes. *J Pharmacol Sci*. 2007; 103(4): 417-426.
504. Li Y, Baylie RL, Tavares MJ, Brayden JE. TRPM4 channels couple purinergic receptor mechanoactivation and myogenic tone development in cerebral parenchymal arterioles. *J Cereb Blood Flow Metab*. 2014; 34(10): 1706-1714.
505. Gong Y, Du MY, Yu HL, Yang ZY, Li YJ, Zhou L, Mei R, Yang L, Wang F. Increased TRPM4 activity in cerebral artery myocytes contributes to cerebral blood flow reduction after subarachnoid hemorrhage in rats. *Neurotherapeutics*. 2019; 16(3): 901-911.
506. Furchgott RF, Zawadzki JV. The obligatory role of endothelial cells in the relaxation of arterial smooth muscle by acetylcholine. *Nature*. 1980; 288(5789): 373-376.
507. Hutchinson PJ, Palmer RM, Moncada S. Comparative pharmacology of EDRF and nitric oxide on vascular strips. *Eur J Pharmacol*. 1987; 141(3): 445-451.
508. Ignarro LJ, Buga GM, Wood KS, Byrns RE, Chaudhuri G. Endothelium-derived relaxing factor produced and released from artery and vein is nitric oxide. *Proc Natl Acad Sci U S A*. 1987; 84(24): 9265-9269.
509. Taylor MS, Francis M. Decoding dynamic Ca²⁺ signaling in the vascular endothelium. *Front Physiol*. 2014; 5: 447.
510. Sandow SL, Senadheera S, Grayson TH, Welsh DG, Murphy TV. Calcium and endothelium-mediated vasodilator signaling. *Adv Exp Med Biol*. 2012; 740: 811-831.
511. Choi S, Saxena N, Dhammu T, Khan M, Singh AK, Singh I, Won J. Regulation of endothelial barrier integrity by redox-dependent nitric oxide signaling: implication in traumatic and inflammatory brain injuries. *Nitric Oxide*. 2019; 83: 51-64.
512. Mehta D, Konstantoulaki M, Ahmmed GU, Malik AB. Sphingosine 1-phosphate-induced mobilization of intracellular Ca²⁺ mediates rac activation and adherens junction assembly in endothelial cells. *J Biol Chem*. 2005; 280(17): 17320-17328.
513. Dalal PJ, Muller WA, Sullivan DP. Endothelial cell calcium signaling during barrier function and inflammation. *Am J Pathol*. 2020; 190(3): 535-542.
514. van Hinsbergh VW. Endothelium – role in regulation of coagulation and inflammation. *Semin Immunopathol*. 2012; 34(1): 93-106.
515. Moccia F, Tanzi F, Munaron L. Endothelial remodelling and intracellular calcium machinery. *Curr Mol Med*. 2014; 14(4): 457-480.

516. Thakore P, Earley S. Transient receptor potential channels and endothelial cell calcium signaling. *Compr Physiol*. 2019; 9(3): 1249-1277.
517. Murphy TV, Sandow SL. Agonist-evoked endothelial Ca²⁺ signalling microdomains. *Curr Opin Pharmacol*. 2019; 45: 8-15.
518. Ledoux J, Taylor MS, Bonev AD, Hannah RM, Solodushko V, Shui B, Tallini Y, Kotlikoff MI, Nelson MT. Functional architecture of inositol 1,4,5-trisphosphate signaling in restricted spaces of myoendothelial projections. *Proc Natl Acad Sci U S A*. 2008; 105(28): 9627-9632.
519. Kansui Y, Garland CJ, Dora KA. Enhanced spontaneous Ca²⁺ events in endothelial cells reflect signalling through myoendothelial gap junctions in pressurized mesenteric arteries. *Cell Calcium*. 2008; 44(2): 135-146.
520. Cohen KD, Jackson WF. Membrane hyperpolarization is not required for sustained muscarinic agonist-induced increases in intracellular Ca²⁺ in arteriolar endothelial cells. *Microcirculation*. 2005; 12(2): 169-182.
521. Nausch LW, Bonev AD, Heppner TJ, Tallini Y, Kotlikoff MI, Nelson MT. Sympathetic nerve stimulation induces local endothelial Ca²⁺ signals to oppose vasoconstriction of mouse mesenteric arteries. *Am J Physiol Heart Circ Physiol*. 2012; 302(3): H594-602.
522. Socha MJ, Domeier TL, Behringer EJ, Segal SS. Coordination of intercellular Ca²⁺ signaling in endothelial cell tubes of mouse resistance arteries. *Microcirculation*. 2012; 19(8): 757-770.
523. Jackson WF. Calcium-dependent ion channels and the regulation of arteriolar myogenic tone. *Front Physiol*. 2021; 12: 770450.
524. Wood PG, Gillespie JJ. Evidence for mitochondrial Ca²⁺-induced Ca²⁺ release in permeabilised endothelial cells. *Biochem Biophys Res Commun*. 1998; 246(2): 543-548.
525. Filippini A, D'Amore A, D'Alessio A. Calcium mobilization in endothelial cell functions. *Int J Mol Sci*. 2019; 20(18).
526. Maarouf N, Sancho M, Fürstenhaupt T, Tran CH, Welsh DG. Structural analysis of endothelial projections from mesenteric arteries. *Microcirculation*. 2017; 24(3).
527. Chalmers S, McCarron JG. Inhibition of mitochondrial calcium uptake rather than efflux impedes calcium release by inositol-1,4,5-trisphosphate-sensitive receptors. *Cell Calcium*. 2009; 46(2): 107-113.
528. Ichas F, Jouaville LS, Mazat JP. Mitochondria are excitable organelles capable of generating and conveying electrical and calcium signals. *Cell*. 1997; 89(7): 1145-1153.
529. Wilson C, Lee MD, Buckley C, Zhang X, McCarron JG. Mitochondrial ATP production is required for endothelial cell control of vascular tone. *Function (Oxf)*. 2023; 4(2): zqac063.
530. Yamamoto K, Imamura H, Ando J. Shear stress augments mitochondrial ATP generation that triggers ATP release and Ca²⁺ signaling in vascular endothelial cells. *Am J Physiol Heart Circ Physiol*. 2018; 315(5): H1477-h1485.
531. Scheitlin CG, Julian JA, Shanmughapriya S, Madesh M, Tsoukias NM, Alevriadou BR. Endothelial mitochondria regulate the intracellular Ca²⁺ response to fluid shear stress. *Am J Physiol Cell Physiol*. 2016; 310(6): C479-490.
532. Yamamoto K, Nogimori Y, Imamura H, Ando J. Shear stress activates mitochondrial oxidative phosphorylation by reducing plasma membrane cholesterol in vascular endothelial cells. *Proc Natl Acad Sci U S A*. 2020; 117(52): 33660-33667.

533. Fernandes J, Lorenzo IM, Andrade YN, Garcia-Elias A, Serra SA, Fernández-Fernández JM, Valverde MA. IP₃ sensitizes TRPV4 channel to the mechano- and osmotransducing messenger 5'-6'-epoxyeicosatrienoic acid. *J Cell Biol.* 2008; 181(1): 143-155.
534. Takahashi N, Hamada-Nakahara S, Itoh Y, Takemura K, Shimada A, Ueda Y, Kitamata M, Matsuoka R, Hanawa-Suetsugu K, Senju Y, Mori MX, Kiyonaka S, Kohda D, Kitao A, Mori Y, Suetsugu S. TRPV4 channel activity is modulated by direct interaction of the ankyrin domain to PI(4,5)P₂. *Nat Commun.* 2014; 5: 4994.
535. Mackrill JJ. Non-inositol 1,4,5-trisphosphate (IP₃) receptor IP₃-binding proteins. *Biochim Biophys Acta Mol Cell Res.* 2023; 1870(5): 119470.
536. Hong K, Cope EL, DeLalio LJ, Marziano C, Isakson BE, Sonkusare SK. TRPV4 (transient receptor potential vanilloid 4) channel-dependent negative feedback mechanism regulates G_q protein-coupled receptor-induced vasoconstriction. *Arterioscler Thromb Vasc Biol.* 2018; 38(3): 542-554.
537. Mendoza SA, Fang J, Gutterman DD, Wilcox DA, Bubolz AH, Li R, Suzuki M, Zhang DX. TRPV4-mediated endothelial Ca²⁺ influx and vasodilation in response to shear stress. *Am J Physiol Heart Circ Physiol.* 2010; 298(2): H466-476.
538. Gao X, Wu L, O'Neil RG. Temperature-modulated diversity of TRPV4 channel gating: activation by physical stresses and phorbol ester derivatives through protein kinase C-dependent and -independent pathways. *J Biol Chem.* 2003; 278(29): 27129-27137.
539. Liedtke W, Friedman JM. Abnormal osmotic regulation in *trpv4*^{-/-} mice. *Proc Natl Acad Sci U S A.* 2003; 100(23): 13698-13703.
540. Sonkusare SK, Bonev AD, Ledoux J, Liedtke W, Kotlikoff MI, Heppner TJ, Hill-Eubanks DC, Nelson MT. Elementary Ca²⁺ signals through endothelial TRPV4 channels regulate vascular function. *Science.* 2012; 336(6081): 597-601.
541. Köhler R, Heyken WT, Heinau P, Schubert R, Si H, Kacik M, Busch C, Grgic I, Maier T, Hoyer J. Evidence for a functional role of endothelial transient receptor potential V4 in shear stress-induced vasodilatation. *Arterioscler Thromb Vasc Biol.* 2006; 26(7): 1495-1502.
542. Bagher P, Beleznai T, Kansui Y, Mitchell R, Garland CJ, Dora KA. Low intravascular pressure activates endothelial cell TRPV4 channels, local Ca²⁺ events, and IK_{Ca} channels, reducing arteriolar tone. *Proc Natl Acad Sci U S A.* 2012; 109(44): 18174-18179.
543. Marziano C, Hong K, Cope EL, Kotlikoff MI, Isakson BE, Sonkusare SK. Nitric oxide-dependent feedback loop regulates transient receptor potential vanilloid 4 (TRPV4) channel cooperativity and endothelial function in small pulmonary arteries. *J Am Heart Assoc.* 2017; 6(12).
544. Pankey EA, Kassan M, Choi SK, Matrougui K, Nossaman BD, Hyman AL, Kadowitz PJ. Vasodilator responses to acetylcholine are not mediated by the activation of soluble guanylate cyclase or TRPV4 channels in the rat. *Am J Physiol Heart Circ Physiol.* 2014; 306(11): H1495-1506.
545. Liu CL, Huang Y, Ngai CY, Leung YK, Yao XQ. TRPC3 is involved in flow- and bradykinin-induced vasodilation in rat small mesenteric arteries. *Acta Pharmacol Sin.* 2006; 27(8): 981-990.
546. Kerr PM, Wei R, Tam R, Sandow SL, Murphy TV, Ondrusova K, Lunn SE, Tran CHT, Welsh DG, Plane F. Activation of endothelial IK_{Ca} channels underlies NO-dependent myoendothelial feedback. *Vascul Pharmacol.* 2015; 74: 130-138.

547. Kochukov MY, Balasubramanian A, Abramowitz J, Birnbaumer L, Marrelli SP. Activation of endothelial transient receptor potential C3 channel is required for small conductance calcium-activated potassium channel activation and sustained endothelial hyperpolarization and vasodilation of cerebral artery. *J Am Heart Assoc.* 2014; 3(4).
548. Senadheera S, Kim Y, Grayson TH, Toemoe S, Kochukov MY, Abramowitz J, Housley GD, Bertrand RL, Chadha PS, Bertrand PP, Murphy TV, Tare M, Birnbaumer L, Marrelli SP, Sandow SL. Transient receptor potential canonical type 3 channels facilitate endothelium-derived hyperpolarization-mediated resistance artery vasodilator activity. *Cardiovasc Res.* 2012; 95(4): 439-447.
549. Quick K, Zhao J, Eijkelkamp N, Linley JE, Rugiero F, Cox JJ, Raouf R, Gringhuis M, Sexton JE, Abramowitz J, Taylor R, Forge A, Ashmore J, Kirkwood N, Kros CJ, Richardson GP, Freichel M, Flockerzi V, Birnbaumer L, Wood JN. TRPC3 and TRPC6 are essential for normal mechanotransduction in subsets of sensory neurons and cochlear hair cells. *Open Biol.* 2012; 2(5): 120068.
550. Pires PW, Sullivan MN, Pritchard HA, Robinson JJ, Earley S. Unitary TRPV3 channel Ca^{2+} influx events elicit endothelium-dependent dilation of cerebral parenchymal arterioles. *Am J Physiol Heart Circ Physiol.* 2015; 309(12): H2031-2041.
551. Sullivan MN, Gonzales AL, Pires PW, Bruhl A, Leo MD, Li W, Oulidi A, Boop FA, Feng Y, Jaggar JH, Welsh DG, Earley S. Localized TRPA1 channel Ca^{2+} signals stimulated by reactive oxygen species promote cerebral artery dilation. *Sci Signal.* 2015; 8(358): ra2.
552. Förstermann U, Sessa WC. Nitric oxide synthases: regulation and function. *Eur Heart J.* 2012; 33(7): 829-837, 837a-837d.
553. Alderton WK, Cooper CE, Knowles RG. Nitric oxide synthases: structure, function and inhibition. *Biochem J.* 2001; 357(Pt 3): 593-615.
554. Palmer RM, Ashton DS, Moncada S. Vascular endothelial cells synthesize nitric oxide from L-arginine. *Nature.* 1988; 333(6174): 664-666.
555. Lee TJ, Sarwinski S, Ishine T, Lai CC, Chen FY. Inhibition of cerebral neurogenic vasodilation by L-glutamine and nitric oxide synthase inhibitors and its reversal by L-citrulline. *J Pharmacol Exp Ther.* 1996; 276(2): 353-358.
556. Stuehr DJ, Haque MM. Nitric oxide synthase enzymology in the 20 years after the Nobel Prize. *Br J Pharmacol.* 2019; 176(2): 177-188.
557. Li H, Jamal J, Plaza C, Pineda SH, Chreifi G, Jing Q, Cinelli MA, Silverman RB, Poulos TL. Structures of human constitutive nitric oxide synthases. *Acta Crystallogr D Biol Crystallogr.* 2014; 70(Pt 10): 2667-2674.
558. Förstermann U, Closs EI, Pollock JS, Nakane M, Schwarz P, Gath I, Kleinert H. Nitric oxide synthase isozymes. Characterization, purification, molecular cloning, and functions. *Hypertension.* 1994; 23(6 Pt 2): 1121-1131.
559. Förstermann U, Pollock JS, Schmidt HH, Heller M, Murad F. Calmodulin-dependent endothelium-derived relaxing factor/nitric oxide synthase activity is present in the particulate and cytosolic fractions of bovine aortic endothelial cells. *Proc Natl Acad Sci U S A.* 1991; 88(5): 1788-1792.
560. McMillan K, Masters BS. Prokaryotic expression of the heme- and flavin-binding domains of rat neuronal nitric oxide synthase as distinct polypeptides: identification of the heme-binding proximal thiolate ligand as cysteine-415. *Biochemistry.* 1995; 34(11): 3686-3693.

561. Ghosh DK, Stuehr DJ. Macrophage NO synthase: characterization of isolated oxygenase and reductase domains reveals a head-to-head subunit interaction. *Biochemistry*. 1995; 34(3): 801-807.
562. Richards MK, Marletta MA. Characterization of neuronal nitric oxide synthase and a C415H mutant, purified from a baculovirus overexpression system. *Biochemistry*. 1994; 33(49): 14723-14732.
563. Raman CS, Li H, Martásek P, Král V, Masters BS, Poulos TL. Crystal structure of constitutive endothelial nitric oxide synthase: a paradigm for pterin function involving a novel metal center. *Cell*. 1998; 95(7): 939-950.
564. Hemmens B, Goessler W, Schmidt K, Mayer B. Role of bound zinc in dimer stabilization but not enzyme activity of neuronal nitric-oxide synthase. *J Biol Chem*. 2000; 275(46): 35786-35791.
565. Smith BC, Underbakke ES, Kulp DW, Schief WR, Marletta MA. Nitric oxide synthase domain interfaces regulate electron transfer and calmodulin activation. *Proc Natl Acad Sci U S A*. 2013; 110(38): E3577-3586.
566. Yokom AL, Morishima Y, Lau M, Su M, Glukhova A, Osawa Y, Southworth DR. Architecture of the nitric-oxide synthase holoenzyme reveals large conformational changes and a calmodulin-driven release of the FMN domain. *J Biol Chem*. 2014; 289(24): 16855-16865.
567. Arnett DC, Persechini A, Tran QK, Black DJ, Johnson CK. Fluorescence quenching studies of structure and dynamics in calmodulin-eNOS complexes. *FEBS Lett*. 2015; 589(11): 1173-1178.
568. Jiang T, Wan G, Zhang H, Gyawali YP, Underbakke ES, Feng C. Probing protein dynamics in neuronal nitric oxide synthase by quantitative cross-linking mass spectrometry. *Biochemistry*. 2023; 62(15): 2232-2237.
569. He Y, Haque MM, Stuehr DJ, Lu HP. Conformational states and fluctuations in endothelial nitric oxide synthase under calmodulin regulation. *Biophys J*. 2021; 120(23): 5196-5206.
570. Abu-Soud HM, Stuehr DJ. Nitric oxide synthases reveal a role for calmodulin in controlling electron transfer. *Proc Natl Acad Sci U S A*. 1993; 90(22): 10769-10772.
571. Davydov R, Labby KJ, Chobot SE, Lukoyanov DA, Crane BR, Silverman RB, Hoffman BM. Enzymatic and cryoreduction EPR studies of the hydroxylation of methylated N^ω-hydroxy-L-arginine analogues by nitric oxide synthase from *Geobacillus stearothermophilus*. *Biochemistry*. 2014; 53(41): 6511-6519.
572. Hedison TM, Hay S, Scrutton NS. A perspective on conformational control of electron transfer in nitric oxide synthases. *Nitric Oxide*. 2017; 63: 61-67.
573. Stuehr DJ, Wei CC, Wang Z, Hille R. Exploring the redox reactions between heme and tetrahydrobiopterin in the nitric oxide synthases. *Dalton Trans*. 2005;(21): 3427-3435.
574. Oliveira-Paula GH, Lacchini R, Tanus-Santos JE. Endothelial nitric oxide synthase: From biochemistry and gene structure to clinical implications of NOS3 polymorphisms. *Gene*. 2016; 575(2 Pt 3): 584-599.
575. Lisanti MP, Scherer PE, Tang Z, Sargiacomo M. Caveolae, caveolin and caveolin-rich membrane domains: a signalling hypothesis. *Trends Cell Biol*. 1994; 4(7): 231-235.
576. Anderson RG. Caveolae: where incoming and outgoing messengers meet. *Proc Natl Acad Sci U S A*. 1993; 90(23): 10909-10913.

577. Feron O, Belhassen L, Kobzik L, Smith TW, Kelly RA, Michel T. Endothelial nitric oxide synthase targeting to caveolae. Specific interactions with caveolin isoforms in cardiac myocytes and endothelial cells. *J Biol Chem*. 1996; 271(37): 22810-22814.
578. Liu J, García-Cardena G, Sessa WC. Biosynthesis and palmitoylation of endothelial nitric oxide synthase: mutagenesis of palmitoylation sites, cysteines-15 and/or -26, argues against depalmitoylation-induced translocation of the enzyme. *Biochemistry*. 1995; 34(38): 12333-12340.
579. Shaul PW, Smart EJ, Robinson LJ, German Z, Yuhanna IS, Ying Y, Anderson RG, Michel T. Acylation targets endothelial nitric-oxide synthase to plasmalemmal caveolae. *J Biol Chem*. 1996; 271(11): 6518-6522.
580. Ju H, Zou R, Venema VJ, Venema RC. Direct interaction of endothelial nitric-oxide synthase and caveolin-1 inhibits synthase activity. *J Biol Chem*. 1997; 272(30): 18522-18525.
581. Trane AE, Pavlov D, Sharma A, Saqib U, Lau K, van Petegem F, Minshall RD, Roman LJ, Bernatchez PN. Deciphering the binding of caveolin-1 to client protein endothelial nitric-oxide synthase (eNOS): scaffolding subdomain identification, interaction modeling, and biological significance. *J Biol Chem*. 2014; 289(19): 13273-13283.
582. Sowa G, Pypaert M, Sessa WC. Distinction between signaling mechanisms in lipid rafts vs. caveolae. *Proc Natl Acad Sci U S A*. 2001; 98(24): 14072-14077.
583. Joshi MS, Mineo C, Shaul PW, Bauer JA. Biochemical consequences of the NOS3 Glu298Asp variation in human endothelium: altered caveolar localization and impaired response to shear. *Faseb j*. 2007; 21(11): 2655-2663.
584. Gratton JP, Fontana J, O'Connor DS, Garcia-Cardena G, McCabe TJ, Sessa WC. Reconstitution of an endothelial nitric-oxide synthase (eNOS), hsp90, and caveolin-1 complex in vitro. Evidence that hsp90 facilitates calmodulin stimulated displacement of eNOS from caveolin-1. *J Biol Chem*. 2000; 275(29): 22268-22272.
585. Xu H, Shi Y, Wang J, Jones D, Weilrauch D, Ying R, Wakim B, Pritchard KA, Jr. A heat shock protein 90 binding domain in endothelial nitric-oxide synthase influences enzyme function. *J Biol Chem*. 2007; 282(52): 37567-37574.
586. Fisslthaler B, Dimmeler S, Hermann C, Busse R, Fleming I. Phosphorylation and activation of the endothelial nitric oxide synthase by fluid shear stress. *Acta Physiol Scand*. 2000; 168(1): 81-88.
587. Wu Y, Ding Y, Ramprasath T, Zou MH. Oxidative stress, GTPCH1, and endothelial nitric oxide synthase uncoupling in hypertension. *Antioxid Redox Signal*. 2021; 34(9): 750-764.
588. Fleming I. Molecular mechanisms underlying the activation of eNOS. *Pflugers Arch*. 2010; 459(6): 793-806.
589. Moncada S, Higgs A. The L-arginine-nitric oxide pathway. *N Engl J Med*. 1993; 329(27): 2002-2012.
590. Kapil V, Khambata RS, Jones DA, Rathod K, Primus C, Massimo G, Fukuto JM, Ahluwalia A. The noncanonical pathway for in vivo nitric oxide generation: the nitrate-nitrite-nitric oxide pathway. *Pharmacol Rev*. 2020; 72(3): 692-766.
591. Stamler JS, Singel DJ, Loscalzo J. Biochemistry of nitric oxide and its redox-activated forms. *Science*. 1992; 258(5090): 1898-1902.

592. Li CG, Karagiannis J, Rand MJ. Comparison of the redox forms of nitrogen monoxide with the nitrenergic transmitter in the rat anococcygeus muscle. *Br J Pharmacol*. 1999; 127(4): 826-834.
593. Kemp-Harper BK. Nitroxyl (HNO): a novel redox signaling molecule. *Antioxid Redox Signal*. 2011; 14(9): 1609-1613.
594. Butler AR, Megson IL, Wright PG. Diffusion of nitric oxide and scavenging by blood in the vasculature. *Biochim Biophys Acta*. 1998; 1425(1): 168-176.
595. Möller MN, Denicola A. Diffusion of nitric oxide and oxygen in lipoproteins and membranes studied by pyrene fluorescence quenching. *Free Radic Biol Med*. 2018; 128: 137-143.
596. Möller MN, Cuevasanta E, Orrico F, Lopez AC, Thomson L, Denicola A. Diffusion and Transport of Reactive Species Across Cell Membranes. *Adv Exp Med Biol*. 2019; 1127: 3-19.
597. Subczynski WK, Lomnicka M, Hyde JS. Permeability of nitric oxide through lipid bilayer membranes. *Free Radic Res*. 1996; 24(5): 343-349.
598. Hobbs AJ, Stasch J-P. Soluble Guanylate Cyclase: Allosteric Activation and Redox Regulation in *Nitric Oxide*. (ed Ignarro LJ) Ch. 9, 301-326 (Academic Press, 2010).
599. Suvorava T, Metry S, Pick S, Kojda G. Alterations in endothelial nitric oxide synthase activity and their relevance to blood pressure. *Biochem Pharmacol*. 2022; 205: 115256.
600. Underbakke ES, Iavarone AT, Chalmers MJ, Pascal BD, Novick S, Griffin PR, Marletta MA. Nitric oxide-induced conformational changes in soluble guanylate cyclase. *Structure*. 2014; 22(4): 602-611.
601. Ignarro LJ, Degan JN, Baricos WH, Kadowitz PJ, Wolin MS. Activation of purified guanylate cyclase by nitric oxide requires heme. Comparison of heme-deficient, heme-reconstituted and heme-containing forms of soluble enzyme from bovine lung. *Biochim Biophys Acta*. 1982; 718(1): 49-59.
602. Montfort WR, Wales JA, Weichsel A. Structure and activation of soluble guanylyl cyclase, the nitric oxide sensor. *Antioxid Redox Signal*. 2017; 26(3): 107-121.
603. Fukao M, Mason HS, Britton FC, Kenyon JL, Horowitz B, Keef KD. Cyclic GMP-dependent protein kinase activates cloned BK_{Ca} channels expressed in mammalian cells by direct phosphorylation at serine 1072. *J Biol Chem*. 1999; 274(16): 10927-10935.
604. Kyle BD, Hurst S, Swayze RD, Sheng J, Braun AP. Specific phosphorylation sites underlie the stimulation of a large conductance, Ca²⁺-activated K⁺ channel by cGMP-dependent protein kinase. *FASEB J*. 2013; 27(5): 2027-2038.
605. Kyle BD, Mishra RC, Braun AP. The augmentation of BK channel activity by nitric oxide signaling in rat cerebral arteries involves co-localized regulatory elements. *J Cereb Blood Flow Metab*. 2017; 37(12): 3759-3773.
606. Xia C, Bao Z, Yue C, Sanborn BM, Liu M. Phosphorylation and regulation of G-protein-activated phospholipase C-β3 by cGMP-dependent protein kinases. *J Biol Chem*. 2001; 276(23): 19770-19777.
607. Sawada N, Itoh H, Yamashita J, Doi K, Inoue M, Masatsugu K, Fukunaga Y, Sakaguchi S, Sone M, Yamahara K, Yurugi T, Nakao K. cGMP-dependent protein kinase phosphorylates and inactivates RhoA. *Biochem Biophys Res Commun*. 2001; 280(3): 798-805.
608. Schlossmann J, Desch M. IRAG and novel PKG targeting in the cardiovascular system. *Am J Physiol Heart Circ Physiol*. 2011; 301(3): H672-682.

609. Wooldridge AA, MacDonald JA, Erdodi F, Ma C, Borman MA, Hartshorne DJ, Haystead TA. Smooth muscle phosphatase is regulated in vivo by exclusion of phosphorylation of threonine 696 of MYPT1 by phosphorylation of Serine 695 in response to cyclic nucleotides. *J Biol Chem.* 2004; 279(33): 34496-34504.
610. Kharitonov VG, Sundquist AR, Sharma VS. Kinetics of nitric oxide autoxidation in aqueous solution. *J Biol Chem.* 1994; 269(8): 5881-5883.
611. Huie RE, Padmaja S. The reaction of NO with superoxide. *Free Radic Res Commun.* 1993; 18(4): 195-199.
612. Xia Y, Dawson VL, Dawson TM, Snyder SH, Zweier JL. Nitric oxide synthase generates superoxide and nitric oxide in arginine-depleted cells leading to peroxynitrite-mediated cellular injury. *Proc Natl Acad Sci U S A.* 1996; 93(13): 6770-6774.
613. Schmidt HH, Hofmann H, Schindler U, Shutenko ZS, Cunningham DD, Feelisch M. NO •NO from NO synthase. *Proc Natl Acad Sci U S A.* 1996; 93(25): 14492-14497.
614. Beckman JS, Koppenol WH. Nitric oxide, superoxide, and peroxynitrite: the good, the bad, and the ugly. *Am J Physiol.* 1996; 271(5 Pt 1): C1424-1437.
615. Kerr PM, Tam R, Narang D, Potts K, McMillan D, McMillan K, Plane F. Endothelial calcium-activated potassium channels as therapeutic targets to enhance availability of nitric oxide. *Can J Physiol Pharmacol.* 2012; 90(6): 739-752.
616. Landmesser U, Dikalov S, Price SR, McCann L, Fukai T, Holland SM, Mitch WE, Harrison DG. Oxidation of tetrahydrobiopterin leads to uncoupling of endothelial cell nitric oxide synthase in hypertension. *J Clin Invest.* 2003; 111(8): 1201-1209.
617. Kuzkaya N, Weissmann N, Harrison DG, Dikalov S. Interactions of peroxynitrite, tetrahydrobiopterin, ascorbic acid, and thiols: implications for uncoupling endothelial nitric-oxide synthase. *J Biol Chem.* 2003; 278(25): 22546-22554.
618. Kohonen SL, Mouithys-Mickalad AA, Deby-Dupont GP, Deby CM, Lamy ML, Noels AF. Oxidation of tetrahydrobiopterin by peroxynitrite or oxoferryl species occurs by a radical pathway. *Free Radic Res.* 2001; 35(6): 709-721.
619. Kleschyov AL, Zhuge Z, Schiffer TA, Guimarães DD, Zhang G, Montenegro MF, Tesse A, Weitzberg E, Carlström M, Lundberg JO. NO-ferroheme is a signaling entity in the vasculature. *Nat Chem Biol.* 2023; 19(10): 1267-1275.
620. DeMartino AW, Poudel L, Dent MR, Chen X, Xu Q, Gladwin BS, Tejero J, Basu S, Alipour E, Jiang Y, Rose JJ, Gladwin MT, Kim-Shapiro DB. Thiol-catalyzed formation of NO-ferroheme regulates intravascular NO signaling. *Nat Chem Biol.* 2023; 19(10): 1256-1266.
621. Dent MR, DeMartino AW, Tejero J, Gladwin MT. Endogenous hemoprotein-dependent signaling pathways of nitric oxide and nitrite. *Inorg Chem.* 2021; 60(21): 15918-15940.
622. Pfeiffer S, Leopold E, Schmidt K, Brunner F, Mayer B. Inhibition of nitric oxide synthesis by N^G-nitro-L-arginine methyl ester (L-NAME): requirement for bioactivation to the free acid, N^G-nitro-L-arginine. *Br J Pharmacol.* 1996; 118(6): 1433-1440.
623. Moore PK, al-Swayeh OA, Chong NW, Evans RA, Gibson A. L-N^G-nitro arginine (L-NOARG), a novel, L-arginine-reversible inhibitor of endothelium-dependent vasodilatation in vitro. *Br J Pharmacol.* 1990; 99(2): 408-412.
624. Leo F, Suvorava T, Heuser SK, Li J, LoBue A, Barbarino F, Piragine E, Schneckmann R, Hutzler B, Good ME, Fernandez BO, Vornholz L, Rogers S, Doctor A, Grandoch M, Stegbauer J, Weitzberg E, Feelisch M, Lundberg JO, Isakson BE, Kelm M, Cortese-Krott

- MM. Red blood cell and endothelial eNOS independently regulate circulating nitric oxide metabolites and blood pressure. *Circulation*. 2021; 144(11): 870-889.
625. Huang PL, Huang Z, Mashimo H, Bloch KD, Moskowitz MA, Bevan JA, Fishman MC. Hypertension in mice lacking the gene for endothelial nitric oxide synthase. *Nature*. 1995; 377(6546): 239-242.
626. Busse R, Edwards G, Feletou M, Fleming I, Vanhoutte PM, Weston AH. EDHF: bringing the concepts together. *Trends Pharmacol Sci*. 2002; 23(8): 374-380.
627. Taylor SG, Southerton JS, Weston AH, Baker JR. Endothelium-dependent effects of acetylcholine in rat aorta: a comparison with sodium nitroprusside and cromakalim. *Br J Pharmacol*. 1988; 94(3): 853-863.
628. Cowan CL, Cohen RA. Two mechanisms mediate relaxation by bradykinin of pig coronary artery: NO-dependent and -independent responses. *Am J Physiol*. 1991; 261(3 Pt 2): H830-835.
629. Mombouli JV, Illiano S, Nagao T, Scott-Burden T, Vanhoutte PM. Potentiation of endothelium-dependent relaxations to bradykinin by angiotensin I converting enzyme inhibitors in canine coronary artery involves both endothelium-derived relaxing and hyperpolarizing factors. *Circ Res*. 1992; 71(1): 137-144.
630. Nagao T, Vanhoutte PM. Hyperpolarization as a mechanism for endothelium-dependent relaxations in the porcine coronary artery. *J Physiol*. 1992; 445: 355-367.
631. Garland CJ, McPherson GA. Evidence that nitric oxide does not mediate the hyperpolarization and relaxation to acetylcholine in the rat small mesenteric artery. *Br J Pharmacol*. 1992; 105(2): 429-435.
632. Bény J. Electrical coupling between smooth muscle cells and endothelial cells in pig coronary arteries. *Pflugers Arch*. 1997; 433(3): 364-367.
633. Garland CJ, Dora KA. Endothelium-dependent hyperpolarization: the evolution of myoendothelial microdomains. *J Cardiovasc Pharmacol*. 2021; 78(Suppl 6): S3-s12.
634. Garland CJ, Dora KA. EDH: endothelium-dependent hyperpolarization and microvascular signalling. *Acta Physiol (Oxf)*. 2017; 219(1): 152-161.
635. Orfali R, Albanyan N. Ca²⁺-sensitive potassium channels. *Molecules*. 2023; 28(2).
636. Ishii TM, Silvia C, Hirschberg B, Bond CT, Adelman JP, Maylie J. A human intermediate conductance calcium-activated potassium channel. *Proc Natl Acad Sci U S A*. 1997; 94(21): 11651-11656.
637. Latorre R, Vergara C, Hidalgo C. Reconstitution in planar lipid bilayers of a Ca²⁺-dependent K⁺ channel from transverse tubule membranes isolated from rabbit skeletal muscle. *Proc Natl Acad Sci U S A*. 1982; 79(3): 805-809.
638. Köhler M, Hirschberg B, Bond CT, Kinzie JM, Marrion NV, Maylie J, Adelman JP. Small-conductance, calcium-activated potassium channels from mammalian brain. *Science*. 1996; 273(5282): 1709-1714.
639. Sandow SL, Grayson TH. Limits of isolation and culture: intact vascular endothelium and BK_{Ca}. *Am J Physiol Heart Circ Physiol*. 2009; 297(1): H1-7.
640. Köhler R, Ruth P. Endothelial dysfunction and blood pressure alterations in K⁺-channel transgenic mice. *Pflugers Arch*. 2010; 459(6): 969-976.
641. Ledoux J, Werner ME, Brayden JE, Nelson MT. Calcium-activated potassium channels and the regulation of vascular tone. *Physiology (Bethesda)*. 2006; 21: 69-78.
642. Wulff H, Zhorov BS. K⁺ channel modulators for the treatment of neurological disorders and autoimmune diseases. *Chem Rev*. 2008; 108(5): 1744-1773.

643. Cox DH. Ca²⁺-regulated ion channels. *BMB Rep.* 2011; 44(10): 635-646.
644. Burnham MP, Bychkov R, Félétou M, Richards GR, Vanhoutte PM, Weston AH, Edwards G. Characterization of an apamin-sensitive small-conductance Ca²⁺-activated K⁺ channel in porcine coronary artery endothelium: relevance to EDHF. *Br J Pharmacol.* 2002; 135(5): 1133-1143.
645. Christophersen P, Wulff H. Pharmacological gating modulation of small- and intermediate-conductance Ca²⁺-activated K⁺ channels (K_{Ca2.x} and K_{Ca3.1}). *Channels (Austin).* 2015; 9(6): 336-343.
646. Chen MX, Gorman SA, Benson B, Singh K, Hieble JP, Michel MC, Tate SN, Trezise DJ. Small and intermediate conductance Ca²⁺-activated K⁺ channels confer distinctive patterns of distribution in human tissues and differential cellular localisation in the colon and corpus cavernosum. *Naunyn Schmiedebergs Arch Pharmacol.* 2004; 369(6): 602-615.
647. Damkjaer M, Nielsen G, Bodendiek S, Staehr M, Gramsbergen JB, de Wit C, Jensen BL, Simonsen U, Bie P, Wulff H, Köhler R. Pharmacological activation of K_{Ca3.1}/K_{Ca2.3} channels produces endothelial hyperpolarization and lowers blood pressure in conscious dogs. *Br J Pharmacol.* 2012; 165(1): 223-234.
648. Xia XM, Fakler B, Rivard A, Wayman G, Johnson-Pais T, Keen JE, Ishii T, Hirschberg B, Bond CT, Lutsenko S, Maylie J, Adelman JP. Mechanism of calcium gating in small-conductance calcium-activated potassium channels. *Nature.* 1998; 395(6701): 503-507.
649. Nam YW, Cui M, Orfali R, Viegas A, Nguyen M, Mohammed EHM, Zoghebi KA, Rahighi S, Parang K, Zhang M. Hydrophobic interactions between the HA helix and S4-S5 linker modulate apparent Ca²⁺ sensitivity of SK2 channels. *Acta Physiol (Oxf).* 2021; 231(1): e13552.
650. Joiner WJ, Wang LY, Tang MD, Kaczmarek LK. hSK4, a member of a novel subfamily of calcium-activated potassium channels. *Proc Natl Acad Sci U S A.* 1997; 94(20): 11013-11018.
651. Halling DB, Kenrick SA, Riggs AF, Aldrich RW. Calcium-dependent stoichiometries of the K_{Ca2.2} (SK) intracellular domain/calmodulin complex in solution. *J Gen Physiol.* 2014; 143(2): 231-252.
652. Bruening-Wright A, Schumacher MA, Adelman JP, Maylie J. Localization of the activation gate for small conductance Ca²⁺-activated K⁺ channels. *J Neurosci.* 2002; 22(15): 6499-6506.
653. Maingret F, Coste B, Hao J, Giamarchi A, Allen D, Crest M, Litchfield DW, Adelman JP, Delmas P. Neurotransmitter modulation of small-conductance Ca²⁺-activated K⁺ channels by regulation of Ca²⁺ gating. *Neuron.* 2008; 59(3): 439-449.
654. Bildl W, Strassmaier T, Thurm H, Andersen J, Eble S, Oliver D, Knipper M, Mann M, Schulte U, Adelman JP, Fakler B. Protein kinase CK2 is coassembled with small conductance Ca²⁺-activated K⁺ channels and regulates channel gating. *Neuron.* 2004; 43(6): 847-858.
655. Stocker M, Hirzel K, D'Hoedt D, Pedarzani P. Matching molecules to function: neuronal Ca²⁺-activated K⁺ channels and afterhyperpolarizations. *Toxicon.* 2004; 43(8): 933-949.
656. Quignard JF, Félétou M, Edwards G, Duhault J, Weston AH, Vanhoutte PM. Role of endothelial cell hyperpolarization in EDHF-mediated responses in the guinea-pig carotid artery. *Br J Pharmacol.* 2000; 129(6): 1103-1112.

657. Edwards G, Dora KA, Gardener MJ, Garland CJ, Weston AH. K^+ is an endothelium-derived hyperpolarizing factor in rat arteries. *Nature*. 1998; 396(6708): 269-272.
658. Bychkov R, Burnham MP, Richards GR, Edwards G, Weston AH, Félétou M, Vanhoutte PM. Characterization of a charybdotoxin-sensitive intermediate conductance Ca^{2+} -activated K^+ channel in porcine coronary endothelium: relevance to EDHF. *Br J Pharmacol*. 2002; 137(8): 1346-1354.
659. Marchenko SM, Sage SO. Calcium-activated potassium channels in the endothelium of intact rat aorta. *J Physiol*. 1996; 492 (Pt 1)(Pt 1): 53-60.
660. Si R, Zhang Q, Cabrera JTO, Zheng Q, Tsuji-Hosokawa A, Watanabe M, Hosokawa S, Xiong M, Jain PP, Ashton AW, Yuan JX, Wang J, Makino A. Chronic hypoxia decreases endothelial connexin 40, attenuates endothelium-dependent hyperpolarization-mediated relaxation in small distal pulmonary arteries, and leads to pulmonary hypertension. *J Am Heart Assoc*. 2020; 9(24): e018327.
661. Brasen JC, de Wit C, Sorensen CM. Myoendothelial coupling through Cx40 contributes to EDH-induced vasodilation in murine renal arteries: evidence from experiments and modelling. *Acta Physiol (Oxf)*. 2018; 222(1).
662. Crane GJ, Neild TO, Segal SS. Contribution of active membrane processes to conducted hyperpolarization in arterioles of hamster cheek pouch. *Microcirculation*. 2004; 11(5): 425-433.
663. Crane GJ, Garland CJ. Thromboxane receptor stimulation associated with loss of SK_{Ca} activity and reduced EDHF responses in the rat isolated mesenteric artery. *Br J Pharmacol*. 2004; 142(1): 43-50.
664. Bolz SS, de Wit C, Pohl U. Endothelium-derived hyperpolarizing factor but not NO reduces smooth muscle Ca^{2+} during acetylcholine-induced dilation of microvessels. *Br J Pharmacol*. 1999; 128(1): 124-134.
665. Loirand G, Pacaud P, Mironneau C, Mironneau J. Evidence for two distinct calcium channels in rat vascular smooth muscle cells in short-term primary culture. *Pflugers Arch*. 1986; 407(5): 566-568.
666. Félétou M. Endothelium-dependent hyperpolarization and endothelial dysfunction. *J Cardiovasc Pharmacol*. 2016; 67(5): 373-387.
667. Smith PD, Brett SE, Luykenaar KD, Sandow SL, Marrelli SP, Vigmond EJ, Welsh DG. K_{IR} channels function as electrical amplifiers in rat vascular smooth muscle. *J Physiol*. 2008; 586(4): 1147-1160.
668. Prior HM, Webster N, Quinn K, Beech DJ, Yates MS. K^+ -induced dilation of a small renal artery: no role for inward rectifier K^+ channels. *Cardiovasc Res*. 1998; 37(3): 780-790.
669. Sonkusare SK, Dalsgaard T, Bonev AD, Nelson MT. Inward rectifier potassium ($K_{IR2.1}$) channels as end-stage boosters of endothelium-dependent vasodilators. *J Physiol*. 2016; 594(12): 3271-3285.
670. Shimokawa H, Yasutake H, Fujii K, Owada MK, Nakaike R, Fukumoto Y, Takayanagi T, Nagao T, Egashira K, Fujishima M, Takeshita A. The importance of the hyperpolarizing mechanism increases as the vessel size decreases in endothelium-dependent relaxations in rat mesenteric circulation. *J Cardiovasc Pharmacol*. 1996; 28(5): 703-711.

671. Sandow SL, Hill CE. Incidence of myoendothelial gap junctions in the proximal and distal mesenteric arteries of the rat is suggestive of a role in endothelium-derived hyperpolarizing factor-mediated responses. *Circ Res.* 2000; 86(3): 341-346.
672. Absi M, Burnham MP, Weston AH, Harno E, Rogers M, Edwards G. Effects of methyl β -cyclodextrin on EDHF responses in pig and rat arteries; association between SK_{Ca} channels and caveolin-rich domains. *Br J Pharmacol.* 2007; 151(3): 332-340.
673. Walker SD, Dora KA, Ings NT, Crane GJ, Garland CJ. Activation of endothelial cell IK_{Ca} with 1-ethyl-2-benzimidazolinone evokes smooth muscle hyperpolarization in rat isolated mesenteric artery. *Br J Pharmacol.* 2001; 134(7): 1548-1554.
674. Sheng JZ, Braun AP. Small- and intermediate-conductance Ca²⁺-activated K⁺ channels directly control agonist-evoked nitric oxide synthesis in human vascular endothelial cells. *Am J Physiol Cell Physiol.* 2007; 293(1): C458-467.
675. Wulff H, Kolski-Andreaco A, Sankaranarayanan A, Sabatier JM, Shakkottai V. Modulators of small- and intermediate-conductance calcium-activated potassium channels and their therapeutic indications. *Curr Med Chem.* 2007; 14(13): 1437-1457.
676. Ishii TM, Maylie J, Adelman JP. Determinants of apamin and *d*-tubocurarine block in SK potassium channels. *J Biol Chem.* 1997; 272(37): 23195-23200.
677. Nolting A, Ferraro T, D'Hoedt D, Stocker M. An amino acid outside the pore region influences apamin sensitivity in small conductance Ca²⁺-activated K⁺ channels. *J Biol Chem.* 2007; 282(6): 3478-3486.
678. Weatherall KL, Seutin V, Liégeois JF, Marrion NV. Crucial role of a shared extracellular loop in apamin sensitivity and maintenance of pore shape of small-conductance calcium-activated potassium (SK) channels. *Proc Natl Acad Sci U S A.* 2011; 108(45): 18494-18499.
679. Lamy C, Goodchild SJ, Weatherall KL, Jane DE, Liégeois JF, Seutin V, Marrion NV. Allosteric block of K_{Ca2} channels by apamin. *J Biol Chem.* 2010; 285(35): 27067-27077.
680. Kuzmenkov AI, Peigneur S, Nasburg JA, Mineev KS, Nikolaev MV, Pinheiro-Junior EL, Arseniev AS, Wulff H, Tytgat J, Vassilevski AA. Apamin structure and pharmacology revisited. *Front Pharmacol.* 2022; 13: 977440.
681. Wulff H, Miller MJ, Hansel W, Grissmer S, Cahalan MD, Chandy KG. Design of a potent and selective inhibitor of the intermediate-conductance Ca²⁺-activated K⁺ channel, IKCa1: a potential immunosuppressant. *Proc Natl Acad Sci U S A.* 2000; 97(14): 8151-8156.
682. Wulff H, Gutman GA, Cahalan MD, Chandy KG. Delineation of the clotrimazole/TRAM-34 binding site on the intermediate conductance calcium-activated potassium channel, IKCa1. *J Biol Chem.* 2001; 276(34): 32040-32045.
683. Jørgensen S, Dyhring T, Brown DT, Strøbæk D, Christophersen P, Demnitz J. A high-throughput screening campaign for detection of Ca²⁺-activated K⁺ channel activators and inhibitors using a fluorometric imaging plate reader-based TI⁺-influx assay. *Assay Drug Dev Technol.* 2013; 11(3): 163-172.
684. Strøbæk D, Brown DT, Jenkins DP, Chen YJ, Coleman N, Ando Y, Chiu P, Jørgensen S, Demnitz J, Wulff H, Christophersen P. NS6180, a new K_{Ca3.1} channel inhibitor prevents T-cell activation and inflammation in a rat model of inflammatory bowel disease. *Br J Pharmacol.* 2013; 168(2): 432-444.

685. Nguyen HM, Singh V, Pressly B, Jenkins DP, Wulff H, Yarov-Yarovoy V. Structural insights into the atomistic mechanisms of action of small molecule inhibitors targeting the KCa3.1 channel pore. *Mol Pharmacol*. 2017; 91(4): 392-402.
686. Hougaard C, Eriksen BL, Jørgensen S, Johansen TH, Dyhring T, Madsen LS, Strøbaek D, Christophersen P. Selective positive modulation of the SK3 and SK2 subtypes of small conductance Ca²⁺-activated K⁺ channels. *Br J Pharmacol*. 2007; 151(5): 655-665.
687. Sankaranarayanan A, Raman G, Busch C, Schultz T, Zimin PI, Hoyer J, Kohler R, Wulff H. Naphtho[1,2-d]thiazol-2-ylamine (SKA-31), a new activator of KCa2 and KCa3.1 potassium channels, potentiates the endothelium-derived hyperpolarizing factor response and lowers blood pressure. *Mol Pharmacol*. 2009; 75(2): 281-295.
688. El-Sayed NS, Nam YW, Egorova PA, Nguyen HM, Orfali R, Rahman MA, Yang G, Wulff H, Bezprozvanny I, Parang K, Zhang M. Structure-activity relationship study of subtype-selective positive modulators of K_{Ca}2 channels. *J Med Chem*. 2022; 65(1): 303-322.
689. Nam YW, Cui M, El-Sayed NS, Orfali R, Nguyen M, Yang G, Rahman MA, Lee J, Zhang M. Subtype-selective positive modulation of K_{Ca}2 channels depends on the HA/HB helices. *Br J Pharmacol*. 2022; 179(3): 460-472.
690. Sandow SL, Neylon CB, Chen MX, Garland CJ. Spatial separation of endothelial small- and intermediate-conductance calcium-activated potassium channels (K(Ca)) and connexins: possible relationship to vasodilator function? *J Anat*. 2006; 209(5): 689-698.
691. Brähler S, Kaistha A, Schmidt VJ, Wölfle SE, Busch C, Kaistha BP, Kacik M, Hasenau AL, Grgic I, Si H, Bond CT, Adelman JP, Wulff H, de Wit C, Hoyer J, Köhler R. Genetic deficit of SK3 and IK1 channels disrupts the endothelium-derived hyperpolarizing factor vasodilator pathway and causes hypertension. *Circulation*. 2009; 119(17): 2323-2332.
692. Weston AH, Absi M, Ward DT, Ohanian J, Dodd RH, Dauban P, Petrel C, Ruat M, Edwards G. Evidence in favor of a calcium-sensing receptor in arterial endothelial cells: studies with calindol and Calhex 231. *Circ Res*. 2005; 97(4): 391-398.
693. Saliez J, Bouzin C, Rath G, Ghisdal P, Desjardins F, Rezzani R, Rodella LF, Vriens J, Nilius B, Feron O, Balligand JL, Dessy C. Role of caveolar compartmentation in endothelium-derived hyperpolarizing factor-mediated relaxation: Ca²⁺ signals and gap junction function are regulated by caveolin in endothelial cells. *Circulation*. 2008; 117(8): 1065-1074.
694. Chen M, Li X. Role of TRPV4 channel in vasodilation and neovascularization. *Microcirculation*. 2021; 28(6): e12703.
695. Sukumaran SV, Singh TU, Parida S, Narasimha Reddy Ch E, Thangamalai R, Kandasamy K, Singh V, Mishra SK. TRPV4 channel activation leads to endothelium-dependent relaxation mediated by nitric oxide and endothelium-derived hyperpolarizing factor in rat pulmonary artery. *Pharmacol Res*. 2013; 78: 18-27.
696. Dora KA, Gallagher NT, McNeish A, Garland CJ. Modulation of endothelial cell K_{Ca}3.1 channels during endothelium-derived hyperpolarizing factor signaling in mesenteric resistance arteries. *Circ Res*. 2008; 102(10): 1247-1255.
697. Chadha PS, Liu L, Rikard-Bell M, Senadheera S, Howitt L, Bertrand RL, Grayson TH, Murphy TV, Sandow SL. Endothelium-dependent vasodilation in human mesenteric artery is primarily mediated by myoendothelial gap junctions intermediate conductance calcium-activated K⁺ channel and nitric oxide. *J Pharmacol Exp Ther*. 2011; 336(3): 701-708.

698. Tran CH, Taylor MS, Plane F, Nagaraja S, Tsoukias NM, Solodushko V, Vigmond EJ, Furstenhaupt T, Brigdan M, Welsh DG. Endothelial Ca^{2+} wavelets and the induction of myoendothelial feedback. *Am J Physiol Cell Physiol*. 2012; 302(8): C1226-1242.
699. Isakson BE. Localized expression of an $\text{Ins}(1,4,5)\text{P}_3$ receptor at the myoendothelial junction selectively regulates heterocellular Ca^{2+} communication. *J Cell Sci*. 2008; 121(Pt 21): 3664-3673.
700. Wei R, Lunn SE, Tam R, Gust SL, Classen B, Kerr PM, Plane F. Vasoconstrictor stimulus determines the functional contribution of myoendothelial feedback to mesenteric arterial tone. *J Physiol*. 2018; 596(7): 1181-1197.
701. Dalsgaard T, Kroigaard C, Misfeldt M, Bek T, Simonsen U. Openers of small conductance calcium-activated potassium channels selectively enhance NO-mediated bradykinin vasodilatation in porcine retinal arterioles. *Br J Pharmacol*. 2010; 160(6): 1496-1508.
702. Eichler I, Wibawa J, Grgic I, Knorr A, Brakemeier S, Pries AR, Hoyer J, Köhler R. Selective blockade of endothelial Ca^{2+} -activated small- and intermediate-conductance K^+ -channels suppresses EDHF-mediated vasodilation. *Br J Pharmacol*. 2003; 138(4): 594-601.
703. Leuranguer V, Gluais P, Vanhoutte PM, Verbeuren TJ, Félétou M. Openers of calcium-activated potassium channels and endothelium-dependent hyperpolarizations in the guinea pig carotid artery. *Naunyn Schmiedebergs Arch Pharmacol*. 2008; 377(2): 101-109.
704. Si H, Heyken WT, Wölfle SE, Tysiac M, Schubert R, Grgic I, Vilianovich L, Giebing G, Maier T, Gross V, Bader M, de Wit C, Hoyer J, Köhler R. Impaired endothelium-derived hyperpolarizing factor-mediated dilations and increased blood pressure in mice deficient of the intermediate-conductance Ca^{2+} -activated K^+ channel. *Circ Res*. 2006; 99(5): 537-544.
705. Taylor MS, Bonev AD, Gross TP, Eckman DM, Brayden JE, Bond CT, Adelman JP, Nelson MT. Altered expression of small-conductance Ca^{2+} -activated K^+ (SK3) channels modulates arterial tone and blood pressure. *Circ Res*. 2003; 93(2): 124-131.
706. Biwer LA, Taddeo EP, Kenwood BM, Hoehn KL, Straub AC, Isakson BE. Two functionally distinct pools of eNOS in endothelium are facilitated by myoendothelial junction lipid composition. *Biochim Biophys Acta*. 2016; 1861(7): 671-679.
707. Höhler B, Holzapfel B, Kummer W. NADPH oxidase subunits and superoxide production in porcine pulmonary artery endothelial cells. *Histochem Cell Biol*. 2000; 114(1): 29-37.
708. Rueckschloss U, Galle J, Holtz J, Zerkowski HR, Morawietz H. Induction of NAD(P)H oxidase by oxidized low-density lipoprotein in human endothelial cells: antioxidative potential of hydroxymethylglutaryl coenzyme A reductase inhibitor therapy. *Circulation*. 2001; 104(15): 1767-1772.
709. Görlach A, Brandes RP, Nguyen K, Amidi M, Dehghani F, Busse R. A gp91phox containing NADPH oxidase selectively expressed in endothelial cells is a major source of oxygen radical generation in the arterial wall. *Circ Res*. 2000; 87(1): 26-32.
710. Matsuzaki I, Chatterjee S, Debolt K, Manevich Y, Zhang Q, Fisher AB. Membrane depolarization and NADPH oxidase activation in aortic endothelium during ischemia reflect altered mechanotransduction. *Am J Physiol Heart Circ Physiol*. 2005; 288(1): H336-343.

711. Lunn SE. *Regulation of mesenteric resistance artery diameter by pharmacological modulators of K_{Ca} channels* Doctor of Philosophy thesis, University of Alberta, (2018).
712. Tare M, Parkington HC, Coleman HA, Neild TO, Dusting GJ. Hyperpolarization and relaxation of arterial smooth muscle caused by nitric oxide derived from the endothelium. *Nature*. 1990; 346(6279): 69-71.
713. Rand VE, Garland CJ. Endothelium-dependent relaxation to acetylcholine in the rabbit basilar artery: importance of membrane hyperpolarization. *Br J Pharmacol*. 1992; 106(1): 143-150.
714. Vanheel B, Van de Voorde J, Leusen I. Contribution of nitric oxide to the endothelium-dependent hyperpolarization in rat aorta. *J Physiol*. 1994; 475(2): 277-284.
715. Bolotina VM, Najibi S, Palacino JJ, Pagano PJ, Cohen RA. Nitric oxide directly activates calcium-dependent potassium channels in vascular smooth muscle. *Nature*. 1994; 368(6474): 850-853.
716. Alaaeddine RA, Mroueh A, Gust S, Eid AH, Plane F, El-Yazbi AF. Impaired cross-talk between NO and hyperpolarization in myoendothelial feedback: a novel therapeutic target in early endothelial dysfunction of metabolic disease. *Curr Opin Pharmacol*. 2019; 45: 33-41.
717. Aird WC. Phenotypic heterogeneity of the endothelium: I. Structure, function, and mechanisms. *Circ Res*. 2007; 100(2): 158-173.
718. Aird WC. Phenotypic heterogeneity of the endothelium: II. Representative vascular beds. *Circ Res*. 2007; 100(2): 174-190.
719. Bennett HS, Luft JH, Hampton JC. Morphological classifications of vertebrate blood capillaries. *Am J Physiol*. 1959; 196(2): 381-390.
720. Adamson RH, Lenz JF, Zhang X, Adamson GN, Weinbaum S, Curry FE. Oncotic pressures opposing filtration across non-fenestrated rat microvessels. *J Physiol*. 2004; 557(Pt 3): 889-907.
721. Pries AR, Kuebler WM. Normal endothelium. *Handb Exp Pharmacol*. 2006;(176 Pt 1): 1-40.
722. Stan RV, Kubitza M, Palade GE. PV-1 is a component of the fenestral and stomatal diaphragms in fenestrated endothelia. *Proc Natl Acad Sci U S A*. 1999; 96(23): 13203-13207.
723. Rostgaard J, Qvortrup K. Electron microscopic demonstrations of filamentous molecular sieve plugs in capillary fenestrae. *Microvasc Res*. 1997; 53(1): 1-13.
724. Griffin CT, Gao S. Building discontinuous liver sinusoidal vessels. *J Clin Invest*. 2017; 127(3): 790-792.
725. Wallez Y, Huber P. Endothelial adherens and tight junctions in vascular homeostasis, inflammation and angiogenesis. *Biochim Biophys Acta*. 2008; 1778(3): 794-809.
726. Vanslebrouck B, Chen JH, Larabell C, van Hengel J. Microscopic visualization of cell-cell adhesion complexes at micro and nanoscale. *Front Cell Dev Biol*. 2022; 10: 819534.
727. Lampugnani MG, Dejana E, Giampietro C. Vascular endothelial (VE)-cadherin, endothelial adherens junctions, and vascular disease. *Cold Spring Harb Perspect Biol*. 2018; 10(10).
728. Hartsock A, Nelson WJ. Adherens and tight junctions: structure, function and connections to the actin cytoskeleton. *Biochim Biophys Acta*. 2008; 1778(3): 660-669.
729. Zihni C, Mills C, Matter K, Balda MS. Tight junctions: from simple barriers to multifunctional molecular gates. *Nat Rev Mol Cell Biol*. 2016; 17(9): 564-580.

730. Cong X, Kong W. Endothelial tight junctions and their regulatory signaling pathways in vascular homeostasis and disease. *Cell Signal*. 2020; 66: 109485.
731. Pogoda K, Kameritsch P, Mannell H, Pohl U. Connexins in the control of vasomotor function. *Acta Physiol (Oxf)*. 2019; 225(1): e13108.
732. Schmidt K, Windler R, de Wit C. Communication through gap junctions in the endothelium. *Adv Pharmacol*. 2016; 77: 209-240.
733. Söhl G, Willecke K. Gap junctions and the connexin protein family. *Cardiovasc Res*. 2004; 62(2): 228-232.
734. Hakim CH, Jackson WF, Segal SS. Connexin isoform expression in smooth muscle cells and endothelial cells of hamster cheek pouch arterioles and retractor feed arteries. *Microcirculation*. 2008; 15(6): 503-514.
735. Hill CE, Rummery N, Hickey H, Sandow SL. Heterogeneity in the distribution of vascular gap junctions and connexins: implications for function. *Clin Exp Pharmacol Physiol*. 2002; 29(7): 620-625.
736. Gabriels JE, Paul DL. Connexin43 is highly localized to sites of disturbed flow in rat aortic endothelium but connexin37 and connexin40 are more uniformly distributed. *Circ Res*. 1998; 83(6): 636-643.
737. Rummery NM, Hickey H, McGurk G, Hill CE. Connexin37 is the major connexin expressed in the media of caudal artery. *Arterioscler Thromb Vasc Biol*. 2002; 22(9): 1427-1432.
738. Severs NJ, Rothery S, Dupont E, Coppens SR, Yeh HI, Ko YS, Matsushita T, Kaba R, Halliday D. Immunocytochemical analysis of connexin expression in the healthy and diseased cardiovascular system. *Microsc Res Tech*. 2001; 52(3): 301-322.
739. van Kempen MJ, Jongsma HJ. Distribution of connexin37, connexin40 and connexin43 in the aorta and coronary artery of several mammals. *Histochem Cell Biol*. 1999; 112(6): 479-486.
740. Yeh HI, Rothery S, Dupont E, Coppens SR, Severs NJ. Individual gap junction plaques contain multiple connexins in arterial endothelium. *Circ Res*. 1998; 83(12): 1248-1263.
741. Rackauskas M, Kreuzberg MM, Pranevicius M, Willecke K, Verselis VK, Bukauskas FF. Gating properties of heterotypic gap junction channels formed of connexins 40, 43, and 45. *Biophys J*. 2007; 92(6): 1952-1965.
742. Martinez AD, Hayrapetyan V, Moreno AP, Beyer EC. Connexin43 and connexin45 form heteromeric gap junction channels in which individual components determine permeability and regulation. *Circ Res*. 2002; 90(10): 1100-1107.
743. Beyer EC, Gemel J, Martínez A, Berthoud VM, Valiunas V, Moreno AP, Brink PR. Heteromeric mixing of connexins: compatibility of partners and functional consequences. *Cell Commun Adhes*. 2001; 8(4-6): 199-204.
744. Wagner C, Kurtz L, Schweda F, Simon AM, Kurtz A. Connexin 37 is dispensable for the control of the renin system and for positioning of renin-producing cells in the kidney. *Pflugers Arch*. 2009; 459(1): 151-158.
745. Beyer EC, Lin X, Veenstra RD. Interfering amino terminal peptides and functional implications for heteromeric gap junction formation. *Front Pharmacol*. 2013; 4: 67.
746. Rodríguez-Sinovas A, Sánchez JA, Valls-Lacalle L, Consegal M, Ferreira-González I. Connexins in the heart: regulation, function and involvement in cardiac disease. *Int J Mol Sci*. 2021; 22(9).

747. Foote CI, Zhou L, Zhu X, Nicholson BJ. The pattern of disulfide linkages in the extracellular loop regions of connexin 32 suggests a model for the docking interface of gap junctions. *J Cell Biol.* 1998; 140(5): 1187-1197.
748. Rahman S, Evans WH. Topography of connexin32 in rat liver gap junctions. Evidence for an intramolecular disulphide linkage connecting the two extracellular peptide loops. *J Cell Sci.* 1991; 100 (Pt 3): 567-578.
749. Martin PE, Evans WH. Incorporation of connexins into plasma membranes and gap junctions. *Cardiovasc Res.* 2004; 62(2): 378-387.
750. Beyer EC, Berthoud VM. Gap junction structure: unraveled, but not fully revealed. *F1000Res.* 2017; 6: 568.
751. Maeda S, Nakagawa S, Suga M, Yamashita E, Oshima A, Fujiyoshi Y, Tsukihara T. Structure of the connexin 26 gap junction channel at 3.5 Å resolution. *Nature.* 2009; 458(7238): 597-602.
752. Solan JL, Lampe PD. Spatio-temporal regulation of connexin43 phosphorylation and gap junction dynamics. *Biochim Biophys Acta Biomembr.* 2018; 1860(1): 83-90.
753. Severs NJ. The cardiac gap junction and intercalated disc. *Int J Cardiol.* 1990; 26(2): 137-173.
754. Windoffer R, Beile B, Leibold A, Thomas S, Wilhelm U, Leube RE. Visualization of gap junction mobility in living cells. *Cell Tissue Res.* 2000; 299(3): 347-362.
755. Beardslee MA, Laing JG, Beyer EC, Saffitz JE. Rapid turnover of connexin43 in the adult rat heart. *Circ Res.* 1998; 83(6): 629-635.
756. Fallon RF, Goodenough DA. Five-hour half-life of mouse liver gap-junction protein. *J Cell Biol.* 1981; 90(2): 521-526.
757. Falk MM, Kells RM, Berthoud VM. Degradation of connexins and gap junctions. *FEBS Lett.* 2014; 588(8): 1221-1229.
758. Veenstra RD. Size and selectivity of gap junction channels formed from different connexins. *J Bioenerg Biomembr.* 1996; 28(4): 327-337.
759. Weber PA, Chang HC, Spaeth KE, Nitsche JM, Nicholson BJ. The permeability of gap junction channels to probes of different size is dependent on connexin composition and permeant-pore affinities. *Biophys J.* 2004; 87(2): 958-973.
760. Harris AL. Connexin channel permeability to cytoplasmic molecules. *Prog Biophys Mol Biol.* 2007; 94(1-2): 120-143.
761. Thuringer D, Boucher J, Jégo G, Pernet N, Cronier L, Hammann A, Solary E, Garrido C. Transfer of functional microRNAs between glioblastoma and microvascular endothelial cells through gap junctions. *Oncotarget.* 2016; 7(45): 73925-73934.
762. Welsh DG, Tran CHT, Hald BO, Sancho M. The conducted vasomotor response: function, biophysical basis, and pharmacological control. *Annu Rev Pharmacol Toxicol.* 2018; 58: 391-410.
763. Hald BO, Welsh DG. Conceptualizing conduction as a pliant electrical response: impact of gap junctions and ion channels. *Am J Physiol Heart Circ Physiol.* 2020; 319(6): H1276-h1289.
764. Figueroa XF, Duling BR. Dissection of two Cx37-independent conducted vasodilator mechanisms by deletion of Cx40: electrotonic versus regenerative conduction. *Am J Physiol Heart Circ Physiol.* 2008; 295(5): H2001-2007.

765. Jobs A, Schmidt K, Schmidt VJ, Lübke-meier I, van Veen TA, Kurtz A, Willecke K, de Wit C. Defective Cx40 maintains Cx37 expression but intact Cx40 is crucial for conducted dilations irrespective of hypertension. *Hypertension*. 2012; 60(6): 1422-1429.
766. Alonso F, Boittin FX, Bény JL, Haefliger JA. Loss of connexin40 is associated with decreased endothelium-dependent relaxations and eNOS levels in the mouse aorta. *Am J Physiol Heart Circ Physiol*. 2010; 299(5): H1365-1373.
767. Novielli-Kuntz NM, Jelen M, Barr K, DeLalio LJ, Feng Q, Isakson BE, Gros R, Laird DW. Ablation of both Cx40 and Panx1 results in similar cardiovascular phenotypes exhibited in Cx40 knockout mice. *Biosci Rep*. 2019; 39(2).
768. Jacobsen JC, Sorensen CM. Influence of connexin40 on the renal myogenic response in murine afferent arterioles. *Physiol Rep*. 2015; 3(5).
769. Rodenwaldt B, Pohl U, de Wit C. Endogenous and exogenous NO attenuates conduction of vasoconstrictions along arterioles in the microcirculation. *Am J Physiol Heart Circ Physiol*. 2007; 292(5): H2341-2348.
770. Emerson GG, Neild TO, Segal SS. Conduction of hyperpolarization along hamster feed arteries: augmentation by acetylcholine. *Am J Physiol Heart Circ Physiol*. 2002; 283(1): H102-109.
771. Wölfle SE, Schmidt VJ, Hoyer J, Köhler R, de Wit C. Prominent role of $K_{Ca}3.1$ in endothelium-derived hyperpolarizing factor-type dilations and conducted responses in the microcirculation *in vivo*. *Cardiovasc Res*. 2009; 82(3): 476-483.
772. Meng T, Cheng G, Wei Y, Ma S, Jiang Y, Wu J, Zhou X, Sun C. Exposure to a chronic high-fat diet promotes atrial structure and gap junction remodeling in rats. *Int J Mol Med*. 2017; 40(1): 217-225.
773. Simon AM, McWhorter AR. Vascular abnormalities in mice lacking the endothelial gap junction proteins connexin37 and connexin40. *Dev Biol*. 2002; 251(2): 206-220.
774. Simon AM, Goodenough DA, Li E, Paul DL. Female infertility in mice lacking connexin 37. *Nature*. 1997; 385(6616): 525-529.
775. Kanady JD, Dellinger MT, Munger SJ, Witte MH, Simon AM. Connexin37 and Connexin43 deficiencies in mice disrupt lymphatic valve development and result in lymphatic disorders including lymphedema and chylothorax. *Dev Biol*. 2011; 354(2): 253-266.
776. Sabine A, Agalarov Y, Maby-El Hajjami H, Jaquet M, Hägerling R, Pollmann C, Bebbler D, Pfenniger A, Miura N, Dormond O, Calmes JM, Adams RH, Mäkinen T, Kiefer F, Kwak BR, Petrova TV. Mechanotransduction, PROX1, and FOXC2 cooperate to control connexin37 and calcineurin during lymphatic-valve formation. *Dev Cell*. 2012; 22(2): 430-445.
777. Xue J, Thomas L, Dominguez Rieg JA, Fenton RA, Rieg T. Genetic deletion of connexin 37 causes polyuria and polydipsia. *PLoS One*. 2020; 15(12): e0244251.
778. Fang JS, Angelov SN, Simon AM, Burt JM. Cx37 deletion enhances vascular growth and facilitates ischemic limb recovery. *Am J Physiol Heart Circ Physiol*. 2011; 301(5): H1872-1881.
779. Le Gal L, Pellegrin M, Santoro T, Mazzolai L, Kurtz A, Meda P, Wagner C, Haefliger JA. Connexin37-dependent mechanisms selectively contribute to modulate angiotensin II-mediated hypertension. *J Am Heart Assoc*. 2019; 8(8): e010823.

780. Meens MJ, Alonso F, Le Gal L, Kwak BR, Haefliger JA. Endothelial connexin37 and connexin40 participate in basal but not agonist-induced NO release. *Cell Commun Signal*. 2015; 13: 34.
781. World Health Organization. *The top 10 causes of death*, <<https://www.who.int/news-room/fact-sheets/detail/the-top-10-causes-of-death>> (2020).
782. Anzell AR, Maizy R, Przyklenk K, Sanderson TH. Mitochondrial quality control and disease: insights into ischemia-reperfusion injury. *Mol Neurobiol*. 2018; 55(3): 2547-2564.
783. Genest J, McPherson R, Frohlich J, Anderson T, Campbell N, Carpentier A, Couture P, Dufour R, Fodor G, Francis GA, Grover S, Gupta M, Hegele RA, Lau DC, Leiter L, Lewis GF, Lonn E, Mancini GB, Ng D, Pearson GJ, Sniderman A, Stone JA, Ur E. 2009 Canadian Cardiovascular Society/Canadian guidelines for the diagnosis and treatment of dyslipidemia and prevention of cardiovascular disease in the adult - 2009 recommendations. *Can J Cardiol*. 2009; 25(10): 567-579.
784. Greenland P, Alpert JS, Beller GA, Benjamin EJ, Budoff MJ, Fayad ZA, Foster E, Hlatky MA, Hodgson JM, Kushner FG, Lauer MS, Shaw LJ, Smith SC, Jr., Taylor AJ, Weintraub WS, Wenger NK, Jacobs AK, Smith SC, Jr., Anderson JL, Albert N, Buller CE, Creager MA, Ettinger SM, Guyton RA, Halperin JL, Hochman JS, Kushner FG, Nishimura R, Ohman EM, Page RL, Stevenson WG, Tarkington LG, Yancy CW. 2010 ACCF/AHA guideline for assessment of cardiovascular risk in asymptomatic adults: a report of the American College of Cardiology Foundation/American Heart Association Task Force on Practice Guidelines. *J Am Coll Cardiol*. 2010; 56(25): e50-103.
785. Wong ND. Epidemiological studies of CHD and the evolution of preventive cardiology. *Nat Rev Cardiol*. 2014; 11(5): 276-289.
786. Testai L, Rapposelli S, Martelli A, Breschi MC, Calderone V. Mitochondrial potassium channels as pharmacological target for cardioprotective drugs. *Med Res Rev*. 2015; 35(3): 520-553.
787. Yellon DM, Hausenloy DJ. Myocardial reperfusion injury. *N Engl J Med*. 2007; 357(11): 1121-1135.
788. Lucas DT, Szweda LI. Cardiac reperfusion injury: aging, lipid peroxidation, and mitochondrial dysfunction. *Proc Natl Acad Sci U S A*. 1998; 95(2): 510-514.
789. Hearse DJ, Humphrey SM, Chain EB. Abrupt reoxygenation of the anoxic potassium-arrested perfused rat heart: a study of myocardial enzyme release. *J Mol Cell Cardiol*. 1973; 5(4): 395-407.
790. Zweier JL. Measurement of superoxide-derived free radicals in the reperfused heart. Evidence for a free radical mechanism of reperfusion injury. *J Biol Chem*. 1988; 263(3): 1353-1357.
791. Morel S, Kwak BR. Roles of connexins in atherosclerosis and ischemia-reperfusion injury. *Curr Pharm Biotechnol*. 2012; 13(1): 17-26.
792. Gros DB, Jongsma HJ. Connexins in mammalian heart function. *Bioessays*. 1996; 18(9): 719-730.
793. Delorme B, Dahl E, Jarry-Guichard T, Marics I, Briand JP, Willecke K, Gros D, Théveniau-Ruissy M. Developmental regulation of connexin 40 gene expression in mouse heart correlates with the differentiation of the conduction system. *Dev Dyn*. 1995; 204(4): 358-371.

794. Gu H, Smith FC, Taffet SM, Delmar M. High incidence of cardiac malformations in connexin40-deficient mice. *Circ Res*. 2003; 93(3): 201-206.
795. Gollob MH, Jones DL, Krahn AD, Danis L, Gong XQ, Shao Q, Liu X, Veinot JP, Tang AS, Stewart AF, Tesson F, Klein GJ, Yee R, Skanes AC, Guiraudon GM, Ebihara L, Bai D. Somatic mutations in the connexin 40 gene (GJA5) in atrial fibrillation. *N Engl J Med*. 2006; 354(25): 2677-2688.
796. Delmar M, Makita N. Cardiac connexins, mutations and arrhythmias. *Curr Opin Cardiol*. 2012; 27(3): 236-241.
797. Gemel J, Simon AR, Patel D, Xu Q, Matiukas A, Veenstra RD, Beyer EC. Degradation of a connexin40 mutant linked to atrial fibrillation is accelerated. *J Mol Cell Cardiol*. 2014; 74: 330-339.
798. Zhang F, Bian Y, Huang L, Fan W. Association between connexin 40 and potassium voltage-gated channel subfamily A member 5 expression in the atrial myocytes of patients with atrial fibrillation. *Exp Ther Med*. 2017; 14(5): 5170-5176.
799. Si R, Cabrera JTO, Tsuji-Hosokawa A, Guo R, Watanabe M, Gao L, Lee YS, Moon JS, Scott BT, Wang J, Ashton AW, Rao JN, Wang JY, Yuan JX, Makino A. HuR/Cx40 downregulation causes coronary microvascular dysfunction in type 2 diabetes. *JCI Insight*. 2021; 6(21).
800. Morel S, Braunersreuther V, Chanson M, Bouis D, Rochemont V, Foglia B, Pelli G, Sutter E, Pinsky DJ, Mach F, Kwak BR. Endothelial Cx40 limits myocardial ischaemia/reperfusion injury in mice. *Cardiovasc Res*. 2014; 102(2): 329-337.
801. Flister MJ, Prokop JW, Lazar J, Shimoyama M, Dwinell M, Geurts A. 2015 Guidelines for Establishing Genetically Modified Rat Models for Cardiovascular Research. *J Cardiovasc Transl Res*. 2015; 8(4): 269-277.
802. Clark K, Karsch-Mizrachi I, Lipman DJ, Ostell J, Sayers EW. GenBank. *Nucleic Acids Res*. 2016; 44(D1): D67-72.
803. den Dunnen JT, Dalgleish R, Maglott DR, Hart RK, Greenblatt MS, McGowan-Jordan J, Roux AF, Smith T, Antonarakis SE, Taschner PE. HGVS Recommendations for the Description of Sequence Variants: 2016 Update. *Hum Mutat*. 2016; 37(6): 564-569.
804. Haefliger JA, Bruzzone R, Jenkins NA, Gilbert DJ, Copeland NG, Paul DL. Four novel members of the connexin family of gap junction proteins. Molecular cloning, expression, and chromosome mapping. *J Biol Chem*. 1992; 267(3): 2057-2064.
805. Beyer EC, Reed KE, Westphale EM, Kanter HL, Larson DM. Molecular cloning and expression of rat connexin40, a gap junction protein expressed in vascular smooth muscle. *J Membr Biol*. 1992; 127(1): 69-76.
806. Narang D, Kerr PM, Lunn SE, Beaudry R, Sigurdson J, Lallies MD, Hudson AL, Light PE, Holt A, Plane F. Modulation of resistance artery tone by the trace amine β -phenylethylamine: dual indirect sympathomimetic and α_1 -adrenoceptor blocking actions. *J Pharmacol Exp Ther*. 2014; 351(1): 164-171.
807. Pakdeechote P, Rummery NM, Ralevic V, Dunn WR. Raised tone reveals purinergic-mediated responses to sympathetic nerve stimulation in the rat perfused mesenteric vascular bed. *Eur J Pharmacol*. 2007; 563(1-3): 180-186.
808. Ralevic V, Aberdeen JA, Burnstock G. Acrylamide-induced autonomic neuropathy of rat mesenteric vessels: histological and pharmacological studies. *J Auton Nerv Syst*. 1991; 34(1): 77-87.

809. Kawasaki H, Urabe M, Takasaki K. Enhanced 5-hydroxytryptamine release from vascular adrenergic nerves in spontaneously hypertensive rats. *Hypertension*. 1987; 10(3): 321-327.
810. Kingma JG, Jr., Laher I. Effect of endothelin on sex-dependent regulation of tone in coronary resistance vessels. *Biochem Biophys Res Commun*. 2021; 540: 56-60.
811. Bülow A. Differentiated effects of vasodilators on myogenic reactivity during partial inhibition of myogenic tone in pressurized skeletal muscle small arteries of the rat. *Acta Physiol Scand*. 1996; 157(4): 419-426.
812. Izzard AS, Heagerty AM. Impaired flow-dependent dilatation in distal mesenteric arteries from the spontaneously hypertensive rat. *J Physiol*. 1999; 518(Pt 1): 239-245.
813. Noble RMN, Jahandideh F, Armstrong EA, Bourque SL, Yager JY. Broccoli sprouts promote sex-dependent cardiometabolic health and longevity in Long-Evans rats. *Int J Environ Res Public Health*. 2022; 19(20).
814. Hem NA, Phie J, Chilton L, Kinobe R. A volume-pressure tail cuff method for hemodynamic parameters: Comparison of restraint and light isoflurane anesthesia in normotensive male Lewis rats. *J Pharmacol Toxicol Methods*. 2019; 100: 106601.
815. Daugherty A, Rateri D, Hong L, Balakrishnan A. Measuring blood pressure in mice using volume pressure recording, a tail-cuff method. *J Vis Exp*. 2009;(27).
816. Wang Y, Thatcher SE, Cassis LA. Measuring Blood Pressure Using a Noninvasive Tail Cuff Method in Mice. *Methods Mol Biol*. 2017; 1614: 69-73.
817. Skrzypiec-Spring M, Grotthus B, Szelag A, Schulz R. Isolated heart perfusion according to Langendorff – still viable in the new millennium. *J Pharmacol Toxicol Methods*. 2007; 55(2): 113-126.
818. Alaaeddine R, Elkhatib MAW, Mroueh A, Fouad H, Saad EI, El-Sabban ME, Plane F, El-Yazbi AF. Impaired endothelium-dependent hyperpolarization underlies endothelial dysfunction during early metabolic challenge: increased ROS generation and possible interference with NO function. *J Pharmacol Exp Ther*. 2019; 371(3): 567-582.
819. Al-Assi O, Ghali R, Mroueh A, Kaplan A, Mougharbil N, Eid AH, Zouein FA, El-Yazbi AF. Cardiac autonomic neuropathy as a result of mild hypercaloric challenge in absence of signs of diabetes: modulation by antidiabetic drugs. *Oxid Med Cell Longev*. 2018; 2018: 9389784.
820. Bielohuby M, Bodendorf K, Brandstetter H, Bidlingmaier M, Kienzle E. Predicting metabolisable energy in commercial rat diets: physiological fuel values may be misleading. *Br J Nutr*. 2010; 103(10): 1525-1533.
821. Sánchez-Peña MJ, Márquez-Sandoval F, Ramírez-Anguiano AC, Velasco-Ramírez SF, Macedo-Ojeda G, González-Ortiz LJ. Calculating the metabolizable energy of macronutrients: a critical review of Atwater's results. *Nutr Rev*. 2017; 75(1): 37-48.
822. Wilson C, Lee MD, McCarron JG. Acetylcholine released by endothelial cells facilitates flow-mediated dilatation. *J Physiol*. 2016; 594(24): 7267-7307.
823. Rhoden A, Speiser J, Geertz B, Uebeler J, Schmidt K, de Wit C, Eschenhagen T. Preserved cardiovascular homeostasis despite blunted acetylcholine-induced dilation in mice with endothelial muscarinic M3 receptor deletion. *Acta Physiol (Oxf)*. 2019; 226(1): e13262.
824. Wessler I, Kirkpatrick CJ, Racké K. The cholinergic 'pitfall': acetylcholine, a universal cell molecule in biological systems, including humans. *Clin Exp Pharmacol Physiol*. 1999; 26(3): 198-205.

825. Habermann E. Apamin. *Pharmacol Ther.* 1984; 25(2): 255-270.
826. Sturgill MG, Kelly M, Notterman DA. Pharmacology of the Cardiovascular System in *Pediatric Critical Care (Fourth Edition)*. (eds Fuhrman BP, Zimmerman JJ) Ch. 25, 277-305 (Mosby, 2011).
827. Heesen BJ, De Mey JG. Effects of cyclic AMP-affecting agents on contractile reactivity of isolated mesenteric and renal resistance arteries of the rat. *Br J Pharmacol.* 1990; 101(4): 859-864.
828. Prehn JL, Bevan JA. Facial vein of the rabbit. Intracellularly recorded hyperpolarization of smooth muscle cells induced by beta-adrenergic receptor stimulation. *Circ Res.* 1983; 52(4): 465-470.
829. Abel P, Rorabaugh B. Isoproterenol in *xPharm: The Comprehensive Pharmacology Reference*. (eds Enna SJ, Bylund DB) 1-7 (Elsevier, 2007).
830. Rees DD, Palmer RM, Schulz R, Hodson HF, Moncada S. Characterization of three inhibitors of endothelial nitric oxide synthase in vitro and in vivo. *Br J Pharmacol.* 1990; 101(3): 746-752.
831. Boer R, Ulrich WR, Klein T, Mirau B, Haas S, Baur I. The inhibitory potency and selectivity of arginine substrate site nitric-oxide synthase inhibitors is solely determined by their affinity toward the different isoenzymes. *Mol Pharmacol.* 2000; 58(5): 1026-1034.
832. Arévalo-León LE, Gallardo-Ortíz IA, Urquiza-Marín H, Villalobos-Molina R. Evidence for the role of α_{1D} - and α_{1A} -adrenoceptors in contraction of the rat mesenteric artery. *Vascul Pharmacol.* 2003; 40(2): 91-96.
833. Minneman KP, Theroux TL, Hollinger S, Han C, Esbenshade TA. Selectivity of agonists for cloned α_1 -adrenergic receptor subtypes. *Mol Pharmacol.* 1994; 46(5): 929-936.
834. Shen JB, Jiang B, Pappano AJ. Comparison of L-type calcium channel blockade by nifedipine and/or cadmium in guinea pig ventricular myocytes. *J Pharmacol Exp Ther.* 2000; 294(2): 562-570.
835. Stork AP, Cocks TM. Pharmacological reactivity of human epicardial coronary arteries: phasic and tonic responses to vasoconstrictor agents differentiated by nifedipine. *Br J Pharmacol.* 1994; 113(4): 1093-1098.
836. Cosconati S, Marinelli L, Lavecchia A, Novellino E. Characterizing the 1,4-dihydropyridines binding interactions in the L-type Ca^{2+} channel: model construction and docking calculations. *J Med Chem.* 2007; 50(7): 1504-1513.
837. Grand T, Demion M, Norez C, Mettey Y, Launay P, Becq F, Bois P, Guinamard R. 9-phenanthrol inhibits human TRPM4 but not TRPM5 cationic channels. *Br J Pharmacol.* 2008; 153(8): 1697-1705.
838. Guinamard R, Hof T, Del Negro CA. The TRPM4 channel inhibitor 9-phenanthrol. *Br J Pharmacol.* 2014; 171(7): 1600-1613.
839. Tanoue A, Nasa Y, Koshimizu T, Shinoura H, Oshikawa S, Kawai T, Sunada S, Takeo S, Tsujimoto G. The α_{1D} -adrenergic receptor directly regulates arterial blood pressure via vasoconstriction. *J Clin Invest.* 2002; 109(6): 765-775.
840. Piascik MT, Hrometz SL, Edelmann SE, Guarino RD, Hadley RW, Brown RD. Immunocytochemical localization of the alpha-1B adrenergic receptor and the contribution of this and the other subtypes to vascular smooth muscle contraction: analysis with selective ligands and antisense oligonucleotides. *J Pharmacol Exp Ther.* 1997; 283(2): 854-868.

841. Chen S, Xu M, Lin F, Lee D, Riek P, Graham RM. Phe³¹⁰ in transmembrane VI of the α_{1B} -adrenergic receptor is a key switch residue involved in activation and catecholamine ring aromatic bonding. *J Biol Chem*. 1999; 274(23): 16320-16330.
842. Hussain MB, Marshall I. Characterization of α_1 -adrenoceptor subtypes mediating contractions to phenylephrine in rat thoracic aorta, mesenteric artery and pulmonary artery. *Br J Pharmacol*. 1997; 122(5): 849-858.
843. Taddei C, Poggesi E, Leonardi A, Testa R. Affinity of different α_1 -agonists and antagonists for the α_1 -adrenoceptors of rabbit and rat liver membranes. *Life Sci*. 1993; 53(12): P1177-181.
844. Angus JA, Broughton A, Mulvany MJ. Role of α -adrenoceptors in constrictor responses of rat, guinea-pig and rabbit small arteries to neural activation. *J Physiol*. 1988; 403: 495-510.
845. Coleman RA, Humphrey PP, Kennedy I, Levy GP, Lumley P. Comparison of the actions of U-46619, a prostaglandin H₂-analogue, with those of prostaglandin H₂ and thromboxane A₂ on some isolated smooth muscle preparations. *Br J Pharmacol*. 1981; 73(3): 773-778.
846. Mufti RE, Zechariah A, Sancho M, Mazumdar N, Brett SE, Welsh DG. Implications of $\alpha_v\beta_3$ integrin signaling in the regulation of Ca²⁺ waves and myogenic tone in cerebral arteries. *Arterioscler Thromb Vasc Biol*. 2015; 35(12): 2571-2578.
847. Mironova GY, Mazumdar N, Hashad AM, El-Lakany MA, Welsh DG. Defining a role of NADPH oxidase in myogenic tone development. *Microcirculation*. 2022; 29(3): e12756.
848. Yasuda N, Miura S, Akazawa H, Tanaka T, Qin Y, Kiya Y, Imaizumi S, Fujino M, Ito K, Zou Y, Fukuhara S, Kunimoto S, Fukuzaki K, Sato T, Ge J, Mochizuki N, Nakaya H, Saku K, Komuro I. Conformational switch of angiotensin II type 1 receptor underlying mechanical stress-induced activation. *EMBO Rep*. 2008; 9(2): 179-186.
849. Schleifenbaum J, Kassmann M, Szijártó IA, Hercule HC, Tano JY, Weinert S, Heidenreich M, Pathan AR, Anistan YM, Alenina N, Rusch NJ, Bader M, Jentsch TJ, Gollasch M. Stretch-activation of angiotensin II type 1_a receptors contributes to the myogenic response of mouse mesenteric and renal arteries. *Circ Res*. 2014; 115(2): 263-272.
850. Hong K, Zhao G, Hong Z, Sun Z, Yang Y, Clifford PS, Davis MJ, Meininger GA, Hill MA. Mechanical activation of angiotensin II type 1 receptors causes actin remodelling and myogenic responsiveness in skeletal muscle arterioles. *J Physiol*. 2016; 594(23): 7027-7047.
851. Yamasaki E, Ali S, Sanchez Solano A, Thakore P, Smith M, Wang X, Labelle-Dumais C, Gould DB, Earley S. Faulty TRPM4 channels underlie age-dependent cerebral vascular dysfunction in Gould syndrome. *Proc Natl Acad Sci U S A*. 2023; 120(5): e2217327120.
852. Hurley M, Kaur S, Walton R, Power A, Haïssaguerre M, Bernus O, Ward ML, White E. Endocardial role in arrhythmias induced by acute ventricular stretch and the involvement of Purkinje fibres, in isolated rat hearts. *Curr Res Physiol*. 2023; 6: 100098.
853. Ma P, Huang N, Tang J, Zhou Z, Xu J, Chen Y, Zhang M, Huang Q, Cheng Y. The TRPM4 channel inhibitor 9-phenanthrol alleviates cerebral edema after traumatic brain injury in rats. *Front Pharmacol*. 2023; 14: 1098228.
854. Kim BJ, Kim SY, Lee S, Jeon JH, Matsui H, Kwon YK, Kim SJ, So I. The role of transient receptor potential channel blockers in human gastric cancer cell viability. *Can J Physiol Pharmacol*. 2012; 90(2): 175-186.

855. Veress R, Baranyai D, Hegyi B, Kistamás K, Dienes C, Magyar J, Bányász T, Nánási PP, Szentandrassy N, Horváth B. Transient receptor potential melastatin 4 channel inhibitor 9-phenanthrol inhibits K(+) but not Ca(2+) currents in canine ventricular myocytes. *Can J Physiol Pharmacol*. 2018; 96(10): 1022-1029.
856. Burris SK, Wang Q, Bulley S, Neeb ZP, Jaggar JH. 9-Phenanthrol inhibits recombinant and arterial myocyte TMEM16A channels. *Br J Pharmacol*. 2015; 172(10): 2459-2468.
857. Garland CJ, Smirnov SV, Bagher P, Lim CS, Huang CY, Mitchell R, Stanley C, Pinkney A, Dora KA. TRPM4 inhibitor 9-phenanthrol activates endothelial cell intermediate conductance calcium-activated potassium channels in rat isolated mesenteric artery. *Br J Pharmacol*. 2015; 172(4): 1114-1123.
858. Simard C, Sallé L, Rouet R, Guinamard R. Transient receptor potential melastatin 4 inhibitor 9-phenanthrol abolishes arrhythmias induced by hypoxia and re-oxygenation in mouse ventricle. *Br J Pharmacol*. 2012; 165(7): 2354-2364.
859. Simard C, Hof T, Keddache Z, Launay P, Guinamard R. The TRPM4 non-selective cation channel contributes to the mammalian atrial action potential. *J Mol Cell Cardiol*. 2013; 59: 11-19.
860. Back G, Strubelt O. Seasonal variations of cardiac output in rats. *Experientia*. 1975; 31(11): 1304-1306.
861. Konior A, Klemenska E, Brudek M, Podolecka E, Czarnowska E, Beręsewicz A. Seasonal superoxide overproduction and endothelial activation in guinea-pig heart; seasonal oxidative stress in rats and humans. *J Mol Cell Cardiol*. 2011; 50(4): 686-694.
862. Ahlersová E, Ahlers I, Garlátiová E, Toropila M, Smajda B. Influence of the seasons on the circadian rhythm of blood glucose and tissue glycogen in male Wistar rats. *Physiol Bohemoslov*. 1982; 31(1): 45-55.
863. Arullampalam P, Preti B, Ross-Kaschitza D, Lochner M, Rougier JS, Abriel H. Species-specific effects of cation channel TRPM4 small-molecule inhibitors. *Front Pharmacol*. 2021; 12: 712354.
864. Kawata N, Kondo R, Suzuki Y, Yamamura H. Increased TMEM16A-mediated Ca²⁺-activated Cl⁻ currents in portal vein smooth muscle cells of caveolin 1-deficient mice. *Biol Pharm Bull*. 2022; 45(11): 1692-1698.
865. Seo Y, Lee HK, Park J, Jeon DK, Jo S, Jo M, Namkung W. Ani9, a novel potent small-molecule ANO1 inhibitor with negligible effect on ANO2. *PLoS One*. 2016; 11(5): e0155771.
866. Al-Hosni R, Ilkan Z, Agostinelli E, Tammaro P. The pharmacology of the TMEM16A channel: therapeutic opportunities. *Trends Pharmacol Sci*. 2022; 43(9): 712-725.
867. Liu S, Feng J, Luo J, Yang P, Brett TJ, Hu H. Eact, a small molecule activator of TMEM16A, activates TRPV1 and elicits pain- and itch-related behaviours. *Br J Pharmacol*. 2016; 173(7): 1208-1218.
868. Namkung W, Yao Z, Finkbeiner WE, Verkman AS. Small-molecule activators of TMEM16A, a calcium-activated chloride channel, stimulate epithelial chloride secretion and intestinal contraction. *Faseb j*. 2011; 25(11): 4048-4062.
869. Crnich R, Amberg GC, Leo MD, Gonzales AL, Tamkun MM, Jaggar JH, Earley S. Vasoconstriction resulting from dynamic membrane trafficking of TRPM4 in vascular smooth muscle cells. *Am J Physiol Cell Physiol*. 2010; 299(3): C682-694.
870. Moccia F, Berra-Romani R, Tanzi F. Update on vascular endothelial Ca²⁺ signalling: A tale of ion channels, pumps and transporters. *World J Biol Chem*. 2012; 3(7): 127-158.

871. Fantozzi I, Zhang S, Platoshyn O, Remillard CV, Cowling RT, Yuan JX. Hypoxia increases AP-1 binding activity by enhancing capacitative Ca^{2+} entry in human pulmonary artery endothelial cells. *Am J Physiol Lung Cell Mol Physiol*. 2003; 285(6): L1233-1245.
872. Gerzanich V, Woo SK, Vennekens R, Tsybalyuk O, Ivanova S, Ivanov A, Geng Z, Chen Z, Nilius B, Flockerzi V, Freichel M, Simard JM. *De novo* expression of Trpm4 initiates secondary hemorrhage in spinal cord injury. *Nat Med*. 2009; 15(2): 185-191.
873. Gottlieb P, Folgering J, Maroto R, Raso A, Wood TG, Kurosky A, Bowman C, Bichet D, Patel A, Sachs F, Martinac B, Hamill OP, Honoré E. Revisiting TRPC1 and TRPC6 mechanosensitivity. *Pflugers Arch*. 2008; 455(6): 1097-1103.
874. Nemeth Z, Hildebrandt E, Ryan MJ, Granger JP, Drummond HA. Pressure-induced constriction of the middle cerebral artery is abolished in TrpC6 knockout mice. *Am J Physiol Heart Circ Physiol*. 2020; 319(1): H42-h50.
875. Hill-Eubanks DC, Gonzales AL, Sonkusare SK, Nelson MT. Vascular TRP channels: performing under pressure and going with the flow. *Physiology (Bethesda)*. 2014; 29(5): 343-360.
876. Knot HJ, Standen NB, Nelson MT. Ryanodine receptors regulate arterial diameter and wall $[Ca^{2+}]$ in cerebral arteries of rat via Ca^{2+} -dependent K^+ channels. *J Physiol*. 1998; 508 (Pt 1)(Pt 1): 211-221.
877. Gul H, Yildiz O, Simsek A, Balkan M, Ersoz N, Cetiner S, Isimer A, Sen D. Pharmacologic characterization of contractile serotonergic receptors in human isolated mesenteric artery. *J Cardiovasc Pharmacol*. 2003; 41(2): 307-315.
878. Watts SW. Serotonin-induced contraction in mesenteric resistance arteries: signaling and changes in deoxycorticosterone acetate-salt hypertension. *Hypertension*. 2002; 39(3): 825-829.
879. Sung DJ, Noh HJ, Kim JG, Park SW, Kim B, Cho H, Bae YM. Serotonin contracts the rat mesenteric artery by inhibiting 4-aminopyridine-sensitive K_v channels via the 5-HT_{2A} receptor and Src tyrosine kinase. *Exp Mol Med*. 2013; 45(12): e67.
880. McCarron JG, Osol G, Halpern W. Myogenic responses are independent of the endothelium in rat pressurized posterior cerebral arteries. *Blood Vessels*. 1989; 26(5): 315-319.
881. Adebisi A, Zhao G, Cheranov SY, Ahmed A, Jaggar JH. Caveolin-1 abolishment attenuates the myogenic response in murine cerebral arteries. *Am J Physiol Heart Circ Physiol*. 2007; 292(3): H1584-1592.
882. Earley S, Straub SV, Brayden JE. Protein kinase C regulates vascular myogenic tone through activation of TRPM4. *Am J Physiol Heart Circ Physiol*. 2007; 292(6): H2613-2622.
883. Sonoyama K, Greenstein AS, Micheletti R, Ferrari P, Schiavone A, Aghamohammadzadeh R, Withers SB, Tripodi G, Ferrandi M, Heagerty AM. Mutation in the beta adducin subunit causes tissue-specific damage to myogenic tone. *J Hypertens*. 2011; 29(3): 466-474.
884. Kotecha N, Hill MA. Myogenic contraction in rat skeletal muscle arterioles: smooth muscle membrane potential and Ca^{2+} signaling. *Am J Physiol Heart Circ Physiol*. 2005; 289(4): H1326-1334.

885. Ochodnický P, Henning RH, Buikema HJ, de Zeeuw D, Provoost AP, van Dokkum RP. Renal vascular dysfunction precedes the development of renal damage in the hypertensive Fawn-Hooded rat. *Am J Physiol Renal Physiol*. 2010; 298(3): F625-633.
886. Uchida E, Bohr DF. Myogenic tone in isolated perfused resistance vessels from rats. *Am J Physiol*. 1969; 216(6): 1343-1350.
887. Hemmings DG, Veerareddy S, Baker PN, Davidge ST. Increased myogenic responses in uterine but not mesenteric arteries from pregnant offspring of diet-restricted rat dams. *Biol Reprod*. 2005; 72(4): 997-1003.
888. Learmont JG, Cockell AP, Knock GA, Poston L. Myogenic and flow-mediated responses in isolated mesenteric small arteries from pregnant and nonpregnant rats. *Am J Obstet Gynecol*. 1996; 174(5): 1631-1636.
889. Looft-Wilson RC, Gisolfi CV. Rat small mesenteric artery function after hindlimb suspension. *J Appl Physiol (1985)*. 2000; 88(4): 1199-1206.
890. Dunn SM, Hilgers R, Das KC. Decreased EDHF-mediated relaxation is a major mechanism in endothelial dysfunction in resistance arteries in aged mice on prolonged high-fat sucrose diet. *Physiol Rep*. 2017; 5(23).
891. Cockell AP, Poston L. Isolated mesenteric arteries from pregnant rats show enhanced flow-mediated relaxation but normal myogenic tone. *J Physiol*. 1996; 495 (Pt 2)(Pt 2): 545-551.
892. Sun D, Messina EJ, Kaley G, Koller A. Characteristics and origin of myogenic response in isolated mesenteric arterioles. *Am J Physiol*. 1992; 263(5 Pt 2): H1486-1491.
893. Johnson PC. Autoregulatory responses of cat mesenteric arterioles measured in vivo. *Circ Res*. 1968; 22(2): 199-212.
894. Johnson PC. The Myogenic Response in *Handbook of Physiology, The Cardiovascular System, Vascular Smooth Muscle*. Vol. II Ch. 15, 409-442 (1981).
895. Davis AJ, Forrest AS, Jepps TA, Valencik ML, Wiwchar M, Singer CA, Sones WR, Greenwood IA, Leblanc N. Expression profile and protein translation of TMEM16A in murine smooth muscle. *Am J Physiol Cell Physiol*. 2010; 299(5): C948-959.
896. Leo MD, Peixoto-Nieves D, Yin W, Raghavan S, Muralidharan P, Mata-Daboïn A, Jaggar JH. TMEM16A channel upregulation in arterial smooth muscle cells produces vasoconstriction during diabetes. *Am J Physiol Heart Circ Physiol*. 2021; 320(3): H1089-h1101.
897. Kondo R, Furukawa N, Deguchi A, Kawata N, Suzuki Y, Imaizumi Y, Yamamura H. Downregulation of Ca²⁺-activated Cl⁻ channel TMEM16A mediated by angiotensin II in cirrhotic portal hypertensive mice. *Front Pharmacol*. 2022; 13: 831311.
898. Heinze C, Seniuk A, Sokolov MV, Huebner AK, Klementowicz AE, Szijártó IA, Schleifenbaum J, Vitzthum H, Gollasch M, Ehmke H, Schroeder BC, Hübner CA. Disruption of vascular Ca²⁺-activated chloride currents lowers blood pressure. *J Clin Invest*. 2014; 124(2): 675-686.
899. van Rijen H, van Kempen MJ, Analbers LJ, Rook MB, van Ginneken AC, Gros D, Jongsma HJ. Gap junctions in human umbilical cord endothelial cells contain multiple connexins. *Am J Physiol*. 1997; 272(1 Pt 1): C117-130.
900. Gustafsson F, Mikkelsen HB, Arensbak B, Thuneberg L, Neve S, Jensen LJ, Holstein-Rathlou NH. Expression of connexin 37, 40 and 43 in rat mesenteric arterioles and resistance arteries. *Histochem Cell Biol*. 2003; 119(2): 139-148.

901. Mather S, Dora KA, Sandow SL, Winter P, Garland CJ. Rapid endothelial cell-selective loading of connexin 40 antibody blocks endothelium-derived hyperpolarizing factor dilation in rat small mesenteric arteries. *Circ Res.* 2005; 97(4): 399-407.
902. Matchkov VV, Rahman A, Bakker LM, Griffith TM, Nilsson H, Aalkjær C. Analysis of effects of connexin-mimetic peptides in rat mesenteric small arteries. *Am J Physiol Heart Circ Physiol.* 2006; 291(1): H357-367.
903. Ellis A, Goto K, Chaston DJ, Brackenbury TD, Meaney KR, Falck JR, Wojcikiewicz RJ, Hill CE. Enalapril treatment alters the contribution of epoxyeicosatrienoic acids but not gap junctions to endothelium-derived hyperpolarizing factor activity in mesenteric arteries of spontaneously hypertensive rats. *J Pharmacol Exp Ther.* 2009; 330(2): 413-422.
904. Haddock RE, Grayson TH, Brackenbury TD, Meaney KR, Neylon CB, Sandow SL, Hill CE. Endothelial coordination of cerebral vasomotion via myoendothelial gap junctions containing connexins 37 and 40. *Am J Physiol Heart Circ Physiol.* 2006; 291(5): H2047-2056.
905. Yu J, Bihari A, Lidington D, Tysl K. Gap junction uncouplers attenuate arteriolar response to distal capillary stimuli. *Microvasc Res.* 2000; 59(1): 162-168.
906. Matchkov VV, Rahman A, Peng H, Nilsson H, Aalkjær C. Junctional and nonjunctional effects of heptanol and glycyrrhetic acid derivatives in rat mesenteric small arteries. *Br J Pharmacol.* 2004; 142(6): 961-972.
907. Chaytor AT, Marsh WL, Hutcheson IR, Griffith TM. Comparison of glycyrrhetic acid isoforms and carbenoxolone as inhibitors of EDHF-type relaxations mediated via gap junctions. *Endothelium.* 2000; 7(4): 265-278.
908. Délèze J, Hervé JC. Effect of several uncouplers of cell-to-cell communication on gap junction morphology in mammalian heart. *J Membr Biol.* 1983; 74(3): 203-215.
909. Guo Y, Martinez-Williams C, Gilbert KA, Rannels DE. Inhibition of gap junction communication in alveolar epithelial cells by 18 α -glycyrrhetic acid. *Am J Physiol.* 1999; 276(6): L1018-1026.
910. Bastiaanse EM, Jongsma HJ, van der Laarse A, Takens-Kwak BR. Heptanol-induced decrease in cardiac gap junctional conductance is mediated by a decrease in the fluidity of membranous cholesterol-rich domains. *J Membr Biol.* 1993; 136(2): 135-145.
911. Bernardini G, Peracchia C, Peracchia LL. Reversible effects of heptanol on gap junction structure and cell-to-cell electrical coupling. *Eur J Cell Biol.* 1984; 34(2): 307-312.
912. Buckley C, Zhang X, Wilson C, McCarron JG. Carbenoxolone and 18 β -glycyrrhetic acid inhibit inositol 1,4,5-trisphosphate-mediated endothelial cell calcium signalling and depolarise mitochondria. *Br J Pharmacol.* 2021; 178(4): 896-912.
913. King DR, Sedovy MW, Leng X, Xue J, Lamouille S, Koval M, Isakson BE, Johnstone SR. Mechanisms of connexin regulating peptides. *Int J Mol Sci.* 2021; 22(19).
914. Chaytor AT, Evans WH, Griffith TM. Peptides homologous to extracellular loop motifs of connexin 43 reversibly abolish rhythmic contractile activity in rabbit arteries. *J Physiol.* 1997; 503 (Pt 1)(Pt 1): 99-110.
915. Warner A, Clements DK, Parikh S, Evans WH, DeHaan RL. Specific motifs in the external loops of connexin proteins can determine gap junction formation between chick heart myocytes. *J Physiol.* 1995; 488 (Pt 3)(Pt 3): 721-728.
916. Evans WH, Leybaert L. Mimetic peptides as blockers of connexin channel-facilitated intercellular communication. *Cell Commun Adhes.* 2007; 14(6): 265-273.

917. Leybaert L, Lampe PD, Dhein S, Kwak BR, Ferdinandy P, Beyer EC, Laird DW, Naus CC, Green CR, Schulz R. Connexins in cardiovascular and neurovascular health and disease: pharmacological implications. *Pharmacol Rev.* 2017; 69(4): 396-478.
918. Chaytor AT, Martin PE, Edwards DH, Griffith TM. Gap junctional communication underpins EDHF-type relaxations evoked by ACh in the rat hepatic artery. *Am J Physiol Heart Circ Physiol.* 2001; 280(6): H2441-2450.
919. Chaytor AT, Martin PE, Evans WH, Randall MD, Griffith TM. The endothelial component of cannabinoid-induced relaxation in rabbit mesenteric artery depends on gap junctional communication. *J Physiol.* 1999; 520 Pt 2(Pt 2): 539-550.
920. Martin PE, Wall C, Griffith TM. Effects of connexin-mimetic peptides on gap junction functionality and connexin expression in cultured vascular cells. *Br J Pharmacol.* 2005; 144(5): 617-627.
921. Billaud M, Dahan D, Marthan R, Savineau JP, Guibert C. Role of the gap junctions in the contractile response to agonists in pulmonary artery from two rat models of pulmonary hypertension. *Respir Res.* 2011; 12(1): 30.
922. Ebong EE, Depaola N. Specificity in the participation of connexin proteins in flow-induced endothelial gap junction communication. *Pflugers Arch.* 2013; 465(9): 1293-1302.
923. Sandow SL, Goto K, Rummery NM, Hill CE. Developmental changes in myoendothelial gap junction mediated vasodilator activity in the rat saphenous artery. *J Physiol.* 2004; 556(Pt 3): 875-886.
924. Rummery NM, Hill CE. Vascular gap junctions and implications for hypertension. *Clin Exp Pharmacol Physiol.* 2004; 31(10): 659-667.
925. Earley S, Resta TC, Walker BR. Disruption of smooth muscle gap junctions attenuates myogenic vasoconstriction of mesenteric resistance arteries. *Am J Physiol Heart Circ Physiol.* 2004; 287(6): H2677-2686.
926. Wang N, De Bock M, Antoons G, Gadicherla AK, Bol M, Decrock E, Evans WH, Sipido KR, Bukauskas FF, Leybaert L. Connexin mimetic peptides inhibit Cx43 hemichannel opening triggered by voltage and intracellular Ca²⁺ elevation. *Basic Res Cardiol.* 2012; 107(6): 304.
927. Goodenough DA, Simon AM, Paul DL. Gap junctional intercellular communication in the mouse ovarian follicle. *Novartis Found Symp.* 1999; 219: 226-235; discussion 235-240.
928. Simon AM, Chen H, Jackson CL. Cx37 and Cx43 localize to zona pellucida in mouse ovarian follicles. *Cell Commun Adhes.* 2006; 13(1-2): 61-77.
929. Dominguez Rieg JA, Burt JM, Ruth P, Rieg T. P2Y₂ receptor activation decreases blood pressure via intermediate conductance potassium channels and connexin 37. *Acta Physiol (Oxf).* 2015; 213(3): 628-641.
930. Undavia SS, Berger V, Kaley G, Messina EJ. Myogenic responses of isolated adipose tissue arterioles. *Microvasc Res.* 2003; 66(2): 140-146.
931. Bai N, Moien-Afshari F, Washio H, Min A, Laher I. Pharmacology of the mouse-isolated cerebral artery. *Vascul Pharmacol.* 2004; 41(3): 97-106.
932. Lagaud GJ, Masih-Khan E, Kai S, van Breemen C, Dubé GP. Influence of type II diabetes on arterial tone and endothelial function in murine mesenteric resistance arteries. *J Vasc Res.* 2001; 38(6): 578-589.

933. Bennett MV, Barrio LC, Bargiello TA, Spray DC, Hertzberg E, Sáez JC. Gap junctions: new tools, new answers, new questions. *Neuron*. 1991; 6(3): 305-320.
934. Laird DW. Life cycle of connexins in health and disease. *Biochem J*. 2006; 394(Pt 3): 527-543.
935. Nishi M, Kumar NM, Gilula NB. Developmental regulation of gap junction gene expression during mouse embryonic development. *Dev Biol*. 1991; 146(1): 117-130.
936. Valdimarsson G, De Sousa PA, Beyer EC, Paul DL, Kidder GM. Zygotic expression of the connexin43 gene supplies subunits for gap junction assembly during mouse preimplantation development. *Mol Reprod Dev*. 1991; 30(1): 18-26.
937. De Sousa PA, Valdimarsson G, Nicholson BJ, Kidder GM. Connexin trafficking and the control of gap junction assembly in mouse preimplantation embryos. *Development*. 1993; 117(4): 1355-1367.
938. Reaume AG, de Sousa PA, Kulkarni S, Langille BL, Zhu D, Davies TC, Juneja SC, Kidder GM, Rossant J. Cardiac malformation in neonatal mice lacking connexin43. *Science*. 1995; 267(5205): 1831-1834.
939. Morley GE, Vaidya D, Samie FH, Lo C, Delmar M, Jalife J. Characterization of conduction in the ventricles of normal and heterozygous Cx43 knockout mice using optical mapping. *J Cardiovasc Electrophysiol*. 1999; 10(10): 1361-1375.
940. Evans WH, Martin PE. Gap junctions: structure and function (Review). *Mol Membr Biol*. 2002; 19(2): 121-136.
941. Rozental R, Giaume C, Spray DC. Gap junctions in the nervous system. *Brain Res Brain Res Rev*. 2000; 32(1): 11-15.
942. Rozental R, Srinivas M, Gökhan S, Urban M, Dermietzel R, Kessler JA, Spray DC, Mehler MF. Temporal expression of neuronal connexins during hippocampal ontogeny. *Brain Res Brain Res Rev*. 2000; 32(1): 57-71.
943. Cina C, Bechberger JF, Ozog MA, Naus CC. Expression of connexins in embryonic mouse neocortical development. *J Comp Neurol*. 2007; 504(3): 298-313.
944. Chang Q, Gonzalez M, Pinter MJ, Balice-Gordon RJ. Gap junctional coupling and patterns of connexin expression among neonatal rat lumbar spinal motor neurons. *J Neurosci*. 1999; 19(24): 10813-10828.
945. Chen W, Guo Y, Yang W, Zheng P, Zeng J, Tong W. Involvement of autophagy in connexin 40 reduction in the late phase of traumatic brain injury in rats. *Brain Res Bull*. 2017; 131: 100-106.
946. Chen B, Sun L, Wu X, Ma J. Correlation between connexin and traumatic brain injury in patients. *Brain Behav*. 2017; 7(9): e00770.
947. Chen W, Guo Y, Yang W, Zheng P, Zeng J, Tong W. Connexin40 correlates with oxidative stress in brains of traumatic brain injury rats. *Restor Neurol Neurosci*. 2017; 35(2): 217-224.
948. Condorelli DF, Trovato-Salinaro A, Mudò G, Mirone MB, Belluardo N. Cellular expression of connexins in the rat brain: neuronal localization, effects of kainate-induced seizures and expression in apoptotic neuronal cells. *Eur J Neurosci*. 2003; 18(7): 1807-1827.
949. Wang YF, Daniel EE. Gap junctions in gastrointestinal muscle contain multiple connexins. *Am J Physiol Gastrointest Liver Physiol*. 2001; 281(2): G533-543.

950. Cho WJ, Daniel EE. Proteins of interstitial cells of Cajal and intestinal smooth muscle, colocalized with caveolin-1. *Am J Physiol Gastrointest Liver Physiol.* 2005; 288(3): G571-585.
951. Li C, Fu J, Liu H, Yang H, Yao L, You K, Xue X. Hyperoxia arrests pulmonary development in newborn rats via disruption of endothelial tight junctions and downregulation of Cx40. *Mol Med Rep.* 2014; 10(1): 61-67.
952. Yin J, Lv L, Zhai P, Long T, Zhou Q, Pan H, Botwe G, Wang L, Wang Q, Tan L, Kuebler WM. Connexin 40 regulates lung endothelial permeability in acute lung injury via the ROCK1-MYPT1-MLC20 pathway. *Am J Physiol Lung Cell Mol Physiol.* 2019; 316(1): L35-144.
953. Hanner F, Sorensen CM, Holstein-Rathlou NH, Peti-Peterdi J. Connexins and the kidney. *Am J Physiol Regul Integr Comp Physiol.* 2010; 298(5): R1143-1155.
954. Nakamura K, Kuraoka A, Kawabuchi M, Shibata Y. Specific localization of gap junction protein, connexin45, in the deep muscular plexus of dog and rat small intestine. *Cell Tissue Res.* 1998; 292(3): 487-494.
955. More HL, Braam B, Cupples WA. Reduced tubuloglomerular feedback activity and absence of its synchronization in a connexin40 knockout rat. *Front Netw Physiol.* 2023; 3: 1208303.
956. Bermudez E, Willson G, Parkinson H, Dodd D. Toxicity of methyl tertiary-butyl ether (MTBE) following exposure of Wistar Rats for 13 weeks or one year via drinking water. *J Appl Toxicol.* 2012; 32(9): 687-706.
957. Bauman DH, Richerson JT, Britt AL. A comparison of body and organ weights, physiologic parameters, and pathologic changes in target organs of rats given combinations of exercise, anabolic hormone, and protein supplementation. *Am J Sports Med.* 1988; 16(4): 397-402.
958. Derwand D, Zierau O, Thieme D, Keiler AM. Up to the maximum — testosterone dose-dependent effects on anabolic and androgen responsive tissues in orchietomized rats. *Andrology.* 2023.
959. Saffitz JE, Kanter HL, Green KG, Tolley TK, Beyer EC. Tissue-specific determinants of anisotropic conduction velocity in canine atrial and ventricular myocardium. *Circ Res.* 1994; 74(6): 1065-1070.
960. Lin X, Gemel J, Glass A, Zemlin CW, Beyer EC, Veenstra RD. Connexin40 and connexin43 determine gating properties of atrial gap junction channels. *J Mol Cell Cardiol.* 2010; 48(1): 238-245.
961. Pogoda K, Kameritsch P. Molecular regulation of myoendothelial gap junctions. *Curr Opin Pharmacol.* 2019; 45: 16-22.
962. Figueroa XF, Lillo MA, Gaete PS, Riquelme MA, Sáez JC. Diffusion of nitric oxide across cell membranes of the vascular wall requires specific connexin-based channels. *Neuropharmacology.* 2013; 75: 471-478.
963. Pogoda K, Füller M, Pohl U, Kameritsch P. NO, via its target Cx37, modulates calcium signal propagation selectively at myoendothelial gap junctions. *Cell Commun Signal.* 2014; 12: 33.
964. Chaston DJ, Baillie BK, Grayson TH, Courjaret RJ, Heisler JM, Lau KA, Machaca K, Nicholson BJ, Ashton A, Matthaai KI, Hill CE. Polymorphism in endothelial connexin40 enhances sensitivity to intraluminal pressure and increases arterial stiffness. *Arterioscler Thromb Vasc Biol.* 2013; 33(5): 962-970.

965. Fang JS, Angelov SN, Simon AM, Burt JM. Compromised regulation of tissue perfusion and arteriogenesis limit, in an AT₁R-independent fashion, recovery of ischemic tissue in Cx40^{-/-} mice. *Am J Physiol Heart Circ Physiol*. 2013; 304(6): H816-827.
966. Cantin M, Araujo-Nascimento MD, Benchimol S, Desormeaux Y. Metaplasia of smooth muscle cells into juxtaglomerular cells in the juxtaglomerular apparatus, arteries, and arterioles of the ischemic (endocrine) kidney. An ultrastructural-cytochemical and autoradiographic study. *Am J Pathol*. 1977; 87(3): 581-602.
967. Yamaguchi H, Gomez RA, Sequeira-Lopez MLS. Renin cells, from vascular development to blood pressure sensing. *Hypertension*. 2023; 80(8): 1580-1589.
968. Schweda F, Friis U, Wagner C, Skott O, Kurtz A. Renin release. *Physiology (Bethesda)*. 2007; 22: 310-319.
969. Martini AG, Danser AHJ. Juxtaglomerular cell phenotypic plasticity. *High Blood Press Cardiovasc Prev*. 2017; 24(3): 231-242.
970. Sequeira-Lopez MLS, Gomez RA. Renin cells, the kidney, and hypertension. *Circ Res*. 2021; 128(7): 887-907.
971. Yang X, Zeng H, Wang L, Luo S, Zhou Y. Activation of Piezo1 downregulates renin in juxtaglomerular cells and contributes to blood pressure homeostasis. *Cell Biosci*. 2022; 12(1): 197.
972. Ortiz-Capisano MC, Ortiz PA, Harding P, Garvin JL, Beierwaltes WH. Decreased intracellular calcium stimulates renin release via calcium-inhibitable adenylyl cyclase. *Hypertension*. 2007; 49(1): 162-169.
973. Potolicchio I, Cigliola V, Velazquez-Garcia S, Klee P, Valjevac A, Kapic D, Cosovic E, Lepara O, Hadzovic-Dzuvo A, Mornjacovic Z, Meda P. Connexin-dependent signaling in neuro-hormonal systems. *Biochim Biophys Acta*. 2012; 1818(8): 1919-1936.
974. Krattinger N, Capponi A, Mazzolai L, Aubert JF, Caille D, Nicod P, Waeber G, Meda P, Haefliger JA. Connexin40 regulates renin production and blood pressure. *Kidney Int*. 2007; 72(7): 814-822.
975. Zhang J, Hill CE. Differential connexin expression in preglomerular and postglomerular vasculature: accentuation during diabetes. *Kidney Int*. 2005; 68(3): 1171-1185.
976. Kurtz L, Madsen K, Kurt B, Jensen BL, Walter S, Banas B, Wagner C, Kurtz A. High-level connexin expression in the human juxtaglomerular apparatus. *Nephron Physiol*. 2010; 116(1): p1-8.
977. Wagner C, de Wit C, Kurtz L, Grünberger C, Kurtz A, Schweda F. Connexin40 is essential for the pressure control of renin synthesis and secretion. *Circ Res*. 2007; 100(4): 556-563.
978. Wagner C, Jobs A, Schweda F, Kurtz L, Kurt B, Lopez ML, Gomez RA, van Veen TA, de Wit C, Kurtz A. Selective deletion of Connexin 40 in renin-producing cells impairs renal baroreceptor function and is associated with arterial hypertension. *Kidney Int*. 2010; 78(8): 762-768.
979. Kurtz A. Connexins, renin cell displacement and hypertension. *Curr Opin Pharmacol*. 2015; 21: 1-6.
980. Machura K, Neubauer B, Müller H, Tauber P, Kurtz A, Kurtz L. Connexin 40 is dispensable for vascular renin cell recruitment but is indispensable for vascular baroreceptor control of renin secretion. *Pflugers Arch*. 2015; 467(8): 1825-1834.

981. Haefliger JA, Demotz S, Braissant O, Suter E, Waeber B, Nicod P, Meda P. Connexins 40 and 43 are differentially regulated within the kidneys of rats with renovascular hypertension. *Kidney Int.* 2001; 60(1): 190-201.
982. Takenaka T, Inoue T, Kanno Y, Okada H, Meaney KR, Hill CE, Suzuki H. Expression and role of connexins in the rat renal vasculature. *Kidney Int.* 2008; 73(4): 415-422.
983. Lin L, Nasjletti A. Role of endothelium-derived prostanoid in angiotensin-induced vasoconstriction. *Hypertension.* 1991; 18(2): 158-164.
984. Wilcox CS, Welch WJ, Snellen H. Thromboxane mediates renal hemodynamic response to infused angiotensin II. *Kidney Int.* 1991; 40(6): 1090-1097.
985. Keen HL, Brands MW, Smith MJ, Jr., Shek EW, Hall JE. Thromboxane is required for full expression of angiotensin hypertension in rats. *Hypertension.* 1997; 29(1 Pt 2): 310-314.
986. Francois H, Athirakul K, Mao L, Rockman H, Coffman TM. Role for thromboxane receptors in angiotensin-II-induced hypertension. *Hypertension.* 2004; 43(2): 364-369.
987. Zhou H, Yan F, Tai HH. Phosphorylation and desensitization of the human thromboxane receptor- α by G protein-coupled receptor kinases. *J Pharmacol Exp Ther.* 2001; 298(3): 1243-1251.
988. Flannery PJ, Spurney RF. Desensitization of the mouse thromboxane A₂ receptor (TP) by G protein-coupled receptor kinases (GRKs). *Prostaglandins Other Lipid Mediat.* 2002; 70(1-2): 79-90.
989. Parent JL, Labrecque P, Orsini MJ, Benovic JL. Internalization of the TXA₂ receptor α and β isoforms. Role of the differentially spliced COOH terminus in agonist-promoted receptor internalization. *J Biol Chem.* 1999; 274(13): 8941-8948.
990. Zhang M, Li C, He C, Cui Y, Li Y, Ma Y, Cheng J, Wen J, Li P, Yang Y. Thromboxane-induced contractile response of mesenteric arterioles is diminished in the older rats and the older hypertensive rats. *Front Pharmacol.* 2022; 13: 1019511.
991. Wilde DW, Massey KD, Walker GK, Vollmer A, Grekin RJ. High-fat diet elevates blood pressure and cerebrovascular muscle Ca²⁺ current. *Hypertension.* 2000; 35(3): 832-837.
992. Ohya Y, Tsuchihashi T, Kagiya S, Abe I, Fujishima M. Single L-type calcium channels in smooth muscle cells from resistance arteries of spontaneously hypertensive rats. *Hypertension.* 1998; 31(5): 1125-1129.
993. Gerzanich V, Ivanova S, Zhou H, Simard JM. Mislocalization of eNOS and upregulation of cerebral vascular Ca²⁺ channel activity in angiotensin-hypertension. *Hypertension.* 2003; 41(5): 1124-1130.
994. Liao J, Zhang Y, Ye F, Zhang L, Chen Y, Zeng F, Shi L. Epigenetic regulation of L-type voltage-gated Ca²⁺ channels in mesenteric arteries of aging hypertensive rats. *Hypertens Res.* 2017; 40(5): 441-449.
995. Zhou Y, Fan J, Zhu H, Ji L, Fan W, Kapoor I, Wang Y, Wang Y, Zhu G, Wang J. Aberrant splicing induced by dysregulated Rbfox2 produces enhanced function of Cav1.2 calcium channel and vascular myogenic tone in hypertension. *Hypertension.* 2017; 70(6): 1183-1192.
996. Pinto YM, Paul M, Ganten D. Lessons from rat models of hypertension: from Goldblatt to genetic engineering. *Cardiovasc Res.* 1998; 39(1): 77-88.
997. DuPont JJ, McCurley A, Davel AP, McCarthy J, Bender SB, Hong K, Yang Y, Yoo JK, Aronovitz M, Baur WE, Christou DD, Hill MA, Jaffe IZ. Vascular mineralocorticoid

- receptor regulates microRNA-155 to promote vasoconstriction and rising blood pressure with aging. *JCI Insight*. 2016; 1(14): e88942.
998. Ji L, Zhu H, Chen H, Fan W, Chen J, Chen J, Zhu G, Wang J. Modulation of Cav1.2 calcium channel by neuropeptide W regulates vascular myogenic tone via G protein-coupled receptor 7. *J Hypertens*. 2015; 33(12): 2431-2442.
 999. Kurjiaka DT, Bender SB, Nye DD, Wiehler WB, Welsh DG. Hypertension attenuates cell-to-cell communication in hamster retractor muscle feed arteries. *Am J Physiol Heart Circ Physiol*. 2005; 288(2): H861-870.
 1000. Lalley PM. Microiontophoresis and pressure ejection in *Modern Techniques in Neuroscience Research*. (eds Windhorst U, Johansson H) Ch. 7, 193-212 (Springer Berlin Heidelberg, 1999).
 1001. Xia J, Duling BR. Electromechanical coupling and the conducted vasomotor response. *Am J Physiol*. 1995; 269(6 Pt 2): H2022-2030.
 1002. Sancho M, Gao Y, Hald BO, Yin H, Boulton M, Steven DA, MacDougall KW, Parrent AG, Pickering JG, Welsh DG. An assessment of K_{IR} channel function in human cerebral arteries. *Am J Physiol Heart Circ Physiol*. 2019; 316(4): H794-h800.
 1003. de Wit C. Different pathways with distinct properties conduct dilations in the microcirculation *in vivo*. *Cardiovasc Res*. 2010; 85(3): 604-613.
 1004. Salameh A, Dhein S. Effects of mechanical forces and stretch on intercellular gap junction coupling. *Biochim Biophys Acta*. 2013; 1828(1): 147-156.
 1005. Johnson TL, Nerem RM. Endothelial connexin 37, connexin 40, and connexin 43 respond uniquely to substrate and shear stress. *Endothelium*. 2007; 14(4-5): 215-226.
 1006. Vorderwülbecke BJ, Maroski J, Fiedorowicz K, Da Silva-Azevedo L, Marki A, Pries AR, Zakrzewicz A. Regulation of endothelial connexin40 expression by shear stress. *Am J Physiol Heart Circ Physiol*. 2012; 302(1): H143-152.
 1007. Yao QP, Qi YX, Zhang P, Cheng BB, Yan ZQ, Jiang ZL. SIRT1 and connexin40 mediate the normal shear stress-induced inhibition of the proliferation of endothelial cells co-cultured with vascular smooth muscle cells. *Cell Physiol Biochem*. 2013; 31(2-3): 389-399.
 1008. Zhang Z, Chen Y, Zhang T, Guo L, Yang W, Zhang J, Wang C. Role of myoendothelial gap junctions in the regulation of human coronary artery smooth muscle cell differentiation by laminar shear stress. *Cell Physiol Biochem*. 2016; 39(2): 423-437.
 1009. Piao H, Sato A, Nozawa Y, Sun W, Morioka T, Oite T. Effects of connexin-mimetic peptides on perfusion pressure in response to phenylephrine in isolated, perfused rat kidneys. *Clin Exp Nephrol*. 2011; 15(2): 203-211.
 1010. Fowler MJ. Microvascular and macrovascular complications of diabetes. *Clinical Diabetes*. 2008; 26(2): 77-82.
 1011. DeFronzo RA, Abdul-Ghani M. Assessment and treatment of cardiovascular risk in prediabetes: impaired glucose tolerance and impaired fasting glucose. *Am J Cardiol*. 2011; 108(3 Suppl): 3b-24b.
 1012. Sitia S, Tomasoni L, Atzeni F, Ambrosio G, Cordiano C, Catapano A, Tramontana S, Perticone F, Naccarato P, Camici P, Picano E, Cortigiani L, Bevilacqua M, Milazzo L, Cusi D, Barlassina C, Sarzi-Puttini P, Turiel M. From endothelial dysfunction to atherosclerosis. *Autoimmun Rev*. 2010; 9(12): 830-834.
 1013. Mudau M, Genis A, Lochner A, Strijdom H. Endothelial dysfunction: the early predictor of atherosclerosis. *Cardiovasc J Afr*. 2012; 23(4): 222-231.

1014. Brisset AC, Isakson BE, Kwak BR. Connexins in vascular physiology and pathology. *Antioxid Redox Signal*. 2009; 11(2): 267-282.
1015. Sato T, Haimovici R, Kao R, Li AF, Roy S. Downregulation of connexin 43 expression by high glucose reduces gap junction activity in microvascular endothelial cells. *Diabetes*. 2002; 51(5): 1565-1571.
1016. Ding H, Hashem M, Wiehler WB, Lau W, Martin J, Reid J, Triggle C. Endothelial dysfunction in the streptozotocin-induced diabetic apoE-deficient mouse. *Br J Pharmacol*. 2005; 146(8): 1110-1118.
1017. Makino A, Platoshyn O, Suarez J, Yuan JX, Dillmann WH. Downregulation of connexin40 is associated with coronary endothelial cell dysfunction in streptozotocin-induced diabetic mice. *Am J Physiol Cell Physiol*. 2008; 295(1): C221-230.
1018. Makino A, Dai A, Han Y, Youssef KD, Wang W, Donthamsetty R, Scott BT, Wang H, Dillmann WH. O-GlcNAcase overexpression reverses coronary endothelial cell dysfunction in type 1 diabetic mice. *Am J Physiol Cell Physiol*. 2015; 309(9): C593-599.
1019. Rai A, Riemann M, Gustafsson F, Holstein-Rathlou NH, Torp-Pedersen C. Streptozotocin-induced diabetes decreases conducted vasoconstrictor response in mouse cremaster arterioles. *Horm Metab Res*. 2008; 40(9): 651-654.
1020. Young EJ, Hill MA, Wiehler WB, Triggle CR, Reid JJ. Reduced EDHF responses and connexin activity in mesenteric arteries from the insulin-resistant obese Zucker rat. *Diabetologia*. 2008; 51(5): 872-881.
1021. Takahashi K, Sasano T, Sugiyama K, Kurokawa J, Tamura N, Soejima Y, Sawabe M, Isobe M, Furukawa T. High-fat diet increases vulnerability to atrial arrhythmia by conduction disturbance via miR-27b. *J Mol Cell Cardiol*. 2016; 90: 38-46.
1022. Liu R, Wu K, Li Y, Sun R, Li X. Human antigen R: a potential therapeutic target for liver diseases. *Pharmacol Res*. 2020; 155: 104684.
1023. Hou CJ, Tsai CH, Yeh HI. Endothelial connexins are down-regulated by atherogenic factors. *Front Biosci*. 2008; 13: 3549-3557.
1024. Chadjichristos CE, Derouette JP, Kwak BR. Connexins in atherosclerosis. *Adv Cardiol*. 2006; 42: 255-267.
1025. Kwak BR, Mulhaupt F, Veillard N, Gros DB, Mach F. Altered pattern of vascular connexin expression in atherosclerotic plaques. *Arterioscler Thromb Vasc Biol*. 2002; 22(2): 225-230.
1026. Yeh HI, Lu CS, Wu YJ, Chen CC, Hong RC, Ko YS, Shiao MS, Severs NJ, Tsai CH. Reduced expression of endothelial connexin37 and connexin40 in hyperlipidemic mice: recovery of connexin37 after 7-day simvastatin treatment. *Arterioscler Thromb Vasc Biol*. 2003; 23(8): 1391-1397.
1027. Simon AM, McWhorter AR, Chen H, Jackson CL, Ouellette Y. Decreased intercellular communication and connexin expression in mouse aortic endothelium during lipopolysaccharide-induced inflammation. *J Vasc Res*. 2004; 41(4): 323-333.
1028. Yeh HI, Lee PY, Su CH, Tian TY, Ko YS, Tsai CH. Reduced expression of endothelial connexins 43 and 37 in hypertensive rats is rectified after 7-day carvedilol treatment. *Am J Hypertens*. 2006; 19(2): 129-135.
1029. Yeh HI, Chang HM, Lu WW, Lee YN, Ko YS, Severs NJ, Tsai CH. Age-related alteration of gap junction distribution and connexin expression in rat aortic endothelium. *J Histochem Cytochem*. 2000; 48(10): 1377-1389.

1030. van Rijen HV, van Veen TA, Hermans MM, Jongsma HJ. Human connexin40 gap junction channels are modulated by cAMP. *Cardiovasc Res.* 2000; 45(4): 941-951.
1031. Bolon ML, Ouellette Y, Li F, Tyml K. Abrupt reoxygenation following hypoxia reduces electrical coupling between endothelial cells of wild-type but not connexin40 null mice in oxidant- and PKA-dependent manner. *Faseb j.* 2005; 19(12): 1725-1727.
1032. Traub O, Eckert R, Lichtenberg-Fraté H, Elfgang C, Bastide B, Scheidtmann KH, Hülser DF, Willecke K. Immunochemical and electrophysiological characterization of murine connexin40 and -43 in mouse tissues and transfected human cells. *Eur J Cell Biol.* 1994; 64(1): 101-112.
1033. Humphries KM, Pennypacker JK, Taylor SS. Redox regulation of cAMP-dependent protein kinase signaling: kinase versus phosphatase inactivation. *J Biol Chem.* 2007; 282(30): 22072-22079.
1034. Tyml K, Wang X, Lidington D, Ouellette Y. Lipopolysaccharide reduces intercellular coupling in vitro and arteriolar conducted response in vivo. *Am J Physiol Heart Circ Physiol.* 2001; 281(3): H1397-1406.
1035. Lidington D, Ouellette Y, Tyml K. Communication of agonist-induced electrical responses along 'capillaries' in vitro can be modulated by lipopolysaccharide, but not nitric oxide. *J Vasc Res.* 2002; 39(5): 405-413.
1036. Bolon ML, Peng T, Kidder GM, Tyml K. Lipopolysaccharide plus hypoxia and reoxygenation synergistically reduce electrical coupling between microvascular endothelial cells by dephosphorylating connexin40. *J Cell Physiol.* 2008; 217(2): 350-359.
1037. Hariri N, Thibault L. High-fat diet-induced obesity in animal models. *Nutr Res Rev.* 2010; 23(2): 270-299.
1038. Buettner R, Schölmerich J, Bollheimer LC. High-fat diets: modeling the metabolic disorders of human obesity in rodents. *Obesity (Silver Spring).* 2007; 15(4): 798-808.
1039. Botchlett R, Wu C. Diet composition for the management of obesity and obesity-related disorders. *J Diabetes Mellit Metab Syndr.* 2018; 3: 10-25.
1040. Heydemann A. An overview of murine high fat diet as a model for type 2 diabetes mellitus. *J Diabetes Res.* 2016; 2016: 2902351.
1041. Hintze KJ, Benninghoff AD, Cho CE, Ward RE. Modeling the Western diet for preclinical investigations. *Adv Nutr.* 2018; 9(3): 263-271.
1042. Bortolin RC, Vargas AR, Gasparotto J, Chaves PR, Schnorr CE, Martinello KB, Silveira AK, Rabelo TK, Gelain DP, Moreira JCF. A new animal diet based on human Western diet is a robust diet-induced obesity model: comparison to high-fat and cafeteria diets in term of metabolic and gut microbiota disruption. *Int J Obes (Lond).* 2018; 42(3): 525-534.
1043. Martin B, Caron N, Jadot I, Colombaro V, Federici G, Depommier C, Declèves A. Evaluation of inducible nitric oxide synthase inhibition on kidney function and structure in high-fat diet-induced kidney disease. *Exp Physiol.* 2018; 103(1): 125-140.
1044. Declèves AE, Mathew AV, Cunard R, Sharma K. AMPK mediates the initiation of kidney disease induced by a high-fat diet. *J Am Soc Nephrol.* 2011; 22(10): 1846-1855.
1045. Sánchez-Navarro A, Martínez-Rojas M, Caldiño-Bohn RI, Pérez-Villalva R, Zambrano E, Castro-Rodríguez DC, Bobadilla NA. Early triggers of moderately high-fat diet-induced kidney damage. *Physiol Rep.* 2021; 9(14): e14937.

1046. Mehmood R, Sheikh N, Khawar MB, Abbasi MH, Tayyeb A, Ashfaq I, Mukhtar M, Fatima N. High-fat diet induced hedgehog signaling modifications during chronic kidney damage. *Biomed Res Int.* 2020; 2020: 8073926.
1047. Maleki MH, Nadimi E, Vakili O, Tavakoli R, Taghizadeh M, Dehghanian A, Bordbar H, Shafiee SM. Bilirubin improves renal function by reversing the endoplasmic reticulum stress and inflammation in the kidneys of type 2 diabetic rats fed high-fat diet. *Chem Biol Interact.* 2023; 378: 110490.
1048. Castro BBA, Foresto-Neto O, Saraiva-Camara NO, Sanders-Pinheiro H. Renal lipotoxicity: Insights from experimental models. *Clin Exp Pharmacol Physiol.* 2021; 48(12): 1579-1588.
1049. Di Marco E, Jha JC, Sharma A, Wilkinson-Berka JL, Jandeleit-Dahm KA, de Haan JB. Are reactive oxygen species still the basis for diabetic complications? *Clin Sci (Lond).* 2015; 129(2): 199-216.
1050. Janssen-Heininger YM, Poynter ME, Baeuerle PA. Recent advances towards understanding redox mechanisms in the activation of nuclear factor κ B. *Free Radic Biol Med.* 2000; 28(9): 1317-1327.
1051. Kobayasi R, Akamine EH, Davel AP, Rodrigues MA, Carvalho CR, Rossoni LV. Oxidative stress and inflammatory mediators contribute to endothelial dysfunction in high-fat diet-induced obesity in mice. *J Hypertens.* 2010; 28(10): 2111-2119.
1052. Rendra E, Riabov V, Mossel DM, Sevastyanova T, Harmsen MC, Kzhyshkowska J. Reactive oxygen species (ROS) in macrophage activation and function in diabetes. *Immunobiology.* 2019; 224(2): 242-253.
1053. Korkmaz S, Radovits T, Barnucz E, Neugebauer P, Arif R, Hirschberg K, Loganathan S, Seidel B, Karcik M, Szabó G. Dose-dependent effects of a selective phosphodiesterase-5-inhibitor on endothelial dysfunction induced by peroxynitrite in rat aorta. *Eur J Pharmacol.* 2009; 615(1-3): 155-162.
1054. El-Remessy AB, Behzadian MA, Abou-Mohamed G, Franklin T, Caldwell RW, Caldwell RB. Experimental diabetes causes breakdown of the blood-retina barrier by a mechanism involving tyrosine nitration and increases in expression of vascular endothelial growth factor and urokinase plasminogen activator receptor. *Am J Pathol.* 2003; 162(6): 1995-2004.
1055. Szabó C, Ischiropoulos H, Radi R. Peroxynitrite: biochemistry, pathophysiology and development of therapeutics. *Nat Rev Drug Discov.* 2007; 6(8): 662-680.
1056. Maneen MJ, Cipolla MJ. Peroxynitrite diminishes myogenic tone in cerebral arteries: role of nitrotyrosine and F-actin. *Am J Physiol Heart Circ Physiol.* 2007; 292(2): H1042-1050.
1057. Bachschmid M, Thureau S, Zou MH, Ullrich V. Endothelial cell activation by endotoxin involves superoxide/NO-mediated nitration of prostacyclin synthase and thromboxane receptor stimulation. *Faseb j.* 2003; 17(8): 914-916.
1058. Aggarwal S, Gross CM, Kumar S, Datar S, Oishi P, Kalkan G, Schreiber C, Fratz S, Fineman JR, Black SM. Attenuated vasodilatation in lambs with endogenous and exogenous activation of cGMP signaling: role of protein kinase G nitration. *J Cell Physiol.* 2011; 226(12): 3104-3113.
1059. Lu H, Boustany-Kari CM, Daugherty A, Cassis LA. Angiotensin II increases adipose angiotensinogen expression. *Am J Physiol Endocrinol Metab.* 2007; 292(5): E1280-1287.

1060. Van Harmelen V, Ariapart P, Hoffstedt J, Lundkvist I, Bringman S, Arner P. Increased adipose angiotensinogen gene expression in human obesity. *Obes Res.* 2000; 8(4): 337-341.
1061. Massiéra F, Bloch-Faure M, Ceiler D, Murakami K, Fukamizu A, Gasc JM, Quignard-Boulangé A, Negrel R, Ailhaud G, Seydoux J, Meneton P, Teboul M. Adipose angiotensinogen is involved in adipose tissue growth and blood pressure regulation. *Faseb j.* 2001; 15(14): 2727-2729.
1062. Massiéra F, Seydoux J, Geloën A, Quignard-Boulangé A, Turban S, Saint-Marc P, Fukamizu A, Negrel R, Ailhaud G, Teboul M. Angiotensinogen-deficient mice exhibit impairment of diet-induced weight gain with alteration in adipose tissue development and increased locomotor activity. *Endocrinology.* 2001; 142(12): 5220-5225.
1063. Yasue S, Masuzaki H, Okada S, Ishii T, Kozuka C, Tanaka T, Fujikura J, Ebihara K, Hosoda K, Katsurada A, Ohashi N, Urushihara M, Kobori H, Morimoto N, Kawazoe T, Naitoh M, Okada M, Sakaue H, Suzuki S, Nakao K. Adipose tissue-specific regulation of angiotensinogen in obese humans and mice: impact of nutritional status and adipocyte hypertrophy. *Am J Hypertens.* 2010; 23(4): 425-431.
1064. Karlsson C, Lindell K, Ottosson M, Sjöström L, Carlsson B, Carlsson LM. Human adipose tissue expresses angiotensinogen and enzymes required for its conversion to angiotensin II. *J Clin Endocrinol Metab.* 1998; 83(11): 3925-3929.
1065. Ruster C, Wolf G. The role of the renin-angiotensin-aldosterone system in obesity-related renal diseases. *Semin Nephrol.* 2013; 33(1): 44-53.
1066. Schling P, Mallow H, Trindl A, Löffler G. Evidence for a local renin angiotensin system in primary cultured human preadipocytes. *Int J Obes Relat Metab Disord.* 1999; 23(4): 336-341.
1067. Gu JW, Wang J, Stockton A, Lokitz B, Henegar L, Hall JE. Cytokine gene expression profiles in kidney medulla and cortex of obese hypertensive dogs. *Kidney Int.* 2004; 66(2): 713-721.
1068. Li C, Lin Y, Luo R, Chen S, Wang F, Zheng P, Levi M, Yang T, Wang W. Intrarenal renin-angiotensin system mediates fatty acid-induced ER stress in the kidney. *Am J Physiol Renal Physiol.* 2016; 310(5): F351-363.
1069. Saddik M, Lopaschuk GD. Myocardial triglyceride turnover and contribution to energy substrate utilization in isolated working rat hearts. *J Biol Chem.* 1991; 266(13): 8162-8170.
1070. Lopaschuk GD, Ussher JR, Folmes CD, Jaswal JS, Stanley WC. Myocardial fatty acid metabolism in health and disease. *Physiol Rev.* 2010; 90(1): 207-258.
1071. Aubert G, Vega RB, Kelly DP. Perturbations in the gene regulatory pathways controlling mitochondrial energy production in the failing heart. *Biochim Biophys Acta.* 2013; 1833(4): 840-847.
1072. Littlejohns B, Pasdois P, Duggan S, Bond AR, Heesom K, Jackson CL, Angelini GD, Halestrap AP, Suleiman MS. Hearts from mice fed a non-obesogenic high-fat diet exhibit changes in their oxidative state, calcium and mitochondria in parallel with increased susceptibility to reperfusion injury. *PLoS One.* 2014; 9(6): e100579.
1073. Inserte J, Aluja D, Barba I, Ruiz-Meana M, Miró E, Poncelas M, Vilardosa Ú, Castellano J, Garcia-Dorado D. High-fat diet improves tolerance to myocardial ischemia by delaying normalization of intracellular PH at reperfusion. *J Mol Cell Cardiol.* 2019; 133: 164-173.

1074. Edland F, Wergeland A, Kopperud R, Åsrud KS, Hoivik EA, Witsø SL, Æsøy R, Madsen L, Kristiansen K, Bakke M, Døskeland SO, Jonassen AK. Long-term consumption of an obesogenic high fat diet prior to ischemia-reperfusion mediates cardioprotection via Epacl-dependent signaling. *Nutr Metab (Lond)*. 2016; 13: 87.
1075. Salie R, Huisamen B, Lochner A. High carbohydrate and high fat diets protect the heart against ischaemia/reperfusion injury. *Cardiovasc Diabetol*. 2014; 13: 109.
1076. Boardman NT, Rossvoll L, Lund J, Hafstad AD, Aasum E. 3-Weeks of exercise training increases ischemic-tolerance in hearts from high-fat diet fed mice. *Front Physiol*. 2019; 10: 1274.
1077. Mahalakshmi A, Kurian GA. Evaluating the impact of diabetes and diabetic cardiomyopathy rat heart on the outcome of ischemia-reperfusion associated oxidative stress. *Free Radic Biol Med*. 2018; 118: 35-43.
1078. Axelsen LN, Calloe K, Braunstein TH, Riemann M, Hofgaard JP, Liang B, Jensen CF, Olsen KB, Bartels ED, Baandrup U, Jespersen T, Nielsen LB, Holstein-Rathlou NH, Nielsen MS. Diet-induced pre-diabetes slows cardiac conductance and promotes arrhythmogenesis. *Cardiovasc Diabetol*. 2015; 14: 87.
1079. Stanley WC, Dabkowski ER, Ribeiro RF, Jr., O'Connell KA. Dietary fat and heart failure: moving from lipotoxicity to lipoprotection. *Circ Res*. 2012; 110(5): 764-776.
1080. Gerges SH, El-Kadi AOS. Sex differences in eicosanoid formation and metabolism: A possible mediator of sex discrepancies in cardiovascular diseases. *Pharmacol Ther*. 2022; 234: 108046.
1081. Elmarakby AA, Katary M, Pollock JS, Sullivan JC. Influence of the selective COX-2 inhibitor celecoxib on sex differences in blood pressure and albuminuria in spontaneously hypertensive rats. *Prostaglandins Other Lipid Mediat*. 2018; 135: 16-20.
1082. Costa G, Garabito M, Jiménez-Altayó F, Onetti Y, Sabate M, Vila E, Dantas AP. Sex differences in angiotensin II responses contribute to a differential regulation of cox-mediated vascular dysfunction during aging. *Exp Gerontol*. 2016; 85: 71-80.
1083. Batres RO, Dupont J. Gender differences in prostacyclin and prostaglandin E2 synthesis by human endothelial cells. *Prostaglandins Leukot Med*. 1986; 22(2): 159-171.
1084. Pabbidi MR, Kuppusamy M, Didion SP, Sanapureddy P, Reed JT, Sontakke SP. Sex differences in the vascular function and related mechanisms: role of 17 β -estradiol. *Am J Physiol Heart Circ Physiol*. 2018; 315(6): H1499-h1518.
1085. Stanhewicz AE, Wenner MM, Stachenfeld NS. Sex differences in endothelial function important to vascular health and overall cardiovascular disease risk across the lifespan. *Am J Physiol Heart Circ Physiol*. 2018; 315(6): H1569-h1588.
1086. Stepan D, Geis L, Pan L, Gross K, Wagner C, Kurtz A. Lack of connexin 40 decreases the calcium sensitivity of renin-secreting juxtaglomerular cells. *Pflugers Arch*. 2018; 470(6): 969-978.

Appendix A: Diet compositions

Control Diet 1: PicoLab® Laboratory Rodent Diet 5L0D

Macronutrients		
	% by weight	% kcal from
Protein	25.0	29.829
Carbohydrates[†]	47.5	56.744
Fat	5.0	13.427
Fiber	5.3	—
Metabolizable Energy	kcal/g	2.91

Amino Acids		
Alanine	g/kg	14.4
Arginine	g/kg	15.7
Aspartic Acid	g/kg	28.1
Cystine	g/kg	3.9
Glutamic Acid	g/kg	47.4
Glycine	g/kg	12.8
Histidine	g/kg	6.2
Isoleucine	g/kg	10.6
Leucine	g/kg	18.9
Lysine	g/kg	14.8
Methionine	g/kg	5.9
Phenylalanine	g/kg	11.1
Proline	g/kg	14.7
Serine	g/kg	11.8
Threonine	g/kg	9.7
Tryptophan	g/kg	2.8
Tyrosine	g/kg	7.7
Valine	g/kg	11.6
Taurine	g/kg	0.3

Vitamins		
Biotin	mg/kg	0.3
Carotene	mg/kg	2.3
Choline	mg/kg	2250
Folic Acid	mg/kg	7.1
Niacin	mg/kg	120
Pantothenic Acid	mg/kg	24
Pyridoxine	mg/kg	6.0
Riboflavin	mg/kg	4.7
Thiamin	mg/kg	16
Vitamin B₁₂	mg/kg	0.051
Vitamin K	mg/kg	1.3
Vitamin A	IU/kg	15000
Vitamin D₃	IU/kg	4600
Vitamin E	IU/kg	42

Minerals		
Calcium	g/kg	9.5
Chlorine	g/kg	6.4
Magnesium	g/kg	2.3
Phosphorus	g/kg	7.0
Potassium	g/kg	12.8
Sodium	g/kg	3.9
Sulfur	g/kg	3.6
Chromium	mg/kg	0.01
Cobalt	mg/kg	0.91
Copper	mg/kg	15
Fluorine	mg/kg	15
Iodine	mg/kg	0.99
Iron	mg/kg	240
Manganese	mg/kg	75
Selenium	mg/kg	0.41
Zinc	mg/kg	85

Carbohydrates		
Fructose	g/kg	2.7
Glucose	g/kg	1.9
Lactose	g/kg	20.1
Starch	g/kg	210
Sucrose	g/kg	38.3

Fatty Acids		
Total Fat	g/kg	50
Saturated Fat	g/kg	14.8
Monounsaturated Fat	g/kg	16.2
Polyunsaturated Fat*	g/kg	14.6
Saturated Fat*	% of fat	32.5
Monounsaturated Fat*	% of fat	35.5
Polyunsaturated Fat*	% of fat	32.0
18:2 Linoleic Acid	g/kg	10.5
18:3 Linolenic Acid	g/kg	0.9
20:4 Arachidonic Acid	g/kg	0.2
Omega-3 Fatty Acids	g/kg	3.00

Other		
Cholesterol	mg/kg	209

Table A.1: Chemical composition of the first control diet, PicoLab[®] Laboratory Rodent Diet 5L0D. Constituent macro- and micronutrient composition of diet 5L0D, which was used as the control diet from the beginning of the study until March 2023. Chemical analyses were performed by LabDiet (Richmond, USA) and data were accessed from www.labdiet.com. †Digestible carbohydrates. *Values not provided by LabDiet, instead calculated from provided data.

Control Diet 2: PicoLab® Rodent Diet 20 5053

Macronutrients		
	% by weight	% kcal from
Protein	21.0	24.517
Carbohydrates[†]	53.4	62.349
Fat	5.0	13.134
Fiber	4.6	—
Metabolizable Energy	kcal/g	3.03

Amino Acids		
Alanine	g/kg	11.9
Arginine	g/kg	12.9
Aspartic Acid	g/kg	21.9
Cystine	g/kg	3.6
Glutamic Acid	g/kg	41.8
Glycine	g/kg	9.7
Histidine	g/kg	5.3
Isoleucine	g/kg	8.6
Leucine	g/kg	15.7
Lysine	g/kg	11.8
Methionine	g/kg	6.2
Phenylalanine	g/kg	9.1
Proline	g/kg	13.1
Serine	g/kg	9.8
Threonine	g/kg	7.8
Tryptophan	g/kg	2.4
Tyrosine	g/kg	6.0
Valine	g/kg	9.7
Taurine	g/kg	0.3

Vitamins		
Biotin	mg/kg	0.30
Carotene	mg/kg	1.5
Choline	mg/kg	2000
Folic Acid	mg/kg	3.0
Niacin	mg/kg	85
Pantothenic Acid	mg/kg	17
Pyridoxine	mg/kg	9.6
Riboflavin	mg/kg	8.0
Thiamin	mg/kg	17
Vitamin B₁₂	mg/kg	0.051
Vitamin K	mg/kg	3.3
Vitamin A	IU/kg	15000
Vitamin D₃	IU/kg	2300
Vitamin E	IU/kg	99

Minerals		
Calcium	g/kg	8.1
Chlorine	g/kg	5.2
Magnesium	g/kg	2.2
Phosphorus	g/kg	6.4
Potassium	g/kg	11.0
Sodium	g/kg	3.0
Sulfur	g/kg	3.3
Chromium	mg/kg	0.01
Cobalt	mg/kg	0.71
Copper	mg/kg	14
Fluorine	mg/kg	9.3
Iodine	mg/kg	0.97
Iron	mg/kg	185
Manganese	mg/kg	84
Selenium	mg/kg	0.37
Zinc	mg/kg	89

Carbohydrates		
Fructose	g/kg	2.4
Glucose	g/kg	1.9
Lactose	g/kg	13.4
Starch	g/kg	282
Sucrose	g/kg	32.5

Fatty Acids		
Total Fat	g/kg	50
Saturated Fat	g/kg	7.8
Monounsaturated Fat	g/kg	9.6
Polyunsaturated Fat*	g/kg	28.5
Saturated Fat*	% of fat	17.0
Monounsaturated Fat*	% of fat	20.9
Polyunsaturated Fat*	% of fat	62.1
18:2 Linoleic Acid	g/kg	21.2
18:3 Linolenic Acid	g/kg	2.7
20:4 Arachidonic Acid	g/kg	0.1
Omega-3 Fatty Acids	g/kg	4.50

Other		
Cholesterol	mg/kg	142

Table A.2: Chemical composition of the second control diet, PicoLab[®] Rodent Diet 20 5053. Constituent macro- and micronutrient composition of diet 5053, which was used as the control diet from March 2023 onward. Chemical analyses were performed by LabDiet (Richmond, USA) and data were accessed from www.labdiet.com. †Digestible carbohydrates. *Values not provided by LabDiet, instead calculated from provided data.

HFD: Teklad custom diet TD.210490 (20% Fructose, 15% Crisco®)

Macronutrients		
	% by weight	% kcal from
Protein	15.8	15.4
Carbohydrates[†]	46.4	45.3
Fat	17.9	39.3
Fiber	2.3	—
Metabolizable Energy	kcal/g	4.1

Amino Acids		
	g/kg	
Alanine	g/kg	0.0
Arginine	g/kg	10.6
Aspartic Acid	g/kg	0.0
Cystine	g/kg	4.2
Glutamic Acid	g/kg	0.0
Glycine	g/kg	0.0
Histidine	g/kg	3.9
Isoleucine	g/kg	7.3
Leucine	g/kg	12.7
Lysine	g/kg	9.6
Methionine	g/kg	2.8
Phenylalanine	g/kg	7.6
Proline	g/kg	0.0
Serine	g/kg	0.0
Threonine	g/kg	6.5
Tryptophan	g/kg	2.0
Tyrosine	g/kg	6.4
Valine	g/kg	8.0

Vitamins		
	mg/kg	
Biotin	mg/kg	0.30
Choline	mg/kg	1628.4
Folic Acid	mg/kg	2.7
Niacin	mg/kg	49.6
Pantothenic Acid	mg/kg	17.1
Riboflavin	mg/kg	6.7
Thiamin	mg/kg	25.1
Vitamin B₆	mg/kg	10.9
Vitamin B₁₂	mg/kg	0.05
Vitamin K	mg/kg	41.6
Vitamin A	IU/kg	12802
Vitamin D₃	IU/kg	2393
Vitamin E	IU/kg	80

Minerals		
	g/kg	
Calcium	g/kg	8.8
Chlorine	g/kg	5.0
Magnesium	g/kg	1.804
Phosphorus	g/kg	6.3
Potassium	g/kg	8.5
Sodium	g/kg	2.2
Chromium	mg/kg	0.31
Copper	mg/kg	21.9
Iodine	mg/kg	2.38
Iron	mg/kg	229.4
Manganese	mg/kg	83.8
Molybdenum	mg/kg	0.10
Selenium	mg/kg	0.21
Zinc	mg/kg	62.6

Carbohydrates		
Fructose	g/kg	≥200.0*
Glucose	g/kg	N/A*
Lactose	g/kg	N/A*
Starch	g/kg	N/A*
Sucrose	g/kg	N/A*

Fatty Acids		
Total Fat	g/kg	179.0
Saturated Fat	g/kg	45.6
Monounsaturated Fat	g/kg	36.2
Polyunsaturated Fat	g/kg	92.0
Saturated Fat	% of fat	26.2
Monounsaturated Fat	% of fat	20.9
Polyunsaturated Fat	% of fat	52.9
12:0 Lauric Acid	g/kg	0.1
14:0 Myristic Acid	g/kg	0.4
16:0 Palmitic Acid	g/kg	29.2
16:1 Palmitoleic Acid	g/kg	0.5
18:0 Stearic Acid	g/kg	15.8
18:1 Oleic Acid	g/kg	35.6
18:2 Linoleic Acid	g/kg	80.2
18:3 Linolenic Acid	g/kg	10.2

Other		
Cholesterol	mg/kg	36.7

Table A.3: Chemical composition of the mild HFD, Teklad custom diet TD.210490. Constituent macro- and micronutrient composition of diet TD.210490, which was formulated in consultation with Dr. Derek Martin, RD, a laboratory animal nutritionist at Envigo (Madison, USA). The diet was created by using Teklad Rodent Diet 8604 as a base and adding fructose and Crisco®. The final composition was 643.85 g/kg of Diet 8604, 200.0 g/kg of added fructose, 150.0 g/kg of Crisco® hydrogenated vegetable shortening and additional vitamin and mineral mixes to replenish diluted micronutrients. Values were provided by Dr. Martin are not experimentally measured but instead are calculated from data of included ingredients. †Digestible carbohydrates. *Values of individual carbohydrates were not provided by Envigo, as the digestible carbohydrate content in the base diet 8604 was calculated by subtraction.

Appendix B: Absolute values of organ weights

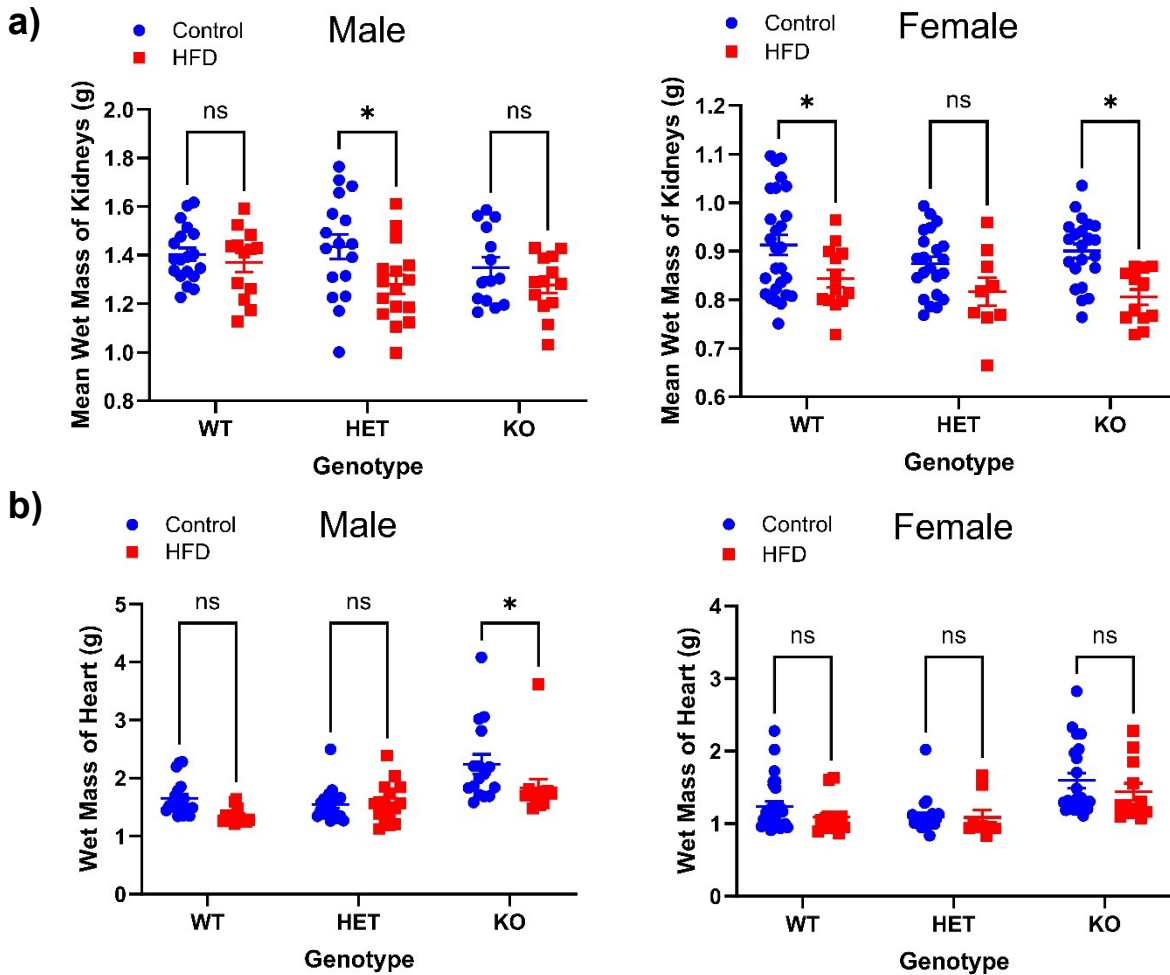


Figure B.1: Weight of kidneys and hearts from control and HFD-fed WT, HET and KO rats before correcting for body weight. Kidneys and hearts of control and HFD-fed male and female WT, HET, and KO rats were weighed and compared on the basis of diet within each genotype-sex group. **a)** Mean kidney weight ($n = 9-22$) showed a significant effect of diet ($P < 0.05$) but effect of genotype ($P > 0.05$). **b)** Heart weight ($n = 9-22$) from male rats showed significant effects of both diet and genotype ($P < 0.05$). Heart weight from female rats did not show a significant effect of diet ($P > 0.05$) but showed a significant effect of genotype ($P < 0.05$). Data are presented as mean \pm SEM. * denotes $P < 0.05$ from control diet; two-way ANOVA with Šídák's multiple comparison tests.